Nanotool-based platform for neuronal activity monitoring at the single cell level

Luca Bettamin

THÈSE

En vue de l'obtention du

DOCTORAT DE L'UNIVERSITÉ DE TOULOUSE

Délivré par l'Université Toulouse 3 - Paul Sabatier

Présentée et soutenue par

Luca BETTAMIN

Le 30 juin 2021

Plate-forme de nano-dispositifs pour le suivi de l'activité neuronale au niveau de la cellule individuelle

---

Ecole doctorale : **GEETS - Génie Electrique Electronique,Télécommunications et Santé : du système au nanosystème**

Spécialité : **MicroNano Systèmes**

Unité de recherche :
LAAS - Laboratoire d'Analyse et d'Architecture des Systèmes

Thèse dirigée par
Guilhem LARRIEU et Daniel DUNIA

Jury
Mme Anne Charrier, Rapporteure
Mme Cécile Delacour, Rapporteure
Mme Esma Ismailova, Examinatrice
Mr Jean-Michel Peyrin, Examinateur
M. Guilhem Larrieu, Directeur de thèse
M. Daniel Gonzalez-Dunia, Co-directeur de thèse

Contents

Abstract

The major goal in modern electrophysiology is to improve the comprehension of the central nervous system functioning. The global population is getting older, therefore neurodegenerative problems are becoming more and more relevant. Hence, the brain, and in particular neurons have been studied with a wide range of devices. Technologies for both *in-vivo* and *in-vitro* recording have been developed to perform studies on this topic. With this objective, our team is developing a bio platform to measure the activity of cultured neurons. The advantages brought by means of micro fabrication allows to improve the performances of this type of chips.

At the same time, it became evident that the sensing of multiple parameters is a great advantage for electrophysiological studies. The co-integration of multiples type of devices on the same substrate is an effective way to provide this possibility. We decided to integrate on the same platform passive devices to record the electrical activity of the cells and active electrodes for the monitoring of pH variation. The electrical signals are recorded with electrodes based on PtSi vertical nanopillars, meanwhile FinFETs are used as pH sensors.

Also, the creation of organized cells network has been an objective of researchers to study neuronal communication. To obtain it, different methods have been considered, but particularly interesting results have been obtained with microchannels. This technology can be easily integrated on planar bio platform. Because of that, we decided to investigate which was the best method to effectively transfer it on our bio platform. One solution was found in the structuration of a photosensitive resist, the SU-8, by photolithography. In alternative, the use of PDMS resulted in reliable microchannels that can be easily integrate on top of the devices.

Finally, the efforts dedicated on the development of this bio platform and the home-made complementary recording setup were validated by several electrical tests and characterizations. In order to perform data analysis, most available commercial setups include a dedicated software, in our case it was necessary the development of both a recording software and a script to extract relevant statistical trends. This manuscript ends with the results obtained on two biologically relevant experiments, the effect of Amyloid-β Peptide and Borna Disease Virus on the electrical activity of cultured primary rat neurons.

Chapter 1

Introduction

In order to fabricate a working bio platform for electrophysiology, all prior knowledge on the topic must be mastered and integrated. The historical reasons to study the electric communication have evolved over time, but these studies are important nowadays more than ever. In the modern research several groups investigate and try to improve those devices as well as several start up and companies put funding and time for the same goal.

Here the history of electrophysiology is described and a description of how electrogenic cells, in particular neurons, work. The modern technologies for electrophysiological studies are shown. In particular, the published works and the state-of-the-art bio platform for electrogenic cells interfacing are presented. Finally, the thesis objectives are disclosed and discussed.

1.1 History of electrophysiology

The electrophysiology (from Greek *electron*, "amber"; *physis*, "nature, origin"; *logia*, "the study of [a certain subject]") is the study of electrical phenomena and properties of biological cells and tissues. The first roots of electrophysiology came from the description of static electricity by Thales (625 547 B.C.), but it was only in the year 1600 that the term electricity appeared in the first scientific essay "*De magnete, magnticisque corporibus, et de magro magnete tellure*" by William Gilbert.

Relatively soon after that, in the last years of the 1700, Alessandro Volta invented the first electric battery and defined the quantitative relation between capacity, charge and electrical potential: $C = \frac{Q}{V}$, giving the name Volt to the unit for the electric potential. During the same last decades of the 1700, a debate regarding metal electricity against animal electricity (Volta against Galvani) started spreading from Italy (Bologna and Pavia) through all Europe. The discussion started from Volta's scepticism regarding earlier publications by John Walsh in 1773 about the possibility to produce electricity form Torpedo fish, on the other hand Luigi Galvani

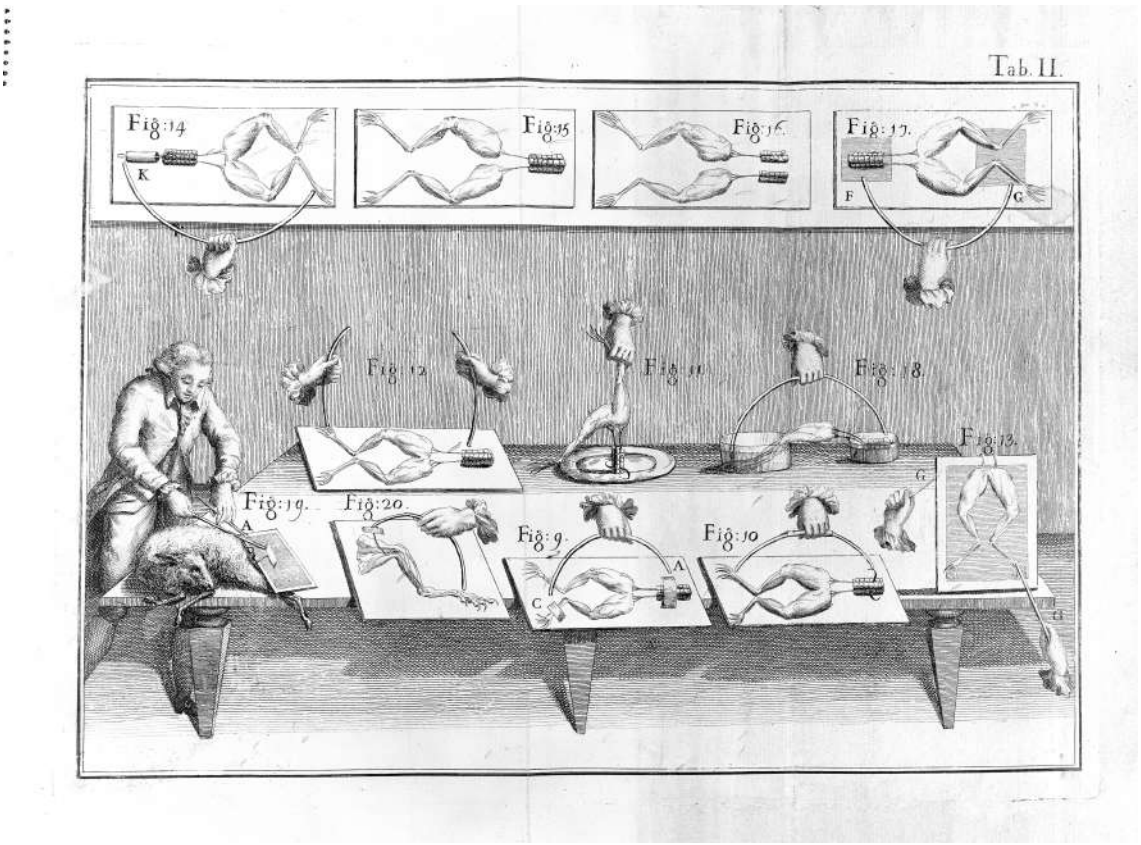

Figure 1.1: Illustration from Galvani's *De viribus electricitatis in motu musculari. Commentarius* essay describing frog muscles contractions due to electrical stimulations. Image from Wellcome Collection.

in 1791 published his work "*De viribus electricitatis in motu musculari. Commentarius*" where he demonstrated the electrical nature of nervous activity obtaining contractions of frog muscles with an electrical stimulation (figure 1.1). Finally, in 1792, another publication by Galvani almost convinced Volta of the existence of this animal electricity, he also wrote that it could be "one of the most surprising findings, and the germ of many others", but at the end of the year he clearly declared his reject for the existence of the animal electricity. Historically, Galvani is now known as one of the pioneers of bioelectricity and electrophysiology.

Carlo Matteucci continued Galvani's work on bioelectricity and in 1840 he was the first to measure muscular current in a frog muscle, thanks to a galvanometer invented by Leopoldo Nobili. He saw that these currents were not constant during the contraction of the muscles and also observed a surface tension of the muscles (first clue for the resting potential of electrogenic cells). Matteucci just worked on muscles, it was Emil Heinrich du Bois-Reymond in 1850 that first was able to measure an action current (later related to the action potential) with a particular sensitive galvanometer. Du Bois-Reymond observed a decrease in the electrical potential where the nerves where stimulated and he postulated the existence of

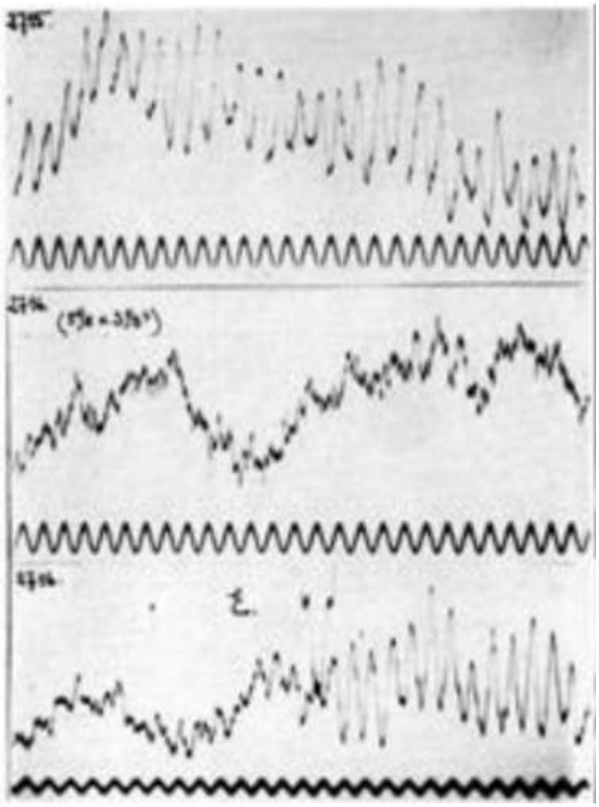

(a) First plot of an EEG by Berger published in 1924 [1].

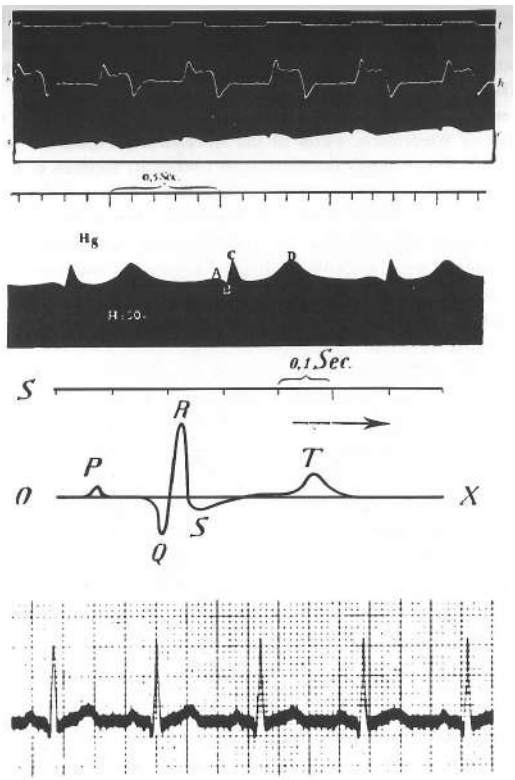

(b) Theory of the ECG published by Einthoven in 1903 [2].

some electrical molecules responsible for the electrical conductivity of these cells. In 1852, Hermann Ludwing von Helmholtz measured nerves response speed about 1 to $100m/s$.

The first measurements of the brain electrical activity were made by Richard Caton in 1875 with some electrodes and a galvanometer on a dog brain. It opened the doors to the electroencephalography (EEG) measurements made by Hans Berger [1] who described the alpha waves in 1924 (figure 1.2a). In the same period, 1885, Sydney Ringer was experimenting on a frog heart varying the concentration of electrolytes in his media and he demonstrated the need of ions for a heart contraction. Therefore later, Willem Einthoven in 1904 obtained the first electrocardiogram [2] (ECG)(figure 1.2b) with, once again, a specifically modified galvanometer (Nobel prize in 1924).

Arriving to modern electrophysiology, Julius Bernstein described the "membrane theory" stating that the cellular membrane has a different permeability to different ions and that this selectivity was varying during the cell activity (the origin of the action potential), he created the first model about bioelectricity in 1902. Later Edgar Adrian stated the all-or-none law of nerves in 1913 and obtained the Nobel prize in 1932. In 1939, Alan Lloyd Hodgkin and Andrew Huxley stated that the value of an action potential peak depends on the sodium potential equilibrium. From 1946, a

collaboration between Kenneth Stewart Cole and Bernard Katz lead at first to the realisation of a feed-back amplifier, the first "voltage-clamp" setup and in 1947 the measure of potassium flow during an action potential of a squid giant axon. Another collaboration between David Goldman, Hodgkin and Katz brought to the definition of a generalization of the Nernst's equation ($E = \frac{RT}{zF} \ln \frac{[ion]_o}{[ion]_i}$):

$$E_m = \frac{RT}{F} \ln\left(\frac{P_{Na^+}[Na^+]_{ext} + P_{K^+}[K^+]_{ext} + P_{Cl^-}[Cl^-]_{ext}}{P_{Na^+}[Na^+]_{int} + P_{K^+}[K^+]_{int} + P_{Cl^-}[Cl^-]_{int}}\right)$$

with E_m for the membrane potential, R is the ideal gas constant, T is the temperature in Kelvin, F is the Faraday constant, P_i are the permeability of the membrane to the different ions and $[i]$ are the concentrations of the ions. The Goldman-Hodgkin-Katz equation gives the value of membrane potential when it has different types of conductivity for the different ions, perfect example for the neuronal action potential.

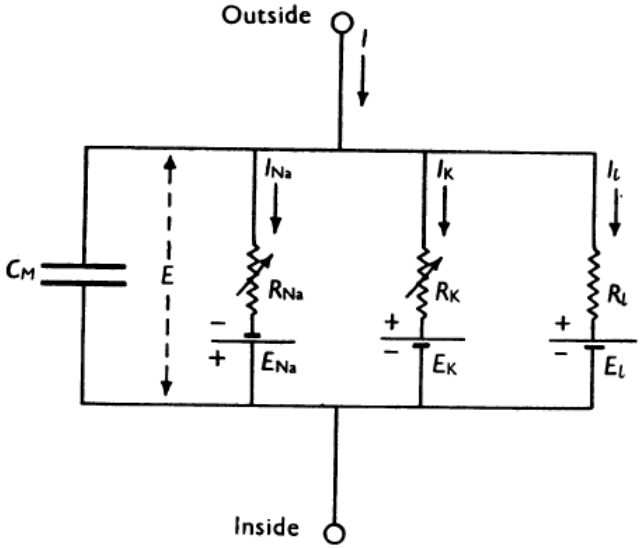

Figure 1.3: Hudgkin-Huxley electrical circuit model of a neuron cellular membrane [3]. Described by a membrane capacitance, C_M and three parallel resistances $R_{Na} = g_{Na}$, $R_K = g_K$, $R_l = g_l$. R_{Na} and R_K in particular vary with time and membrane potential, the other elements are constant.

In the following years, 1952, Hodgkin and Huxley, thanks to their experience with the voltage-clamp, described the movements of the ions through a neuronal membrane and the existence of ionic channels that could be activated and deactivated [3]. It brought them to the creation of the Hodgkin-Huxley electrical equivalent model of a neuronal membrane (figure 1.3) and to win the Nobel prize in 1963.

The main technique used for electrophysiology since works from Hodgkin and Huxley is the patch-clamp and all its variants, in particular, in 1978 Ervin Neher and Bert Sakmann developed a technique called "gigaseal" that allows to record the activity of a single ionic channel [4] and won them the Nobel prize in 1991.

Since then, electrophysiology by patch-clamp allowed to largely investigate the different families of ionic channels and the proteins that they are made out of. In 1998, Roderick Mackinnon did a complete crystallization of a potassium channel and studied it by x-rays diffraction, he won the Nobel prize in 2003. Other modern techniques are for example the discovery of the green fluorescent protein (GFP) by Roger Yonchien Tsien (Nobel prize in 2008) that brought to optogenetics: calcium imaging, light-gated channels and the measure of action potentials with Fluorescent Resonance Energy Transfer (FRET).

Nowadays, thanks to development of micro- and nanotechnology and their means of fabrication, new technologies are being developed to deepen electrophysiology knowledge. Intra cortical probes, flexible electrodes, multi electrode arrays and CMOS devices are constantly improved by companies, start-ups as well as scientific researchers to have better performances and open the possibility to new types of investigation in the electrophysiology field.

1.2 Electrogenic cells

1.2.1 The neuron

The human nervous system is made up of specialized cells: nerve cells (or ***neurons***), known as the grey matter; glial cells, oligodendrocytes and astrocytes, known as the white matter. Neurons are the basic building blocks of the nervous system: They quickly transmit information over long distances using electrical signals called action potentials. In a healthy adult human brain, they are estimated to be around 100 billion with more than 100 trillion synaptic connections. Oligodendrocytes, astrocytes and glial cells mostly have a role of support to the neurons as transport nutrients, clean up brain debris, digest dead neurons and hold neurons in place. There are two main zones in which the human nervous system can be divided: the central nervous system, including brain and spinal cord; the peripheral nervous system, including sensory neurons, the enteric nervous system and motor neurons in the rest of the body. The information are analysed in the central nervous system and transmitted in the peripheral one, where axons travelling together forms nerves that connect to muscles or provide information about touch, position, pain and temperature.

A neuron has three main functions: receive signals, integrate incoming signals and communicate signals. These functions are mirrored in the anatomy of the cell itself (figure 1.4). The **dendrites** are where the receiving function takes place, in-

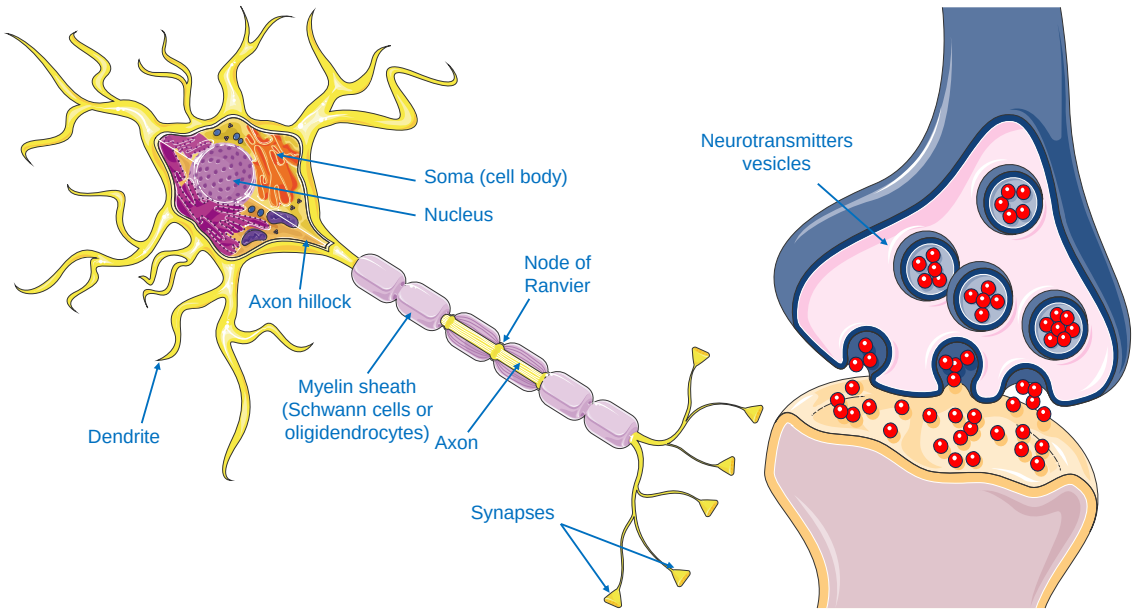

Figure 1.4: Left, the representation of a generic neurons with its different anatomic parts. Right, an example of two synapses connection with neurotransmitter working mechanism illustration. [Image composed using material from SMART]

coming signals can be **excitatory** or **inhibitory**. A neuron can have several sets of dendrites, therefore it can receive thousands of input signals. The activation of a neuron depends on the sum of all the excitatory and inhibitory signal it receives. This integration of the information is made in the cell body (or **soma**), where the nucleus is containing the cell DNA. If the addition of the received signals exceeds a certain threshold, an electric signal is generated in the axon hillock, called **action potential**. From here, the action potential is transmitted along the axon, to the **synapses**. The axons length can variate from fractions of millimetres up to tens of centimetres depending on the location of the target cell. Several types of neuronal axons are covered in myelin sheaths, that helps for a better propagation of the electrical signal, spaced out by the so-called nodes of Ranvier, where the signal is boosted with a mechanism later explained. Myelin is produced by the oligodendrocytes in the CNS or the Schwann cells in the PNS. Synapses are found in neuron-to-neuron connections, the neuron sending a signal is the **presynaptic neuron** and the target one is the **postsynaptic neuron**. At synapses, the information is transmitted via chemical messengers called **neurotransmitters** (that can be amino acids, peptides or monoamines) to dedicated receptors (GABA, NMDA, AMPA, ...).

1.2.2 Electrical signals

Electrogenic cells are capable of generating electrical signals, neurons are a part of this family of cells. In order to create an electrical signal an electric potential is needed, and the variation of this potential determines the intensity, shape and frequency of the generated signal. Intuitively, the neurons naturally have an electric potential, defined by the voltage difference between the interior and the exterior of the cell, this is called **resting membrane potential** and the membrane is said to be polarized. This resting potential ranges from $-30mV$ to $-90mV$, with the inside of the cell being more negative than the outside, usually the value of $-70mV$ is a good approximation. An increase of this resting potential defines a depolarization, a decrease defines a hyperpolarization.

The resting membrane potential is due to an unequal distribution of ions between two sides of the cell membrane, and by the permeability of the membrane to these ions. In particular, ions such as $\mathbf{K}^+$, $\mathbf{Na}^+$ and $\mathbf{Cl}^-$ are usually the most abundant. The ions flow from inside to outside of the membrane lipid bilayer, or vice versa, through specific channels (sodium channel, potassium channel, ...). The sodium-potassium pumps in particular act to maintain the resting membrane potential. The flow of the ions is due to the natural electrochemical potential (difference in potential and concentration) but also to the activation of ions channels in response to external stimuli such as neurotransmitters from the synapses.

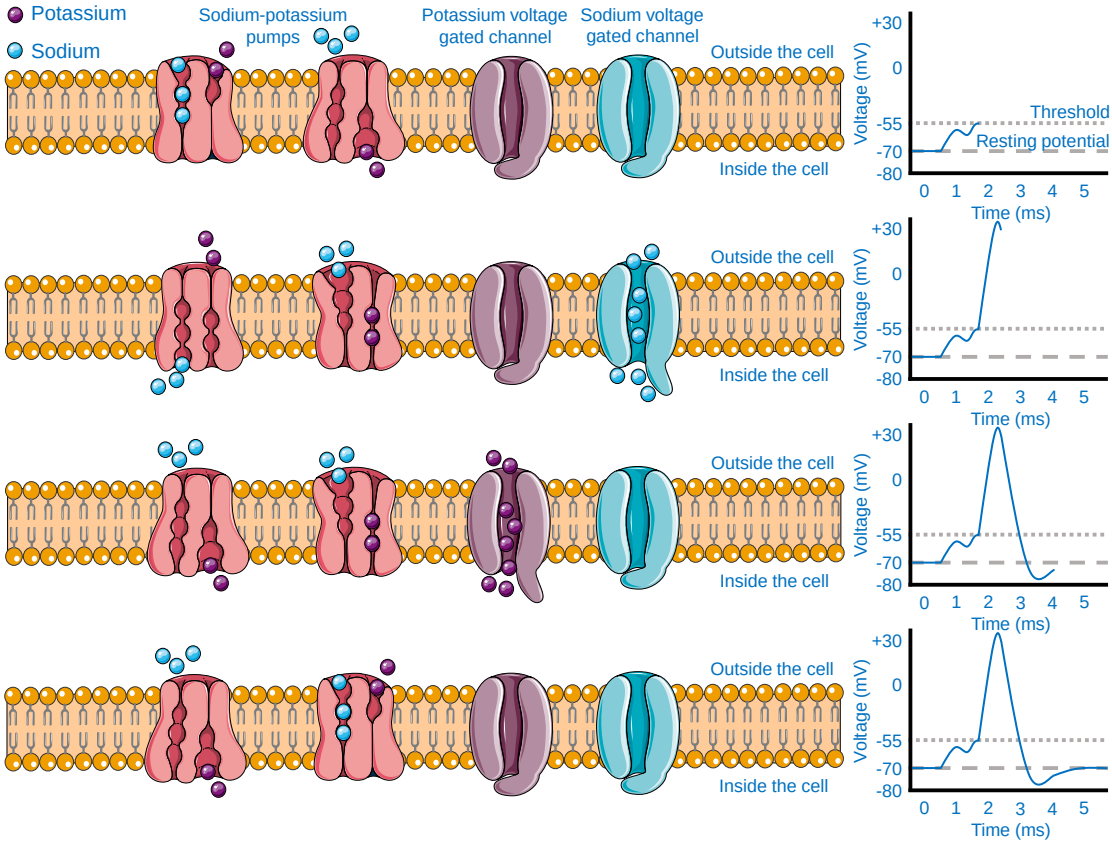

Figure 1.5: The four main parts of the activation mechanism of a neuron. From top to bottom: the resting potential controlled by sodium-potassium pumps and the reach of the threshold; the membrane potential is surpassing the threshold the sodium voltage gated channels open and there is a polarization of the cell; opening of the potassium voltage gated channel and consequent repolarization of the membrane potential; hyperpolarization and return to resting potential. [Image composed using material from SMART]

The activation of a neuron is a all-or-none response, only if the membrane potential reaches a certain threshold at the axon hillock, specific voltage gated channels will activate. These channels have defined potentials for activation and deactivation, based on the type of ions that are paired. To simplify, let us consider only $\mathbf{Na}^+$ channels and $\mathbf{K}^+$ channels. Starting from $-70mV$ at resting potential, an increase to $-55mV$ will activate the sodium voltage gated channels, increasing the permeability of the membrane to this type of ion. The sodium flow modifies the electrochemical membrane potential depolarizing it up to $+30mV$ where the sodium voltage gated channels will deactivate and, at the same time, the potassium voltage gated channels will activate. The potassium flow will re-polarize the membrane down to $-80mV$ causing also a hyperpolarization and deactivating the potassium voltage gated channels. This sequence of events take place in the axon hillock as well as along the axon, in particular, in the nodes of Ranvier. The membrane potential will thereafter return to the resting membrane potential. This variation of the mem-

brane potential is called **action potential** and it is transmitted along the axon to the synapses (figure1.5).

1.2.3 Neurodegenerative diseases

Knowing the fundamental role of the brain and its complex structure, it is also important to understand how a failure at any level can impact the normal life of a human being [5]. The World Health Organization (W.H.O.) published several reports and books regarding neurological disorders, in particular, the 2006 report sent a clear message stating that, unless immediate action is taken globally, neurological burden will become a very serious threat to public health. Citing Rita Levi-Montalcini in the foreword of the same report: "At the beginning of the third millennium, due to prolonged ageing, neurodevelopmental disorders are growing, and a much deeper knowledge of the brain is necessary. Scientific and technological research, from molecular to behavioural levels, have been carried out in many different places but they have not been developed in an interdisciplinary way. Research should be based on the convergence of different interconnected scientific sectors, not in isolation, as was the case in the past."

Neurodegenerative diseases are part of the neurological disorders and they are caused by the degeneration of the brain abilities. The most important neurodegenerative diseases are Alzheimer's disease, Parkinson's disease and Huntington's disease with the first one accounting between 60% and 80% out of all cases. These diseases are linked to neuronal plasticity perturbation, reduced possibility of receiving or communicating signals and neuronal death. For Alzheimer's disease in particular, the accumulation of amyloid-beta oligomers may contribute to the damage and death of neurons (neurodegeneration) by interfering with neuron-to-neuron communication at synapses. The complete sequence of events is still unclear and none of the pharmacologic treatments (medications) available today slow or stop the damage and destruction of neurons. According to the 2020 Alzheimer's association report projections, the number of people in the U.S.A. with Alzheimer's disease will more than double (increase of 2.4 factor) in the next 30 years, moreover the Alzheimer's disease as a cause of death at all ages between 2000 and 2018 increased of 146.2%.

To fight the growth of these disorders and to enhance the knowledge about the mechanisms at their base, several institutions found the scientific research on this theme, such as the National Institute of Environmental Health Sciences (NIEHS) in the U.S.A, and in Europe the EU Joint Programme - Neurodegenerative Disease Research (JPND).

1.3 Technology for neuronal electrical recording

The modern technologies to record and study cells activity divide between *in-vivo* and *in-vitro*, the first being focused on a more global level of investigation of cells networks or brain zones and the second one that aims to the understanding of the basic mechanisms of cell functioning at the single cell level or of a few cell clusters.

1.3.1 In-vivo

For *in-vivo* studies, it exists two main categories of technologies, non-invasive and invasive ones. These are nowadays the most used devices in medicine to investigate pathologies linked to malfunctioning of brain areas.

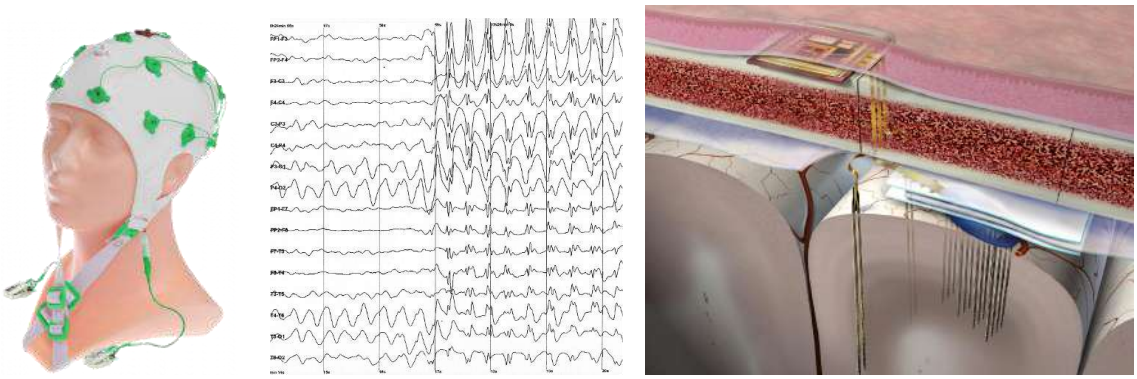

(a) EEG. (b) Neural probes.

Figure 1.6: a. An example of EEG setup and recorded graph. b. Neural probes example [6], neural microsystem consisting of arrays of cortically implanted electrodes.

Electroencephalography, or EEG, is the technology that allows to record the activity generated by the brain via electrodes placed on the scalp surface. These electrodes are normally mounted in elastic caps and they are distributed on the surface of the scalp to record the activity from different brain areas (figure1.6a). This technology aims to record a global activity of the brain coming from thousands of neurons that generate electrical signal in synchronous. The EEG records 4 main areas of the brain:

Occipital cortex Is the visual processing centre of the brain, is the rearmost portion of the skull.

Parietal cortex Here the brain merges information into a coherent representation of how all things relate to us spatially.

Temporal cortex It is associated with visual memories, language and emotional associations.

Frontal cortex It is all about executive function, maintain control, plan for the future and monitor our behaviour.

The EEG frequency ranges from 1 to $50Hz$, from lower to higher waves frequency: delta $(1-4Hz)$, theta $(4-7Hz)$, alpha $(7-12Hz)$, beta $(12-30Hz)$ and gamma $(30-50Hz)$.

Even if this technique has some advantages like having a **relatively simple setup** and being **totally non-invasive**, it also has several disadvantages: a **very low spatial resolution** of the brain, it needs intense interpretation of the data to deduce which area of the brain is activated; **poor detection** of the activity below the upper layers of the brain; **very low signal-to-noise ratio** add the necessity of sophisticated data analysis.

Other indirect measurement at the macro-scale of large areas of brain's activity are the functional magnetic resonance imaging (fMRI) and the positron emission tomography (PET).

On the other hand, a very intrusive *in vivo* recording technique is based on the positioning of intra-cortical probes (figure1.6b). These types of electrodes are implanted directly in the brain, close to the signal source. The intra-cortical probes are used for neuroscience and electrophysiology research but also for brain computer interfaces that are being developed in the recent decades. It exists a variety of implantable devices, divided in single recording methods (single wire, glass pipette) and multichannel recordings (micro-wires, silicon probes and platforms with micro-electrode arrays) [6, 7, 8, 9, 10, 11].

The intra-cortical probes have **much higher sensitivity**, being in direct contact with the brain and record the activity of **smaller population of neurons**. Nevertheless, they require **intrusive surgical operation** to be positioned, moreover the vascularization of the brain and the presence of glial cells could degrade the recorded signals.

To improve our comprehension of the brain's basic mechanisms, as well as its malfunctioning, it is therefore necessary to integrate to this more global reading of the brain activity an investigation at a smaller level. With this idea, in vitro devices have been developed to allow the study of cultured cells and the basic mechanisms at the cellular level.

1.3.2 In-vitro

Moving to the *in-vitro* technologies, these are divided in two main types: the patch-clamp and the Multi Electrode Arrays (MEAs). These devices are used to study cell networks simpler that the ones in the brain and to get to the comprehension of the building blocks of the nervous system. These simplified systems can allow to verify

the effect of stimuli or the impact of specific substances on the cells.

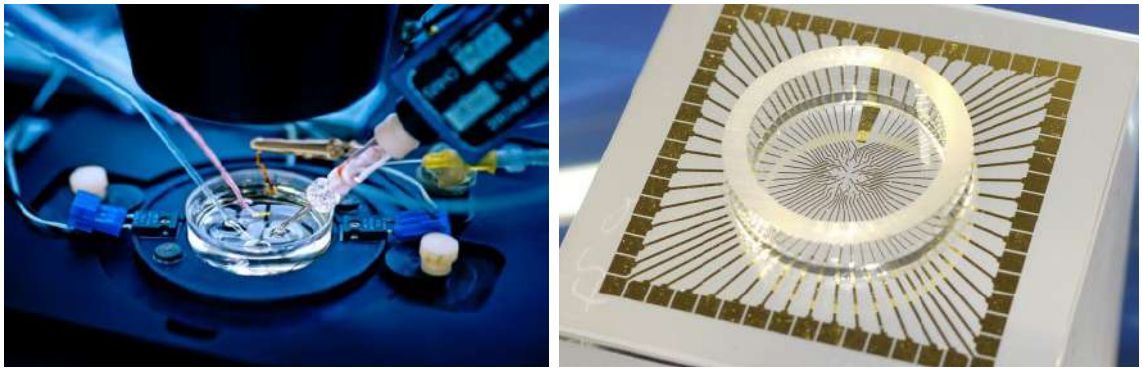

(a) Patch-clamp. (b) MEA.

Figure 1.7: a. Image of a patch-clamp setup with different electrodes under an optical microscope. b. Standard MEA device with 60 electrodes.

The patch-clamp technique is a very powerful and versatile method for studying electrophysiological properties of biological membranes. After its development, this technique was adopted by numerous laboratories and constantly improved ever since. Several ramifications of this technique were developed, from voltage-clamp to current-clamp and from whole-cell type of measurement to single-channel currents flowing across biological membranes through ion channels. Being nowadays the most used technique to study it brought an expansion of the commercial supply industry and equipment, making also impossible to define a "standard" patch-clamp setup. In its simplest form, the patch-clamp setup consists of a microscope on a vibration isolation table within a Faraday cage, an amplifier and a pulse generator for voltage-clamping the cells, a micromanipulator to position the micropipettes and a data recording device.

In general, the patch-clamps have a very **high sensitivity** and an **excellent signal-to-noise ratio**, it allows to study the total amplitude of the cells electrical activity and the details of a single ionic channel activation. On the other hand, patch-clamps have several limitations: it has a **complex setup** [12], needing a lot of experience to master it; it can interface only one cell at a time, **few neurons per experiment**, limiting the cells network behaviour study [13]; it often implies the cellular death at the end of the recording, there is no possibility of long time or repeated experiments.

The MEAs started to be fabricated when the technologies for silicon structuration, as photolithography and plasma etch, reached the micro metric dimensions in the middle of last century [14], it then allowed to produce devices with many electrodes even smaller than the cells dimensions. MEAs usually have between 60 to 256 electrodes and the most common used materials are: gold (Au), titanium nitride (TiN), platinum (Pt), stainless steel aluminium (Al) and other alloys as iridium ox-

ide (IrOx). Several terms have been used to describe and refer to the different types of MEAs developed (microelectrode array, multi-electrode array, multi-transistor array, ...), the substrate used (active array, passive array, CMOS array [15, 16, 17], ...), the electrode density (HDMEA [18, 19, 20]) or the application [21, 22, 23, 24]. This technology became commercially available in the late 90s, giving a boost to its application in electrophysiological investigation. Moreover the integration of active electronic components on the same substrate increased the possibility of higher electrode number, density and additional functionality [25, 26].

Even if the possibility that MEAs bring to electrophysiology are numerous, such as the possibility of **long-term experiments** and to record data on **multiple locations**, these devices are limited by their resolution. The micro metric dimensions of the electrodes have as consequence **high interface impedances**, and the **planar geometry** does not promote the interaction with the cells.

In-vivo	Advantages	Drawbacks
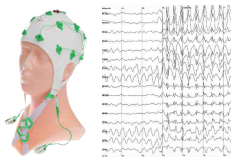	• Global brain reading • Non-invasive setup	• Low spatial resolution • Low sensitivity • Difficult interpretation
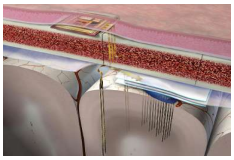	• Higher resolution • Precise localization	• Very intrusive • No permanent
In-vitro	Advantages	Drawbacks
	• Maximal resolution • Intracellular measure • Single cell interfacing	• Limited in multiplexing • Not repeatable measures
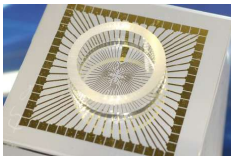	• Multi-sites measurement • Long term recordings • Repeatable experiments	• Not single cell interfacing • Weak cell interaction • High impedance

1.3.3 Co-integration and multi-sensing

The possibility to add other modalities of recording to MEAs devices was recently investigated. It can be done adding different types of electrodes or sensing transducers, obviously it is easily done on CMOS MEAs devices thanks to their possibility

to multiplexing channels onto fewer wires. Some examples of these alternative measuring modalities are:

Electrical stimulation The electrodes are able to bidirectionally record and electrically stimulate the cells [27, 28].

Optical recording Angle-sensitive pixels and sensors can be used to stimulate or record light sensitive cells or proteins [29, 30, 31, 32, 33].

Temperature sensors These sensors can readout the temperature of the culture media or the environment [29].

Molecules sensors Used for localization of bio particles or to determine the concentration of molecules in the media [34, 35].

Ion sensors These devices can determine the pH of the media measuring ions concentration [29, 30].

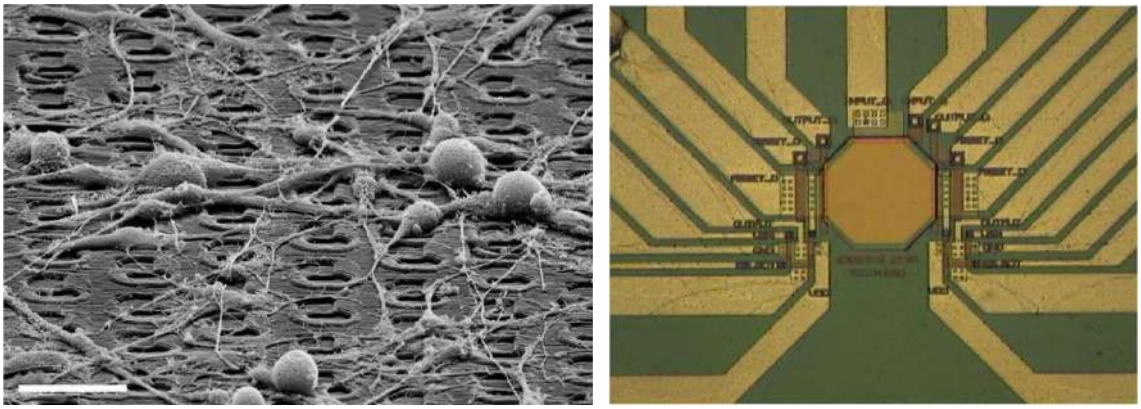

(a) Bidirectional electrodes. (b) Photo- and ion-sensor.

Figure 1.8: a. SEM image of a high-density bidirectional microelectrode array with a fixed neuronal cell culture [28]. b. Optical image of a combined photo- and ion-sensor [30].

Several combinations of co-integrated devices may be found in the literature but none of these devices provided evidence of the possibility to measure multiple parameters down at the cellular level. For example, some devices having bidirectional electrodes showed to have the possibility to record the activity of electrogenic cells, as cardiomyocytes and neurons, before and after localized electrical stimulations [28]. Anyway, this kind of stimulation cannot be proved to be addressed to a single cell, given the planar nature of the electrodes and therefore its weak interaction with the cells, but a global reading of the cellular network has been shown. Other devices proved the theoretic possibility to combine field potential measurements and optical readout [30, 33], but unfortunately it has never been shown practically on a living

cell culture. Anyway, the electrodes and pixels dimensions do not allow this co-integration on a single cell level of interaction, but only for a broader kind of global characterization.

Those modalities were therefore until now used to determine one of the previous parameters at the **global scale** of a cell culture in parallel to **spatially broad measure** of the neuronal network field potential. The co-integration of multiple sensing techniques is for this reason not yet demonstrated on a single cell or subcellular scale, which is definitely important if we want to focus on the study of single cells basic mechanisms functioning when they are part of a wider cell network. Combining two of these measurements techniques at this level of miniaturization would open the possibility for new studies addressing unknown cell malfunctions.

To what degree pH changes during normal brain function is unclear, but neuronal activity could cause transient localized pH changes via several mechanisms [36]. Increased neuronal activity can produce lactic acid and CO_2, large ion fluxes, HCO_3^- transport and acidic synaptic vesicles realising protons. Localized acidosis might have a number of consequences for brain physiology [37, 38], activating some ion channels and receptors and inhibiting others. For this reason, monitoring the pH level at a global scale as well as in specific location might help understand the causes of numerous brain diseases.

1.3.4 Measurements using active devices

Since the end decade of last century another type of devices have been studied and used as bio-platform, the fields effect transistors (FET), as active devices able to detect the variation of field potential. The first studies were done by Fromherz in the first half the 90s, in particular these first studies showed that the FETs were able to measure a signal coming from a cell, even if this current came from a stimulation of a patch-clamp attached to the cell [39, 40]. Not much later, arrays of FETs were developed to reach the dimensions of the cells and to give the possibility of a long-term monitoring of the cellular activity [41]. Moreover, demonstration of the possibility to use these substrates also with brain slices were made, obtaining electrical recordings of field potential coming from different zones of the brain slice [42]. The integration of these devices on CMOS substrates allowed also to record the network dynamics of cells and brain slices and to map them thanks to high density of recording sites [43]. Generally, resolution around few hundreds of microvolts were achieved [44], comparable to MEAs performances.

Lieber's laboratory too, since the early 2000s, was very implicated in the study of these active devices showing their capabilities as ultra-sensitive bioassays or sensors of biological species and even single viruses or cancer markers thanks to specifically

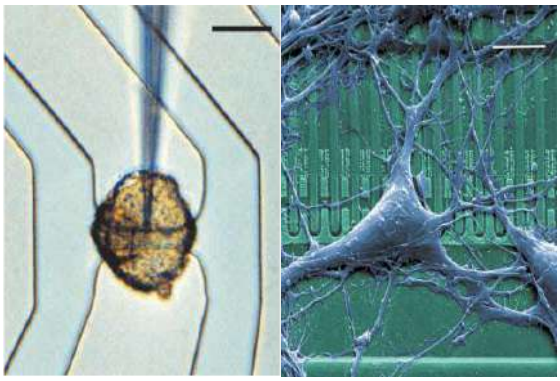

(a) Patch clamp impaled cell on single active device and nerve cell on FET array.

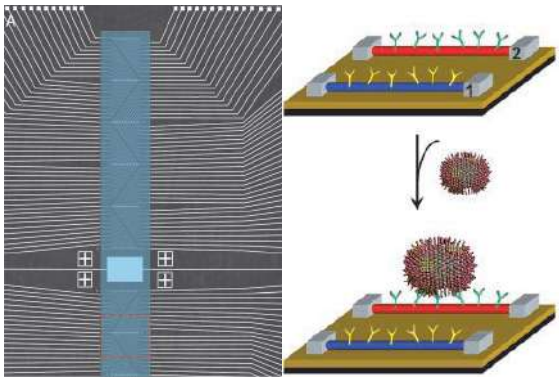

(b) Nanowire device array and schematic of virus detection.

Figure 1.9: a. Left, nerve cell from a leech on the gate of a FET, the cell is impaled with a glass capillary. Right, colourized nerve cell from rat brain on a silicon chip, the surface is made of silicon dioxide the FETs are visible as dark squares. [Scale bars are, left, 50μm and right, 10μm] b. Left, optical image of an active device FET array, white lines are the metal electrodes connecting to individual nanowire devices. Right, schematic showing the dynamic of specific single virus receptor binding mechanism.

functionalized transistor channels [45, 46, 47, 48]. Arrays of FETs were used to detect and stimulate neuronal signals with success and a demonstration of the possibility to follow the signal propagation along a neuronal axon was done with a series of up to fifty transistors [49].

Also, other approaches have been attempted, as the use of open gate FETs [50], metal insulator semiconductor FETs [51] or nanowire-nanotube heterostructures with integrated FETs for intracellular approaches [52, 53] Very high resolution has been achieved by these devices but always with a trade-off between the possibility to multiplex the recordings and the system sensitivity. Very unique solution as the heterostructures may reach intracellular recordings but at the cost of the possibility to interface multiple cells at the same time, exactly as a CMOS substrate can guarantee the spatial resolution needed to map an entire cell network, but lack of the better interaction obtained with more particular structures. The recording of potentials made with active devices did not brought until now a major advantage to the resolution of passive electrodes at a cost of a much more complex system design.

1.3.5 Commercial systems and other solutions

In 1996, the two main companies that now sell commercially available MEAs were founded and in the last decades several other companies and start-ups have emerged.

The European Multi Channel System (MCS) was founded in Germany in the Science and Technology Park in Reutlingen, it then became a division of Harvard Bioscience, Inc. This company sells both MEA-systems or patch-clamps as well as

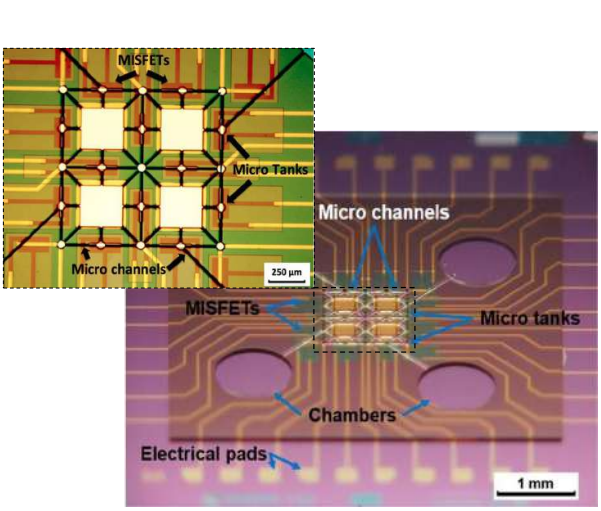

(a) Metal insulator semiconductor FETs.

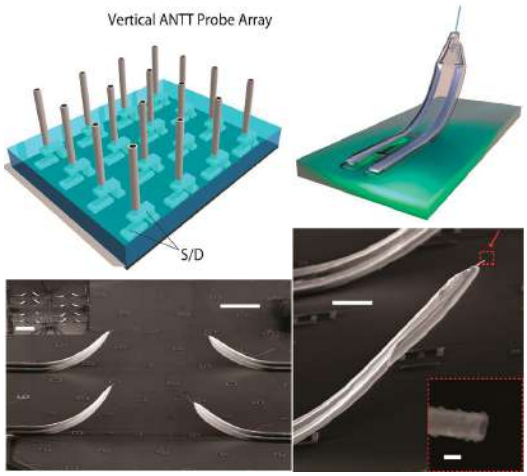

(b) Nanowire-nanotube heterostructures with integrated FETs.

Figure 1.10: a. Optical microscopy images of a substrate with metal insulator semiconductor FETs and in the inset the integrated SU-8 microfluidics system is visible. b. Top left, schematic of chip-based vertical active nanotube transistor. Bottom left, SEM image of part of an active nanotube transistor probe array. Top right, schematic of a completed active nanotube transistor probe following release from the substrate. Bottom right, SEM image of a active nanotube transistor probe and inset of the probe tip. [Scale bars are, bottom left 2μm, bottom right 10μm and 100nm for the inset]

several other setups. They managed to compose and sell a complete MEAs setup from the microelectrode arrays device, to custom amplifiers, data acquisition cards and proprietary software for data acquisition and data analysis. Their devices are mainly used for non-clinical investigations and the commercial MEAs reach up to 256 standard planar electrodes excluding the CMOS solutions.

At the same time in Japan Alpha MED Scientific born inside Panasonic developed the MED64 as their first commercially available in-vitro microelectrode array. They later spun off Panasonic and focused their products on MEAs complete setups, as for MCS, from the device itself to the amplifiers and software.

Regarding other solutions, several start-ups managed to be incredibly well funded promising to create neural interfaces to improve or accelerate the human's ability to recover from trauma or chronic health conditions for neuro-rehabilitation and also to control external systems thanks to AI implementation. Some examples are the now well-known Neuralink from the entrepreneur Elon Musk, or Kernel from Bryan Johnson. In Europe, other companies examples are the Swiss MindMaze, the English BIOS or the French NextMind.

1.4 State-Of-The-Art

What else can be done? From the discussion of the previous section, it can be deducted that there is the need to develop devices able, at the same time, to electrically interface single cells, or even down to the subcellular level, with high-resolution on multiple sites of a neuronal network [54] and to combine it with another local sensing technique in order to be able to screen multiple parameters at the same time. It would open the possibility to better understand the reasons of a cell behaviour given multiples readouts of the cells environment.

To address the MEAs limitation in terms of resolution, the structuration at the micro- and nano-scale of the electrodes has been investigated in the last decades. Several approaches were explored with excellent results and demonstrating the worth of this approach. Here it is presented the state-of-the-art of micro and nano-structuration of the electrodes and their performances, afterwards the previous accomplishments of our team are shown to determine the starting point of this thesis work.

1.4.1 3D electrode devices

The limiting aspect of an MEAs is the scarce interaction with the cell, the cellular membrane is just in contact with the planar electrodes and this interaction is rather weak. This does not allow the MEAs to record signals with a good enough sensibility to detect subthreshold excitatory- and inhibitory-postsynaptic potentials (EPSPs and IPSPs, respectively), and subthreshold membrane oscillations [54]. To increase this *cells/electrode* interaction the geometry of the electrodes has been modified to achieve the **engulfment** of the electrode by the cell. The engulfment depends on the dimensions of the electrodes, tuning these parameters and the materials used equals tuning the neuron-device electrical coupling. Mainly passive multi electrodes arrays integrating nanowires, nanotubes or mushroom-like electrodes were investigated [55].

Chronologically, the first published attempt to improve the *cells/electrode* interaction came from Spira's laboratory in 2011 [56]. They developed gold mushroom-shaped microelectrodes (gMμE) showing a tight seal and describing how the engulfment of this micro metric structures can improve the neuron-device electrical coupling (figure 1.11a). They reported a so called "IN-CELL" recording configuration, not to be confused with an intracellular recording. This configuration showed the engulfment of structures around 1μm in size, the formation of tight cleft that enhances the *cells/electrode* interaction and localized increased conductance of the membrane patch facing the gMμE. The same type of devices was used to study membrane kinetics dynamics [59] by means of an electroporation procedure and consequent recording of the cell electrical activity. Later, it was also demonstrated

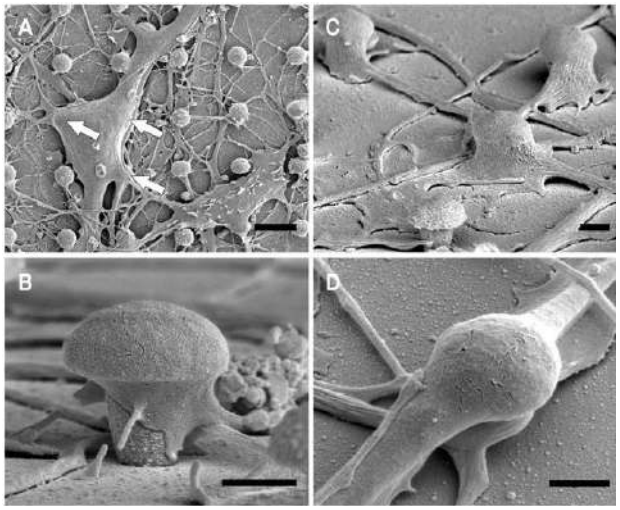

(a) Mushroom-like electrodes.

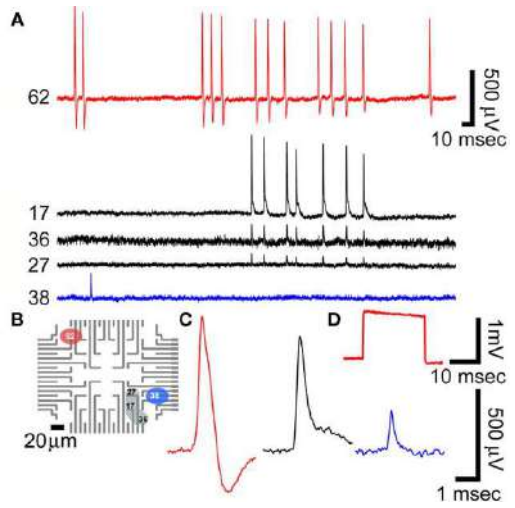

(b) Mushroom-like electrodes recordings.

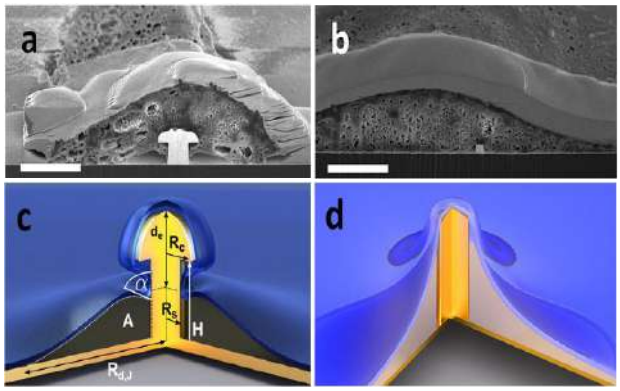

(c) Cell/electrode interface study.

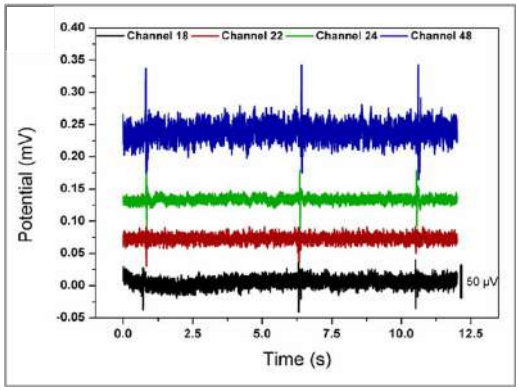

(d) 3D electrode recordings.

Figure 1.11: a. SEM images of dissociated cultured rat hippocampal cells grown on a matrix of gMμE [56].[Scale bars are 5μm for (A) and 1μm for (B-D)] b. Spontaneous fast monophasic positive action potentials generated by cultured hippocampal neurons grown on gMμE based MEA for 10 days. c. Investigation of junctional membrane deformation in the centre of the cell [57]. [Scale bars are 1μm for (A-B)]. e. Spontaneous action potentials recorded by 3D electrodes in a time frame of 12s [58].

the possibility to record up to 60 microelectrodes at the same time with a maximal resolution of few millivolts in amplitude [60]. These devices have been used with *Aplysisa* neurons, rat hippocampal primary neurons and glial cells. In particular with the rat primary neurons good performances have been demonstrated with a maximal recorded amplitude of several millivolts and an average amplitude still well above planar MEA performances. This demonstrates the validity of this approach and the importance of the electrode engulfment, increasing the interaction with the cell.

Similar mushroom-shaped devices were also used in Offenhausser's laboratory to study the electrical coupling with the cells and in particular the combination of cell guidance and extracellular recordings on a chip at the same time [58]. Also later, an in depth study of the cell interface with mushroom-like electrodes and

nanopillar was published [57], it linked the shape of the nano structuration and its position relative to the cell, to the electrical coupling via a deformation model of the cellular membrane demonstrating once again that the better is the *cells/electrode* interaction the better are the consequent electrical recordings (figure 1.11c). These publications used HL-1 cardiomyocytes as cultured cells showing consistent spontaneous recording around one hundred millivolts amplitude, not far from standard MEA platform.

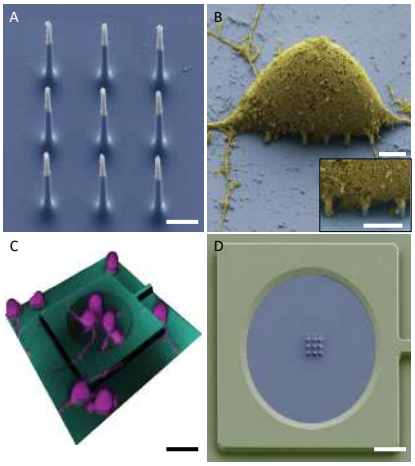

(a) Vertical nanowires arrays.

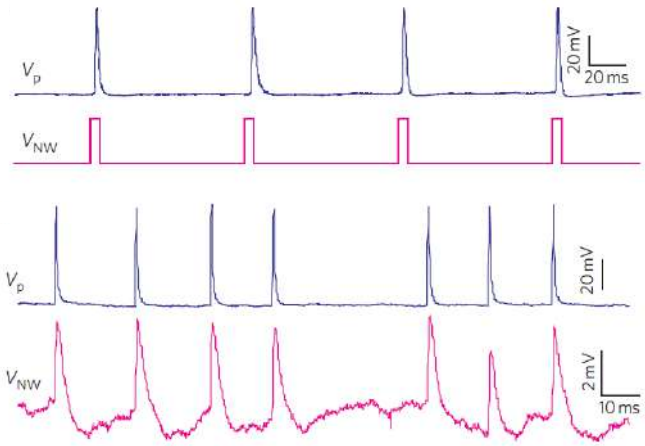

(b) VNEA recordings.

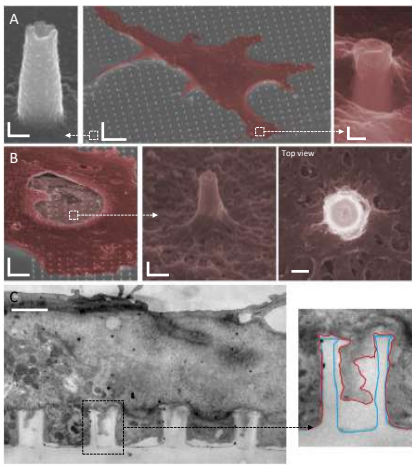

(c) Iridium Oxide nanotubes.

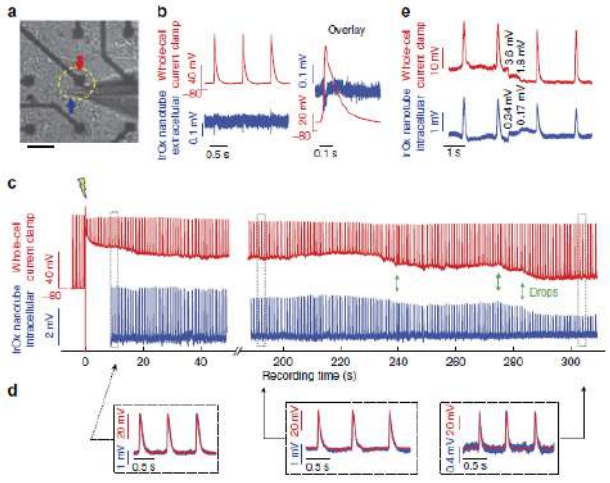

(d) Iridium Oxide nanotubes recordings.

Figure 1.12: a. VNEA used for interrogating neural networks [61]. [Scale bars are 1μm for (A), 2, 5μm for (B and the inset), 40μm for (C) and 10μm for (D)] b. Stimulation and recording of rat cortical neurons using a VNEA. c. Cardiomyocyte interfacing with vertical nanotube arrays [62]. [Scale bars are: 100nm left image, 5μm centre image and 100nm right image for (A); 5μm left image, 200nm centre image and 100nm right image for (B); 1μm for (C)] d. Simultaneous recording by IrOx nanotube electrodes and patch-clamp.

Soon after the first demonstration with mushroom-like shaped electrodes also simpler nanopillars (nanopillars and nanotubes) were published. From Park's laboratory in 2012, vertical nanowires, called vertical nanowires electrodes array (VNEA), made out of silicon and silicon dioxide with metal coated tips of titanium/gold were

fabricated [61] aiming to intracellular recording. It demonstrated that the nanowires are also a feasible structuration to improve MEAs planar electrodes, that it could be used both to record and stimulate the cells and it could be coupled with more classical patch-clamp technique (figure 1.12a). They after moved to a CMOS approach (CNEA), showing the possibility to use these platforms for pharmacological screening and studies of electrogenic cells networks [63]. The VNEA and CNEA platforms where respectively used with rat cortical primary neurons and rat neonatal ventricular cardiomyocytes, their performances constantly reach one millivolt of recorded amplitude demonstrating that with a nanopillar structuration the performances of a standard MEA can also be largely improved. The first demonstration paper, with parallel patch-clamp stimulation, showed the reliability of the platform, and in the latest an electroporation protocol was used to reach up to 15mV of recorded amplitude.

In the same year 2012 from Cui's laboratory platinum nanopillars were fabricated and used to demonstrate that it was possible to pass from extracellular recording to intracellular recording thanks to specific electroporation procedures [64]. This transient electroporation drastically improved the recorded signal but for a limited period of time due to the sealing of membrane pores. They later demonstrated once again that the geometry, and the material choice, of the electrodes can improve the resolution of the device comparing gold nanopillar and iridium oxide nanotubes [62]. The IrOx nanotubes were shown to have a larger surface area and better electrical coupling with the cells and the positive curvature of the cell membrane inside the nanotubes were supposed to have a role in the enhanced device performances (figure 1.12c). The devices have been used with HL-1 cardiomyocytes showing spontaneous recording around one hundred millivolts of amplitude both with platinum nanopillars and iridium oxide nanotubes. After attempted electroporation, the advantage of the nanotube geometry was demonstrated reaching 15mV amplitude against the 10mV of more traditional nanopillars.

Another approach to the use of the three dimensional vertical micro- and nanostructures included the utilisation of lasers to induce plasmonic electron movement at the probes surface. In 2017 at the IIT, it was demonstrated the possibility to use the surface plasmons to obtain the, so called, opto-poration and continuously record both extracellular and intracellular like activity of the cell [65]. The opto-poration happens only at the tip of the gold coated nanopillar and it allows to obtain intracellular reading of specific subcellular location (figure 1.13a). Spontaneous recorded activity of rat hippocampal primary neurons has been shown with an amplitude around seven hundred millivolts, once the opto-poration protocol was used on the cells an increase in recorded amplitude up to 1.5mV was achieved.

Still in 2017 from Dayeh's laboratory excellent results in terms of recorded am-

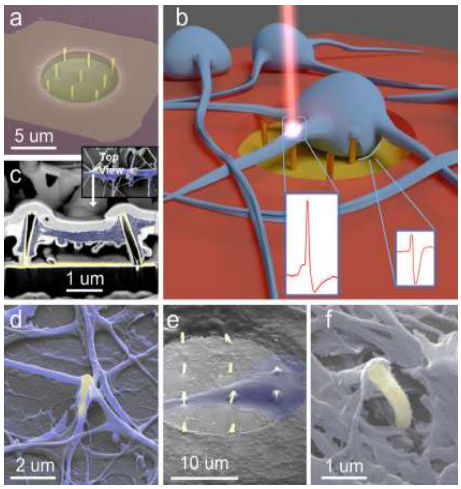

(a) Plasmonic nanolectrodes.

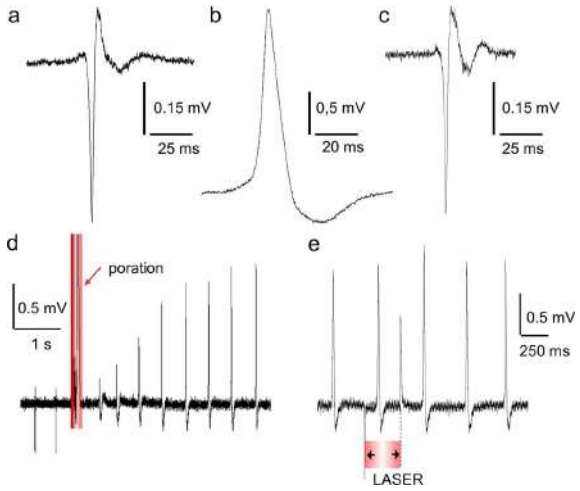

(b) Plasmonic nanoelectrodes recordings.

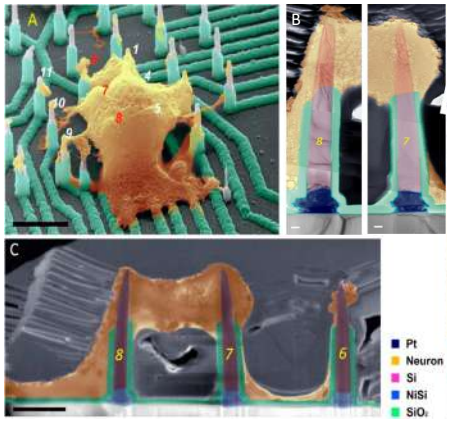

(c) High density nanowires.

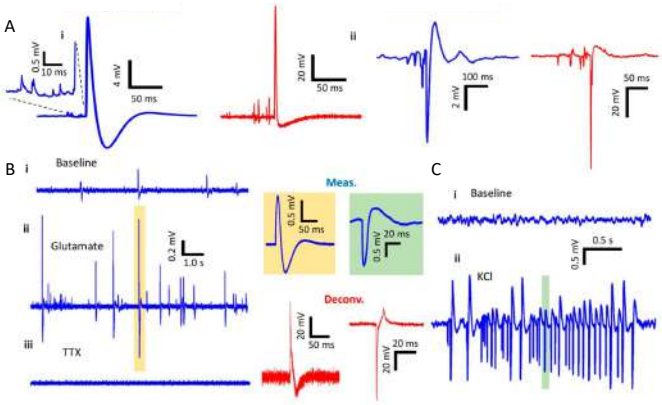

(d) High density nanowires recordings.

Figure 1.13: a. Schematic illustration of the plasmonic opto-poration platform integrated with a hippocampal neural culture-system [65]. b. Extracellular and intracellular-like firing activity recordings of HL-1 cells before and after plasmonic opto-poration. c. Images from a fixed cell culture on the VNEA platform [66]. [Scale bars are 4μm for (A), 200nm for (B) and 2μm for (C)] d. Measurements of the electro-neural system on mouse hippocampal neurons.

plitude and resolution were obtained with high density nanowire arrays [66]. To obtain intracellular like recording they opted for a very high aspect ratio of the probes that pinned the cells above the planar region of the platform, therefore it could compromise the formation of a mature neuronal network (figure 1.13c). The very high nanowires were used to impale mouse and rat hippocampal primary neurons and (hiPSC)-derived neurons, these devices showed impressive high amplitude already with spontaneous activity thanks to their mechanical interaction with the cells, several millivolts of amplitudes were achieved as an average.

A summary of the state-of-the-art devices is done in the table1.1. As it can be noticed, few devices can be compatible with a large-scale production process, this is a limitation in terms of comparison with more standard commercial devices and for an eventual foreseen production. As cells, primary rat neurons were mainly used

but on a large variety of electrodes structuration type, therefore a large spectrum of different results have been obtained.

1.4.2 Previous accomplishments of our team

This thesis work is the consequent follow-up of a previous thesis work done by Adrien Casanova [67]. Our group already managed to obtain a platform based on nanowires for the cellular interfacing, recordings of neuronal electrical activity were demonstrated with the vertical nanoprobes and horizontal finFETs devices.

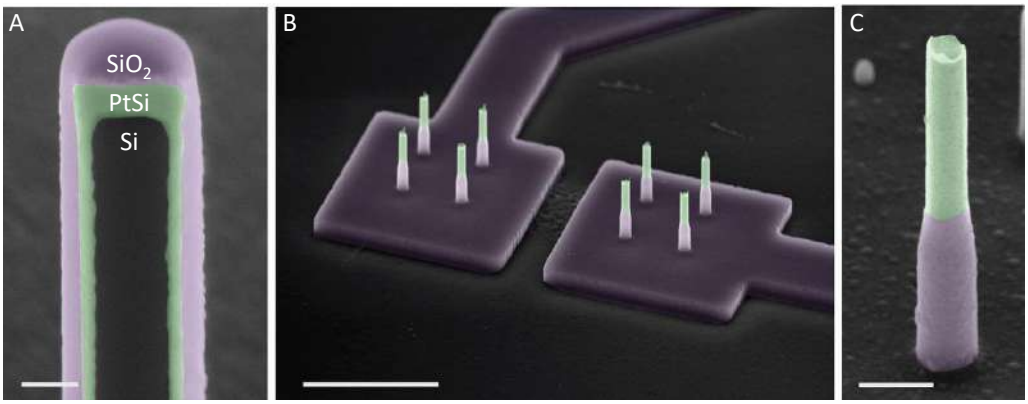

(a) Vertical nanowire probes.

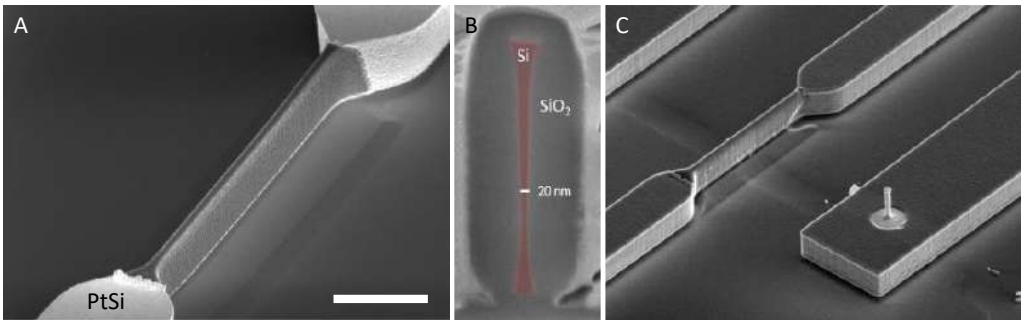

(b) FinFET active device.

Figure 1.14: a. Vertical nanowire probes [55]. (A) FIB colourized cross-section of a nanowire. (B) Colourized SEM image of two electrodes with four nanowires each. (C) Zoom on a single colourized core-shell type device. [Scale bars are, 200nm for (A), 5μm for (B) and 500nm for (C).] b. FinFET active device [68]. (A) SEM image of a single transistor with source and drain contacts in PtSi. (B) FIB colourized cross-section of the transistor channel. (C) Co-integration of active and passive devices on the same platform. [Scale bar for (A) is 2μm]

The first generation of the devices were obtained with a CMOS compatible process, using large scale compatible processes. The electrodes active surface material chosen was platinum silicide (PtSi), because of its biocompatibility, the metal behaviour in terms of conductivity and its possibility to be easily fabricated. Each electrode had four $1,5\mu$m nanowires in size and 300nm in diameter with a pitch of 2μm. A core-shell type device was built to guarantee the probes mechanical stabil-

ity, the exposed tip is therefore PtSi and the insulation layer was made of deposited silicon dioxide. Moreover, our team investigated the possibility to co-integrate passive and active devices on the same platform [68]. A series of finFETs devices were fabricated, in parallel to the passive nanoprobes, with the idea to verify the performances of both device types. A difference in signal-to-noise ratio was demonstrated, respectively a factor 40 for the passive nanoprobes and 8 for the active finFETs, showing that thanks to the major interaction with the cells, the 3D structured passive electrodes have better resolution.

We already showed the possibility of the devices to record spontaneous electrical activity from a culture of primary rat cortical neurons with very good resolution. Moreover, we tested some basic chemical protocols to either silence or activate the cells activity. Silencing was done with a cocktail of drugs (TTX, APV and CNQX). The chemical stimulation with potassium chloride (KCl) being generally used to emulate epilepsy, or using bicuculline and localized one with electrical impulses, all with success [68, 55].

The previous work on this project also includes the development of a surface functionalization based on perfluorodecyltrichlorosilane (FDTS). This functionalization is very stable and could be easily obtained with a final photolithography process. It created hydrophobic zones of the surface and allows to guide the cell growth on planar surfaces. Later, a different solution to control cell axogenesis that we recently investigated is described together with its results. Also, a first generation of the recording setup were built with a simple electronic card and a software to control it. At the time, we had the possibility to address only three electrodes at the same time and the software was still quite limited. This first generation was especially used to verify the electrical noise and the possibility of this approach. In this manuscript the evolution of the recording setup is going to be described.

1.5 Thesis work objectives

As presented in this first chapter, the brain is an extremely complex organ and the knowledge of its **basic mechanisms** is far from acquired. The study of its **basic building blocks**, the neurons, has been thoroughly addressed with many different approaches since electrophysiology beginning in the 18^{th} century to nowadays. The world population is growing older and because of that **neurodegenerative diseases** are most relevant than ever, therefore a major effort in scientific research must be devoted to neurosciences and electrophysiology.

Knowing the big achievement of the scientific community until now and the existing developed devices, our group wanted to bring its contribution to increase the quality of scientific means and open the possibility to new type of electrophysiological investigations. To this aim, a bio platform based on nanowires for the neuronal interfacing at the single cell level has been designed with the intention to co-integrate on the same platform the possibility to record the electrical activity of a neuronal network with high resolution and to measure locally its chemical environment variations. This work is divided in three major parts.

Performance and multi-sensing possibility

The fabrication of an NEA device, by means of **large-scale** compatible processes is described. The co-integration of passive devices (the vertical nanoprobes) and active devices (the FinFETs) is explained, which gives **multi-sensing** capabilities to the platform. The passive devices allow to record the neuronal **electrical activity** with very high resolution thanks to the quality of the nano engineered surface and its very good mechanical interaction with the cell membrane. The active devices are used to monitor the **pH variation** in a cell environment, this allows us to detect small variations in the ion concentration of the media. The chip packaging quality is verified and the printed circuit board (PCB) designed to be compatible with currently available commercial systems.

Subcellular interfacing and axogenesis

The possibility to interface cells at **subcellular** level is investigated and two main technological solutions for the **axogenesis** are described. Both methods are based on the device's surface structuration with **microchannels** guiding the neuritic extensions along electrodes array and determining the connection of the neuronal network. The two possibilities are: a SU-8 structuration is obtained with a photolithography step which guarantees the perfect alignment of the microchannels system to the platform; a PDMS microchannel system is obtained with a resist mould, allowing

the production and study of different types of geometries and their use on different substrates.

Theoretical modelling and biological question

In order to deepen the understanding of the biological interface, an equivalent electrical model is proposed and studied for the device characterization and as well as for the cellular membrane. The recording setup is presented, together with its evolution, and its effect on the measures is studied to avoid misinterpretation of the recorded signals. Having the possibility to multiplex the recordings up to 16 electrodes, the data analysis can be expanded, statistics and trends can be calculated. Therefore, a MATLAB script is used to do an offline analysis of the data, filtering and averaging are implemented and a script for spike detect and signal reconstruction are tested. Finally, studies on biologically relevant cell manipulation are presented. Effects of pH variations on the cell culture are used to validate the platform. The Amyloid Beta Peptide is used as a model for Alzheimer's disease, its effect on the cell electrical activity is presented. The same study is also conducted using neurons infected by Borna disease virus type-1 (BoDV-1).

Chapter conclusion

In this introduction to the thesis work, the historical evolution of electrophysiology was narrated up to modern electrophysiology research. The electrogenic cell mechanism to send and receive electrical signals were described in detail.

The *in-vivo* and *in-vitro* technologies for neuronal electrical recording are presented. Moreover, the introduction of active devices measurement and the numerous co-integration examples of this devices with more classical passive electrode is described. The state-of-the-art devices published by several other research groups are presented and their performances is discussed.

Finally, the already achieved accomplishments from a previous PhD student work on the bio platform are described and the objectives of this thesis as presented as divided in three main areas: performance and multisensing possibility of the bio platform; subcellular interfacing and axogenesis studies, theoretical modelling and biological question investigated.

Device	Description	Fabrication	Cells	Permformances	Reference
	Gold mushroom-shaped electrodes	Conventional lithography	Rat hippocampal primary neurons, *Aplysia* neurons and glia cells	• Spontaneous from $0.3mVto5mV$	[56, 59, 60]
	Gold mushroom-shaped electrodes	Electron-beam lithography	HL-1 cardyomiocites	• Spontaneous around $0.1mV$	[58, 57]
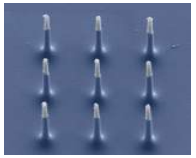	Silicon nanowires with metal tip	Electron-beam lithography	Rat cortical primary neurons and rat neonatal ventricular cardiomyocites	• Spontaneous around $1mV$ • Stimulated from $4mVupto15mV$	[61, 63]
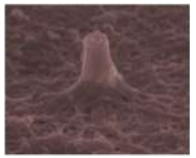	Platinum nanopillars and IrOx nanotubes	FIB assisted deposition and electron-beam lithography	HL-1 and primary rat cardyomiocites	• Spontaneous around $0.1mV$ • Stimulated from $4.6mVupto15mV$	[64, 62]
	Planar MEA with gold nanocylinders	FIB milling and patterning	Rat hippocampal primary neurons and HL-1 cardiac cells	• Spontaneous around $0.7mV$ • Stimulated around $1.4mV$	[65]
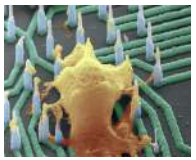	Doped silicon nanowires	Electron-beam lithography	Mouse and rat hippocampal primary and (hiPSC)-derived neurons	• Spontaneous around $6.3mV$	[66]
	Doped silicon and PtSi core-shell nanowires	Conventional photolithography (i-line stepper)	Rat hippocampal primary neurons	• Spontaneous around $0.1mV$	[68, 55]

Table 1.1: Summary of the presented state-of-the-art devices with focus on the technology and use.

Chapter 2

Towards multi-sensing platform: device fabrication and characterization

The micro fabrication of a bio platform is composed by series of steps than can be very critical or of complicated execution. Here, the large-scale compatible processes that we employed are described, with a focus on the most relevant ones. Moreover, a study on the packaging of these devices has been done, the flip chip technological solution is compared to the screen printing with soldering paste. The passive electrode fabrication and characterization, with the extraction of its parameters thanks to an equivalent circuit model are explained. We want also to open the possibility to measure multiple parameters at the same time, therefore our platform co-integrates passive and active devices. In this section, the main steps of fabrication and co-integration of these devices is explained, then, their functioning and performance are shown.

2.1 Fabrication of an NEA chip

Obtaining a good cell/electrode interface is key to have optimal performance when recording the cells electrical activity. The electrode dimensions necessary to record signals from a single cell or axon, at the subcellular level, induce a high surface impedance. In order to avoid the drawback of a high surface impedance, a structuration of the electrodes geometry has proven to be a great solution, as explained in the previous chapter. The 3D geometry gives the electrodes much greater active surface and increases the interaction with the cell for better recording performance.

2.1.1 Large-scale fabrication of nano electrode arrays

In this section, the clean room micro fabrication process is going to be explained, in particular, the most relevant steps are going to be detailed and the changes leading to improvement of previous generations Nano Electrode Arrays (NEA) bio platform are shown. The reasons for any particular choice are going to be discussed. The process has been vastly developed by the already cited previous PhD student and partially explained in related scientific publications [67, 68, 55].

The first step to the realization of a bio platform is the design of photolithography masks. Besides the pure geometrical perspective, these masks have to take into account other important aspects of the micro fabrication process, as for example the resist polarity, or the machine that is going to be used for any particular step. It is fundamental to know which materials are exposed at any point in time, a misconception in the photolithography result may end with an unwanted chemical reaction (for example piranha solution with aluminium). Differences in the mask design as well as in the machine photolithography technology must be forecast and combined.

A part of this project was to adapt masks for several process steps that were designed for a stepper (short for step-and-repeat) machine to a more classical semi-automatic mask aligner. The two machines in particular are: Canon FPA 3000$i4$ projection stepper from 1995, at the LAAS since 2009, that uses a 365nm UV light source (i-line) and can work with up to 6 inches wafers; MA6 gen4 SUSS MicroTec mask aligner, at the LAAS since 2018, that can work with up to 6 inches wafers. These technological solutions are preferred to electron-beam processing to guarantee cost-efficient and a large-scale fabrication process [69, 70].

(a) Canon FPA 3000$i4$.

(b) MA6 gen4 SUSS MicroTec.

Figure 2.1: a. Stepper machine, used for the most critical process steps capable of 400nm resolution and extremely precise alignment. b. Mask aligner for classical photolithography process. Images taken from MyFabLIMS.

The stepper is used for the first two photolithography steps because of its very

high resolution and precise alignment. This machine can reach up to 400nm resolution thanks to its projection lens that reduce of five times the mask design (2.2b). A specific recipe for each photolithography step can be created, including the control of the UV exposure dose and the focus of the light beam and several other parameters. These parameters will be more detailed in a later section of the manuscript for the photolithography of SU-8 resist in order to obtain microfluidics channels. Critical dimensions are bounded by the Rayleigh scattering law, for this stepper in particular the minimal dimension (d_{min}) is given by: $d_{min} = k\frac{\lambda}{NA}$, where $k = 0.7 - 0.8$, λ is the used wavelength and NA is the numerical aperture (between 0.45 and 0.63). The alignment has a precision in the order of $100nm$. The first two steps of the process are done thanks to this machine. The mask design is transferred 68 times on a 4 inches silicon on insulator wafer (SOI) creating the structure for the bio platform.

It is therefore clear that our approach to the structuration of the device is a top-down one (2.2a). It means that, thanks to photolithography, the desired design is transferred on the SOI wafer with specific resists and then etched with the use of plasma reactive ions. This approach is limited only by the resolution of the photolithography machines and guarantees excellent control and reproducibility. The most critical steps for the correct fabrication of the bio platform include, at first, the realization of the vertical nanopillars for the electrodes structuration (2.2b,2.2c) and at second the etch of the finFETs together with pads and accessing lines (2.2d,2.2e).

Another important technique to describe of these first two steps is the plasma etch. In order to obtain a high aspect ratio etch, a machine capable of performing Deep Reactive Ion Etch (DRIE) was chosen, a technique largely used in micro fabrication [71, 72, 73, 74], the machine in particular is the Alcatel AMS 4200. The possibility to control the gas mix and flow, the pressure and the power inside the reactor, the chuck temperature and the etch time allowed us to create a specific recipe obtaining anisotropic etch, with vertical profiles, and with a high selectivity between silicon and resist. The structured nanopillars have a height of 3.5μm and a diameter of $450nm$.

The fabrication steps that do not need a very high level of resolution have been adapted, from the previous process design, for the transfer from the stepper to the mask aligner. This machine can reach up to 1μm of resolution and includes the possibility to use automatic alignment mode with dedicated alignment marks. Switching to a more classical photolithography process resulted in saving both time and money on the project, without compromising any technological output. The mask design has been realized in order to maintain a perfect alignment with the stepper grid reticule. The MA6 allows to expose the resist using the so called "proximity mode", which position the mask at a chosen distance from the substrate. With this mode, it is possible to avoid possible damages that may occur, with the

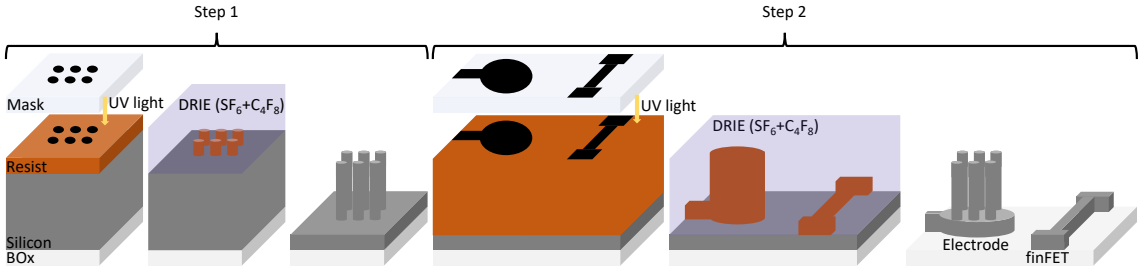

(a) Schematic representation of the first two micro fabrication steps.

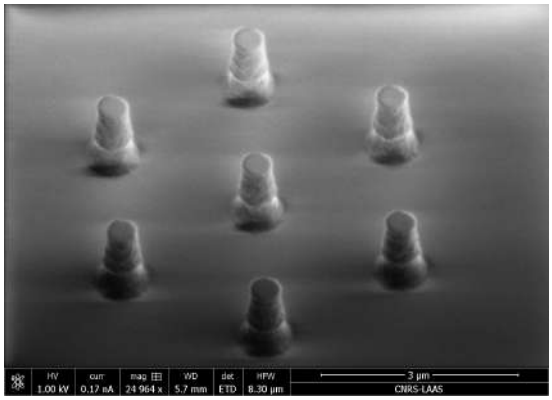

(b) Resist nano dots.

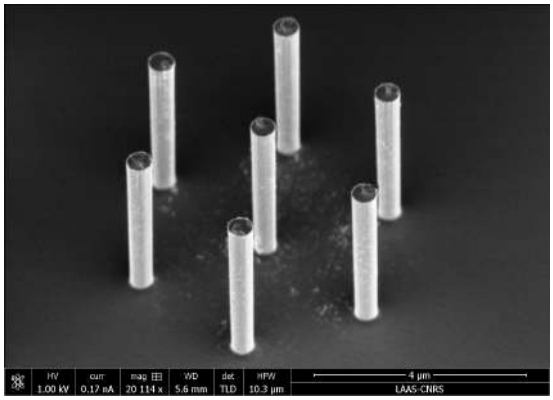

(c) Nanopillars.

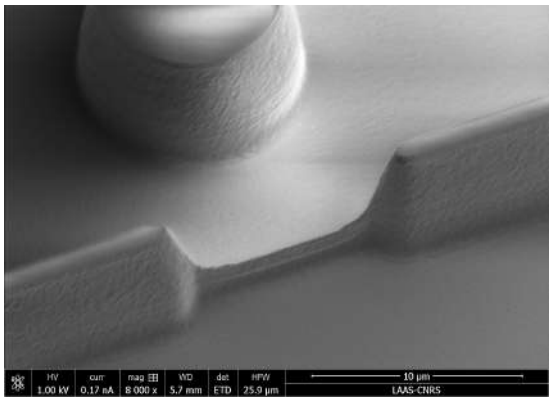

(d) FET Structuration.

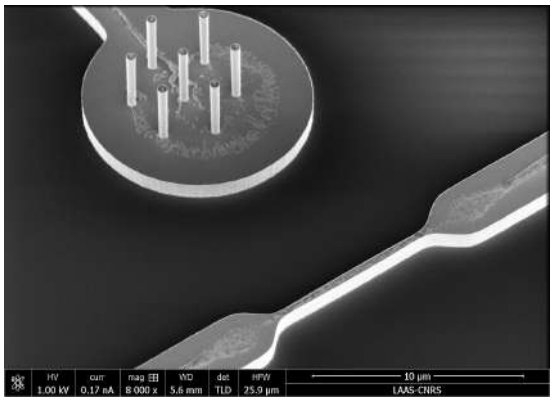

(e) FinFET.

Figure 2.2: a. Description of the first two micro fabrication steps. b. Resist nano dots realization with stepper photolithography machine. c. Nanopillars resulting after plasma etch. d. Second level photolithography transferring finFETs design and access lines onto the substrate. e. Co-integrated structures result on the bio platform after. Every resist residue was carefully removed before the next steps. [Scale bars inside the SEM images]

contact between mask and substrate, to the vertical structures already realized, but losing in maximal resolution. Moreover, these machines allows for the processing of cleaved silicon pieces, down to the single chip processing, very useful for post process testing.

To have a functional device and the completion of the bio platform several other steps are needed. Described not in a specific order:

Sacrificial oxide The nanopillars diameter can be further tuned with a thermal oxidation of the substrate and a wet etch (2.5a) with hydrofluoric acid (HF). It

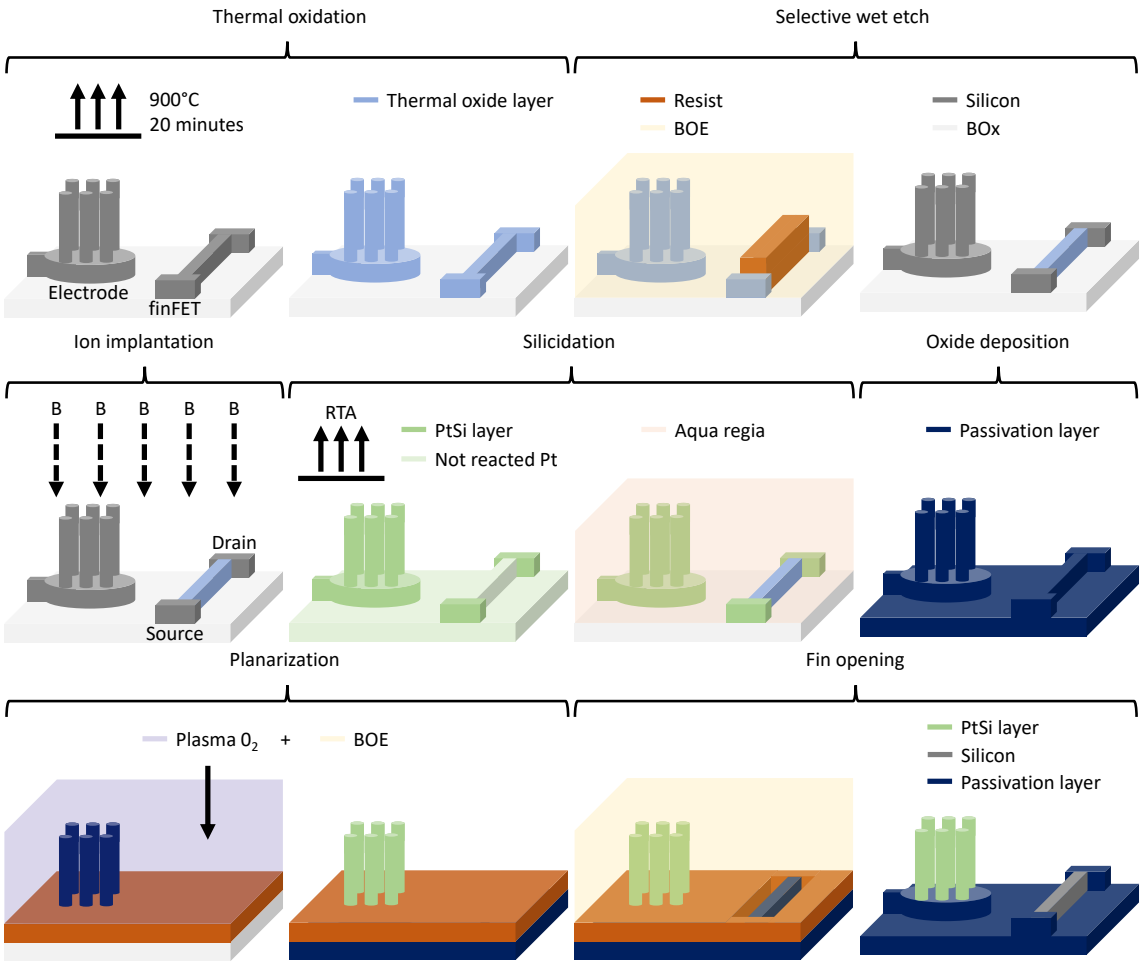

Figure 2.3: Schematic representation of the most important micro fabrication steps needed to complete the bio platform.

allows to reduce the nanopillar diameter, controlling the amount of consumed silicon during the formation of the oxide layer.

Semiconductor doping The substrate is doped with boron in order to obtain source and drain contacts of the finFETs and to reduce the resistivity of the silicon probes [75, 76]. Specific attention must be dedicated to the protection of the transistor channel to avoid the doping of this region.

Metal deposition The biocompatibility and high resolution of the probes are guaranteed by the exterior platinum silicide (PtSi) layer [77, 78, 79], therefore a deposition of $80nm$ platinum by metal evaporation is necessary (2.4c). Also $500nm$ aluminium are deposited, almost at the end of the process, to ensure feasible metal contacts for the packaging.

Rapid thermal processing The PtSi layer is created with a two phases thermal reaction between the silicon and the deposited platinum layer (2.4d 2.5b 2.6a). A rapid annealing process assures the silicide formation [80, 81, 82, 83, 84].

Oxide deposition To ensure the insulation of each conductive line from the saline media a double layer coating is used. A first deposition of $50nm$ aluminium oxide (alumina or Al_2O_3) by Atomic Layer Deposition (ALD) and a sequent deposition of $200nm$ SiO_2 by Plasma Enhanced Chemical Vapour Deposition (PECVD) are performed.

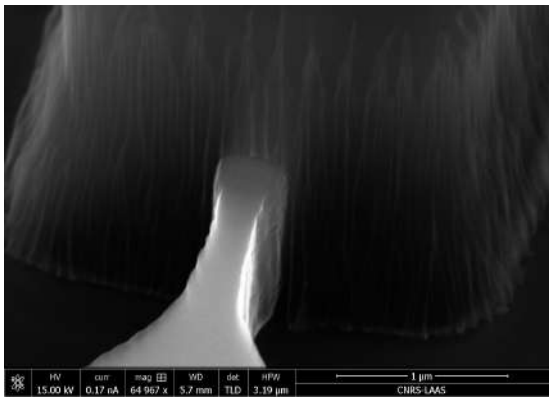

(a) Fin resist mask.

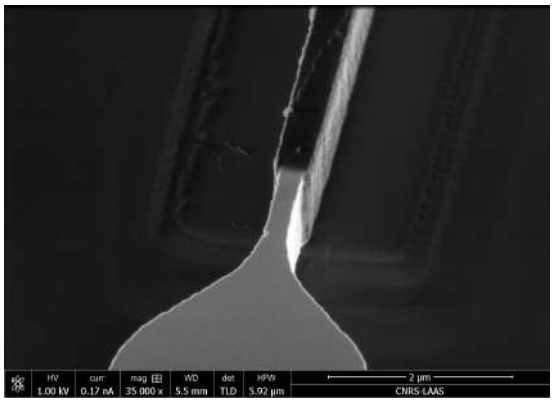

(b) Fin thermal oxide.

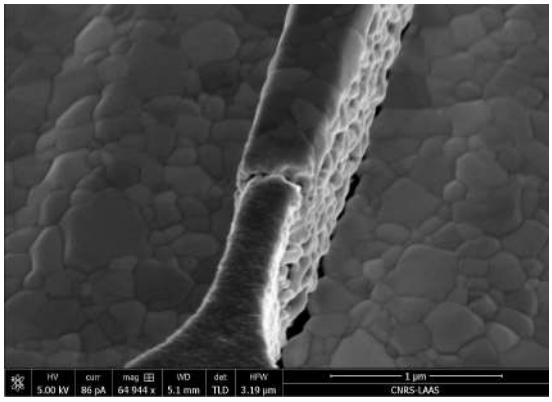

(c) Annealed platinum.

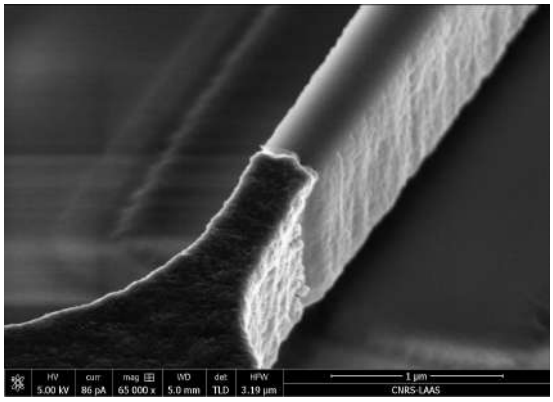

(d) PtSi and thermal oxide.

Figure 2.4: a. SEM image of the resist mask protecting the fin oxide from wet etching. b. SEM image of the finFET structure having thermal oxide as insulating layer. c. SEM image of the platinum deposition on the entire surface once the RTA process is complete. The difference between the not reacted platinum and the formed PtSi layer is evident. d. SEM image of the resulting fin structure once the platinum residues are etched. The external layer is PtSi for the source and drain contacts but not on the fin and substrate because of the oxide presence. [Scale bars inside the SEM images]

In between these processes several photolithography steps are necessary to define the design of each material layer (2.4a). Wet chemical etches are performed to remove unwanted metals or oxides from specific zones (2.6b). Aqua regia, aluminium etch back solution and Buffered oxide etch (BOE) are used at different points in time during the micro fabrication. A special attention is needed once the plasma etch reaches the buried oxide (BOx) of the SOI wafer, each use of HF must be carefully evaluated. The most important fabrication steps are schematically described in the image 2.3.

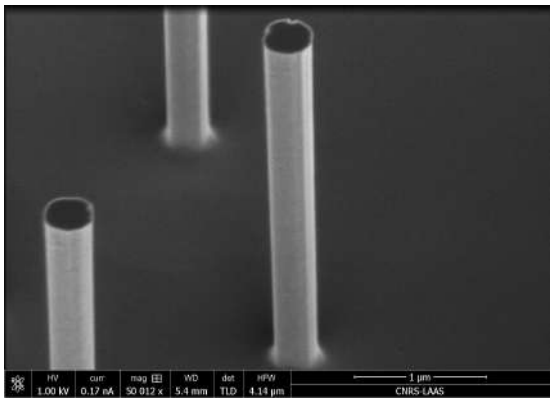

(a) Silicon nano pillars.

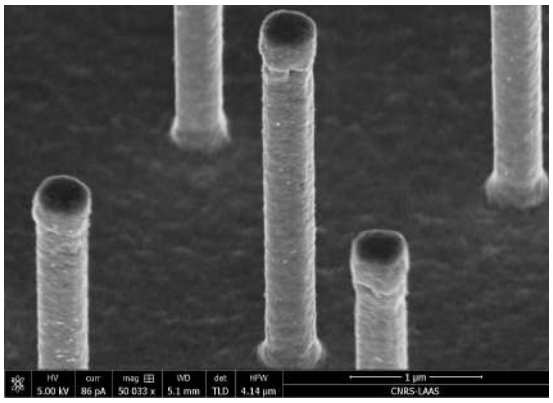

(b) PtSi nano pillars.

Figure 2.5: a. SEM image of the nano pillars after diameter the sacrificial thermal oxide wet etch. b. SEM image of the nano pillars once the PtSi silicide layer is formed on the surface. A very uniform surface topology can be observed. [Scale bars inside the SEM images]

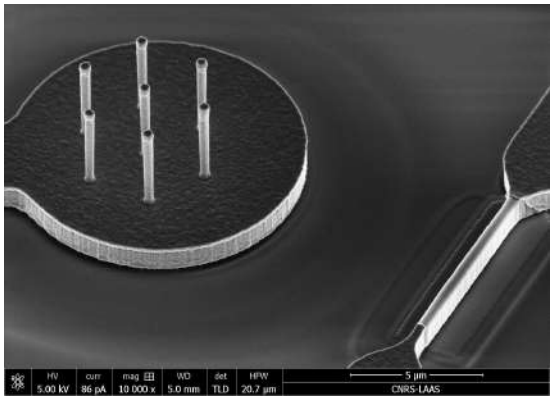

(a) Active and passive electrode.

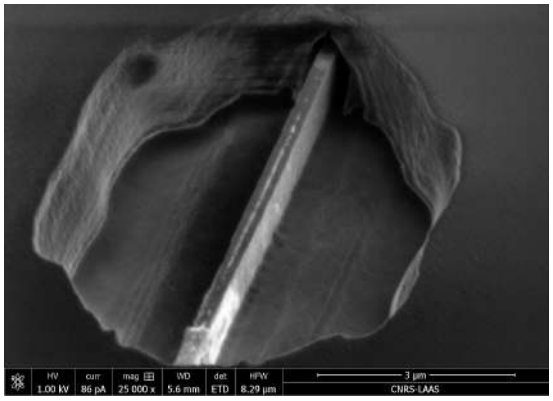

(b) Fin oxide etching.

Figure 2.6: a. SEM image of the active and passive electrode couple after the PTSi silicide formation. b. SEM image of the opening in the resist aligned on the transistor fin once the wet oxide etch is completed. From this step the transistor gate insulating layer can be changed. [Scale bars inside the SEM images]

The resulting electrodes array (2.7a) consists of 48 passive electrodes, composed of vertical nanopillars, and 8 active electrodes, the FinFETs, creating the co-integration between passive and active devices (2.7b). On each substrate, a total of 68 chips were fabricated and usually a good rate around 75% of chips were potentially fully functional if no major problem occurred during any step.

2.1.2 Co-integration of active devices: sensing interface of the FinFETs

The co-integration of two or more devices to measure different variables of a *in-vitro* cellular culture for the published works has already been described in the subsection

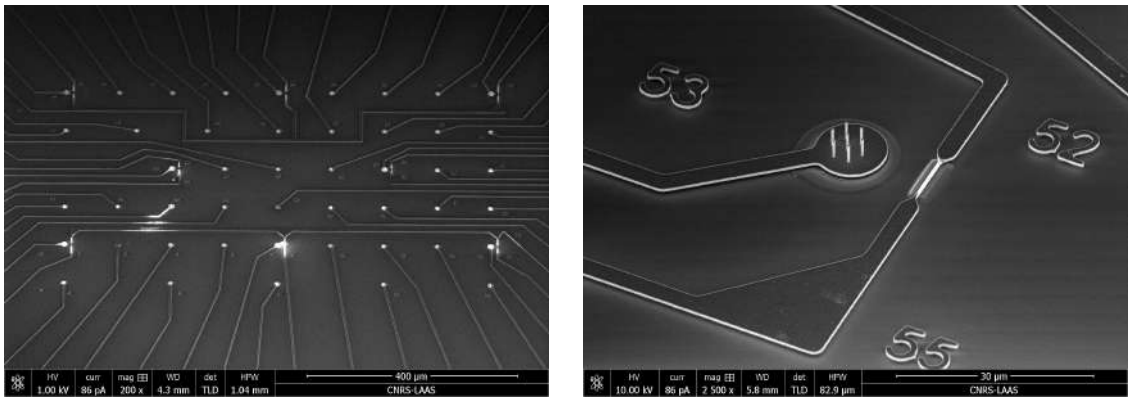

(a) Electrodes array. (b) Example of device co-integration.

Figure 2.7: a. SEM image of the electrodes array resulting at the end of the micro fabrication process. b. SEM image of one of the eight couples of co-integrated passive and active devices on each bio platform. [Scale bars inside the SEM images]

1.3.3. It is demonstrated the possibility to record multiple parameters at the same time on a global scale on the culture. Our project aims to bring this possibility also down at the cellular and subcellular level.

In order to obtain both nanoprobes and finFETs perfectly working, the process steps must be each individually characterize with SEM observations. It is fundamental to assure the protection of the nanopillars at the time of the second dry etching, as well as it is critical to leave a protection layer on the transistor channels to avoid undesired doping. The source and drain contacts are formed with this boron doping step, and they have an external layer of PtSi as the access lines and the nano pillars. The transistor channels are again subject to processing at the very last step of the micro fabrication, here the oxide protective layer is carefully removed using BOE after a photolithography at the MA6. This step allows us to modify the gate sensitive oxide layer, choosing the most convenient material for the application.

Two choices were made in order to try to find the best sensitivity of the finFETs: (i) to leave the gate contact open, and therefore only few nanometres of native silicon oxide layer would be in contact with the saline media [85, 86]; (ii) to deposit $5nm$ layer of Al_2O_3, a material already known for its good behaviour in saline media and often used as sensitive layer for Ion Sensitive Field Effect Transistors (ISFET) [87, 88].

FIB characterization of the transistor channels allowed to observe that on some chips the oxide underlying the transistor fin was over etched, creating a floating fin, detached from the buried oxide of the SOI. This brought to a difference in the characterization of the devices modifying the effect of the bulk polarization of the chip on the transistor currents. The characterization of the active devices is shown in a next section of the manuscript, discussing the variation due to the gate oxide and bulk polarization.

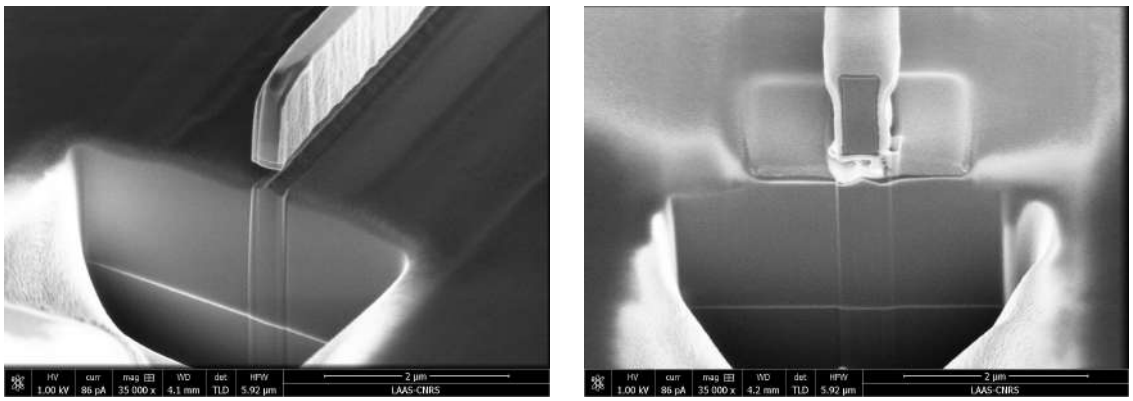

(a) FIB slice side view. (b) FIB slice front view.

Figure 2.8: a. SEM image of a transistor fin FIB slice. It can be observed that the oxide underlying the fin has been completely etched. b. SEM image of a transistor fin FIB slice after the deposition of carbon and platinum layer for a better contrast.

2.1.3 Packaging

At the end of the micro fabrication process, the remaining steps to perform in the clean room are the manual cleavage of each chip chosen to be used and their packaging. After a careful SEM observation of the 68 chips, the ideal ones, without any major defect, are selected. The wafer cleavage was performed manually, this choice has been made to avoid any possible damage to the nano probes. An automatic wafer dicing made by a machine includes a mechanical saw and a constant flow of water on the substrate. This flow could easily destroy the electrodes if the liquid exercise too much force on the nano probes. Therefore, the cleavage is manually executed taking advantage of the crystalline directions of the silicon (100) substrate that, once carefully scraped with a dedicated instrument, determine the direction of the cut. With this method, single chips are obtained, ready for the packaging.

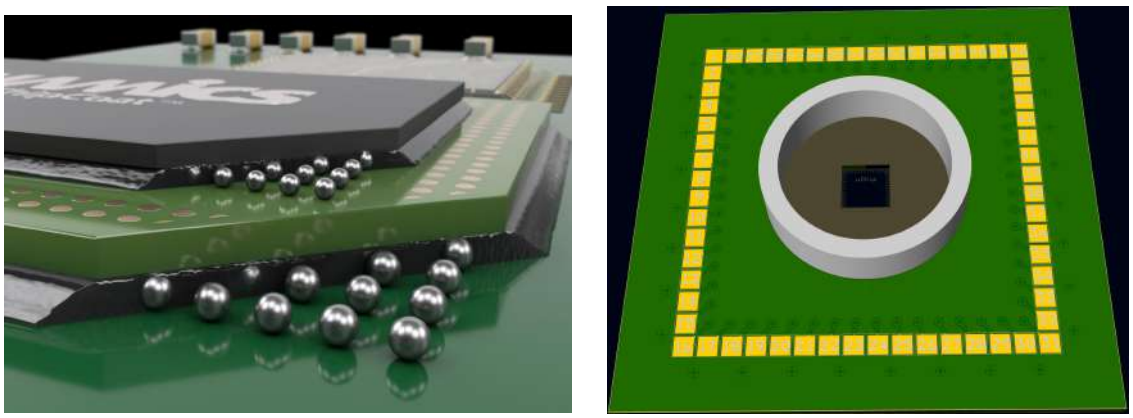

(a) Flip chip IC. (b) MCS board configuration.

Figure 2.9: a. Examples of a flip chipped IC on a board with metallic bumps and underfill. Image taken from NAMICS website. b. CAD image of our PCB design compatible with standard available recording platforms.

The method chosen for the chips packaging is the flip-chip. This technique is a standard procedure for Integrated Circuits (IC) chips or Microelectromechanical systems (MEMS) in order to connect them to an external circuitry [89, 90, 91]. For our platform, the connection is made to a Printed Circuit Board (PCB), designed at the LAAS in order to be compatible with the standard recording platforms available on the market. The flip chip is known to be a technique particularly sensitive to mechanical stress and planarity of the substrate, due to its extremely short contact distance, therefore it is not always the most advantageous one.

The flip chips includes few steps:

Gold bumps One gold bump needs to be manually made and positioned on the relative PCB pad. These pads are also made out of gold, so the soldering between the bumps and the pads is going to be optimal. The average dimension and shape of a gold bump is a $60 - 70\mu$m diameter sphere (figure 2.10a and 2.10c).

Alignment The alignment between PCB with gold bumps and each single chip is performed with a machine, the SET FC150 at the LAAS since 2001, with a very small alignment of $\pm 3\mu$m.

Soldering The same equipment performs the soldering step. As already said, the contact between gold bump and PCB pad is optimal. It is not the same for the contact between gold bump and the chip pads. Those pads are 200μm side squares made of aluminium, unfortunately this material is not easily soldered, therefore the electrical contact here is mostly a mechanical one. Alternatives have been explored and are going to be described in this section.

Epoxy glue The final step for the flip chip is the use of an underfill glue that can have various characteristics. For our application we choose an insulating epoxy glue that prevents short circuits between contacts and improves the mechanical stability of the connection. It is also certified to be biocompatible, in order to avoid any problems.

Two interns worked in our team for a few weeks to verify the flip chip procedure reliability for our platform. At first, the possible introduction of any type of defects that would drastically increase the electrode impedance has been studied. Then, the use of an alternative technique and material to the gold bumps have been explored. The study on the flip chip process reliability concluded that there was no major problem introduced by the flip chip. Testing the impedance at each step of the packaging showed that there was no leap in impedance value. Therefore, from the simple PCB and chip, separate, to the complete recording setup with liquid media, the impedance of the electrodes was always coherent. More details on the

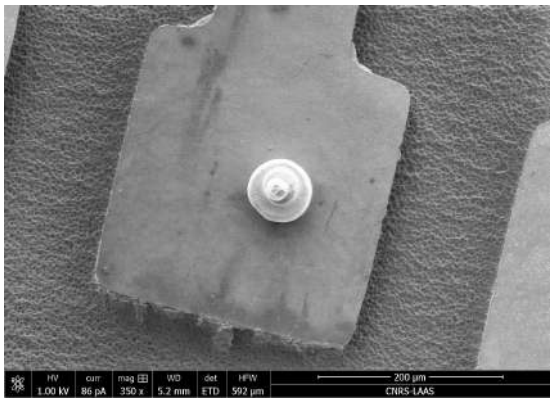

(a) Gold bump.

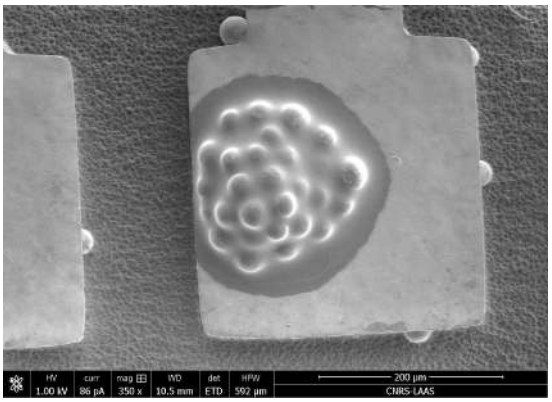

(b) Soldering paste.

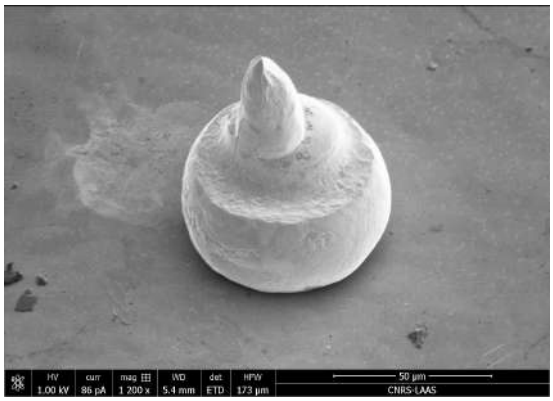

(c) Gold bump tilted.

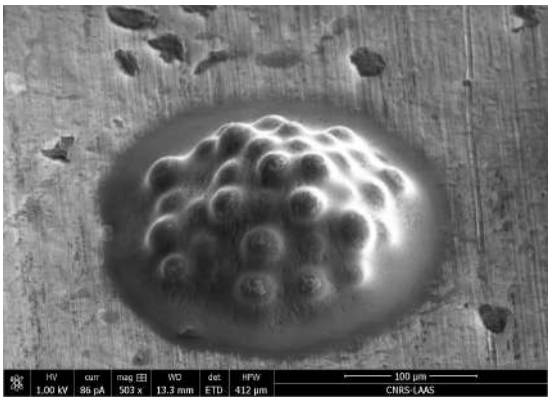

(d) Solder paste tilted.

Figure 2.10: a. SEM image of a manually deposited gold bump on a PCB gold pad. b. SEM image of screen-printed solder paste on a PCB gold pad. c. SEM image of a manually deposited gold bump tilted to see its typical profile. d. SEM image of solder paste on copper plate for annealing testing. [Scale bars inside the SEM images]

methodology used for the impedance characterization are further developed in this section. Because the flip chip is extremely sensitive to mechanical characteristics of the substrate, as previously said, some contacts happened to fail before the characterization. The broken contacts usually were adjacent between them, indicating that the mechanical failure could be linked to a defect in the planarity of the cleaved chip.

The alternatives to the gold bump explored were the solder paste (Chipquik SMDLTLFP60T4) and solder glue (Polytec EC 112-L). This was a choice based on the high economic cost, being packaging by far the most expensive step, and long time needed per flip chip if the gold bumps are used. Moreover, a less mechanical sensible method would guarantee lower contact failure rate. With the use of a metallic stencil for screen printing on PCB and a semi-automatic machine, the solder material can be reported with extremely good alignment and precise control of the thickness.

For our testing, we limited the process to a prototype like procedure. A stainless-

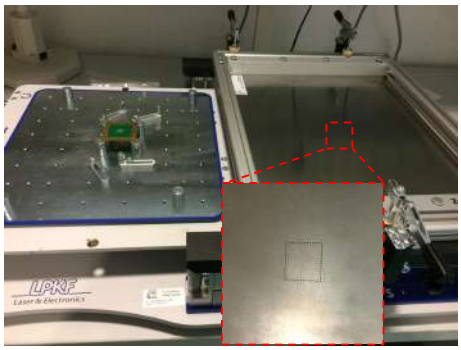

(a) Screen printing setup.

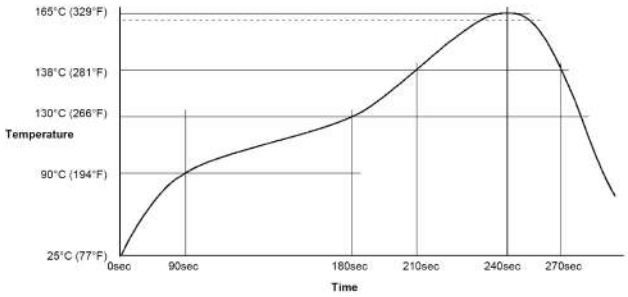

(b) Soldering paste annealing profile.

Figure 2.11: a. Photo of the screen-printing equipment with the stainless steel stencil positioned. Optical alignment was available with the help of a magnifying glass to correctly position the PCB underneath. b. Image of the annealing profile for the solder paste from its data sheet.

steel stencil was fabricated with an array of holes corresponding to the PCB pads. It was compatible with a manual equipment that allowed us to optically align the stencil and the PCB (2.11a). As it can be seen from the image 2.10b, the solder paste is composed by metallic micro spheres and a flux that acts as temporary adhesive. Moreover, it is obvious that the quantity of material is much higher with the solder paste, leading to a more even contact covering and less mechanical stress related failure. An annealing is necessary for the solder paste to melt the metal microspheres and remove the flux, the heating profile is usually available in the solder paste data sheet (2.11b). Once the solder paste is ready the flip chip procedure is exactly as the previously explained.

We decided to proceed with the solder paste being easier to use and because the glue needed to be prepared each time few minutes before use, being a two-component epoxy.

A study on the annealing profile was conducted on a copper substrate before the actual use on PCB to identify the perfect parameters for our equipments. Even if the data sheet suggested reaching a temperature of 165 °C, it was necessary to reach a higher temperature at 180 °C to obtain satisfying results (2.12b).

Once the correct annealing was obtained, we measured the series resistance introduced by the contact. In order to do it, a layer of $500nm$ aluminium was deposited on a simple silicon wafer, in order to simulate a standard contact on our chip. The wafer was then cleaved at the size of a regular chip, these chips were connected via flip chip to our PCBs, with gold bumps and with the solder paste to compare the contact quality. The measures were done with an oscilloscope, two micromechanical tips were used to connect the PCB pads and the aluminium layer. An equivalent circuit of the system includes three series resistances, R_{PCB} for the PCB resistance, R_{Alu} for the aluminium layer resistance and R_{Gb} for the gold bump or R_{Sp} for the

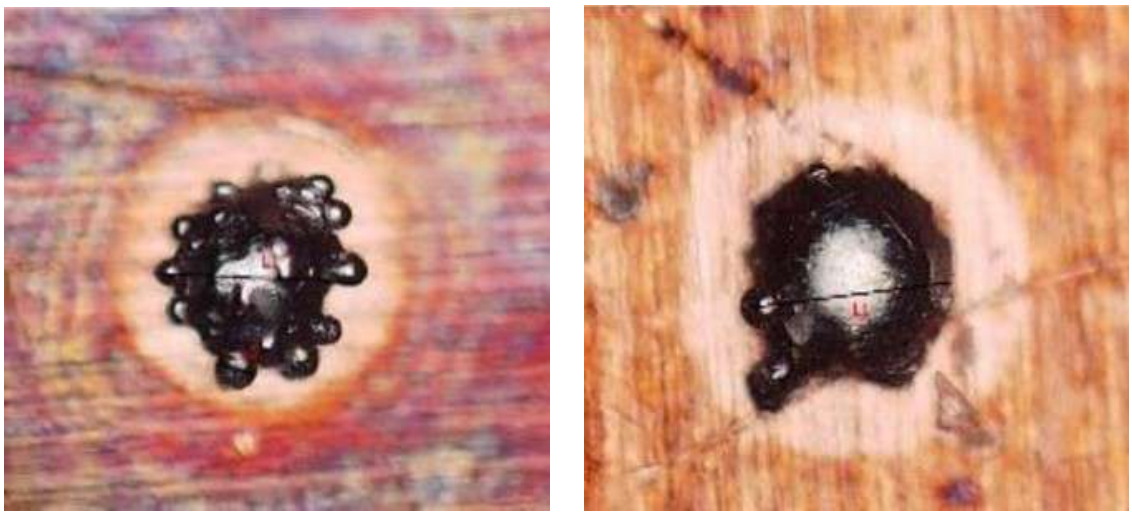

(a) Not ready solder paste. (b) Annealed solder paste.

Figure 2.12: a. Optical photo of the solder paste not correctly annealed. The microspheres profile is still clearly visible therefore the metal did not react completely b. Optical photo of the solder paste once the thermal reaction is completed and the flux is removed. The previous microspheres are almost non identifiable here.

solder paste resistances. The PCB and aluminium resistances are fixed, therefore the only difference in the measure must come from the contact resistance.

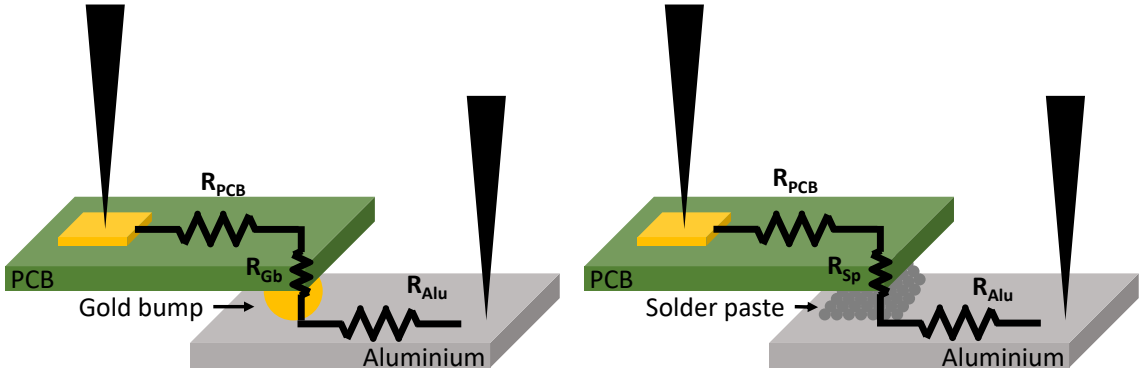

Figure 2.13: Schematic representation of the two packaging method and their characterization. Two micromechanical metal tips were positioned to measure the resistance of the system.

From our preliminary testing, there was a 0% contact failure rate with the solder paste against 10% of contact failure with the gold bump. It means that the solder paste is even more reliable of the gold bumps. From the resistance characterizations, the difference from a gold bump contact and a solder paste one are totally negligible, being around 100Ω, compared to the much greater order of magnitude of the electrode impedances.

From this study, it is possible to plan some changes in the packaging process of our platform. If further testing is going to be done, this could lead to an improvement

of the platform reliability. Moving the screen printing of solder paste to a semi-automatic machine capable of laser alignment, already present at the LAAS, with the possibility of preparing several PCBs at the same time, this step could become less time and cost consuming without losing any performance from the bio platform. A summary of the packaging study result can be found in the table 2.1.

Gold bump	Solder paste
• Very high cost	• Low material cost
• 70μm spheres	• 200μm deposition
• 10% failure rate	• 0% failure rate
• Very time demanding step	• Large scale compatible
• Very reproducible	• Very reproducible
• Very low ohmic resistance	• Negligible ohmic resistance

Table 2.1: Comparison between the two studied methods for chip packaging.

2.2 Electrical field potential

The recording of the activity of electrogenic cells is based on measures of changes in electrical field potentials. The exchange of ions through the cell membrane creates variation of electrochemical potential inside and outside the cell, details may be found in the section 1.2.2. Also, as already described in the section 1.4.1, the geometry of the electrodes and their structuration have been studied from different scientific teams. In this section, the physical principles behind the electrical field potential sensing with passive electrodes are explained together with a description of our particular technological application and the obtained performances on the bio platform.

2.2.1 Potential measurement theory

Measuring the potential of an electrolyte with a metal electrode has been studied for well over a century now. It is also a very important topic in scientific research regarding supercapacitors and batteries. The first model proposed for the metal-electrolyte interface is the Helmholtz model in 1879. This is also the simplest one where the spatial charge distribution is represented as a double layer of opposite charges facing at the interface of the electrode. Each ion in the electrolyte is balanced by an electron in the metal, and a compact monolayer of ions is formed on the surface of the electrode. The potential difference therefore is proportional to the one calculated on a capacitor $\phi_{metal} - \phi_{electrolyte} = Q/C$.

This model was developed considering thermal fluctuation, Boltzmann law for the energy distribution ($N_i(x) = N_i \exp^{-z_i e(\phi_x - \phi_{electrolyte})/kT}$), Poisson electrostatic law ($\Delta\phi_x = -\rho_x/\epsilon$) and diffuse ion distribution from Fick's first law (J=-D$\frac{d\Phi}{dx}$). With ions considered as point charges, this is known as the Gouy-Chapman model from 1913. This was combined with the Helmholtz model and, once added the finite size of each ion type and the solvated shell of the liquid media, it is known as the Stern model from 1924.

A last modification of this model was done by Grahame in 1947. He considered the possibility to have some adsorbed ions on the electrode surface capable of losing the solvation shell and penetrate the Stern layer. This model is divided in three specific layers: Inner Helmholtz plane (IHP), outer Helmholtz plane (OHP) and a diffusion layer. The electrical potential has a value in the metal bulk that is proportional to the ion charges at the interface between solid and liquid. A first drop of the electrical potential happens at the supposed position of the adsorbed ions ($x_1 = IHP$), a second one at the position of the solvated ions ($x_2 = OHP$). Then, the electrical potential gradually reaches a value fixed by the ion concentration in the liquid medium (2.14).

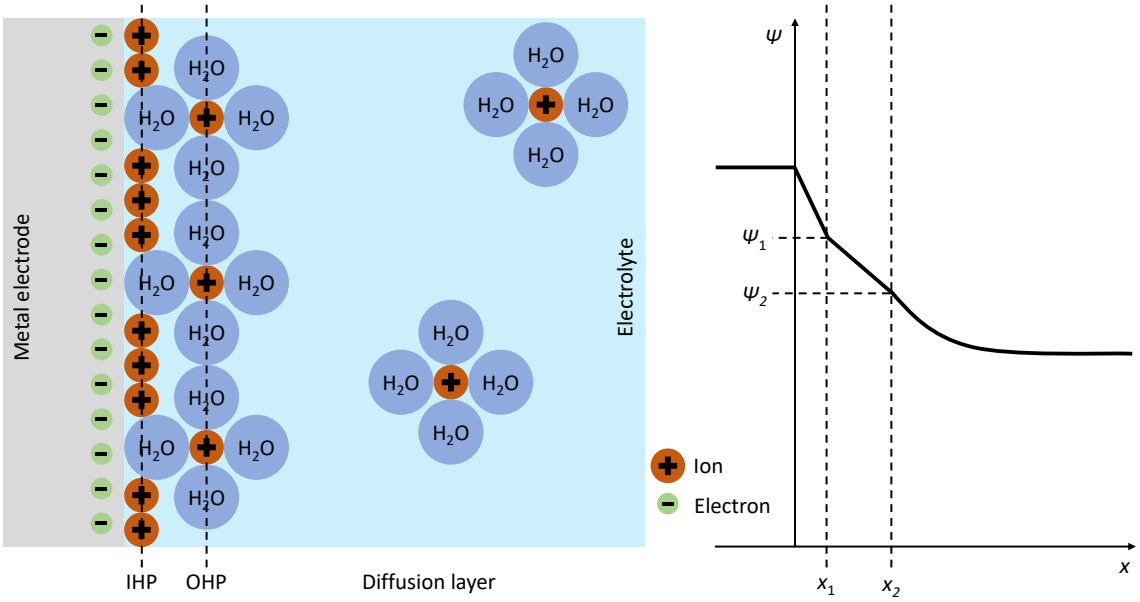

Figure 2.14: Schematic representation of the different layers of the Grahame model and profile of the corresponding electrical potential (Ψ). When $x = x_1$ Ψ_1 is the electrical potential of the IHP, when $x = x_2$ Ψ_1 is the electrical potential of OHP.

2.2.2 The passive nano probes

The main factor modifying electrical recordings are the interfaces between different layers, in our case the interface between PtSi and liquid media [92, 93]. A key point is the difference in mobility of the charge carriers: electrons in the solid silicide lattice and ions in a polar fluid, respectively being $10^3 cm^2/Vs$ and $10^{-3} cm^2/Vs$. The passive nano-probe structures are vertical nano pillars, as previously described, of 3.5μm height and 450nm diameter. Each electrode has three or seven nano pillars with a pitch of 2μm that were proven to be optimum for cell/electrode interaction from the previous studies on the project. The surface is made of platinum silicide (PtSi), giving metal like conductivity qualities to the layer, mechanical stability, being made from crystalline silicon, and a bio compatible interface. The only surface directly exposed to the electrolyte is the nano pillars surface, everything else is insulated by the double layer of deposited oxide. All the details are explained in the section 2.1.1. Whereas the liquid media is either classical phosphate-buffered saline (PBS) solution, for characterizations, or Neurobasal medium for the use with living cell.

All the eventual electrochemical processes take place at this interface, that from the Grahame's model, is represented as a double layer condenser constituted by two charged areas separated by a dielectric [94, 95]. The dielectric thickness corresponds to the ionic radius. To evaluate the total capacitance of the solid/electrolyte interface it is necessary to consider both layers of the capacitor: $C^{-1} = C_G^{-1} + C_H^{-1}$. The first one is the Gouy-Chapman capacitance, the one depending on the capacitance of the

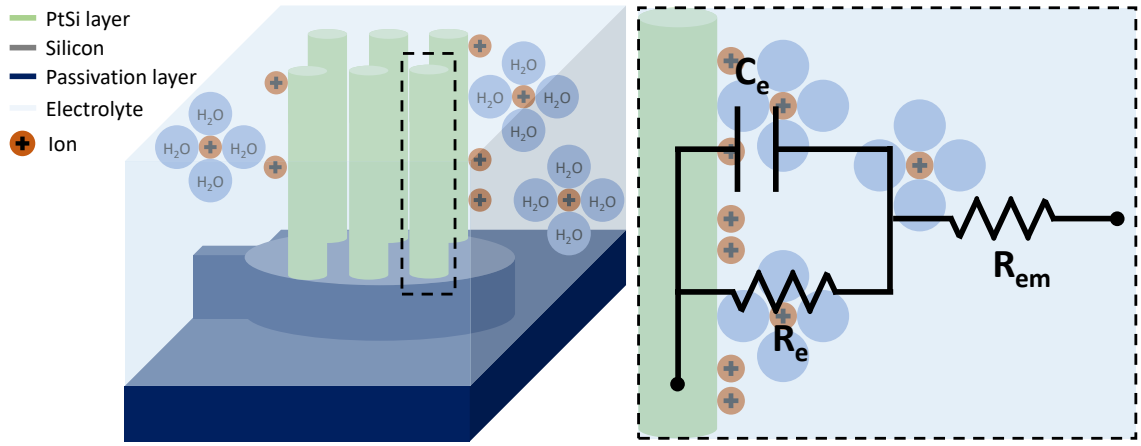

Figure 2.15: Schematic representation of the typical sensing mechanism of the passive electrodes. The PtSi nano pillars electrical potential in a ionic medium varies with the ion concentration. The equivalent circuit model on the right is the simplified Randles' circuit. C_e is the electrode capacity, R_e is the electrode resistance and R_{em} is the electrolyte resistance.

Outer Helmholtz Plane. The second one is the Helmholtz capacitance, that depends on the capacitance of the Inner Helmholtz Plane.

The usual electrode/electrolyte interface is described with an equivalent electrical model known as the Randles' model (2.15), consisting of an interface capacitance (C_e) shunted by a charge transfer resistance (R_l) in series with the medium resistance (R_{em}) [96]. The impedance expression here is composed of a real and imaginary part, depending on the resistive and capacitive elements, giving ohmic and faraidic current to the system. A simplified Randles' circuit is shown in the image 2.15. This model can be therefore applied to evaluate also all the possible source of current leakage. In particular on the bio platform, this refers to the insulating oxide layers present on the access lines that theoretically prevent any loss of signal, measurement away from the actual electrode or cross talk between conductive lines. The values for the two Randles' circuit in parallel must have very different values for each element due to the nature the materials (2.16a).

In order to evaluate the quality of the electrode/electrolyte interface, the Electrochemical Impedance Spectroscopy (EIS) technique was used. This measurement was done with a massive platinum counter electrode, in order to have a minimal difference in the working functions of the materials, and a negligible interface impedance. The liquid media used was a standard PBS solution, with a pH of 7.4 and a conductivity of $1.6 S/m$. The working electrode is considered, once at time, the electrodes on the bio platform. We chose to have two different electrode designs, with three and seven nano pillars, keeping the dimensions and pitch already described. From the EIS characterization of the bio platform, it was possible to distinguish the difference in PtSi surface exposed to the medium having different trends for the average values.

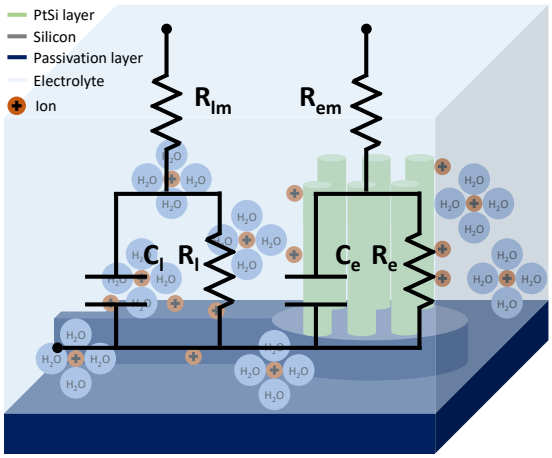

(a) Equivalent circuit of the bio platform.

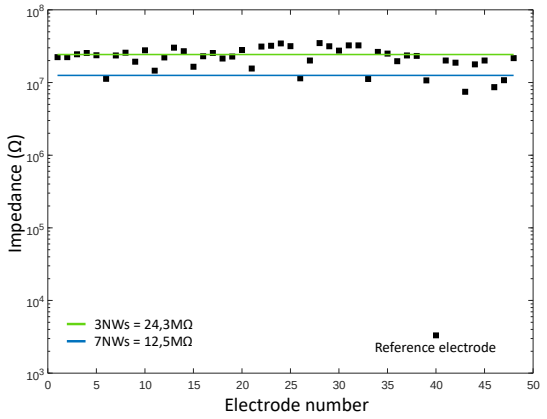

(b) Impedance values at 1kHz.

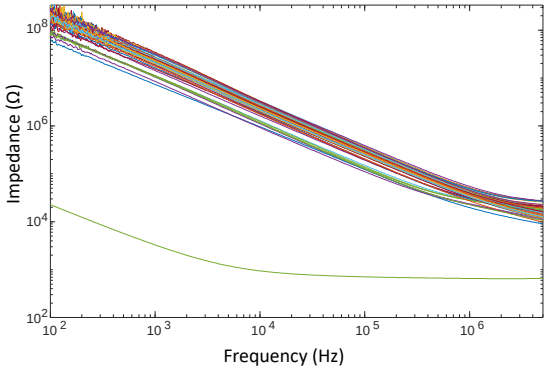

(c) Impedances measurements.

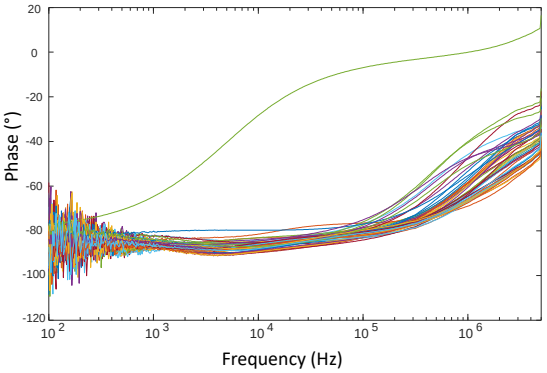

(d) Phase measurements.

Figure 2.16: a. Schematic representation of the equivalent circuit for the electrode/electrolyte interface. The Randles' circuit is used for both electrode and insulated access lines. b. Values of the impedance for each electrode at 1kHz. Different trends may be recognised for the electrodes with three or seven nanopillars, showing the sensibility of the technique. c and d. Graphic of the impedance and phase measurement obtained from the EIS. The capacitive behaviour of the electrodes is clear from this plots.

An electrode with three nano pillars has an exposed surface around $15.32\mu m^2$ and a corresponding average impedance value of $23.4M\Omega \pm 6.2M\Omega$, for an electrode with seven nanopillars instead the exposed surface is around $35.75\mu m^2$ for an impedance of $12.5M\Omega \pm 2.5M\Omega$ (2.16b). The theoretical inverse proportionality between exposed surface and impedance value is therefore respected, the impedance doubles with half of the nano pillars. The average value of the impedance is taken at $1kHz$ because it is the theoretical frequency of a neuronal action potential. The variability of the measure is linked to the PtSi exposed surface of the electrode. This step is done with a wet etch, therefore the control even if all precautions are taken is still limited and a slight over etch can occur. If the oxide layers at the bottom of the nano pillars is etched, even partially, the electrode base must be taken into consideration. Its influence is significant being the planar surface at the bottom 6 or 3 times bigger than, respectively, 3 or 7 nano pillars sidewall surface.

From the plots 2.16c and 2.16d the capacitive behaviour of the electrode can be seen. The Bode plot for the impedance does not have a clear plateau at low frequency that would correspond to a value of the system resistance, meaning that it is overcome from the capacitive component. Moreover, in the second plot, the phase is around -90 degrees, corresponding to a mostly capacitive behaviour of the system. At higher frequencies the system deviates from this characteristic because the capacitive resistance decreases: $X_C = \frac{1}{2\pi fC}$, where X_C is the capacitive resistance, f is the frequency and C the capacitance. Principle used also for the high pass and low pass filters in electronics. Giving to the system a more resistive behaviour, as visible from the plots where the impedance tends to reach a plateau at very high frequency and the phase increase towards 0 degrees. Differently from all the other electrodes, it can be distinguished the behaviour of the "reference electrode". The "reference electrode" is simply a large planar electrode, always made of platinum silicide, that was designed on the bio platform to act as on chip reference electrode. The characterization of this electrode allows to easily verify the correct functioning of the contacts, having a massive surface, compared to the other electrodes, its impedance value is easily recognize in the order of a few $k\Omega$ ($3.3k\Omega$ in the example). It was also designed with the intent of having the possibility to bring a polarization to the liquid media, feature later used for the characterization of the active transistors.

To better understand the characteristics of our electrodes, a theoretical simulation was done, based on the previously represented equivalent circuit. Each element that was already explained for the electrode interface has an equivalent one for the insulating layer (2.16a). Being this second Randles' circuit present to assess the values corresponding to leakage or modification of the measured potential they are called: leakage resistance (R_l), leakage capacitance (C_l) and medium leakage resistance (R_{lm}).

Given the equivalent electrical circuit a function transfer can be calculated taking in consideration all the elements in parallel and in series:

$$Z = \frac{1}{\frac{1}{R_{em}+\frac{R_e}{1+2\pi f R_e C_e i}} + \frac{1}{R_{lm}+\frac{R_l}{1+2\pi f R_l C_l i}}} \tag{2.1}$$

where f is the frequency and every other element has already been presented. This equation can be obtained knowing that the impedance of a resistor and capacitor in parallel is calculated as:

$$Z = \frac{R}{1 + 2\pi f RCi} \tag{2.2}$$

Therefore, the impedance of the system is of course a complex value. Its modulus would give the absolute value of the impedance ($|Z|$), instead the argument is the

phase (ω). Other interesting values that can be extracted are the total parallel resistance and capacitance of the system, respectively R_p and C_p. Those values are relevant because the system is composed of two main elements in parallel to each other, so it is possible to calculate their value:

$$R_p = \frac{|Z|}{\cos\omega} \qquad and \qquad C_p = -\frac{\sin\omega}{2\pi f|Z|} \tag{2.3}$$

they are definitely an approximation of the total, more complex, system characteristics, but are useful to understand which element has most impact at each frequency.

From the plots 2.17a and 2.17b good coherence can be observed between the measured and simulated impedance and phase. The discrepancies are most likely due to the simplified equivalent circuit model that is in use. The oscillation in the phase plot suggests the existence of some other elements that would slightly modify the obtained values and make a better fit between measure and simulation. It would be interesting to further develop this topic an in-depth study of the system model and simulation in order to try to address each element of a more complex model and its behaviour. Measure and simulated values for R_p and C_p are also visible in the plots 2.17c and 2.17d. Here also a good fit is obtained further confirming the validity of the equivalent circuit model used. From these plots, the total values for R_p and C_p are visible at low frequencies and their evolution in function of the frequency. In particular at low frequency the value of C_p is the sum of the capacitance C_e and C_l being in parallel. Instead, at high frequencies the value of R_p is the value of R_{em} and R_{el} as parallel resistor, being the capacitors considered as short circuits.

The same EIS measures were done also in distilled water to verify that the media did not have any major influence on the behaviour of the electrode and insulating layer. Moreover, in the equivalent circuit the R_{em} and R_{lm} elements are also considered to be dependent on the type of electrolyte used, so a measurable difference should be visible. A comparison of the measured and simulated impedance value for each condition can be found in table 2.2. A difference minor than 5% between measure and fit is obtained in most cases, validating the method used. It is possible

Impedance at $1kHz$	3NWs (PBS)	7NWs (PBS)	3NWs (H_2O)	7NWs (H_2O)
Measured	$24,3M\Omega$	$12,5M\Omega$	$28,2M\Omega$	$14,9M\Omega$
Simulated	$22,6M\Omega$	$12,2M\Omega$	$28,8M\Omega$	$14,4M\Omega$

Table 2.2: Values for the measured and simulated impedance at $1kHz$.

to compare the electrode impedances obtained to those found in the literature (as we did in this paper [55]) and verify that the same order of magnitude is obtained,

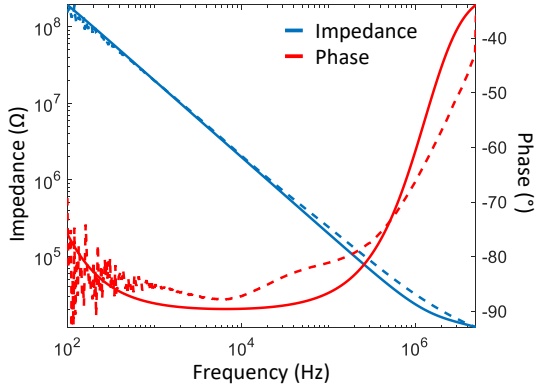

(a) Impedance and phase for three nanopillars.

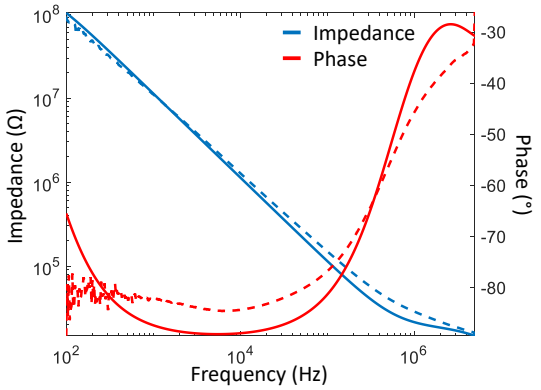

(b) Impedance and phase for seven nanopillars.

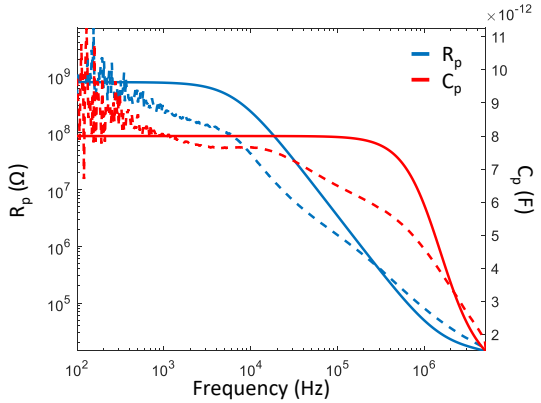

(c) Resistive and capacitive components for three nanopillars.

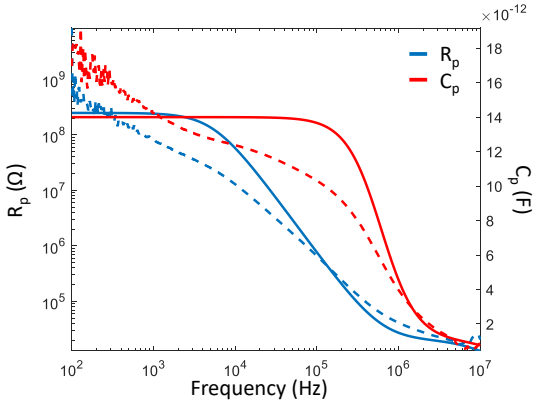

(d) Resistive and capacitive components for seven nanopillars.

Figure 2.17: a. Plot of impedance and phase measurement and simulation for an electrode with three nanopillars. b. Plot of impedance and phase measurement and simulation for an electrode with seven nanopillars. c. Plot of R_p and C_p measurement and simulation for an electrode with three nanopillars. d. Plot of R_p and C_p measurement and simulation for an electrode with three nanopillars. [Dashed lines are the measurements, bold lines are the simulations]

positioning the theoretical performance of the passive nanoprobes at the state-of-the-art level. Moreover, a lower impedance is obtained compared to the previous generations of the bio platform, showing an improvement in the technological control and optimization of the micro fabrication process.

Finally, the value used for the simulation fitting are presented in table 2.3. Here, a variation for R_{em} and R_{lm} is notable, varying from PBS to distilled water as expected because of the difference in ion concentration and, therefore, conductivity of the electrolyte. The values of R_e and C_e are coherent with dependence of the impedance to the surface. More electrode surface means having a bigger capacitance value, obtaining a reduction in the impedance of the electrode. The value of R_l was found to be much greater than the other resistances in the system, this was expected

being R_l a representation of the insulating layer. This means that the oxide behaves correctly avoiding any ohmic leakage. C_l was found to have a different value between the two electrolytes, meaning that the ions may have an interaction with the oxide layer that modifies its value.

Circuit element	3NWs (PBS)	7NWs (PBS)	3NWs (H_2O)	7NWs (H_2O)
R_{em} (Ω)	$15k\Omega$	$20k\Omega$	$300k\Omega$	$300k\Omega$
R_e (Ω)	$0.8G\Omega$	$0.25G\Omega$	$1G\Omega$	$0.5G\Omega$
C_e (F)	$7pF$	$13pF$	$5.5pF$	$11pF$
R_{lm} (Ω)	$10k\Omega$	$10k\Omega$	$100k\Omega$	$100k\Omega$
R_l (Ω)	$> 50G\Omega$	$> 50G\Omega$	$> 50G\Omega$	$> 50G\Omega$
C_l (F)	$1pF$	$1pF$	$0.1pF$	$0.1pF$

Table 2.3: Obtained values for each element of the equivalent circuit model used in the simulation to fit the impedance measurements.

Using the equation 2.2 and the extracted values of each element of the equivalent circuit, the theoretical impedance of singularly electrode (Z_e, given by $R_e//C_e$) and insulating layer (Z_l given by $R_l//C_l$) can be calculated. Z_e varies coherently with the number of nano pillars, being respectively $22,7M\Omega$ for three and $12,2M\Omega$ for seven. These values remain close to the measured ones, underlying that the EIS definitely focus the PtSi electrode measure. To do so, the parallel impedance, Z_l must have a much higher value, which coherently is above $100G\Omega$ in both cases. Once again confirming the correct behaviour of the insulating layer on the conductive lines. The two layers have been chosen for the known excellent electrical insulating characteristics, for the Al_2O_3, and its proven biocompatibility for the SiO_2. Arguably, the thickness or material of the layers may be varied to further improve the performance of the bio platform. A largely used material and valid alternative is the silicon nitride (Si_3N_4), often chosen for the use of electrical devices in saline liquid media.

The EIS measure and simulation have been done for each micro fabrication run of the bio platform, giving the possibility to estimate the performances of the devices and verify their correct functioning. Test runs of the chips, with variations in electrode number, dimensions, surface or geometry always reported coherent results with the expected values and a good fit of the equivalent circuit model.

2.2.3 Performance discussion

In the previous 1.4 section the state-of-the-art publication were discussed, some of these works also included a study of the equivalent circuit and its characteristics. A large variation in materials and structuration of the electrodes as well as materials and thickness of the insulating layers can be found [55]. In table 2.4 a summary of the state-of-the-art electrodes structuration and material used, as well as of the insulating layer chosen and circuit element values extracted is shown. Notably, each team operated differently but came to the same observation that these devices have principally a capacitive behaviour, once again respecting the potential measurement theory and the Grahame model. Differences are due to the method of extraction of the values or fitting of the characterizations. Our results also varied from previous works because we moved to a more accurate method, with the theoretical fit of measured characterizations.

In general, the results give the same trend, with an insulating layer that behaves almost only in a capacitive way (some groups did not even add an parallel resistance to the model, because of its huge value) and an electrode/electrolyte interface parameters that vary with the structuration and materials.

This range of choices shows how different approaches can bring to similar working devices. Anyway, the performances also are different, as shown in the plot 2.18, highlighting the best overall selection of parameters. It can be noticed that most

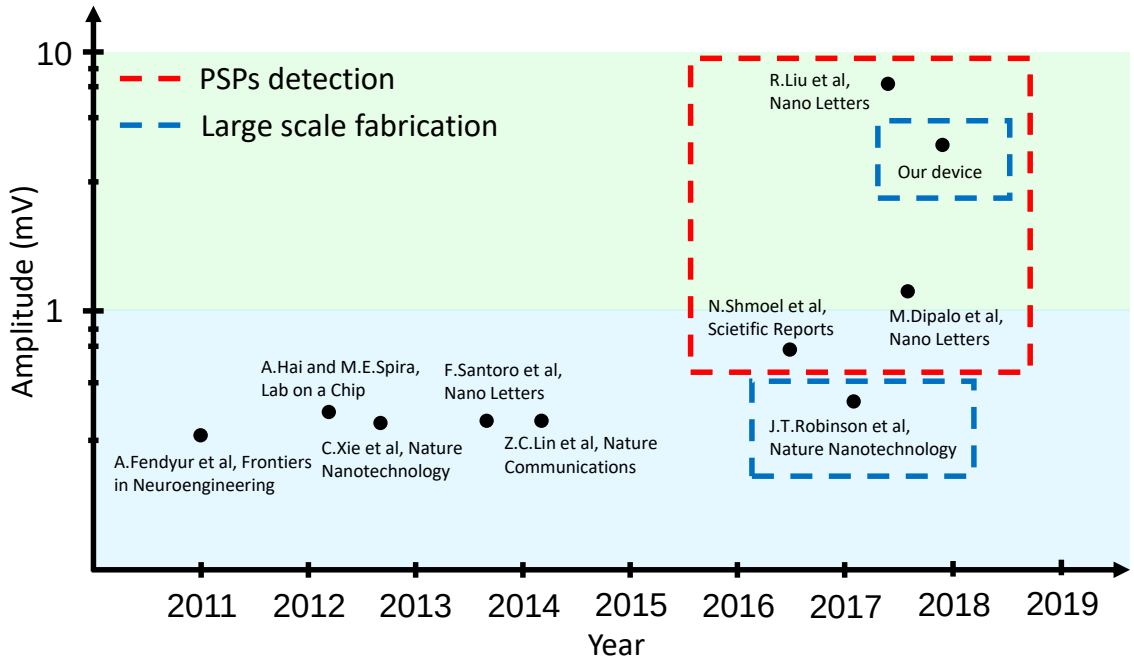

Figure 2.18: Plot showing the average performance of some of the most relevant publication in the state-of-the-art during the years and our positioning comparing to them In the y-axis, the peaks average amplitude showed in the publication.

Electrode structuration	Electrode material	Insulating layer	Circuit elements
Mushroom-shaped electrodes [56, 59, 60]	Gold	$400nmSiO_2$	$R_e = 1500G\Omega$ $C_e = 5pF$ $C_l = 8pF$
Mushroom-shaped electrodes [58, 57]	Gold	None	Not available
Nanowires [61, 63]	Silicon and metal tip	$50nmAl_2O_3$	$R_e = 300M\Omega$ $C_e = 1pF$ $C_l = 150pF$
Nanopillars and nanotubes [64, 62]	Platinum and IrOx	Si_3N_4/SiO_2	$R_e = 141M\Omega$ $C_l = 3.8pF$
Nanocylinders [65]	Gold	$3\mu m$ polyimide	$R_{e1}50G\Omega$ $C_{e1} = 0.8pF$ $R_{e2} = 1G\Omega$ $C_{e2} = 20pF$
Nanowires [66]	Doped silicon	$200/400nmSiO_2$	$R_e = 65M\Omega$ $C_e = 8pF$ $C_l = 8pF$
Nano pillars [68, 55]	Doped silicon and PtSi	$50nmAl_2O_3$ $200nmSiO_2$	$R_e = 2G\Omega$ $C_e = 10pF$ $R_l = 150M\Omega$ $C_l = 1pF$
Nano pillars (This work)	Doped silicon and PtSi	$50nmAl_2O_3$ $200nmSiO_2$	$R_e = 0.25G\Omega$ $C_e = 13pF$ $R_l = 50G\Omega$ $C_l = 1pF$

Table 2.4: Summary of the different used insulating layer in the state-of-the-art bio platforms and the extracted circuit elements values for each type of electrode.

of the devices are not compatible with a large scale fabrication process, limiting the industrialization of them and their reproducibility. Also, only a few publication reached average peak amplitudes that really determined a step forward compared to more classical MEA devices, going above $1mV$ average amplitude. Moreover, still less of these works showed to have the possibility of recording pre- or post-synaptic potentials (PSPs), being a consequence of the electrode high sensitivity and signal to noise ratio. Our device is compatible with large, have the possibility to record PSPs and have a high average recorded amplitude, showing that it is well positioned in the state-of-the-art solution for this type of bio platform. Moreover, a comprehensive equivalent for the system was proposed and verified by EIS characterization fitting.

A more in-depth study of the interfaces may be done performing EIS measures on several electrodes with variation in exposed surface and geometry. It would allow to try to do predictions on the characteristics of a specific combination of electrode parameters.

2.3 Chemical sensing

As previously explained, the bio platform also bears active electrodes (1.3.3), to perform two type of biological analyses on a cell culture at the same time. The finFETs on the chip were designed to be used as ISFET devices, taking advantage of their sensitivity to the chemical environment to detect variations in the pH of the medium. In this section, the functioning principle of this device is explained, our approach and solutions are described and the obtained performances are shown.

2.3.1 ISFET theory

Most of the electrochemical detection is done with potentiometric sensors, meaning that to determine the ion concentration the difference in electrical potential is measured. Following the Nernst equation:

$$\Delta\phi = \frac{RT}{F} \ln \frac{a_{i1}}{a_{i2}} \tag{2.4}$$

where R is the gas constant, T the temperature in Kelvin and F the Faraday constant. The ion concentration c_i is usually noted as $a_i = f_i c_i$, f_i being the activity coefficient. These sensors always need a reference electrode with a stable potential in order to detect the variation in ion concentration.

The alternative to these sensors was created from the MOSFET technology, known as Ion Sensitive Field Effect Transistors (ISFET). The idea was to create interfaces where the Nernst equation is respected, or in solid state physics terms, where the Fermi level of charge carriers can become equal throughout the whole system. The functioning principle of an ISFET can be explained starting from a classical electronic MOSFET, where the the metal gate is replaced by a reference electrode immersed in the liquid that makes contacts with the gate insulator layer (Image2.19).

For both devices, in the non-saturated region, the drain current may be written as the following equation [97]:

$$I_d = \beta(V_{gs} - V_T - \frac{1}{2}V_{ds})V_{ds} \qquad with \qquad \beta = \frac{\mu C_{ox} W}{L} \tag{2.5}$$

where μ is the electron mobility, C_{ox} is the insulator capacitance per unit area and W/L is the width to length of the transistor channel. For an ISFET the threshold voltage equation has to integrate terms relatives to the interface between the gate oxide and the electrolyte and the interface between electrolyte and reference

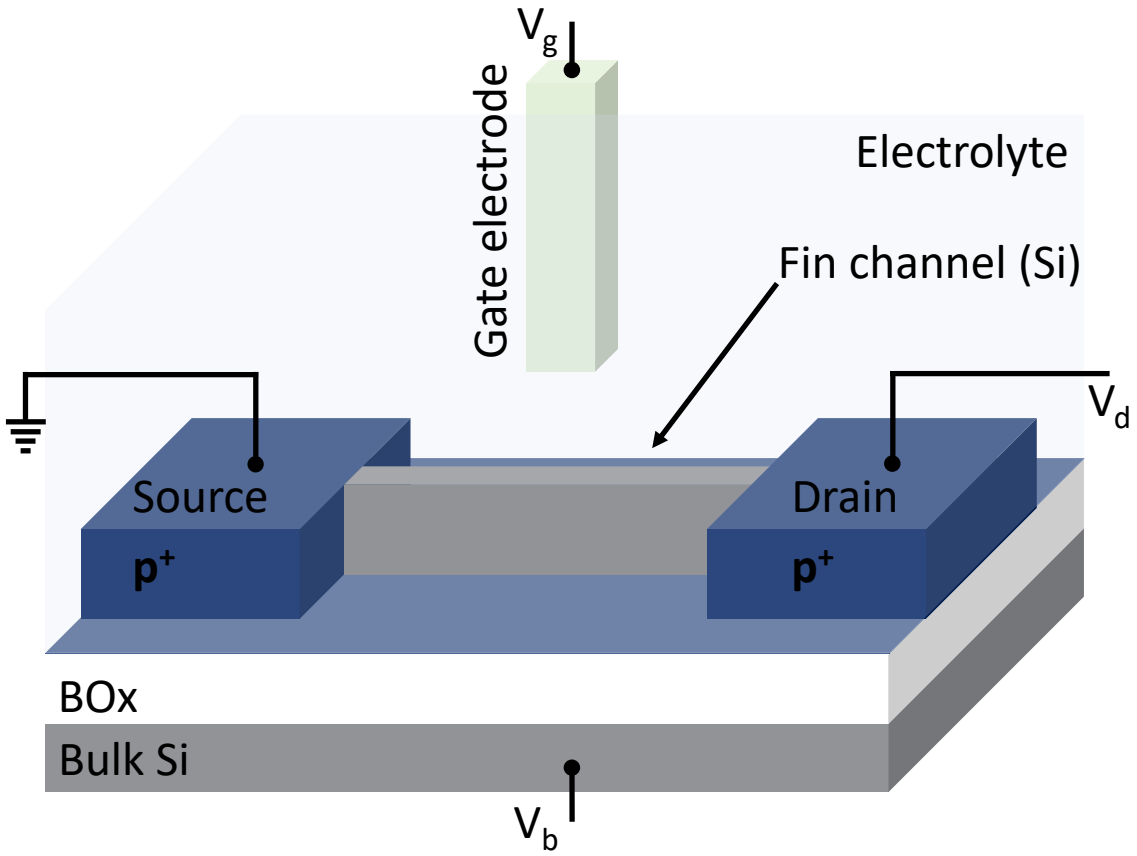

Figure 2.19: Schematic representation an ISFET device.

electrode. If the threshold is:

$$V_T = V_{FB} - \frac{Q_B}{C_{ox}} + 2\phi_F \tag{2.6}$$

where V_{FB} is the flatband voltage, Q_B the charge in the silicon and ϕ_F the Fermi potential. So the equation for the flatband voltage is:

$$V_{FB} = E_{ref} - \Psi_0 + \chi_{sol} - \frac{\phi_{Si}}{q} - \frac{Q_{ss} + Q_{ox}}{C_{ox}} \tag{2.7}$$

where E_{ref} is the reference electrode potential relative to vacuum, χ_{sol} is the dipole potential of the solution, ϕ_{Si} is the silicon workfunction, Q_{ss} is the surface state density and Q_{ox} is the fixed oxide charge. All of these terms are constant but Ψ_0 which is the surface potential. This is the term that makes the ISFET sensitive to the electrolyte pH and depends also on the material chosen as gate insulating layer and therefore the oxide/electrolyte interface.

The general expression for pH sensitivity of an ISFET is [98, 99]:

$$\frac{\delta\Psi_0}{\delta pH} = -2.3\frac{kT}{q}\alpha \qquad with \qquad \alpha = \frac{1}{\frac{2.3kTC_{dif}}{q^2\beta_{int}} + 1} \tag{2.8}$$

where α varies between 0 and 1. It depends on the buffer intrinsic capacity, β_{int}, of the oxide surface and the differential double layer capacitance, the same from the Grahame model, C_{dif}, respectively:

$$\beta_{int} = -\frac{1}{q}\frac{\delta\sigma_0}{\delta pH_S} \qquad and \qquad C_{dif} = \frac{\delta\sigma_0}{\delta\Psi_0} \tag{2.9}$$

where σ_0 is the surface charge density, pH_S is the pH at the oxide interface. When $\alpha = 1$ the ISFET reaches the so-called Nernst sensitivity limit of $59.2mV/pH$, theoretical being the limit without any particular modification of the device.

2.3.2 ISFET as pH sensors

Is therefore since the mid-60s that, with the evolution of the MOSFET technology, that the transistor principles are known. Its application to biological issues came, after the computing field, in the early 70s [100]. ISFET for biomedical application were largely studied during the years [101, 102], examples are: protein detection [103], DNA detection [104], blood gas analysis [105], genome sequencing [106], water analysis [107, 108] or multiple ions sensing [109, 110]. These devices were also used with cells as already described in section 1.3.4.

The ISFET as pH sensors are a category of devices largely studied with numerous technological variations: multiple transistors on CMOS technology [111, 112], organic semiconductors [113], flexible substrates [114] and amorphous gate oxides [115].

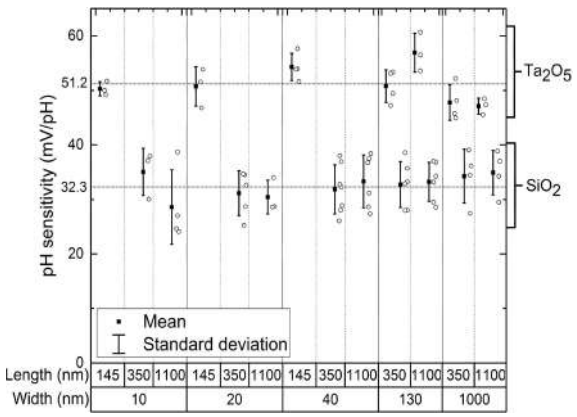

(a) pH sensitivity in function of channel length and width.

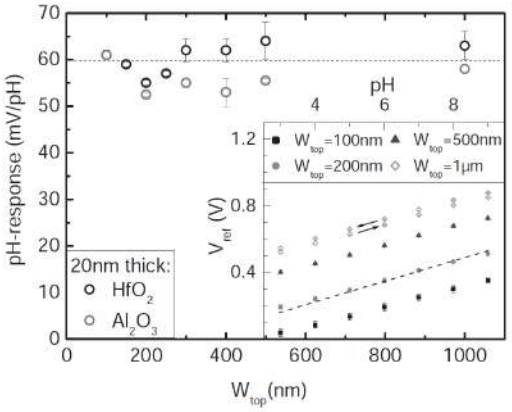

(b) pH sensitivity in function channel width.

Figure 2.20: a. Experimental pH sensitivity for different finFET geometrical dimension. SiO_2 and Ta_2O_5 were used as sensing surfaces [99]. b. The pH response of different finFET channel widths. HfO_2 and Al_2O_3 were used as sensing surfaces [116].

A lot of investigation on ISFET were done on the dependence of the pH sensitivity on the FET geometrical dimensions and there is no consensus to date [99].

More recent results determined that the size, as width and length, of the transistor channels does not influence the pH sensitivity of these devices [116, 99]. As it can be observed in image 2.20a and 2.20b, normally an ISFET device has a sensitivity around or below the theoretical Nernstian value of $59.2mV/pH$.

Differences in the sensitivity of the devices may be found with variations in the sensing layers. Some of the more classical gate oxide are SiO_2, Si_3N_4 ,Al_2O_3, HfO_2 and Ta_2O_5. In general, results depend largely on the method of deposition and quality of the oxide. The amphoteric surface groups (M−OH) protonation or deprotonation determine the surface potential (Ψ_0) and therefore transistor current variation with pH. Following the Site Binding Model, it was known that cations and anions present in the electrolyte equally interact with the oxide surface. Recent studies proposed modification to this model for better fitting experimental data, suggesting that anions directly interact with the hydroxyl surface groups and replace previously adsorbed protons from the surface [117, 118] (image 2.21). It also demonstrates that the pH sensitivity does not depend on ion concentration of the electrolyte ($< 10mM$). This result is particularly interesting for biochemical application, where the electrolyte concentration may vary with time.

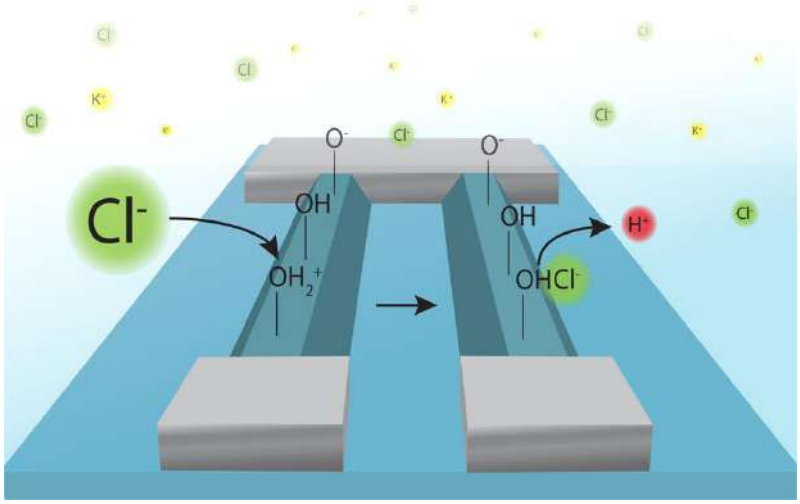

Figure 2.21: Schematic representation an ISFET device sensing layer influenced by the ions in the electrolyte [117].

On our bio platform, we characterized ISFET devices with two different oxides configurations: (i) native silicon oxide; (ii) aluminium oxide. Open-gate ISFET are typically used to easily introduce a functionalization of the transistor channel, enhancing its selective sensitivity to particular ionic species or molecules [86, 85]. Otherwise, the chosen sensing layer for our application was a thin layer of $5nm$ Al_2O_3, a material that already demonstrated near ideal Nernstian response [88] and negligible hysteresis effect [87].

Devices with performances capable of surpassing the Nernst limit of sensitivity

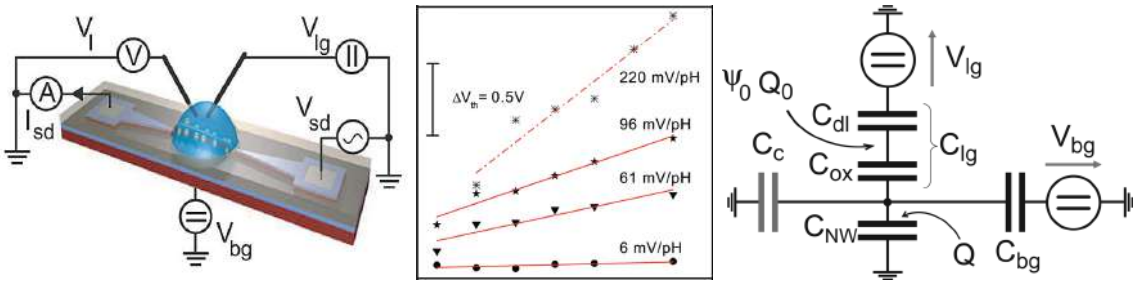

Figure 2.22: Left, schematic representation an ISFET measurement setup with the use of a back-gate (V_{bg}). Centre, measured threshold voltages V_{th} in different pH buffers for a series of fixed liquid potentials. Right, schematic model that defines the charge states for small source-drain polarizations. [119].

have been already published. In particular, the explication for these result above a theoretical law was found to be linked to the use of a double gate effect [120, 119]. When two gates are used on an ISFET device, as in the example in figure 2.22, the Nernst law is no longer correct. Nernst assumed the capacitance of the double layer (C_{dl} in the model) to be much larger than the capacitance of the sensing oxide layer, the intrinsic charging of the ISFET channel and an eventual back-gate contact, respectively C_{ox}, C_{NW} and C_{bg} in the model. For typical high ion concentration of the buffer solution $C_{dl} >> C_{ox}$, therefore the voltage divider of the model is given in practice by the ratio C_{ox}/C_{bg}. Whenever $C_{bg} < C_{ox}$ the result is an apparent sensitivity exceeding the Nernst limit. The device functioning physics itself is not modified, the result is only cause of an amplification of the system, not improving the signal to noise ratio.

2.3.3 FinFET device characterization as pH sensor

A FinFET device to be used a pH sensor allowing to probe the chemical environment of the cells has to satisfy certain working conditions. The liquid electrode should have a natural null polarization, and its variation from zero will modulate the current in the transistor channel, the I_{ds} current has to be already measurable at these polarizations. Also, to avoid heating, that would interfere with the cells spontaneous behaviour, a low V_{ds} polarization has to be used. Finally, the pH range relevant for neurons cells is between 6.5 and 7.5, the cells would not survive to more drastic conditions, meaning that the device has to be capable to measure small pH variations inside this range.

During the micro fabrication, two type of devices were done, the first leaving only native SiO_x oxide after a complete wet etch of the protective layer and the second with a deposited $5nm$ Al_2O_3 sensing layer. Moreover, a difference in the transistor channel width was obtained during the micro fabrication. The widths were between $150nm$ and $350nm$, consequently, being exposed to the same wet etch

time to remove the protective layer, the thinner channels almost completely lost the oxide connecting them to the substrate. It allowed us to study two different sets of parameters and determine which one performed best.

All the characterizations were done with a Agilent 4265C, a prevision parameter analyser for semiconductor devices, together with a semi-automatic probe system, the SUSS PA200.

Basic FinFET characterization with back-gate

Firstly, the transistor behaviour was tested via a first characterization without any electrolyte. The transistors are fabricated with boron doped source and drain (p^+) and with non-intentionally doped SOI substrate, so the choice was to have a device working with holes as charge carriers. First, the conservation between drain and source current was verified, respectively I_d and I_s. In the plot 2.23a an example of the two currents mirroring each other can be seen, showing the correct functioning of these contacts and the conservative current behaviour without parasitic leakage.

Then, the transistor effect with the use of a bulk polarization was verified with different V_{ds} polarizations (plot 2.23b). When the oxide underneath the transistor channel was over etched (as in the image 2.8a and 2.8a) the transistor did not seem to be working. This was happening because the polarization applied to the bulk wafer did not had a correct effect on the channel and the gate effect was therefore insufficient. The effect of the back-gate polarization was used later, in order to modify the threshold voltage of the transistor.

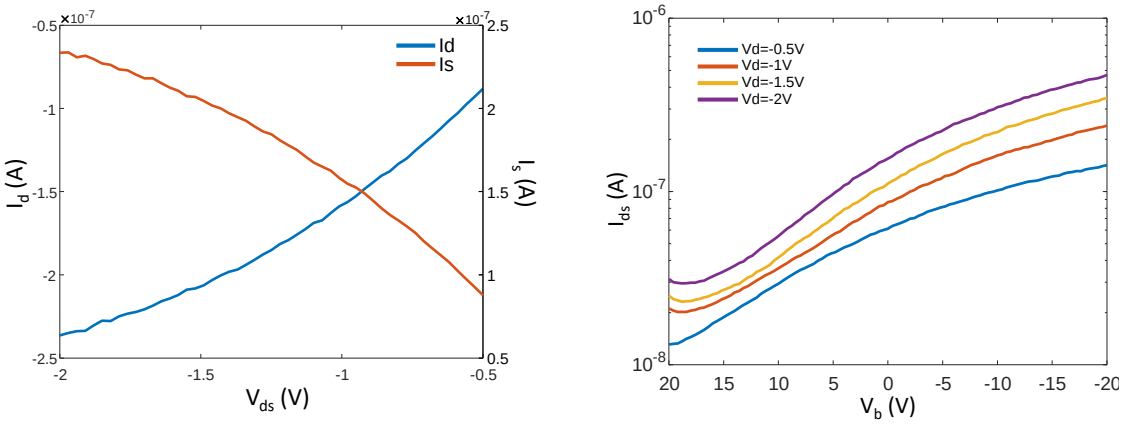

(a) I_d and I_s proportionality.

(b) Back-gate polarization effect.

Figure 2.23: a. First test to verify the correct working of the transistors drain and source contacts with I_d I_s proportionality. b. Transistor effect control with the bulk polarization.

Liquid gate FinFET characterization

Once the basic functioning of the device was correctly verified, the transistors were tested with an electrolyte gate. The transistor functioning as an ISFET device was found to be optimal between $150mV$ and $-400mV$ of V_{gs} with a drain current modulation (I_{on}/I_{off} ratio) around 5 order of magnitude 2.24a. The behaviour of the ISFET was independent from the gate oxide, at least for the basic functioning with liquid gate, showing that the quality of the oxide. The native silicon oxide SiO_x, was good as a correct characterization was obtained. It also confirms that the double layer capacitance from the Grahame's model strongly participates to the gate effect for the transistor channel. Also as expected, with an increasing negative V_{ds} polarization the I_{ds} current correctly increases.

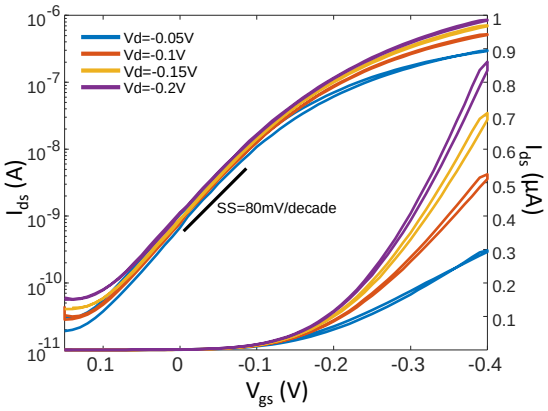

(a) I_dV_g characterization with PBS electrolyte of a FinFET with native SiO_2.

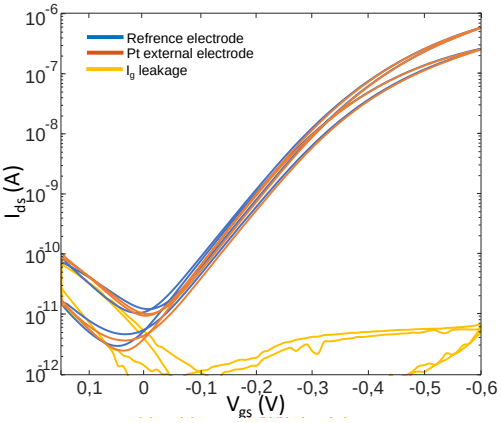

(b) External Pt vs on-chip gate electrodes and the leakage current I_g.

Figure 2.24: a. ISFET I_{ds} in function of V_{gs} characterization with PBS gate electrolyte at different V_{ds} polarizations (V_{ds} from $-50mV$ to $-200mV$). b. Comparison between reference on-chip electrode and platinum external electrode used as gate electrode to bring the V_{gs} in the electrolyte ($V_{ds} = -100mV$ and $-200mV$). The I_g leakage current is also plotted to show its negligible value.

The reliability of the reference electrode, built into the chip surface, was also evaluated using it as gate electrode to fix a polarization into the electrolyte. It was compared to an external platinum electrode dipped in the electrolyte (2.19). The plot 2.24b shows that no evident differences may be found in the use of either of the gate electrodes, therefore from the other characterizations were done using the on-chip reference electrode for simplicity. This is a great advantage, it reduces the complexity of the setup, avoiding the need for an external electrode, the need for eventual additional cable, connectivity or alimentation and shows once again the quality of the PtSi layer and its metallic behaviour. Moreover, an example of the leakage gate current I_g is plotted to show that its negligible value, that stayed between $10fA$ and $10pA$, in the system for both the use with a on-chip gate electrode

or the platinum external one. The subthreshold slope (SS) of the transistor resulted to be of $80mV/decade$, showing that already with a small polarization of the V_{ds}, and its variation necessary to drive the transistor, optimal performance can be obtained. This result is really interesting because the ideal ISFET designed to be used with neuron cells, as previously said, should work with small V_{ds} polarization to avoid an undesired heating of the transistor surface and the interference with culture media temperature and cells electrical behaviour. Finally, the hysteresis width results to be very small with a maximum value of $10\mu V$ calculated in the linear region at $5nA$, showing the negligible effect of charge transfer from adsorbated molecules or charge injection into trap sites on the dielectric substrate.

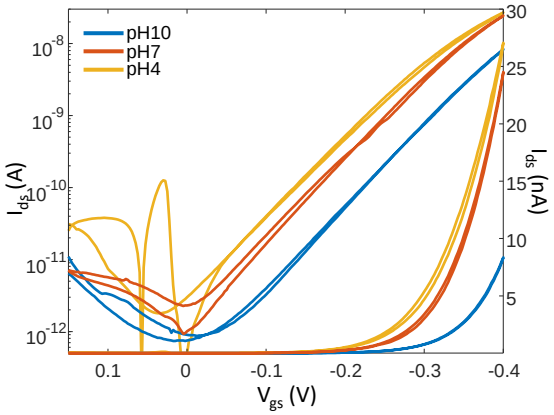

(a) ISFET I_{ds} characterization in different pH solutions.

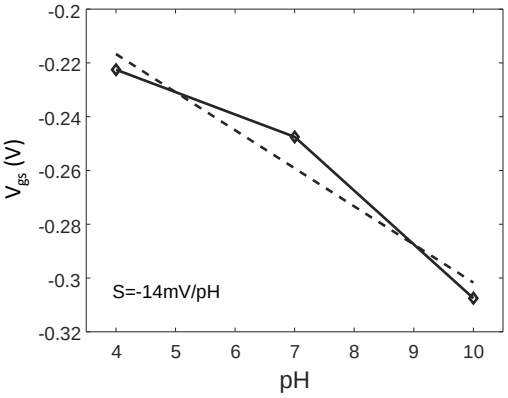

(b) Nernstian response of the device with native silicon oxide sensing layer.

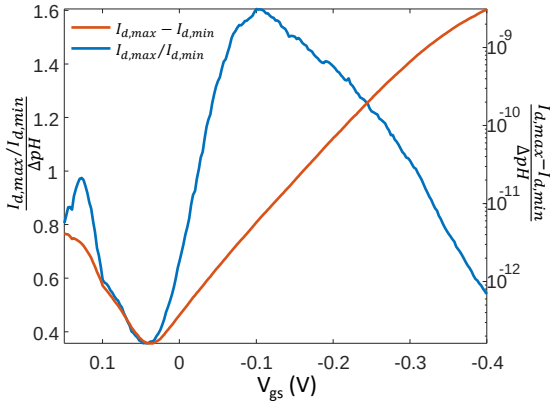

(c) pH sensitivity with native silicon oxide as gate sensing layer.

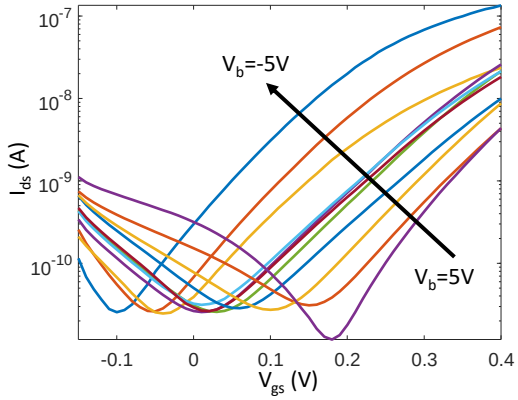

(d) V_b polarization effect on the ISFET characterization as V_{th} shift.

Figure 2.25: a. ISFET characterization with three different buffered pH solutions at 4, 7 and 10 pH ($V_{ds} = -100mV$). b. Nernstian response of the ISFET calculated with the method of constant current at $1nA$. c. Sensitivity of the ISFET without any deposited gate oxide. d. Effect of the bulk polarization V_b between $\pm 5mV$.

ISFET sensitivity to pH with SiO_x

The FinFET device sensitivity to pH was then studied, at first with only native silicon oxide as gate dielectric layer. At first, the sensitivity with three different pH buffer solutions were tested at 4, 7 and 10 pH, in order to have a first confirmation of the correct pH response of the devices (image 2.25a). The transistors with a layer around $2-3nm$ estimated thickness of native silicon oxide as gate dielectric has Nernstian response resulting to be quite weak at $14mV/pH$ (image 2.25b), calculated with the constant current method at $1nA$.

To determine quantitatively the sensitivity of the device according to the range of polarization, we defined two figures of merit:

$$\frac{I_{d,max}/I_{d,min}}{\Delta pH} \qquad and \qquad \frac{I_{d,max}-I_{d,min}}{\Delta pH} \tag{2.10}$$

where $I_{d,max}$ is the current value for the most acid pH and $I_{d,min}$ is the current value for the most basic pH, to assess respectively the sensibility of the transistor on the whole characterization and the measurable current range, both normalized per pH unit. Knowing that the transistor would work in a not polarized media, it is supposed to have high sensitivity and high current around $V_{gs}=0V$. This is not the case for the device with native silicon oxide as gate dielectric, both characteristics are close to their resulting minimum 2.25c.

Therefore, we decided to use the possibility to polarize the substrate bulk to shift the threshold polarization V_{th} with the influence of the back-gate and the added capacitor and gain current at a gate polarization closer to zero. As it can be observed, the V_b polarization was coherently shifting the V_{th} relatively to its value 2.25d, increasing the value of I_{ds} at null gate polarization.

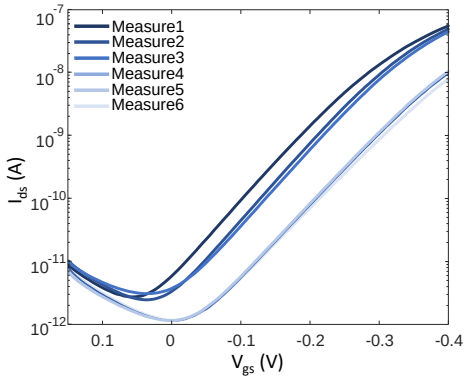

Figure 2.26: Native oxide degradation with a series of measurements.

The native silicon oxide finally resulted to not be enough stable for long term use, after several characterizations of the devices it would not behave correctly any more. As reported in the example of figure 2.26, a device already used for several characterizations often rapidly shifted its characterization losing any sensibility to pH variations for further use. Our hypothesis is that the oxide layer degrades with time and with the numerous variations of electrolyte pH, losing the sensing layer the device could not be used any more. Therefore, we decided to use a reliable conformal and chemically stable deposited sensing layer that would not degrade.

ISFET sensitivity to pH with sensing layer: Al_2O_3

Having verified the possibility to shift V_{th} and the ISFET sensitivity to pH, we decided to search for the best working conditions. The objective was therefore to obtain a response close to the Nernstian theory in a range of pH meaningful for neurons cells, with a high enough level of I_{ds} to be easily observable (close to $10nA$). The low level needed of V_{ds} to drive the transistor had already been verified multiple times. A linear Nernstian response to small pH steps was never

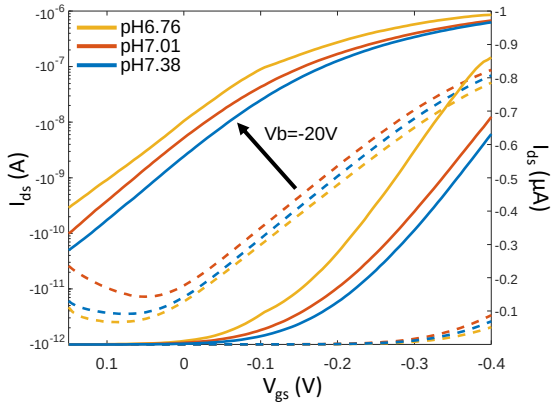

(a) ISFET characterization with ALD sensing layer and back-gate effect.

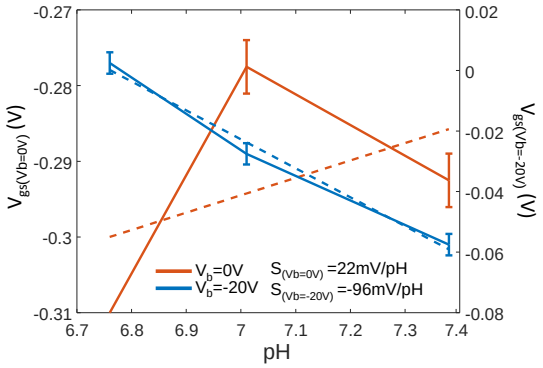

(b) pH sensitivity with and without back-gate polarization.

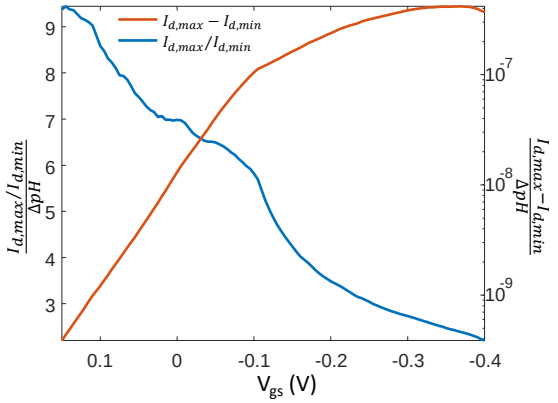

(c) Sensitivity of the ISFET device and I_{ds} range per pH unit.

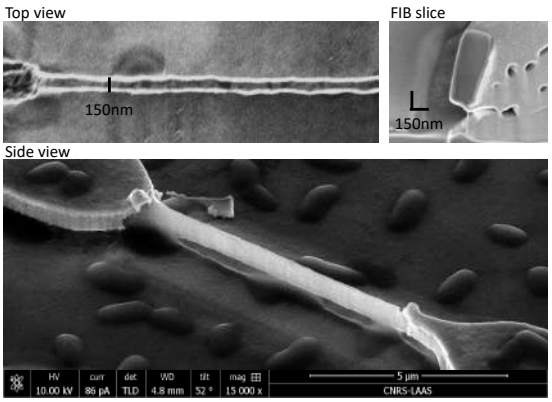

(d) ISFET SEM images of the channel top and side view.

Figure 2.27: a. ISFET characterization with solution at different pH values, respectively 6.76, 7.01 amd 7.38. ($V_{ds} = -100mV$, $V_b = -20V$) b. Nernstian response of the ISFET calculated with the method of constant current at $1nA$. c. Sensitivity of the ISFET with ALD sensing layer. d. SEM image of the transistor after numerous uses and characterizations. The oxide underneath the transistor channel is mostly being etched.

achieved with the native silicon oxide as sensing layer and gate oxide. Therefore, the introduction of $5nm$ layer of Al_2O_3 as sensing layer was motivated by (i) its known good performances in this role, (ii) its easy integration and (iii) already tested compatibility with the fabrication process. Devices having this sensing layer

showed the possibility to obtain a coherent pH sensitivity down to 0.3 pH units (figure 2.27a). The pH solutions were prepared the same day with a sterile medium ready for use with the neurons and its pH value was modified with KCl and NaOH while being measured. Its Nernstian response was linear and even above the one at $-96mV/pH$ (figure 2.27b), result that can be explained with the influence of the back-gate polarization and the charges added by the buried oxide capacitance effect, as discussed in the previous section 2.3.2. To obtain this result, multiple back-gate polarization were tested. It resulted necessary a V_b polarization of $-20V$ to increase the sensitivity of the device in order to obtain a linear Nernstian response to the pH variation, as can be observed in plots 2.27a and 2.27b. With smaller V_b polarization the response to pH steps between 0.2 and 0.3 was not linear. The value of the back-gate polarization was explained by the etch of the oxide underneath the transistor channel, as it can be observed in the transistor top and side view and FIB slice SEM images 2.27d. The width of the fin was of $150nm$, which means that the oxide connecting it to the bulk wafer was of the same dimension. The sensitivity of the device with back-gate polarization was calculated and can be observed in figure 2.27c. Its values in the linear part of the characterization was at a relative maximum between $0V$ and $-100mV$, corresponding to the rising part of the current range. It means that the device can sense small pH variation resulting in measurable drift of the drain current value. Moreover, in an interesting pH range for biological application and without the need of a polarization in the media.

To go further, we investigated the effect of the oxide underneath the transistor channel on its performance. A device with a robust remaining layer of the buried oxide was characterised 2.28d. Doing a screening for the back-gate polarization effect, the effect of V_b was found to be stronger than previously even at lower polarization values. With just $-2.5V$ on the back-gate a greater shift in the V_{th} could be observed. It is coherent with the fin width of $350nm$, that also determines the oxide width, and the presence of this layer on the underneath the entire FinFET channel, increasing the effect of the back-gate polarization on the charge carriers. Its working parameters were the same for V_{ds} at $-100mV$ but the range for V_{gs} was found to be much larger, between $800mV$ and $-400mV$ consequence of the different geometry 2.28d. The I_{ds} obtained values at $V_{gs} = 0V$ were in the order of $10nA$ for $V_b0 = V$, and $150nA$ for $V_b = -2.5V$, being higher than the minimum measurable from our recording setup, at few nano Ampere (figure 2.28a). Already at zero back-gate polarization a linear Nernstian response was obtained, at $-46mV/pH$. Moreover, the effect of the larger capacitance from the back-gate brought the sensitivity to pH even higher than before at $125mV/pH$ with step of $0.2pH$ (figure 2.28b). Its $I_{d,max}/I_{d,min}$ resulted in a maximal value at $0.5V$ for the gate polarization, decreasing close to zero V_{gs} but still with a relative high value. On the other hand, the $I_{d,max} - I_{d,min}$

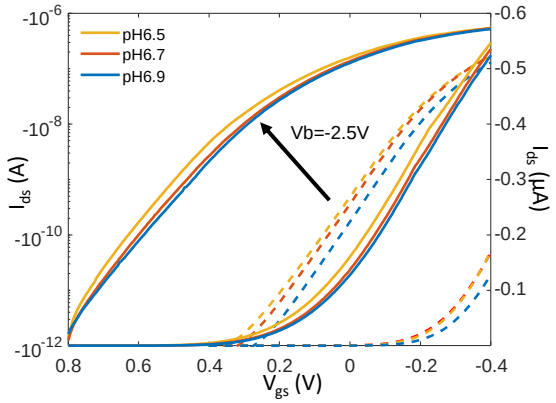

(a) ISFET characterization with ALD sensing layer and back-gate effect.

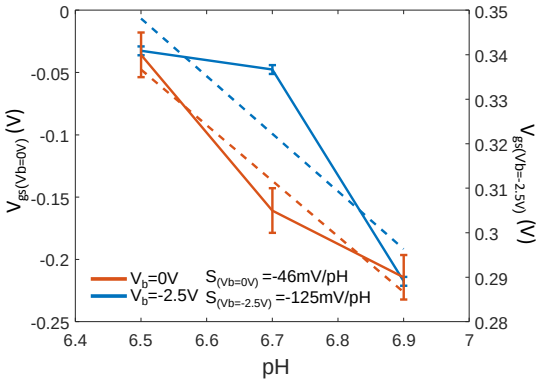

(b) pH sensitivity with and without back-gate polarization.

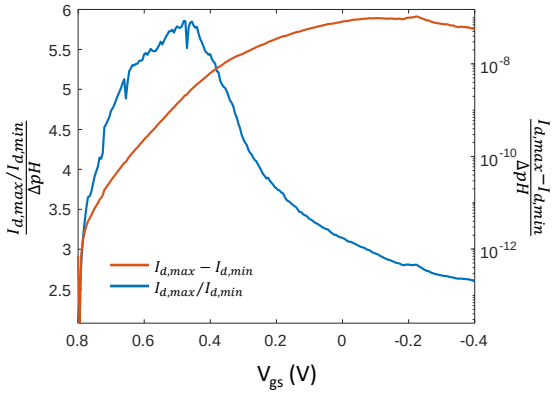

(c) Sensitivity of the ISFET device and I_{ds} range per pH unit.

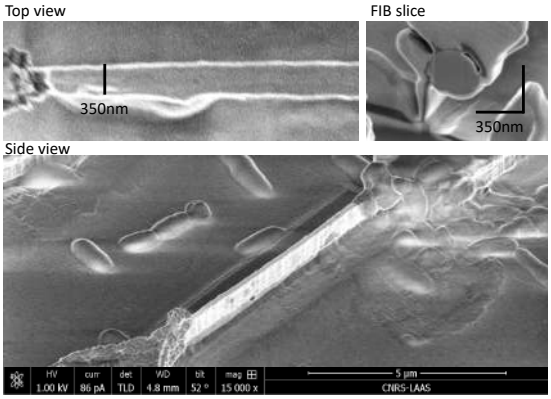

(d) ISFET SEM images of the channel top and side view.

Figure 2.28: a. ISFET characterization with solution at different pH values, respectively 6.3, 6.7 and 7.1 ($V_{ds} = -100mV$, $V_b = -2.5V$). b. Nernstian response of the ISFET calculated with the method of constant current at $1nA$. c. Sensitivity of the ISFET with ALD sensing layer and oxide underneath the channel. d. SEM image of the transistor after numerous uses and characterizations. The oxide underneath the transistor channel is still largely present connecting fin and the SOI substrate.

showed a value close to the maximum right around $V_{gs} = 0V$ (figure 2.28c). It means that the device still offered the possibility to determine small pH shifts with even higher level of current drain variation at zero gate polarization.

Hence, the cause of the over etch of the oxide connecting the transistor fin to the bulk of the SOI wafer was identified to be linked to structural variations. During the micro fabrication process the transistor design is transferred with a thick photoresist of $5\mu m$, needed to assure the protection of the nanopillar from the plasma etch. This thick photoresist induces a variability in the critical dimension obtained on the wafer. The transistor channel width varied from 150 to 350 nm determining also the width of the underneath oxide. Being exposed to the same wet etch time, some devices happened to almost completely lose the underneath oxide and be only

slightly connected to the wafer surface. This geometry irregularity, on the other hand, gave us the opportunity to study different set of conditions and the effect of these parameters on the transistor characteristic and sensitivity to pH. The height and length of transistor fin were unchanged, being determined respectively by the thickness of the remaining crystalline silicon on the SOI at $1\mu m$ and by the mask design at $7\mu m$.

The most optimized ISFET device is therefore obtained when the geometry allowed to preserve the connection between channel and substrate and with the ALD sensing layer deposition as gate oxide. The double gate effect and the quality of the Al_2O_3 layer allows to obtain pH sensitivity above the Nernst limit. Moreover, the devices function with high level of I_{ds} current, if a V_b bulk polarization is applied, when no V_{gs} liquid gate polarization is used. This is perfect for a device that is going to be used with cells, because the electrolyte polarization is naturally going to be null.

Chapter conclusion

In this chapter the fabrication of the nano electrode array was presented, putting an accent on the large-scale compatibility of the process and describing the most relevant and critical steps. Also, in particular the co-integration of electrode and finFETs was explained. To end the clean room fabrication section, a study on the packaging method of the chip was done and its results were described. It is shown that using the solder paste may bring considerable advantages on the gold bump technique.

Then, the theory regarding the measure of electrical potential in liquid media with a metal electrode was presented. A correlation to our specific electrodes was done with the classical Randles' cell model. Moreover, an investigation via electrochemical impedance spectroscopy characterization of the electrode impedance value and its simulation with the presented equivalent circuit was explained. The excellent fit between characterization and simulation means that the equivalent circuit model is a good representation of the system and it allows to extract the indicative values of the circuit elements. The characteristics of our electrodes were then compared to the state-of-the-art similar published devices.

Finally, the theory regarding pH sensing with transistor devices was presented. To conclude, our study on the performance of the finFETs with different sensing layers (native silicon oxide and Al_2O_3) is presented. Moreover, the effect of the back-gate polarization increasing pH sensitivity and Nernstian response was shown, obtaining above Nernst limit pH sensibility with small pH steps and in a range relevant for biological study of neurons.

Chapter 3

Towards subcellular interfacing and axogenesis

It has already discussed in the first chapter 1.3 the numerous technologies that have been developed to interface living cells, being *in-vivo* or *in-vitro*. These solutions are aiming to study and understand the basic mechanisms of cell functioning. In order to study the cells, several techniques to culture different types of cells had to be refined. In particular here the culture of rat primary cells on our bio platform is explained. Also, another critical point is the possibility to define a network of cells down to single axon connection. To this goal, the most efficient methods were found to be the surface functionalization, already used by our team, and the use of microchannels, that we studied here. In this section, two different explored alternatives are described and the results are discussed.

3.1 Cell culture

During the project, we studied and focused on the use of rat primary neurons. These cells come directly from the brain of rat embryos and need to be dissected for each new culture. It is the main difference from immortalized cell lines, where the cells can proliferate thanks to mutations that remove cell senescence. The embryonic cells that we used are not very advanced in the differentiation phase. These cells just finished migrating to the cortex or hyppocampus areas of the rat brain and do not have created any connections. Once plated, the cells will go past the mitotic phase creating connections and a mature network. The cellular nucleus has dimensions of a sphere between $5 - 10\mu m$ in diameter. Even if it can be complex to operate a dissection before each cell culture and create strong constraints due to cell availability and their fragility, primary cell culture has its advantages. Primary neurons, being post-mitotic and non-transformed are closer to *in-vivo* neurons than any dividing

cell lines. Hence these cells are more appropriate for biologically relevant studies, even if it is still a reductionistic system not having support from glial cells or myelin.

3.1.1 Primary rat neurons

The primary cell culture was possible thanks to the collaboration with the team of Daniel Gonzalez-Dunia, PhD co-tutor during this project, at the Toulouse Institute for Infectious and Inflammatory Diseases - Inserm (Infinity), recently created from the ex CPTP-Inserm laboratory. We had the chance and opportunity to took advantage of their expertise in rat primary cell culture to have regular access to these cells synchronizing our work to their dissection schedule. At the LAAS, Marie-Charline Blatche, the engineer in charge of the area dedicated to cell culture, largely helped in taking care of the cells during the project and to perform several experiments and tests.

The neurons are taken from embryos brain of Sprague-Dawley rats. The animals are sacrificed on the 17^{th} day of the embryos life, the brains are dissected manually under a binocular microscope. The cerebral tissue is then dissociated with a solution of $10U/ml$ of papain (Serlabo Technologies), this process is stopped with a solution of Low-ovomucoide containing 0.15% of bovine serum albumin (BSA) and 0.15% of Trypsin inhibitor. The solution containing the cells is filtered at $70\mu m$ and centrifuged for 10 minutes at $1000rpm$. It is then kept in Cortex medium: Neurobasal media (Gibco) with the addition of 2% B-27 supplement, 1.2% GlutaMAX and $120U : 120\mu g/ml$ penicillin:Streptomycin (Life Technologies). This is deposited in $3ml$ of BSA at 4% in Neurobasal media and centrifuged at $1000rpm$ for 9 minutes. This last step allows to separate neurons to the glial cells because of their higher density to obtain culture with a high cellular purity. To the bottom of the solution, containing almost exclusively neurons, is then added the Cortex media. This final solution is brought back to the LAAS in a polystyrene box kept at 37 °C. Here the cell concentration is corrected and the cells are plated onto the bio platform.

One key point about *in-vitro* neurons culture is the adhesion of the cells to the substrate. The cells react to their environment and have the possibility of little migration in order to reach a more suitable adhesion position for their development. The most effective methods to seed neurons on our devices has already been largely studied and optimized by the previous PhD student [67, 121], therefore the same technique has been used during the project. The result is that a double deposition of poly-ornithine (PO) and laminin (LN) is the more reliable solution for long term cell studies. Moreover, the chip surface material biocompatibility (SiO_2) was already been verified via MTT assay to assess cell metabolic activity even at very low cell concentration.

A very precise protocol is established and needed to be followed to assure repeatable and consistent experiments.

Sterilization The samples have to be sterilized with ethanol (70% in distilled water), it cleans any eventual contaminants.

First coating The first molecule for adhesion is used, PO ($0.5mg/ml$ in sterile water), it is typically left for the weekend in a fridge or overnight at 37 °C in humid atmosphere with 5% CO_2 in an incubator.

Second coating The dissection day, the PO is rinsed with sterile water and the LN coating is done ($5\mu g/ml$ in Neurobasal media). This coating is left at least 3 hours in the incubator and rinsed just before the cell plating.

Cell plating Cell concentration is corrected for any specific use in $1ml$ of Neurobasal media with the addition of 2% B-27, $2mM$ of L-Glutamine and $100\mu g/ml$ of Penicillin/Streptomycin (Invitrogen).

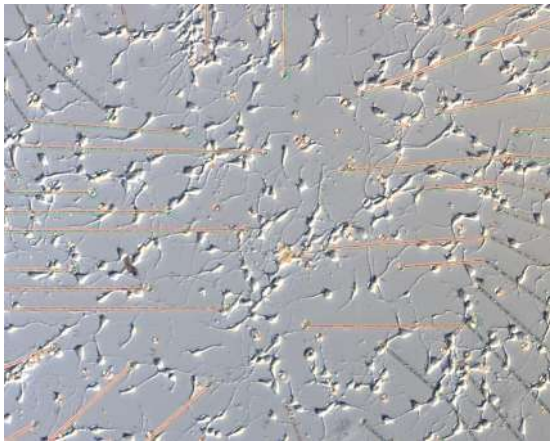

(a) Optical image of cell culture on bio platform at 1 DIV.

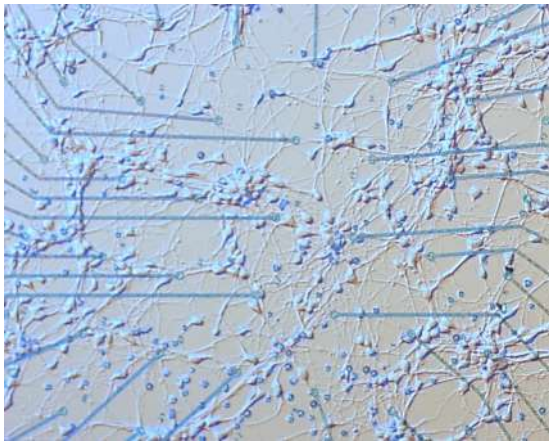

(b) Optical image of cell culture on bio platform at 3 DIV.

Figure 3.1: An example of a cell culture as it develops after being plated. From 1 to 3 day-in-vitro the most part of the connections are created.

During the culture period on chip, or on test substrates, the cells are observed with optical microscopes directly inside the cell culture area of the laboratory. An example of the neuronal culture on the chips can be observed in the images 3.1a and 3.1b at respectively 1 and 3 day-in-vitro (DIV). As the culture develops some cell might slightly migrate from their original position and few cluster of cells can appear. If the coatings are effective the distribution of cells is homogeneous on the chip surface for the entire duration of the culture. An example of a cell culture at $10DIV$ can be observed in image 3.2a. The cells are kept in the incubator until maturity is reached around 15 DIV, and the recording session can start. To increase

the survival rate of cells at long term, the Neurobasal conditioned media is used. This media is obtained with a separated culture of glial cells, which release nutriments for the neurons in the media. The Neurobasal conditioned media is collected from the glial culture and used to partially renew the media, and substitute any evaporation, for the neuronal culture.

(a) Optical image of cell culture on bio platform at 10 DIV.

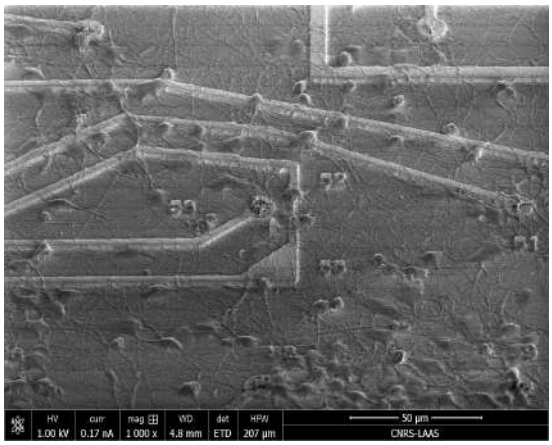

(b) SEM image of cell fixed with glutaraldehyde at 15DIV.

Figure 3.2: a. Optical image, example of cell culture at $10DIV$. The primary neurons are completely developed as wells as their connections. Few cell clusters can be observed due to cell migration. b. SEM image of a mature fixed culture at $15DIV$. The image allows to see how most of the electrodes are engulfed by a neuron or some neurites.

At the end of the experiment, cells may be fixed using glutaraldehyde 3.2b or para-formaldehyde respectively for SEM characterization or immunofluorescence imaging. Otherwise the devices were cleaned with the use of trypsin, that is classically used to cleave proteins holding the cultured cells to the substrates, in order to easily remove the cells. Then rinsing the device in 5% SDS (Sodium dodecyl sulphate), an anionic surfactant typically used in cleaning products, the device can be totally cleaned. Another cell culture could be started again on the device from the sterilization and following the already presented protocol.

Mastering primary cell culture on a bio platform and keeping the cells in good conditions until reached maturity is a complex task that demands a fine-tuning of several parameters. Achieving this goal is already an excellent result and not many research groups are able to achieve it. We wanted also to try to control the neuronal network that would form on our bio platform, obtaining the control of the axogenesis and determining the path for the neuronal growth.

3.2 Possibilities to guide neuronal growth

Going from cell cultures with random positioned cells to organised *in-vitro* neuronal culture creating a controlled network of connection is a key point to bring the study of cell electrical activity to a further level of understanding. Three main methodologies have been adopted trying to achieve this goal:

Topographic structuration Design three dimensional geometries in order to constrain the cell growth. Numerous studies have been done on cell adhesion, viability, morphology of cells, their development and guiding properties [122, 123, 124, 125, 126].

Surface functionalization Chemical confinement with adhesion molecules to promote cellular growth in defined areas. This can be done by micro-contact printing or photolithography [127, 128, 129, 130, 131, 132, 133, 134].

Microchannels Especially used for microfluidics, microchannel structuration has been largely used to geometrically constrain axons and dendrites and guide their growth [135, 136].

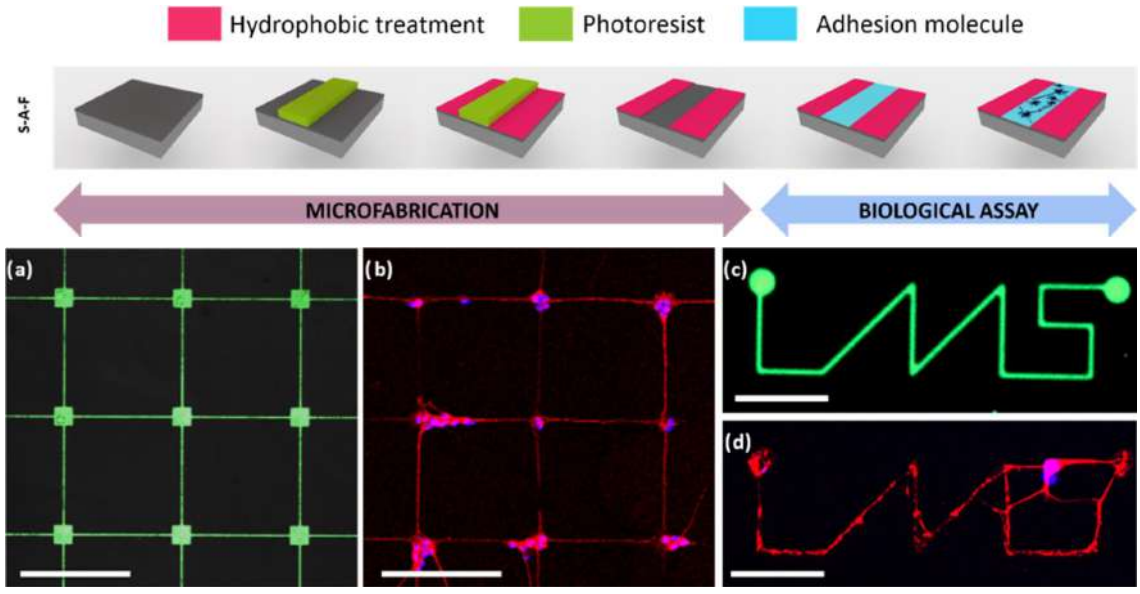

Figure 3.3: Fabrication of the self-aligned functionalization and the possibilities to guide cells growth. The hydrophobic treatment is the FDTS, and the adhesion molecules are the PO and LN.

Our team already achieved great results using a surface functionalization based on the deposition of a hydrophobic molecule, the Perfluorodecytriclhlorosilane (FDTS), able to form monolayers on an oxide surface. In a published paper [55] it was demonstrated how this specific self aligned functionalization, realized thanks to a

photolithography step, could guide the growth of neuronal axons and dendrites, especially at very low cell concentration (figure 3.3).

In order to go further a study was conducted to interface the cells along the axons to bring the analysis of the electrical activity to subcellular level. In order to completely determine the axogenesis of the neurons a fixed three-dimensional structure aligned with the electrode array of the device. It was for that reason that we opted for the realization of a series of microchannels that would constraint the cells in specific areas. Moreover, this approach also opens the possibility to foresee culture of different cell types (or co-culture), determining the connection between the different species and study the exchanged electrical signals.

3.2.1 State-of-the-art

Microchannels have been largely used in microfluidics and they have been applied in various disciplines as chemistry, biology or medicine [135]. Microchannels were also used for various purposes as cell culture, manipulation and differentiation, or neuropharmacology, electrophysiology and on various biosensors. Neurons, more than other cell types, are very sensitive to the environment such as substrate roughness [137, 138], temperature [139], composition of the medium [140, 141, 142], pH value and ions concentration. Very important roles are also the device material and its microstructure. Many materials have been employed to fabricate microfluidics devices for cell culture: silicon [143, 144], glass, quartz [145, 146], PDMS [147, 148] and many others. Moreover, different structures are also commonly used in combination with microchannels, for example grooved structures [149, 127] or nanometre-seized and micrometre-sized columns [150, 151].

The basic design of these devices type includes two main fluidically-isolated culture chambers and media wells connected by microchannels into which only neurites can grow. Classically, the channel dimensions are designed to be too narrow and low for neuronal cell bodies to enter. An example can be seen in image 3.4a, the two chambers separate somatic culture and neurites growth inside the channels. The fluorescence imaging allows to demonstrate the correct separation and the possibility to control the cellular network.

Some designs allowed to create chemical gradient combined with channels for neurites' growth [156, 157], or orienting the network connection in one direction [154]. Also, the channels size influences on the axonal growth were studied [155]. As can be observed in image 3.4c as the width of the channels decrease, also the number of axons in the channels decreases down to a few. Moreover, the directionality of the network can be mostly determined with geometric variation of the channel width. In image 3.4b single cells are positioned inside culture wells con-

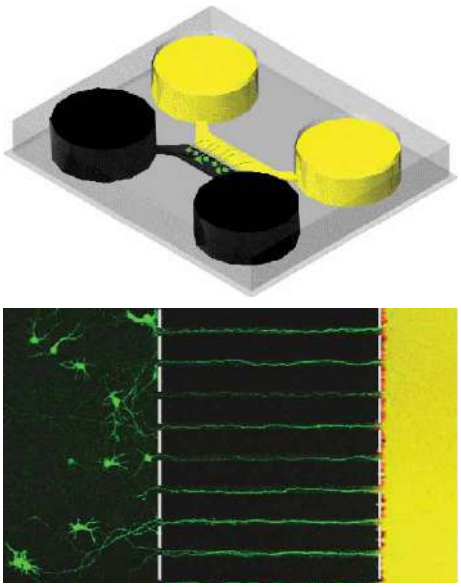

(a) Microfluidic-based platform for direct axonal growth.

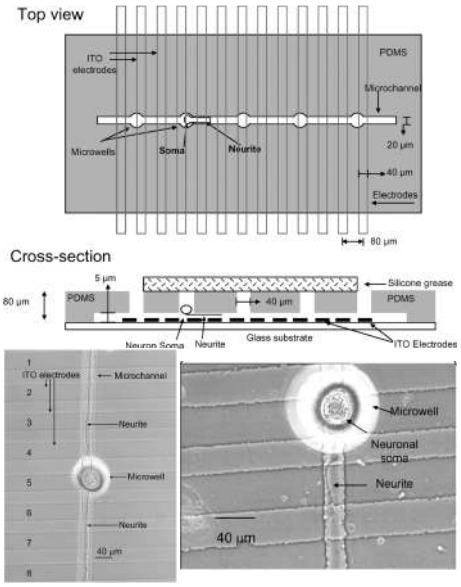

(b) Soma and neurites separation and recording.

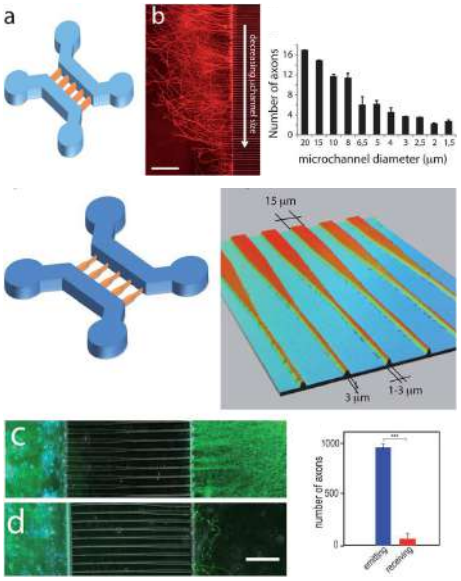

(c) Microchannels to study width effect and network conditioning.

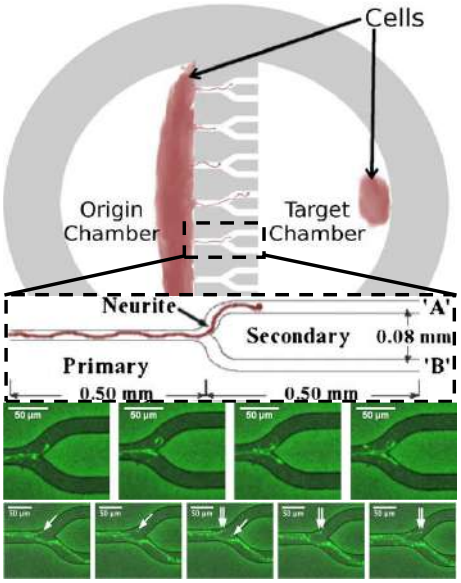

(d) Depiction of the device with bifurcating microchannels.

Figure 3.4: a. Microfluidic-based culture platform for CNS neurons axonal growth [152]. The chambers consist of PDMS connected by microgrooves $10\mu m$ side and $3\mu m$ height. Merge fluorescence image of soma (red) and axonal (green) trackers. b. Multielectrode device with an overlaying polymer film including microwells and microchannels. Phase contrast images of confined neurons growing neurites along the microchannels [153]. c. Primary cortical neuron seeded in microfluidic chip with variable width from 20 to $1.5\mu m$ and the quantification of the number of axons exiting the micro-channels [154]. d. Culturing device origin and target chambers with seeded cells [155]. Bifurcating microchannel design. Example images of the neurites at the decision bifurcation taken 1 hour apart. Images providing an example of the exploratory behaviour of growth cones.

nected by microchannels and the confined growing of the neurites can be observed. The exploratory behaviour of the growth cones can be observed in the image 3.4d, where the bifurcating microchannels oblige the axon to choose a preferred direction to develop.

Often, these systems are used in combination with microscopy, but when they are combined with extracellular electrodes, they allow electrophysiological studies separated for somas outside the of channels and for axons inside of channels. The amplification of the signal inside microchannels was proven [158], thanks to the increased extracellular sealing resistance. Structures to separate soma and axons have been proven functional, with the possibility to record from the different zones of the cell monitoring the propagation of the action potentials, their direction and velocity [159, 153, 160].

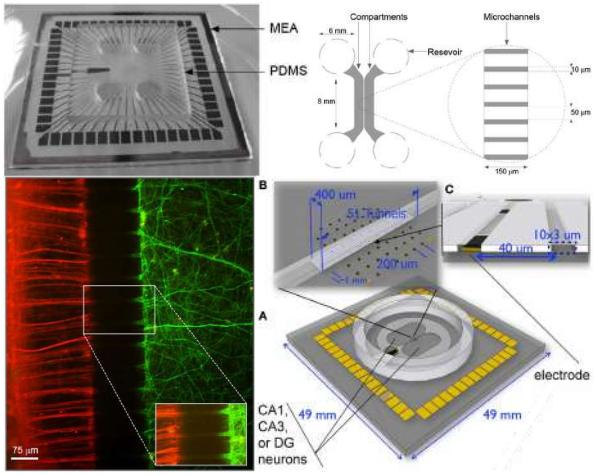

(a) Dual compartment devices used for co-culture and network conditioning.

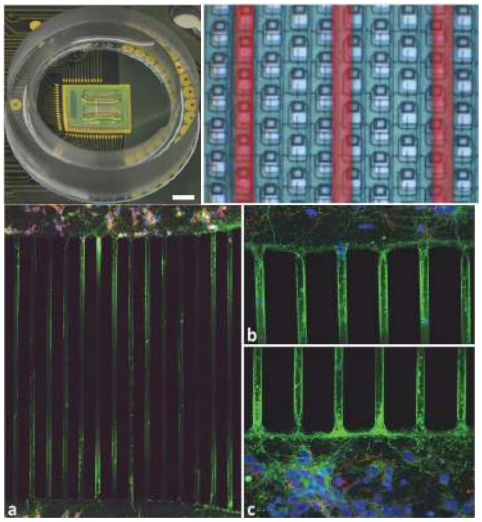

(b) Geometry and layout of PDMS channels on CMOS.

Figure 3.5: a. Schematic layout of the dual-compartment devices, both planar MEAs substrates have custom PDMS microchannels. Example of co-culture fluorescent imaging of cortical (red) and thalamic (green) cells [161, 162]. b. Packaged CMOS chip on PCB cross and zoom on the electrode and channels. Immunostained cells primarily extended axons into the channels [136].

In particular, a number of groups have integrated custom microchannels on commercial MEA systems, typically with 60 electrodes, in order to functionally connect cultures of one or more cell types, demonstrating also self-network orientation [163, 161, 162]. Two planar MEA devices with PDMS microchannels can be seen in image 3.5a with the typical two main chambers design connected by the microchannels. The co-culture in the same image shows effective connections between cortical and thalamic cells demonstrating the possibility to perform cell co-cultures.

Finally, these microchannels were also applied on high-density MEAs and CMOS devices [136, 164]. In image 3.5b, the high density array of electrodes can be seen un-

derneath the microchannels. This allows to precisely follows the electrical potentials and its propagation thanks to the high spatial resolution of the device.

3.2.2 Why the subcellular interfacing?

Information in the brain is processed by the extremely numerous connections between neurons. The need to study these connections, synapses, dendrites and axons remains one of the main objectives of modern electrophysiology [165]. Developing a platform that allows the study of these electrical signals has been the objective of various research teams, as presented in the previous section. Even if great advances have been done in terms of cell culture manipulation and spatially accurate electrical recordings, the recording resolution is still lacking and could be optimized. Having shown how our bio platform has been built to optimize the recording resolution, we wanted to integrate this type of microchannels to achieve very high resolution even at a subcellular level. This would allow us to follow the propagation of the signal along the axons and to study the communication between cells, even of different types.

3.3 Microchannels on NEA chip

In order to create custom microchannels on NEA chips, two methods were identified and investigated:

Direct SU-8 structuration by photolithography The first is based on a photolithography process of the SU-8 photoresist. It can be integrated at the end of the micro fabrication process using the stepper equipment.

PDMS structuration by moulding The second is based on the micro structuration of the PDMS thanks to a wafer used as mould. It can be done separately from the micro fabrication, after that the chip have been cleaved.

Both methods have advantages and drawbacks. The SU-8 is perfectly aligned with the electrode array with sub-micro scale precision, but it is a complex process and can be done only on a whole wafer. The PDMS requires precise manual alignment but it is easily fabricated and can be used even on single chips. Those key point are going to be comprehensively illustrated in the next sections.

3.3.1 Direct SU-8 structuration by photolithography

A structuration method for the SU-8 photoresist has already been effectively proved in the past from a different research team at the LAAS. The use of the stepper by single step projection photolithography gives the possibility to control the focus depth and therefore obtain buried microchannels [166]. The SU-8 is a high contrast epoxy based negative photoresist widely used for MEMS production. Also, SU-8 can be made completely bio compatible with the same coatings that were already described in the previous section [167].

In the image 3.6, the principle of projection lithography and focus depth (d_f) variation is illustrated, known as the "diabolo" effect. With projection lithography, the designed mask is projected onto a focal plane in the photoresist through the projection lens. The projection occurs with a cone of opening angle θ_0, the distance between substrate and lens (Δ_z) can be varied. Where $\Delta_{z,m}$ corresponds to a focal plane in the middle of the photoresist, so $d_f = d_{f,m}$ is the focus depth equivalent to the focus plan at half height of the photoresist. If the focus depth is shifted downward where $d_f < d_{f,m}$, it can be observed that the darker and lighter shades, representing respectively lower and higher effective exposure of the photoresist, also shift coherently. The darker zones, where exposure dose does not reach critical point $D_{exp} < D_{exp,cr}$, corresponds to the buried microchannels. Here the dissolution of the photoresist allows the correct opening of the microstructure.

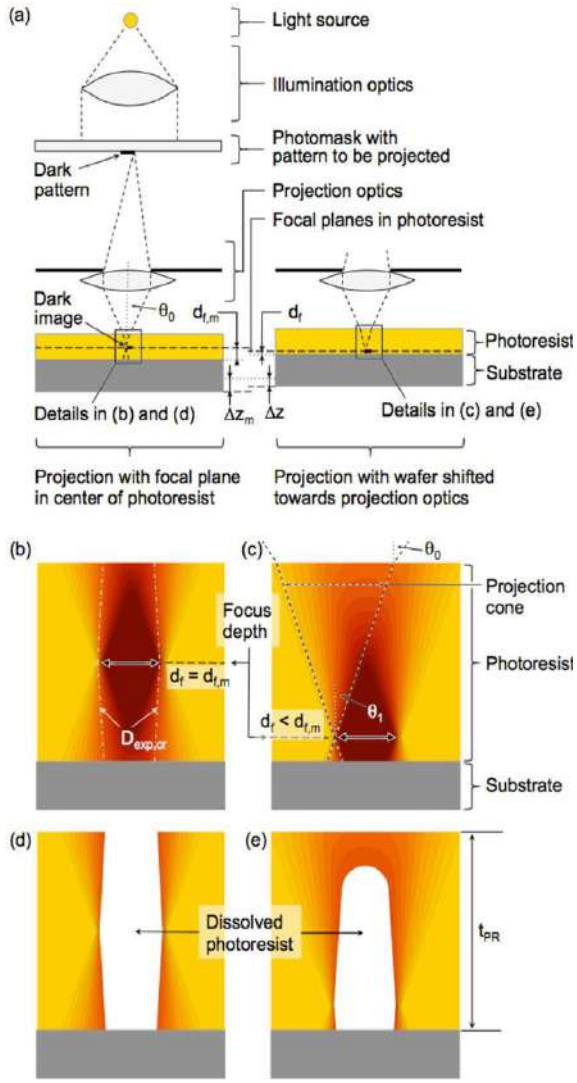

Figure 3.6: Principle of projection lithography and focus depth variation in negative photoresist [166].

Following the already acquired knowledge in this field in the laboratory and taking advantage of the equipment in the clean room, a specific mask for this study was designed and fabricated 3.7. The mask traces the classical design with two main chambers connected via microchannels, these are $10\mu m$ wide with pitch of $300\mu m$ to be aligned with the electrode array underneath. The distance between the two chambers is $1500\mu m$ therefore the channels length is of $1350\mu m$ being reduced by the V shaped opening on one side. The channel length guarantees that only the axons would be able to form connections, being too long for the dendrites. Moreover, the V shaped opening on one side, against the right angle opening on the other one, has been designed to obtain directional cell network connections. Having easier access to the microchannels on one side of the structure than the other, the axons would tend to explore the microchannel connecting to the cells on the other side. The mask design includes four rows of five electrodes equally spaced of $300\mu m$. These electrodes are already adjusted to be used with the PDMS microchannels, the electrode base is $150\mu m$ large with a total of 38 nano pillars, to compensate an eventual misalignment of the microchannels.

The photolithography process was optimized for a photoresist thickness of $50\mu m$, resulting in a microchannels height of $40\mu m$. Several tests were necessary to determine the correct focus and exposure dose parameters. The stepper can perform these tests with a single photolithography step, creating a matrix with the different combinations, 68 in this situation, of focus and exposure dose. It allows to easily find the correct set of parameters with a wide screening as shown in image 3.8a. Then perform more refined tuning was performed by reducing the screening range for both conditions. As it can be observed in images 3.8b and 3.8c, the desired result

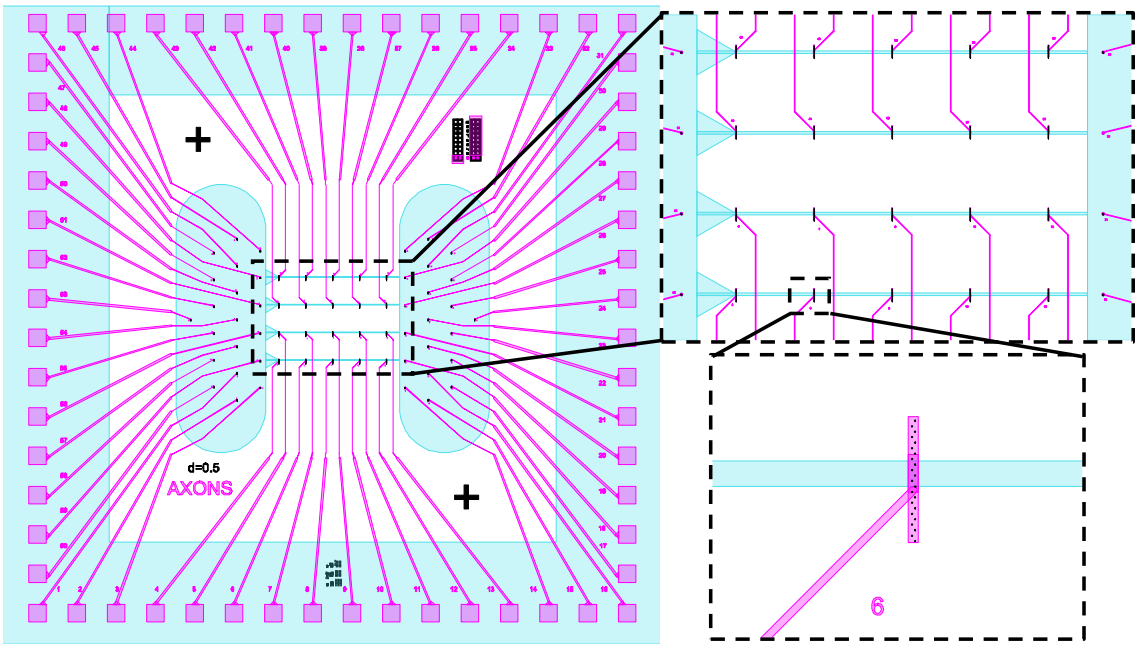

Figure 3.7: The mask design to fabricate SU-8 microchannels on an NEA chip. On the right, the zoomed details of the aligned microchannels on the electrodes.

was obtained. All the channels were correctly opened and the two main chambers were connected by them.

The main advantage of this method is the automatic alignment provided by the stepper. The projection photolithography can perform alignment down to few tens of nanometres, with a good calibration, allowing to design any type of electrode array and then perfectly connecting them through the microchannels. However, this technique also has few drawbacks. Variations in channel dimensions would require to completely change the photolithography parameters, it is a very sensible step that can easily fail if the optimal conditions are not respected. Therefore, each configuration needed a separated fabrication step. Also, this step, needing the stepper, implied the use of a full wafer and it cannot be done on cleaved pieces. Moreover, this would be a wafer at the very end of the micro fabrication process, meaning that an eventual failed photolithography step would condemn the whole substrate and several weeks of work. Because of this, it is a high-risk step, that could potentially made useless an entire substrate with functional chips.

In the interest of the project, we decided to avoid taking such high risk step at the very end of the micro fabrication process. The micro fabrication is already very complex, time and money consuming, therefore adding this step would be excessive, especially having other possibilities. Moreover, it would be interesting to have the possibility to perform different tests and use the chips also for distinct applications.

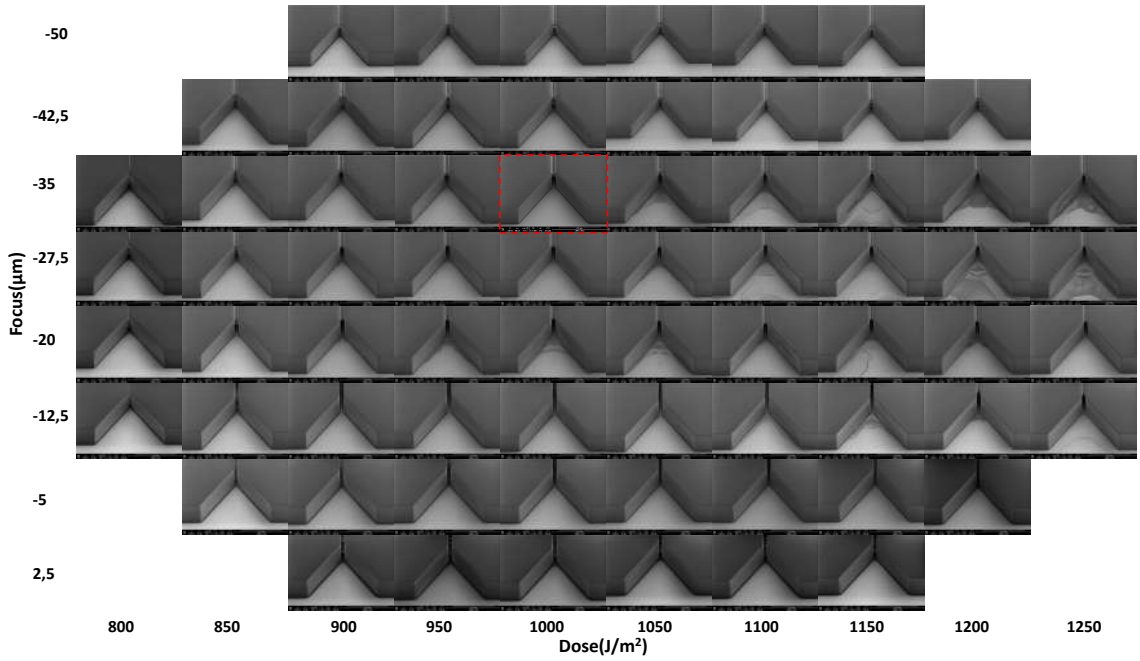

(a) SEM characterization for different focus/dose parameters.

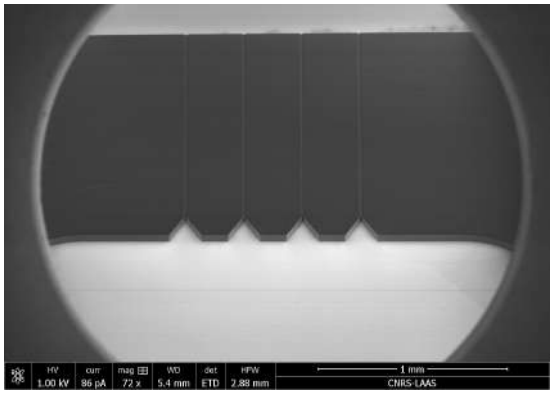

(b) The two main chambers connected by SU-8 microchannels.

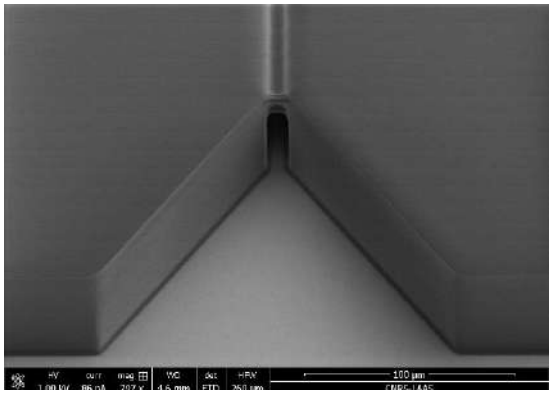

(c) SU-8 microchannel perfectly opened after photoresist revelation.

Figure 3.8: a. SEM images of the V shaped microchannel opening for each couple of focus and dose parameters. This characterization allowed to find the best conditions for the SU-8 photolithography. b. SEM image of the SU-8 photoresist after photolithography and revelation. The microchannels are $10\mu m$ wide and $40\mu m$ height. c. SEM image of the resulting SU-8 microchannel opening, its shape is given by the photolithography effect. [Scale bars inside the SEM images]

3.3.2 PDMS structuration by moulding

The alternative studied method to obtain microchannels was the structuration of polydimethylsiloxane (PDMS). As previously said, PDMS ($-[O-Si(CH_3)_2]_n-$) is a organosilicon compound largely used because of its versatility. Being optically clear, generally inert, non-toxic and bio compatible its applications range from elastomers to several medical devices.

In order to obtain a structuration of this silicon, a mould is necessary. An

easy and cost-effective way to obtain it is to fabricate it with a photolithography process. Here again the SU-8 photoresist is used because it allows to create really solid micro-metrics designs once it is reticulated.

In figure 3.9 the design adapted to the NEA chip can be observed. It has the same characteristics of the previously presented SU-8 based mask, only it is designed at inverse polarity, needing the negative photoresist to define the mould structure. Different channel dimensions were studied, from $100\mu m$ to $5\mu m$. Also, four $1mm$ circle areas were added to create the inlets and outlets for the cells and media. The square PDMS structure side had to be $5mm$ large at maximum to be compatible with the PCB, otherwise it would not be possible to get in contact with the chip. The inlets and outlets were manually created with a PDMS puncher, or biopsy punch, of $1mm$ diameter in order to obtain a clean cut of the silicon.

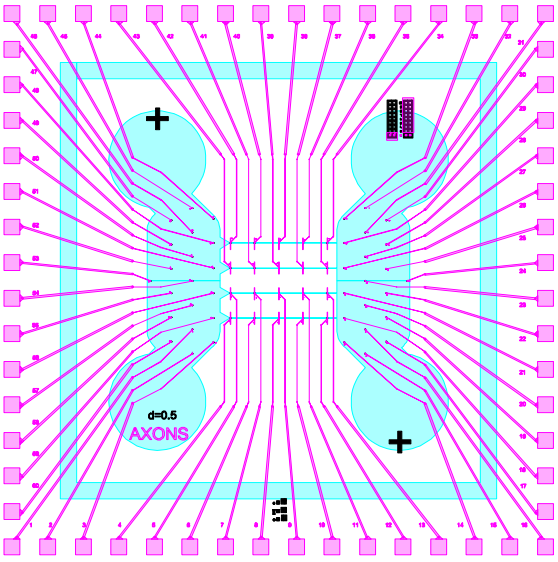

Figure 3.9: Mask design to obtain a wafer mould for PDMS microchannels.

The resulting SU-8 negative moulds were produced on a standard 4 inches wafer as it can be observed in the image 3.10a. Here the wafer is fixed inside a large plastic dish and covered by a layer of PDMS. It is then left in a furnace at 60 °C overnight to let the polymer cross-link and solidify. The PDMS system could be cut with a scalpel and positioned on a glass coverslip in order to test the correct functioning. The bonding between freshly produced PDMS and the glass happens spontaneously providing a sealed structure. If the PDMS was not brand new, the surface dangling bonds could be reactivated with a simple oxygen plasma treatment. After that, the system should rest few hours in the furnace at 60 celsius. This way it was possible to simply have numerous test samples, an example is showed in the image 3.10b. When the PDMS system was carefully cut at the correct dimensions, it was possible to integrate it on the bio platform, as previously planned. An example of the complete system composed by the chip, the PCB, the glass ring and the PDMS microchannels is presented in image 3.10c. The drawback of this method of microchannels fabrication is the alignment on the chip. It is not automatic as for the SU-8 structuration, but it has to be done manually with the help of a binocular microscope. The dimension of the electrodes, $150\mu m$ large, were designed to take account of a possible misalignment during this procedure. As it can be observed in

image 3.10d, being really careful, the microchannels can be correctly aligned. If the PDMS is meticulously cut, the dimensions are designed to fit exactly in the PCB inner hole and align on the electrode array. The worst PDMS alignment obtained was near the upper end of the $150\mu m$ electrodes, therefore it can be assessed an error around $\pm 75\mu m$ for this procedure.

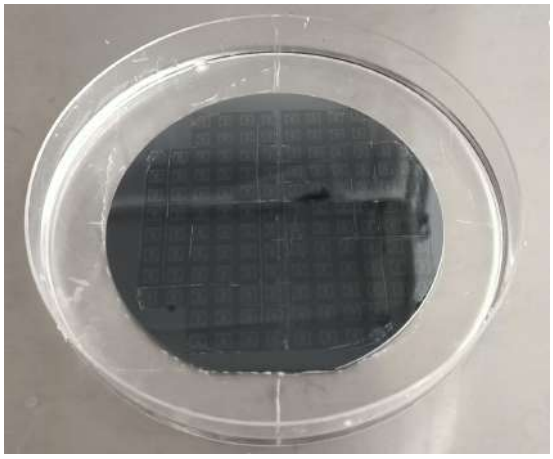

(a) SU-8 mould for PDMS.

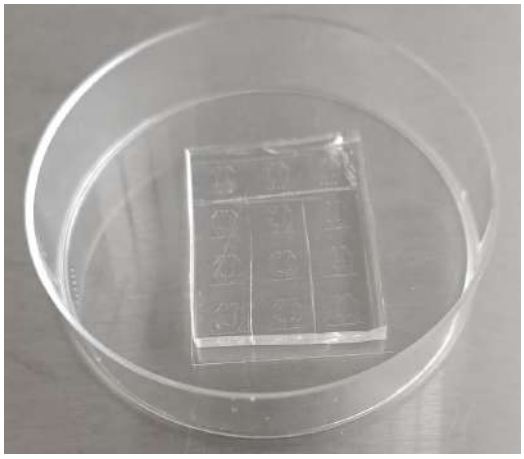

(b) PDMS test sample.

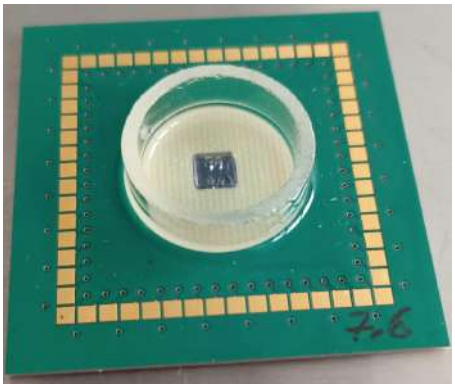

(c) PDMS system on NEA.

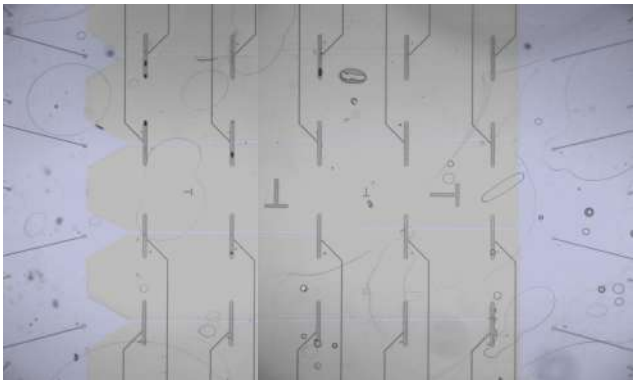

(d) PDMS microchannels on chip.

Figure 3.10: a. Photo of the SU-8 mould fabricated on a 4 inches wafer for PDMS microchannels. b. Photo of the test sample of the PDMS system bonded on glass coverslip. c. Photo of the complete NEA system with integrated PDMS microchannels system bonded on the chip. d. Colourized optical image by microscope of the PDMS microchannels aligned on NEA chip.

PDMS is commonly known to be hydrophobic, but there are different ways to make it hydrophilic. One way is to deposit a thin layer of SiO_x, or otherwise a oxygen plasma treatment can have the same effect temporarily. The second method was chosen because easily implemented and could be done punctually on single chip as well as multiples at the same time. Therefore, after the PDMS bonded with the chip surface, a treatment of 30 seconds at $0.3mbar$ and $50Watts$ oxygen plasma can make the microchannels totally hydrophilic. The only slight disadvantage is that the microchannels would be hydrophilic for only a few minutes, so this treatment needed to be done just before the preparation of the chips for cell culture. To verify

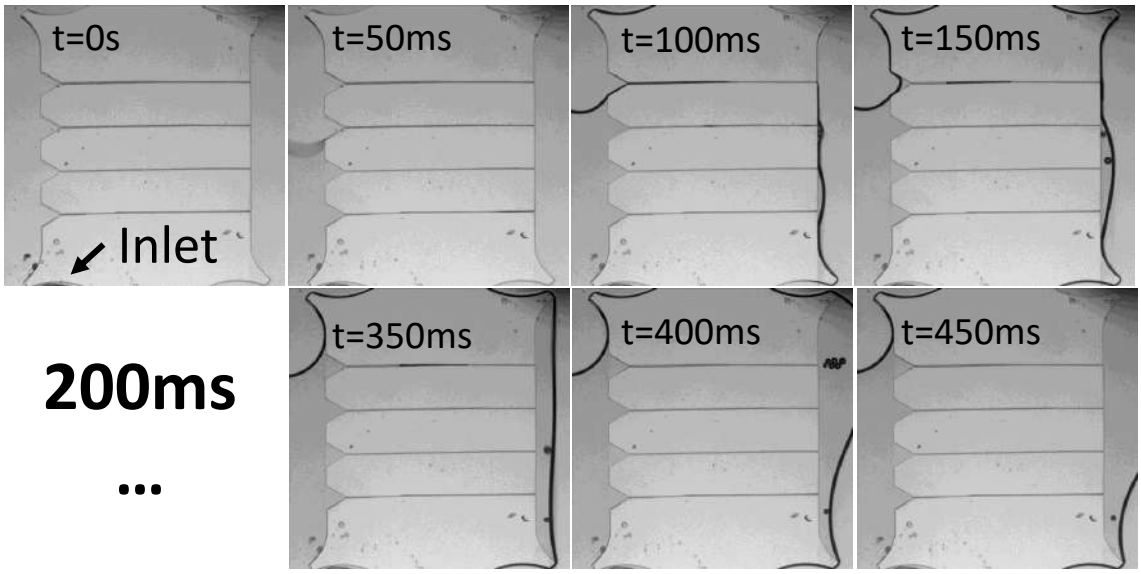

(a) PDMS microchannels with plasma treatment.

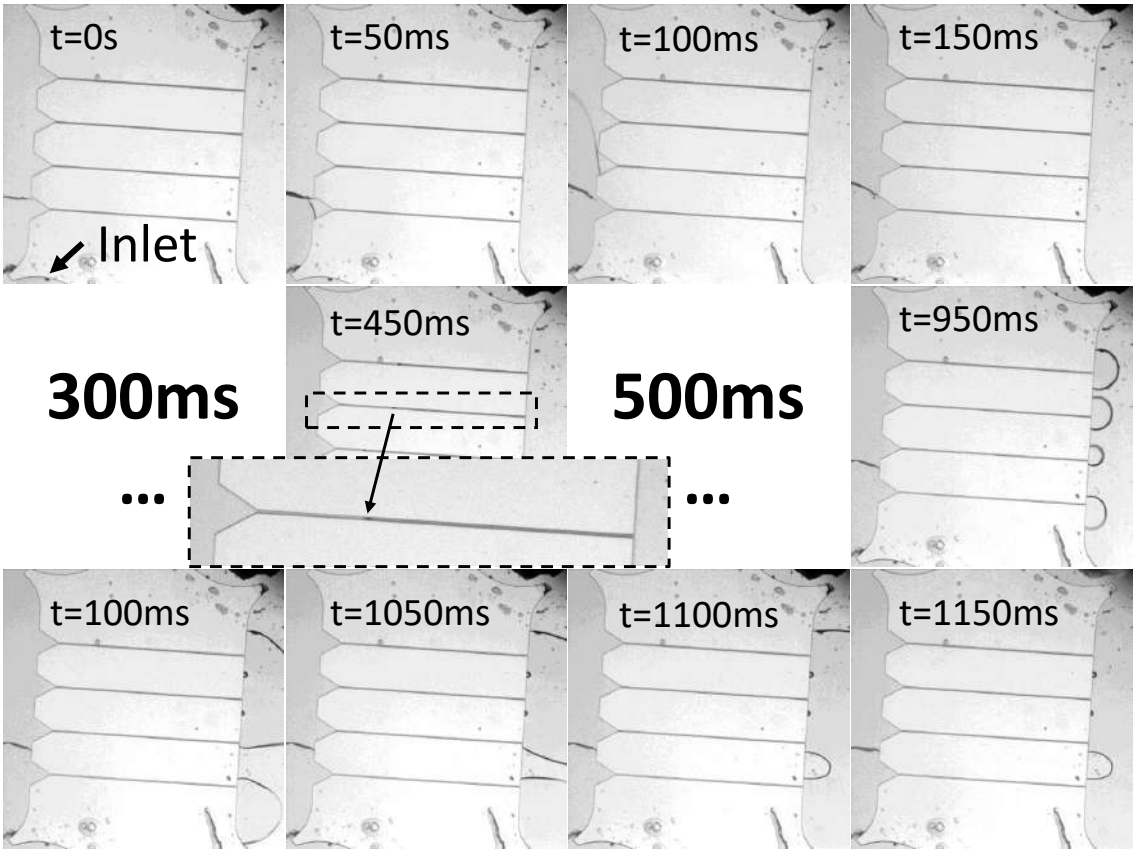

(b) PDMS microchannels without plasma treatment.

Figure 3.11: a. Optical images of the $5\mu m$ wide PDMS microchannels on glass substrate being completely filled with water in few frames being hydrophilic after a plasma treatment. b. Optical images of the $5\mu m$ wide PDMS microchannels on glass substrate without plasma treatment. It can be observed that being hydrophobic the PDMS system is much more difficult to fill with water. [frame rate of $25ms$]

that the complete system would be correctly hydrophilic, optical imaging has been done meanwhile the PDMS system was filled with water, as it can be seen in image 3.11a, all with microchannels of $5\mu m$. It was clearly more difficult to fill the exact same system, with the same channel dimensions, but without the previous plasma treatment. As it can be observed in the image 3.11b the PDMS channels need almost the triple of time to get completely filled. In particular the channels needed longer constant liquid pressure from the inlet without plasma treatment. On the other hand, when hydrophilic, the micro channels would immediately fill with the liquid. In the same manner, the coating for cell culture was then verified to be effective with fluorescence imaging.

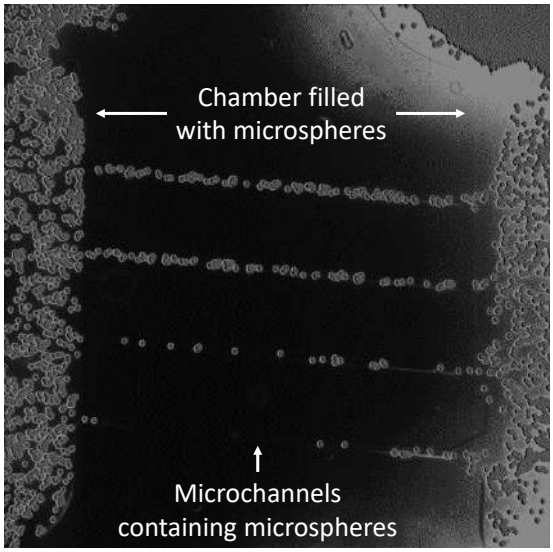

(a) $25\mu m$ wide PDMS microchannels on glass.

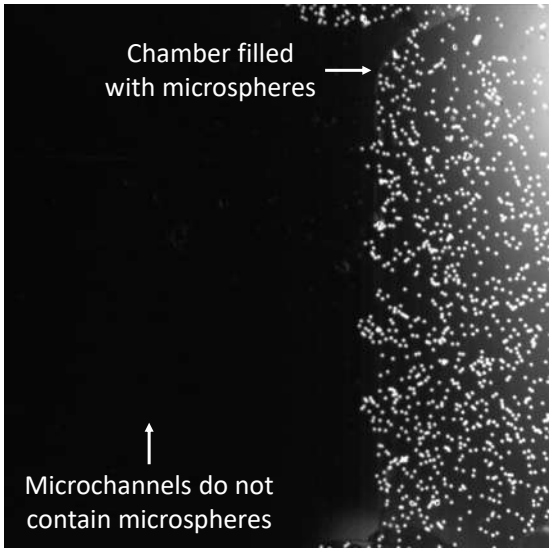

(b) $5\mu m$ wide PDMS microchannels on glass.

Figure 3.12: a. Fluorescent imaging of the $25\mu m$ wide PDMS microchannels on glass substrate being completely filled with auto fluorescent microspheres. b. Fluorescent imaging of the $10\mu m$ diameter spheres correctly filtered by the PDMS $5\mu m$ wide microchannels.

The microchannels tested were all $50\mu m$ in height but with different width. So, it was necessary to choose which channel dimensions could correctly avoid that the cellular somas enter in the microchannels. In order to verify it before the cell culture, some auto fluorescent microspheres of $10\mu m$ diameter were used to simulate the cell soma dimensions. As it can be observed in the example image 3.12a, the microchannels $25\mu m$ wide could not filter the microspheres and would fill with them both main chambers. On the contrary, the microchannels $5\mu m$ wide could correctly filter the microspheres, avoiding passing through to the other main chamber. It means that, theoretically, the cell somas would not be able to go inside the microchannels and only axons could form connections between the two chambers, as supposed to. The dimensions of the microchannels were found to be critical in height to width ratio. The microchannels a few times happened to block because of the material elasticity.

This problem can be eliminated with a reduction of the photoresist thickness for the mould fabrication.

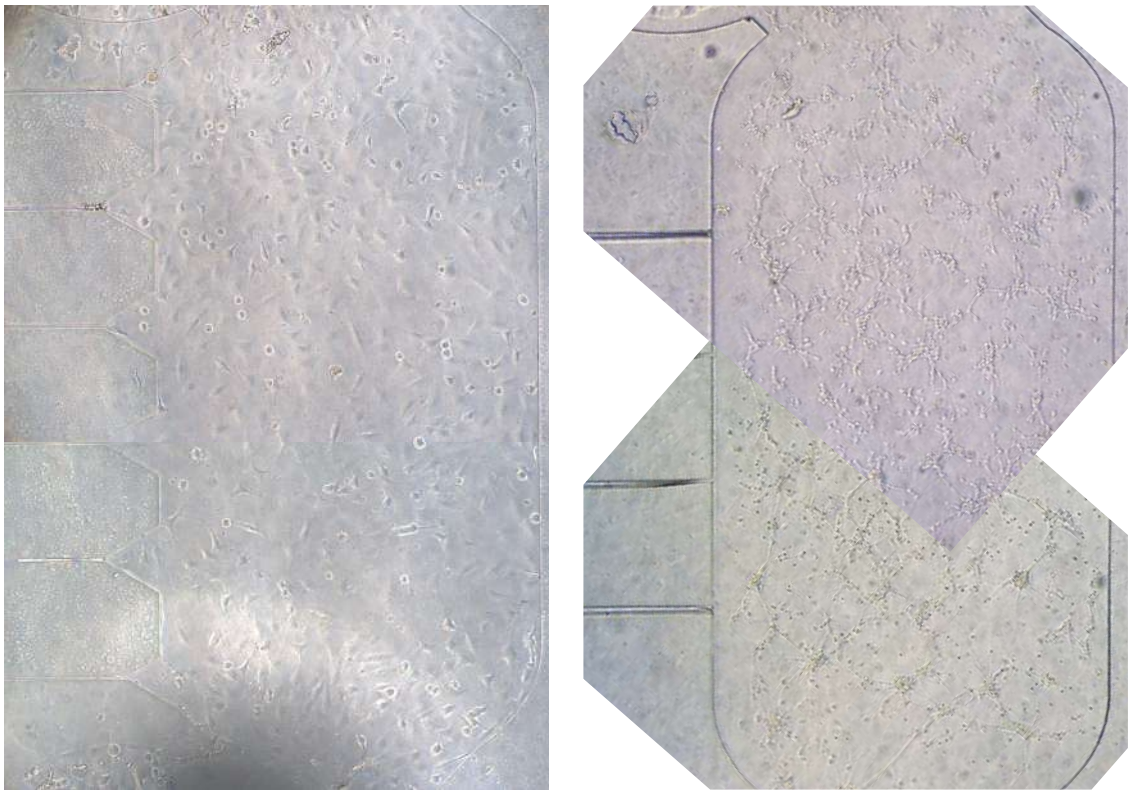

(a) SH-SY5Y cells at 3DIV in PDMS chamber.

(b) Primary cortical rat neurons at 3DIV in PDMS chamber.

Figure 3.13: a. Optical image of an SH-SY5Y cell culture at 3 days-in-vitro used to verify culture conditions. b. Optical image of the rat cortical primary cells at 3 days-in-vitro confirming that the PDMS chamber are a good environment for cell culture.

One final test before moving to primary culture was to verify that the system was suited for cell culture. In order to do it, we choose SH-SY5Y cells for a first validation. SH-SY5Y is a human derived neuroblastoma cell line that was available at the laboratory. The media used for this culture was DMEM medium with and addition of 10% FBS and 1% penicillin:Streptomycin supplements. Looking at the cell culture in figure 3.13a, it could be deducted that the cells are correctly growing inside the PDMS chamber. It confirms that the PO and LN coatings are effective and that the conditions to have a living culture are fulfilled.

The PDMS system was also confirmed to be suitable for cell culture with primary rat cortical neurons. Meaning that it guarantees a correct exchange of oxygen between cells and environment, it does not block the cells access to nutriments, it does not modify the media pH value and neither induce any other evident stress on the neurons. In image 3.13b a culture at 3DIV can be observed, all the principal network connections are being formed and the cells have a good survival rate. On the other hand, with simple optical check it was not possible to verify the connection

between the two main chambers. Therefore, cells fluorescence imaging was necessary and the culture inside the PDMS system needed to be fixed.

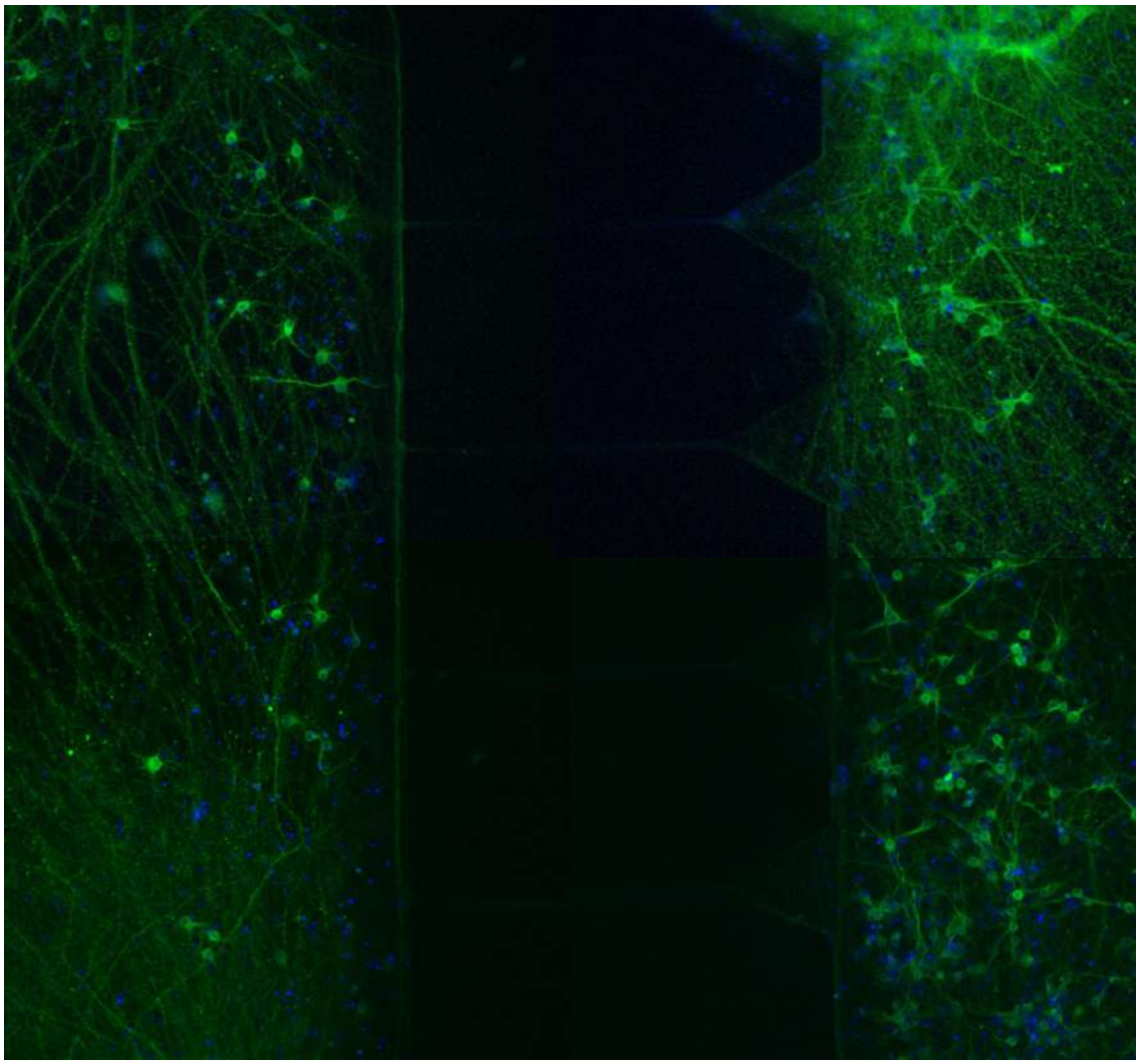

Figure 3.14: Fluorescent imaging of somas (DAPI, blue) and neurites (Phalloidin, green) inside the PDMS system. It can be observed that the axons are connecting the two main chambers via the microchannels. The cell culture were fixed at 7 DIV.

Several tests were done to optimize the fluorescence imaging, for example for the day of fixation and the protocol for the fluorescence agents. The DAPI fluorescent stain was chosen to mark the cells somas because it binds to the nucleic acid of the DNA passing through the cellular membrane. The Phalloidin Alexa Fluor 488 was also chosen to mark the cytoskeleton of the neurons, these molecules binds to the F-actin proteins. The long axonal connection between the two chambers was found to actually need at least 7 days-in-vitro to be effective. Hence, the image 3.14 was done after culture fixation with formaldehyde at 7DIV. The fluorescence is rather weak in the microchannels, but the PDMS system behaves as supposed and allows to condition the network connection between the cells. In the image 3.15 it is possible to see the detail of the axon entering the PDMS microchannel.

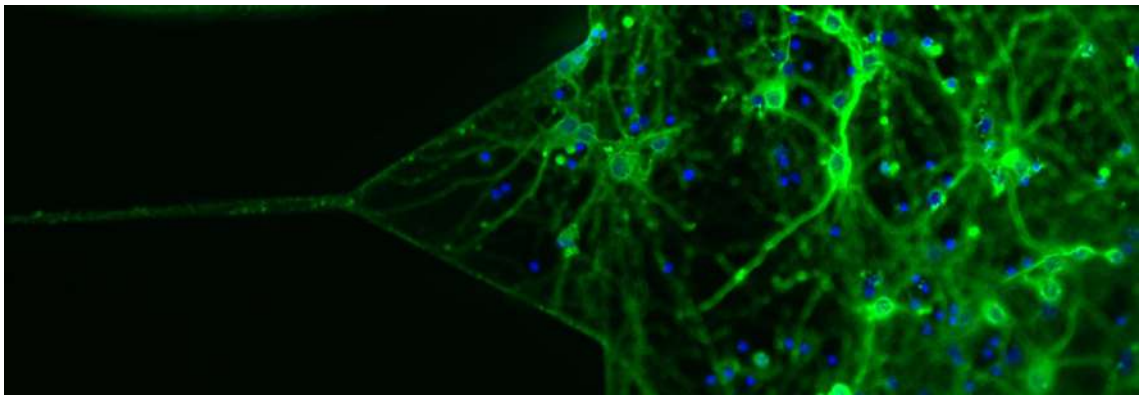

Figure 3.15: Fluorescent imaging of somas (DAPI, blue) and neurites (Phalloidin, green) inside the PDMS system. Details on the channel entrance with the axon growing inside it. The cell culture was fixed at 7 DIV.

Microchannels discussion

The comparison between the two method of microchannels fabrication is here summarized in the table 3.1. As previously said, the SU-8 fabrication has the advantage of being done by photolithography. It means that with just one micro fabrication step a perfectly aligned series of microchannels would be positioned on the electrode arrays. On the other hand, even if the large-scale compatible process is an advantage, it can be useful to run some test samples as single unit and not use an entire wafer each time, because of the long time needed for the entire process. These key points are reversed for the PDMS structuration. The PDMS has to be manually aligned, which is a complex method, but because of the easy samples production, numerous tests can be performed to improve all the parameters. Moreover, the PDMS is biocompatible and bonds naturally with the oxide surface of the chips. A critical drawback is that the channels may block because of the elastic nature of the material, improvements in these terms could be achieved changing the height to width ratio dimensions.

Unfortunately, we never had the possibility to test the PDMS microchannels on a working chip. It would have been great to measure the signal transmission along the axon connecting the two chambers and study the synchronization of the two main cell cultures. Many other uses for this system could be foresee, as the study of communication in a co-culture or the effect of different perturbation introduced only on one of the two PDMS chambers.

SU-8	Advantages	Drawbacks
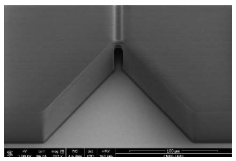	• Automatic alignment with nano metric precision • Large-scale fabrication via photolithography	• High risks, final micro fabrication step • Only doable on a not cleaved wafer
PDMS	Advantages	Drawbacks
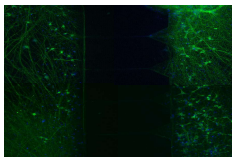	• Easy fabrication with wafer mould • Naturally biocompatible material	• Complex manual alignment, $\pm 75 \mu m$ error • Channels could block because of dimensions ratio

Table 3.1: Summary of the presented state-of-the-art devices with focus on the technology and use.

Chapter conclusion

In this chapter the cell culture protocol for primary rat cortical neurons on NEA chip was presented. This protocol resulted in very consistent long period cell culture that allowed to realize several studies that are presented in the next chapter.

Also, the strategies to create controlled network of cells of already published works was presented. From this knowledge, the photolithography masks were designed to investigate two different possibilities in order to obtain microchannels. Those have been fabricated via the peculiar "diabolo" effect obtained with the projection lithography using SU-8 photoresist. This approach guaranteed an automatic alignment of the microchannels on the electrode array of the chip but being a high risk step it was decided to not chose it as definitive solution. A second approach was presented, the micro structuration of PDMS with a mould wafer, once again obtained with a photolithography step of SU-8. This method was extensively investigated and the possibility to correctly conduce long term primary neurons culture was verified, as well as the axonal connection between the two main chamber of the PDMS system.

Chapter 4

Theoretical modelling and application to biological studies

To perform measurements of neuronal electrical activity, a very sensible setup is needed. The control of this setup and the experimental conditions are fundamental. The experimental setup is described in the first part of this chapter with the home-made electronic card and software. Then, some examples of spontaneous electrical recordings will be presented with the analysis of the bio platform performances and possibilities. The cell electrode interaction model and its simulations are also described. A semi-automatic algorithm wrote with MATLAB is used to perform the spike detect from the electrical recordings and allowing statistical analysis of the results. These instruments presented in the first part of the chapter are then used to investigate the behaviours of biological cells in some particular conditions: being influenced by the Amyloid Beta Peptide and the Borna Disease Virus.

4.1 Electrophysiology recording system

In order to record the electrical signal from a cell culture, a dedicated setup is needed. The experimental setup had reserved place in one of the laboratory rooms, it can be observed in photo 4.1. It includes a computer, where an home made software allows to control and guide the experiment, a furnace, where the chips are placed once outside the incubator, and the recording setup. Some precautions are needed for this type of measurements: the preservation of cells conditions and the minimizing of electrical noise. To ensure a minimal external electrical noise, the desk is shielded with a metal plate, connected to the building electrical ground, where all the ground terminals of the entire setup are also connected. Moreover, the chip is placed inside the furnace, and its metal exterior is also connected to the ground. In the furnace the temperature can be controlled and it is kept at 37 °C and the atmosphere CO_2

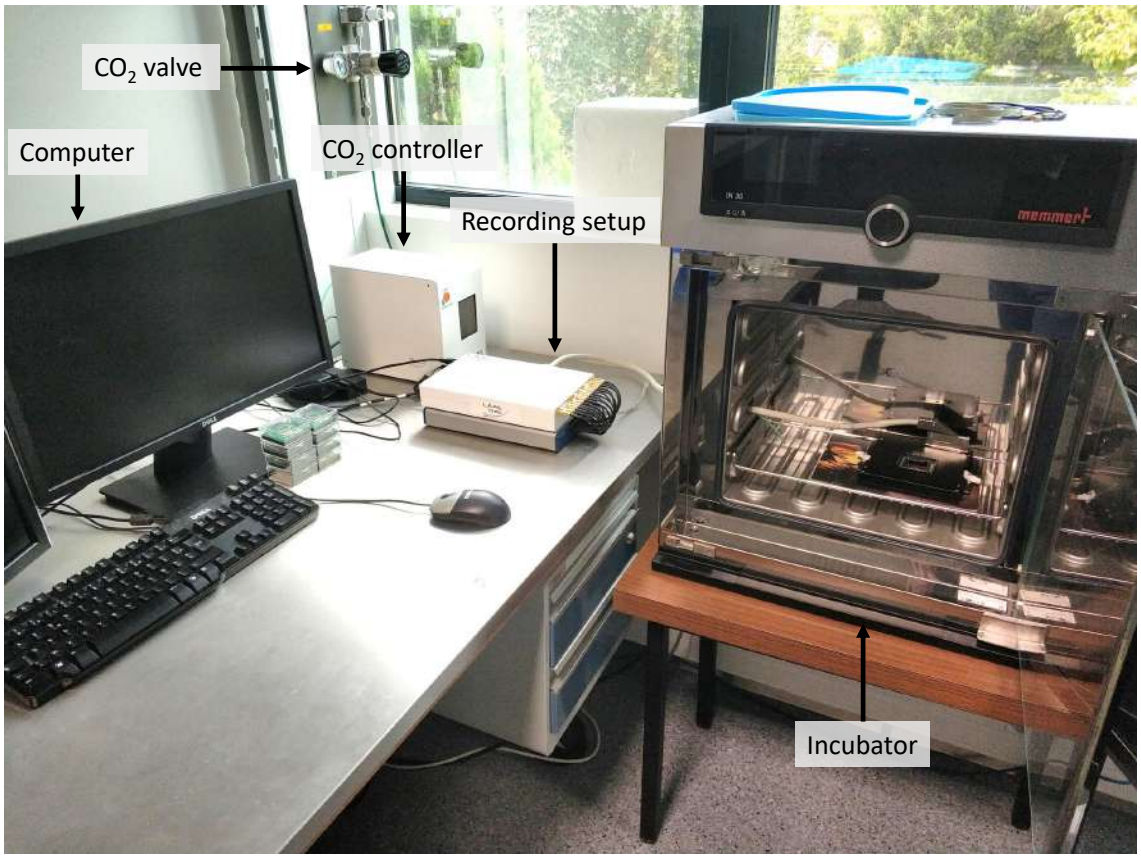

Figure 4.1: Photo of the experimental setup dedicated to the electrical recording of neuronal activity. From left to right, the computer to control the setup, CO_2 delivery system (valve and controller), the recording setup and the furnace.

concentration is also controlled and kept at 5%.

The one described here is the last evolution of the setup. Before that, over the duration of the project, we passed from having the possibility to record only three electrodes at the same time, to six with two channels to record current from the transistors. The evolution of the system was based on the evolution of the electronic cards (last one called multiplexer), that increased in size and complexity with each iteration. The work of the electronic research engineer Mathieu Fabrice was fundamental to the project for the realization of the setup. This multiplexer has been designed taking into consideration numerous key points, that are later explained, but in particular to be adaptable to any type of device design. This aspect is fundamental because it allowed to not put any limitation in the chip design, which is a great advantage.

The schematic description of the recording setup can be seen in the image 4.2. Inside the furnace, the chip is placed in a commercial MEA holder (MEA 1060-Inv-BC) from Multichannel System, this holder does not contain any form of amplifiers or filter built inside. The choice was made in order to be able to design a home-made electronic card with the desired filtration and amplification functions. The holder

is connected to the electronic card, called multiplexer, via a SCSI cable with 64 channels. The multiplexer is the home-made designed electronic card that allowed us to customise the measurements, later described with more details. Then, it is connected with a maximum of 16 cables to an acquisition card from National Instruments (USB-6353) which allows us to record up to 1 million point per second globally. This card also guarantees an extremely low level of crosstalk, an unwanted transfer of signals between communication channels, at $-75dB$. Both multiplexer and acquisition card are connected via USB to the computer that control the setup where a home-made software coded with LabVIEW is installed.

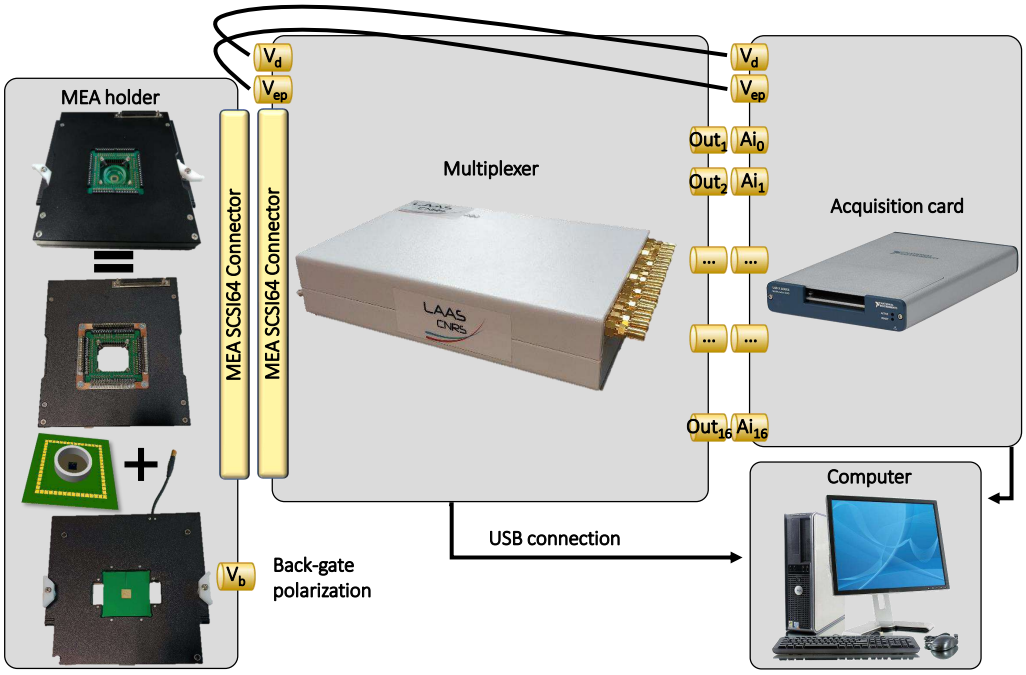

Figure 4.2: Setup main elements and their connections.

The electronic card is the part of the setup that has most evolved during the project, from more simple electronic cards with few channels (three or six for tension measure and one or two for current measure) we managed to design and realize a much more complete multiplexer thanks to expertise of the engineer working on the project. Inside the multiplexer a complex system of more than a thousand elements has been designed and soldered to two printed circuit boards, its schematic representation can be seen in image 4.3. The most relevant elements in the multiplexer are the first multiplexer inputs and the amplifiers and passband filters. The multiplexer input elements are CMOS analog matrix switches (ADG 1438) that have been chosen because of their very low series resistance at 9.5Ω that would not modify the recorded signal from the chip electrodes. This element connects each of the 60 inputs to 5 possible channels: potential measurement, current measurement, two potential stimulations or the ground connection. For the measurement channels the

following element is the amplifiers (ADA 4000). This amplifier is chosen because of its very high input impedance at $10G\Omega$, it prevents the creation of a tension divider and the lowering of the recorded signal. For the voltage measurement, the amplifier is used as an operational amplifier of gain equal to 1, that does not modify the recorded signal. For the transistor current measurement, the amplifiers are used as transimpedance amplifiers with a gain (k) of $-10^5 A/V$. In series with the amplifiers a passband filter is used, filtering the frequencies below $0.7Hz$ and above $30kHz$. The low frequencies are filtered to avoid static polarization to drift the measure baseline and the high frequencies are filtered because not relevant and allowing to reduce the electrical background noise. From here, the channels are then connected to the 16 channels of the acquisition card. Therefore, the multiplexer allows us to address each of the 60 contacts on the chip to 5 different channels and then to the acquisition card. This way, we could choose to perform on each contact the needed measure (transistor current or electrode potential) or polarization (V_{ds} or V_{gs} and eventual electroporation), independently from the chip design that could be modified in future generations of the bio platform.

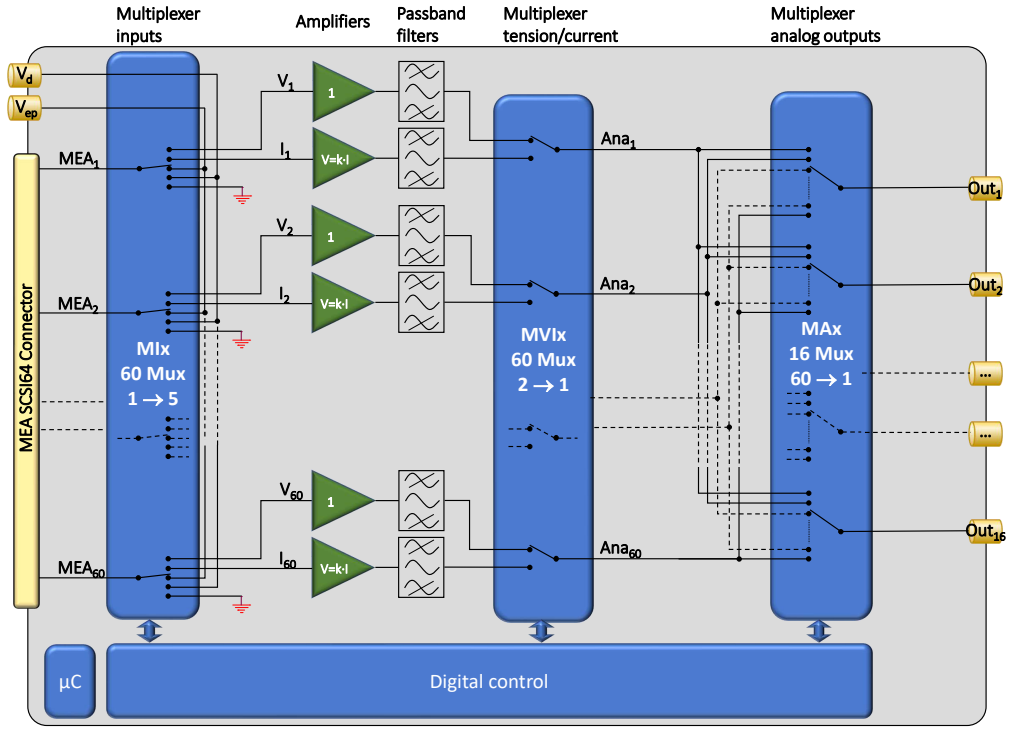

Figure 4.3: Schematic representation of the multiplexer PCB design. From left to right, the SCSI connection and two channels dedicated to electrical stimulation, the first multiplexer level (1 to 5 connections), the amplifiers and passband filter, the tension or current measurement switch and the final multiplexer level (60 to 1 connections).

Multiplexer and acquisition card are connected via USB to a computer. Here a software coded with LabVIEW allows to control the multiplexer, choosing the configuration of the different channels, and the acquisition card to determine the

acquisition data rate, the polarization range and save the recorded data as TDMS files. The advantage of this file format is that being mostly binary it can store large amount of data in a relative small size file. Moreover, it is already structured in data set and channels, so that it can be easily read. The polarization range is particularly important because it can help reducing the noise. The acquisition card is a 16 bits model, meaning it can divide the chose polarization range in 2^{16} steps, therefore taking a measure range of $200mV$ polarization ($\pm 100mV$ is the minimum for the acquisition card) would optimize the recording conditions. Increasing this range would just the influence the measurable amplitude step in tension, without providing any additional information, and increasing the background noise.

The setup possibility to correctly measure the I_{ds} current in the transistors was tested by applying a $V_{ds} = -100mV$ and varying the V_{gs} polarization in the liquid, with the on chip reference electrode, between $-100mV$ and $-400mV$. As it can be

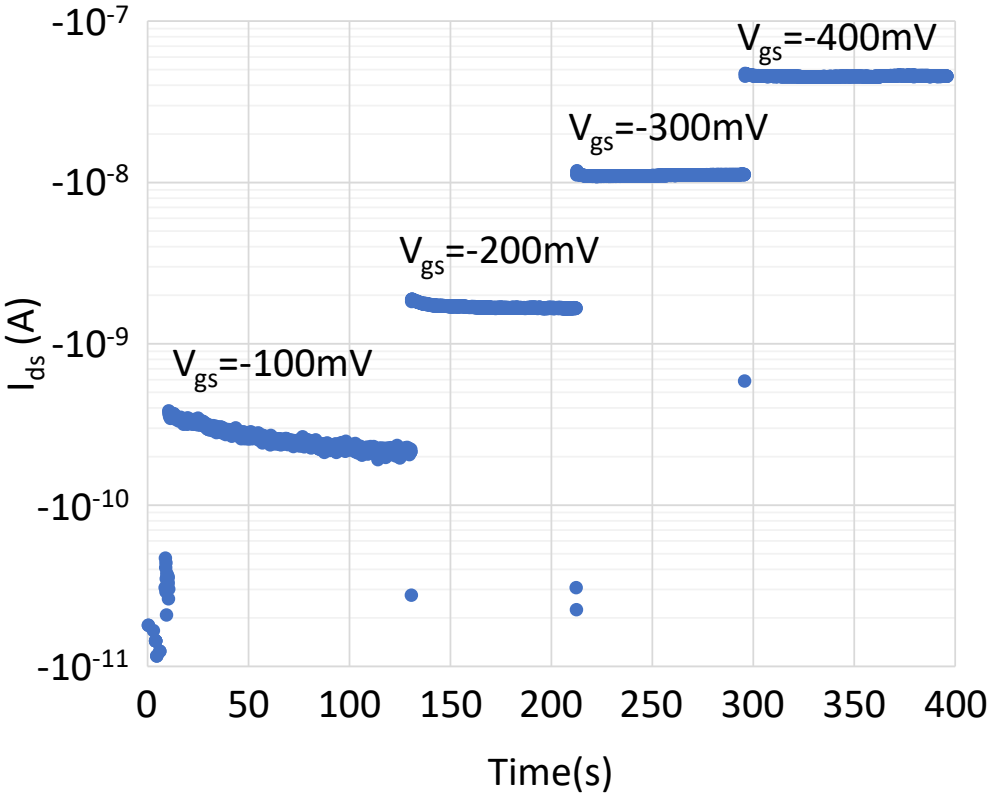

Figure 4.4: Measure of the transistor I_{ds} current with the multiplexer for different liquid gate polarizations.

observed in image 4.4, the current increases with the gate polarization as expected. The variability for $V_{gs} = -100mV$ is probably due to the very low level of current, above $1nA$. At ideal condition the recording setup has a limit of detection around $100pA$, considering the use of the chip in liquid and with biological samples that is why we choose to use the transistor with a minimum of $1nA$.

The recording setup also allows to measure the amplitude of signals coming from the passive electrodes. As it can be observed in the image 4.5, the electrical background noise without any signal treatment is at $120\mu V$. It corresponds to the red plot at the top and the normal distribution standard deviation on the left. In order to improve it a moving average, with a window of 10 points, can be implemented. It allows to greatly improves the signal to noise ratio reducing the last one to one third of its original value, at less than $40\mu V$. It corresponds to the blue plot and the standard deviation analysed on the right of the same image. The moving average

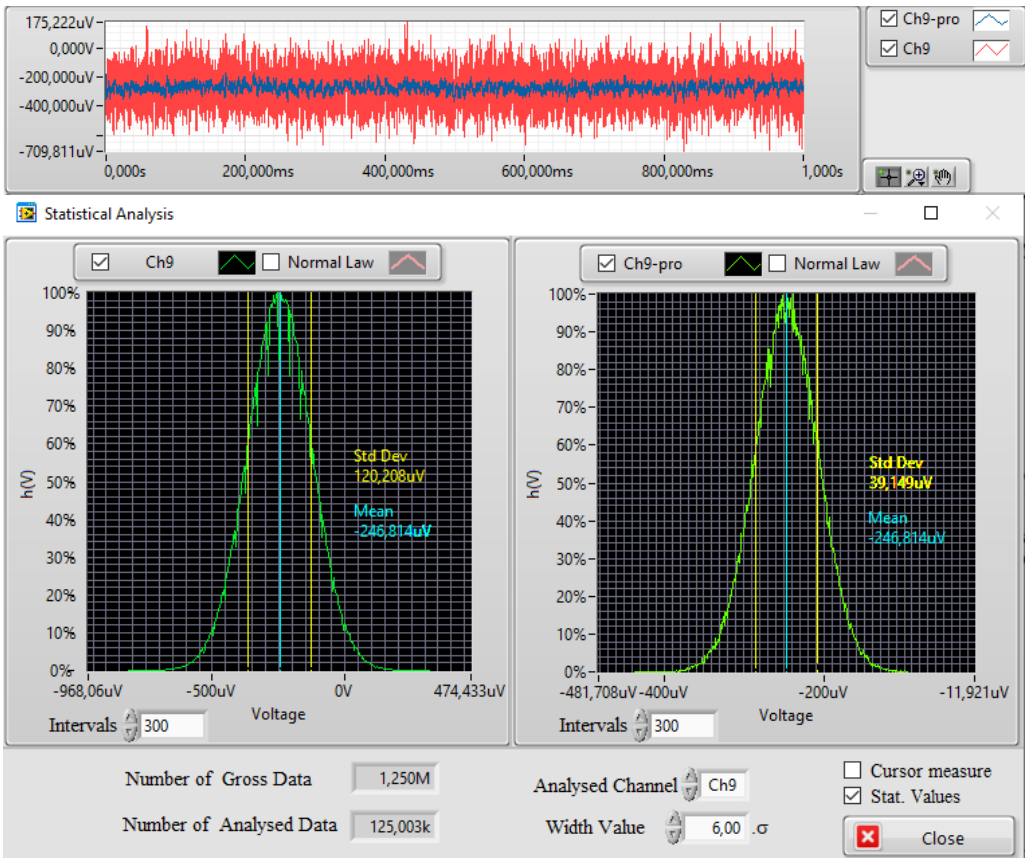

Figure 4.5: Measure of the electrical noise of the recording setup and improved signal.

is used because it act as a low pass filter, reducing the noise of the measure. It is necessary to use it carefully to not impact the amplitude of recorded spikes. One last post treatment of the signal is the application of a $1Hz$ high pass filter to shift the plots exactly around zero and simplifying the data analysis. Together with the analogical high pass filter integrated in the multiplexer it results in a second order filter.

4.2 Electrical recordings

The bio platform focus is therefore to perform accurate electrical recordings of the cells activity. This activity can be a spontaneous one, obtained by the cells typically around the fourteenth day-in-vitro (DIV), when the maturation switch is reached. The spontaneous activity is often used as a baseline for the study of any sequent modification. Here are presented some examples of typical recorded spontaneous activity on the chip, the performance of the device and the possibility to record synaptic potentials. Also a necessary validation of the device has been conducted chemically silencing the culture activity and then reactivating it and performing chemical stimulations.

4.2.1 Spontaneous recordings

Once the chips are ready, finished the micro fabrication, packaging and characterization, it is possible to use them and verify the performance of the bio platform. A last preparation step is needed after packaging, a glass ring is fixed on the PCB to be the culture well with a thin layer of polydimethylsiloxane (PDMS), a silicon largely used for its versatility and biocompatibility qualities. The details regarding cellular culture materials and methods are described in the next chapter. Here, some examples of the passive nano probes used with primary rat neurons to verify the performance of the system. Also a validation of the complete recording system is shown in a next section.

To verify the performances of the nanoprobes, a limited analysis to few electrodes was used each time, focusing on the spontaneously active ones. The example of parallel recordings of six electrodes during five minutes is shown in image 4.6. The amplitude axis is fixed on the same value for all the plots to better compare the difference in recorded amplitudes. These are the traces from six electrode in a square array with a distance of $100\mu m$ between each electrode. In the trace in the fourth plots the activity of an active cell in contact with the electrode itself is visible. The peaks in the plot reaches more than $4mv$ of total amplitude in different cases, showing the capability to easily outperform standard MEA devices. Some smaller peaks are also visible in the fifth and sixth plots, possibly due to the transmission of the signal along the cell extensions or as recorded signal from other cells further positioned. Also, in the first three channels smaller signals, around $500\mu V$, can be identified from the background noise. This plot shows how a single passive nano probe electrode can have a really high sensitivity and at the same time being completely insulated from the other nearer electrodes avoiding electrical crosstalk. The activity recorded on the other electrodes, even if less important, is still well distinguished from the electrical background noise.

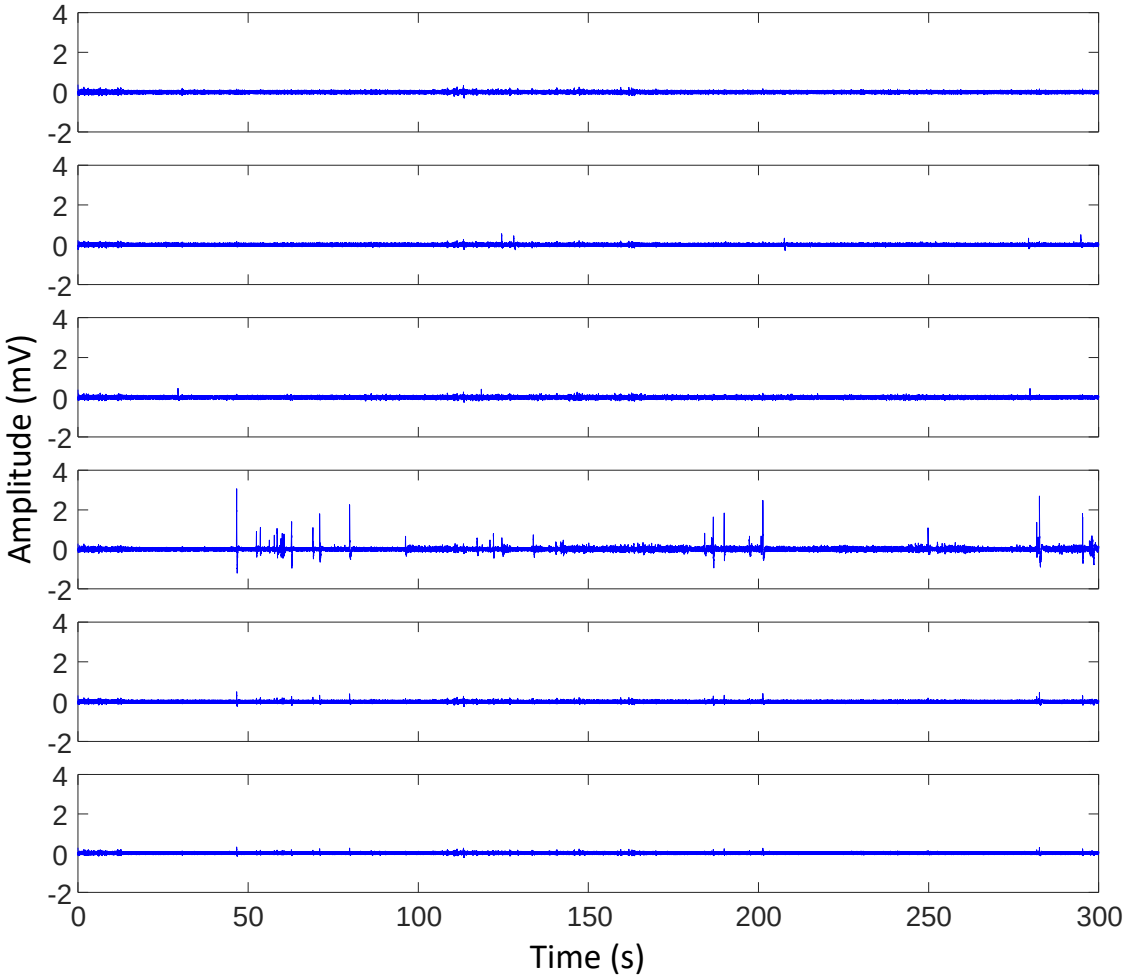

Figure 4.6: Example of a recording with six passive nano probes from a spontaneously active primary rat cortical neurons culture at 14 DIV. The activity of a cell in contact with an electrode can be observed in the fourth plot. Signal transmission, or activity from further cells, can be identified as smaller signals in the other channels.

The level of resolution of our nano probes is shown with a second recording example of a cell spontaneously activating (4.7). Three high amplitude peaks are recorded by an electrode on the chip, and a series of smaller peaks can be also identified. The magnification of the trace in the image allows to see that what could be identify as electrical noise in the first plot is in fact a recording of a series of peaks with an amplitude around 300 to 500μV. Those signals being recorded just before a major peak can be identified as pre-synaptic potentials leading to the activation of the neuron. Remembering the 40μV background electrical noise the signal-to-noise ratio is above 100 for these major spikes.

From the recording obtained with our bio platform, the average amplitude of the major peaks was usually well above 1mV, result which confirmed the theoretical state-of-the-art ([55]) expected performances from the electrode characterizations. Moreover, the electrode resolution gives the possibility to investigate the pre- or

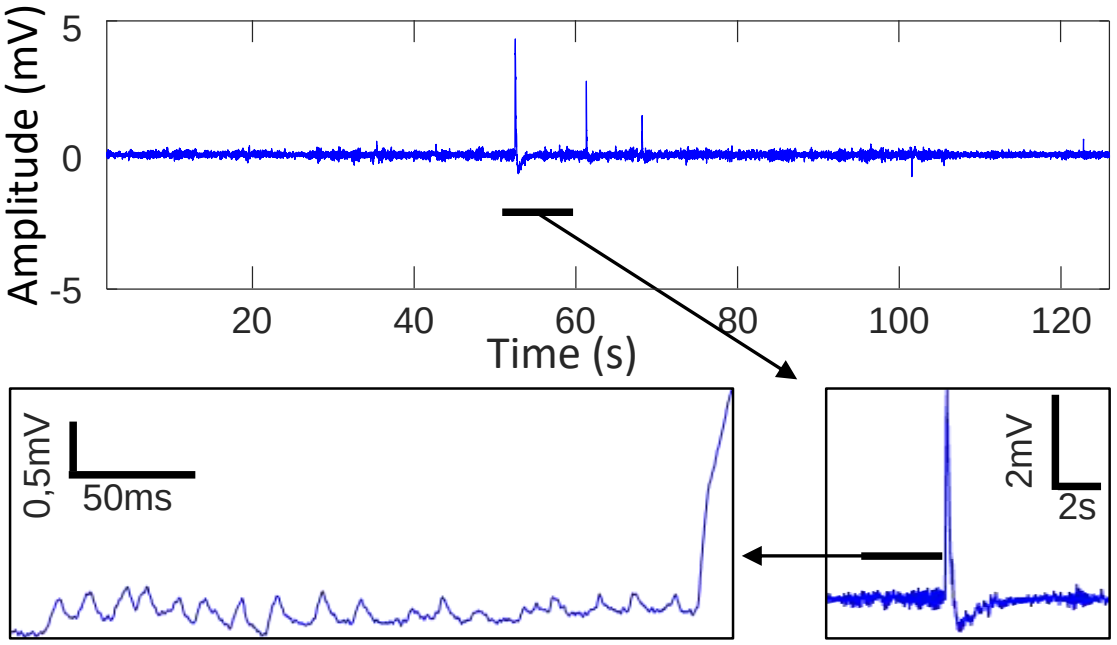

Figure 4.7: Example of a recording from a primary rat cortical neurons culture at 14 DIV with high amplitude peaks and the details of a smaller recorded activity that can be identified as pre-synaptic potentials.

post synaptic potentials (PSPs), much harder to identify as usually drowned in the background noise when the sensitivity is not optimal, as in commercial devices. This is important for the study of the communication in a neuronal network of cells, these classically invisible signals could help to deepen our understanding of the cell basic mechanisms.

4.2.2 Recording setup validation

The recording setup already demonstrated possibility to obtain high resolution recordings with great sensibility. In order to further confirm the validity of the recorded signal a methodical validation was needed. To perform it, a chip with cells at 16 DIV and a regular spontaneous activity was used.

The protocol was based on the use of three chemical compounds:

TTX Tetrodotoxin, it is a potent neurotoxin, the name comes from the Tetrodon(Fugu) fish that carry this toxin. In neuroscience it is classically used because it is a selective inhibitor of voltage-dependet Sodium channels.

APV It is a selective NMDA receptor antagonist that inhibits the glutamate ligand binding NMDA receptors. Also used to isolate the action of other glutamate receptors, as the AMPA receptors.

CNQX Cyanquixaline, it is an antagonist of the AMPA and kainate receptors often

used in electrophysiology. Similarly to the APV it is used to isolate activity of other receptors.

The cocktail of these drugs guarantee the cell culture to be silenced in a few minutes and until rinse of the media. A very important point is that these drugs have completely reversible effects if rinsed away from the cell culture, not influencing permanently the activity of the cells. In the image 4.8, it is possible to see how the regular spontaneous activity of the culture was completely silenced by this drug cocktail, from the first to the second plot. Moreover, in the third plot, once the cell media is rinsed and the complete neurobasal media is used again, in a few minutes the activity is back to normal. To measure the baseline, or spontaneous activity, of the first plot, the complete neurobasal media was substituted with Tyrode solution ($NaCl$ $119mM$, KCl $5nM$, Hepes $25nM$, $CaCl_2$ $2mM$, $MgCl_2$ $2mM$). And to block the neuronal activity a Tyrode solution with the addition of the drug cocktail was used (Tyrode with APV $50\mu M$, CNQX $20\mu M$ and TTX $1\mu M$).

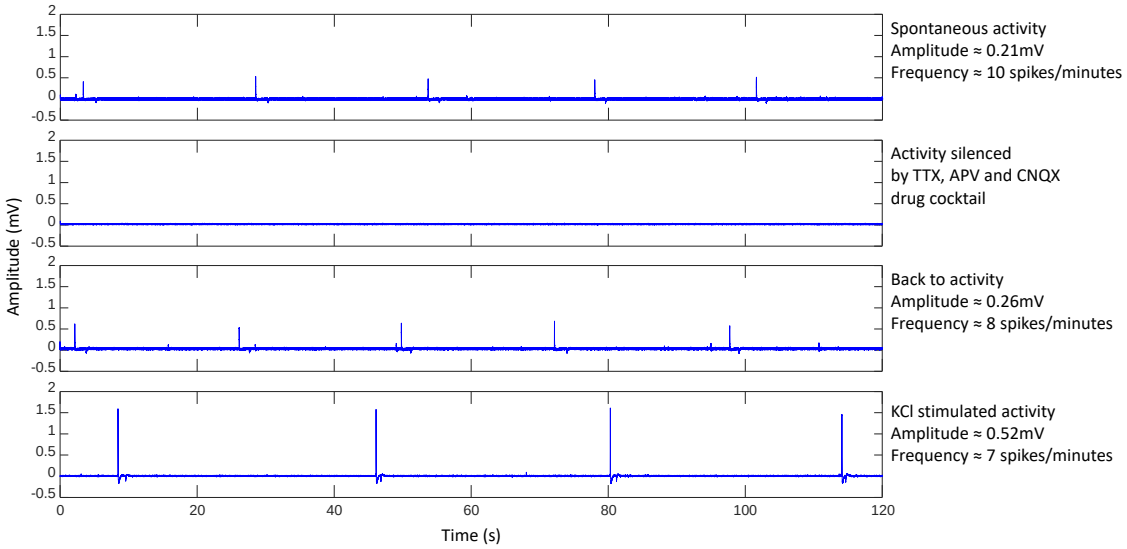

Figure 4.8: Example of a series of recordings on a primary rat cells culture. First, the spontaneous activity, or baseline, followed by the electrical activity silenced by a drug cocktail. The activity comes back to normal if the drugs are rinsed away, and the effect of KCl chemical stimulation can also be observed at 16 DIV.

After that, a depolarization was induced on the cell culture using a highly-concentrated KCl solution ($NaCl$ $54mM$, KCl $70nM$, Hepes $25nM$, $CaCl_2$ $2mM$, $MgCl_2$ $2mM$). These solution is left few minutes on the cells and it is then rinsed. The purpose of this type of chemical stimulation is to generate a concentration gradient in K^+ ions between the inside and the outside of the cells, leading to a large entry of these ions and an increase of the intracellular potential. These triggers the cell network to strongly activate to recreate the equilibrium in ions concentration. Once again in Tyrode, the cells have an activity increased in amplitude, as expected

with this treatment.

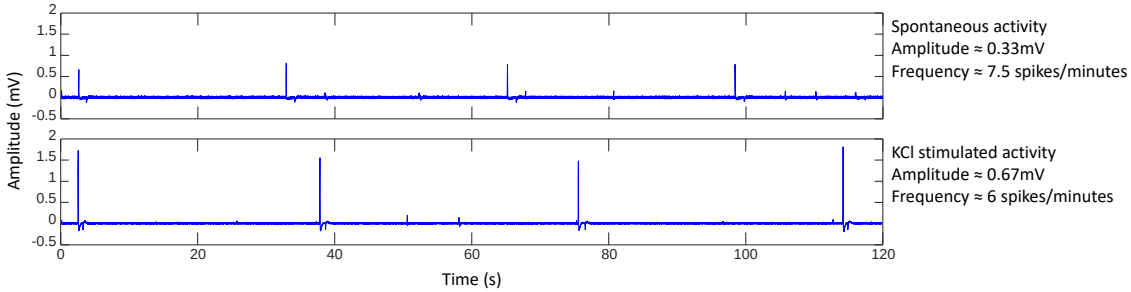

Figure 4.9: Example of a recording, of the same previous culture, at 17 DIV, the baseline was back to normal activity and the response to KCl stimulation was still strong.

The same chemical stimulation with KCl solution was repeated for the following day at 17 DIV to further confirm the previous results. Coherently, the recorded spikes were higher in amplitude both in Tyrode media, to assess the baseline and after the chemical stimulation as shown in image 4.9. This experience was done concentrating on the activity of electrodes where spontaneous activity could be originally found and monitoring its evolution. In particular, the recording shown in the plots are from the same electrode on consecutive days.

This culture was then used to pursue this study verifying the impact of the KCl stimulation over several days and, at the same time, have a first insight of the cell lifespan on the bio platform with this kind of protocol. As it can be see by the plot in image 4.10, generally both spike amplitude and frequency where increasing with each day of chemical stimulation. The experiment where paused for a couple of days because each time that the media is changed the cells can be subjected to stress. Giving the time to the cell culture to recover a normal spontaneous activity allowed us to repeat the stimulation procedure and validate both the results and the methodology. The data variability can be justified with the small amount of electrodes recorded. At the time of the experiment the multiplexer was not yet developed. Therefore, being complicated to obtain data from all the electrodes, only a small part of the electrodes were used for this study. In particular, the measurements concentrate on the electrodes with evident spontaneous activity in the first recording days. To end the experiment, the measurement were done until 30 DIV of the cell culture, assessing a long term possibility of 2D low density cell culture in the bio platform.

With this experiment, we proved that the electrical recorded activity could only came from the cell network. Otherwise during the period when the cell culture was supposed to be silenced, any other signal source or perturbation would have been measured. Moreover, it was proved that a simple treatment as the KCl stimulation and its result can be detected by the bio platform. It demonstrates that if some

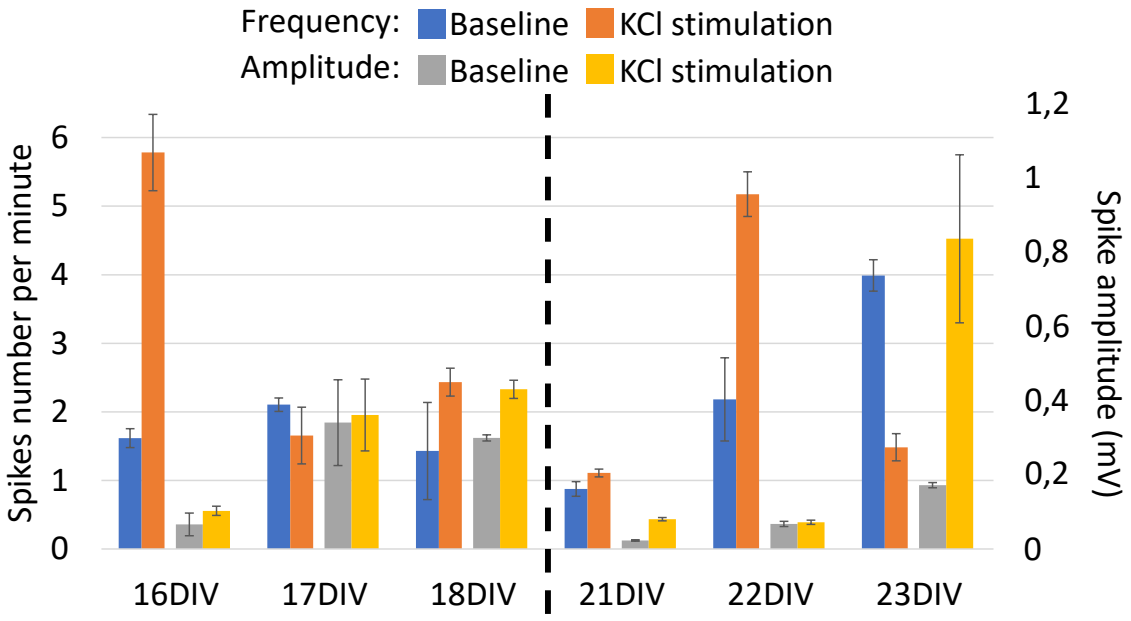

Figure 4.10: Results of the two part experiment about KCl stimulation on primary rat cortical neurons culture. Both plot trends signal the effective increasing of spike amplitude and frequency due to the daily chemical stimulation.

external factor is modifying the electrical activity of the cell network, both in amplitude or frequency of activation, these variation can be easily observed. The bio platform sensibility is going to be used for the biological investigation that were performed during the project. Statistical analysis of the spikes frequency and amplitude are going to be explained in a next section.

4.2.3 Spike detection and analysis

The amount of recorded data made impossible to analyse them without the use of a written script to extract significant statistical trend and values. Usually companies include the data treatment in the proprietary software, but we did not have access to any of these instruments. MATLAB was therefore chosen once again to perform this statistical analysis. The logic and bases for the script were wrote with the help of Timothée Levi (Associate professor at the University of Bordeaux and Project associate professor at the University of Tokyo, met during a visiting period at the LIMMS-CNRS) and his previous work, then it was rewrote and adapted for our particular situation.

The acquisition card and recording software being developed by National Instruments allowed us to save the data in TDMS format. This format has many advantages, such as being already structured and having a relative small size, compared with other formats, being mainly composed by binary data. Native compatibility for this format exists for LabVIEW and DIAdem, being developed by National In-

struments too. Saving the recordings with any other format would have increase the file dimensions and made more complex to operate them. If we consider two minutes of recording at 10000 points per second it means saving 1.2 million data, for each channel. For a regular format, as xlsx for Excel, it is an huge amount of data and severely slows any operation. To open these files with MALTAB an already developed script called TMDS Reader allows to get the structure of the file itself. After defining the path to the data folder, and recovering the file list from the directory, it is possible to extract the data as a matrix of cell elements. This way, it is possible to get any number of electrodes from different files in the same folder, eventually with a different amount of recorded points, otherwise MATLAB does not accept matrices with different number of points. Here, just an example for the time dataset and the first electrode are shown. This script can be extended to include the other recorded electrodes copying the code or via a loop.

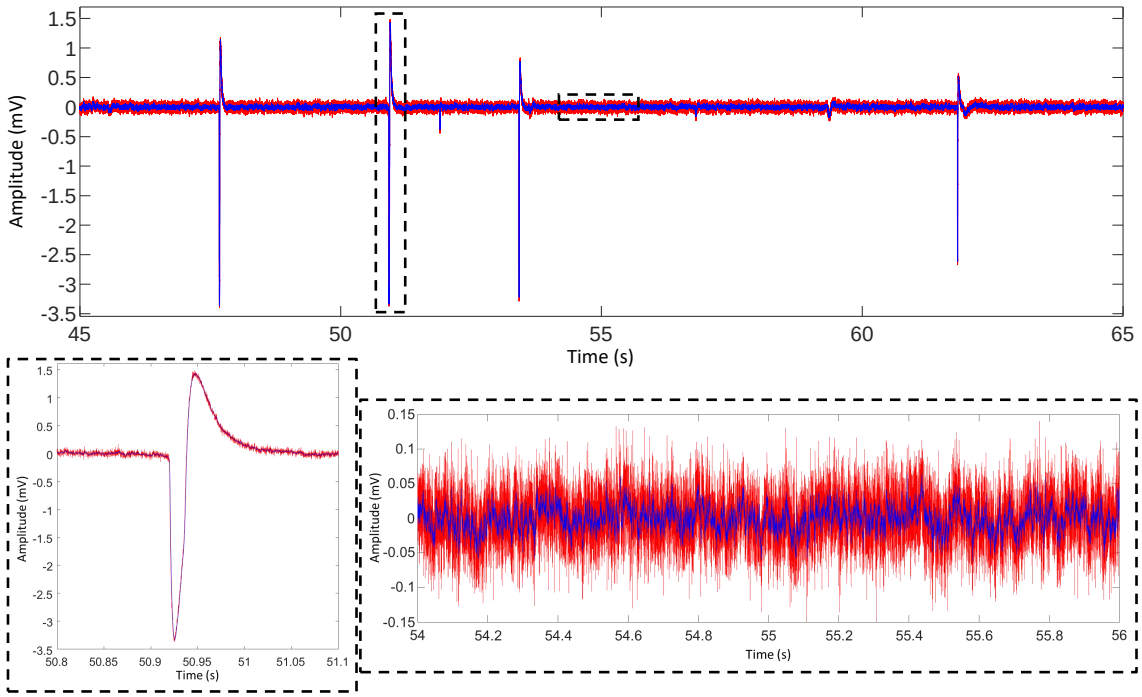

Figure 4.11: Example of a recording before that the moving average is done (red) and after (blue). The background noise is substantially reduced improving the signal to noise ratio.

Once the data are stored in matrices of cell elements, they need to be converted as floating-point values, or "double", the default numeric data type in MATLAB. This data type is compatible for most computational tasks. The recordings are then filtered and a moving average is also applied, as shown before it is useful to reduce the background noise and improve the signal to noise ratio. The filter used is a high-pass Butterworth type, with cut-off frequency at $1Hz$, used to avoid any long term oscillations of the potential. The moving average had a window of 10 points, to

reduce the noise without impacting the maximal recorded amplitudes. An example of the average and filter effect can be observed in the image 4.11. The noise is largely reduced meanwhile the amplitude of the spikes is almost not affected.

Moving to the spike sorting part of the the script, at first it is necessary to perform an evaluation of the background noise. The recordings were divided subset of data in order to create a threshold for the detection of a spike that would vary with the electrical noise. The subset were chosen as a number of point equal to a power of 2, typically 1024 or 2048 points. These values are chosen because it is the fastest way to store data and perform computation on them being multiples of a byte. For each subset of data the noise is evaluated and stored as a threshold value.

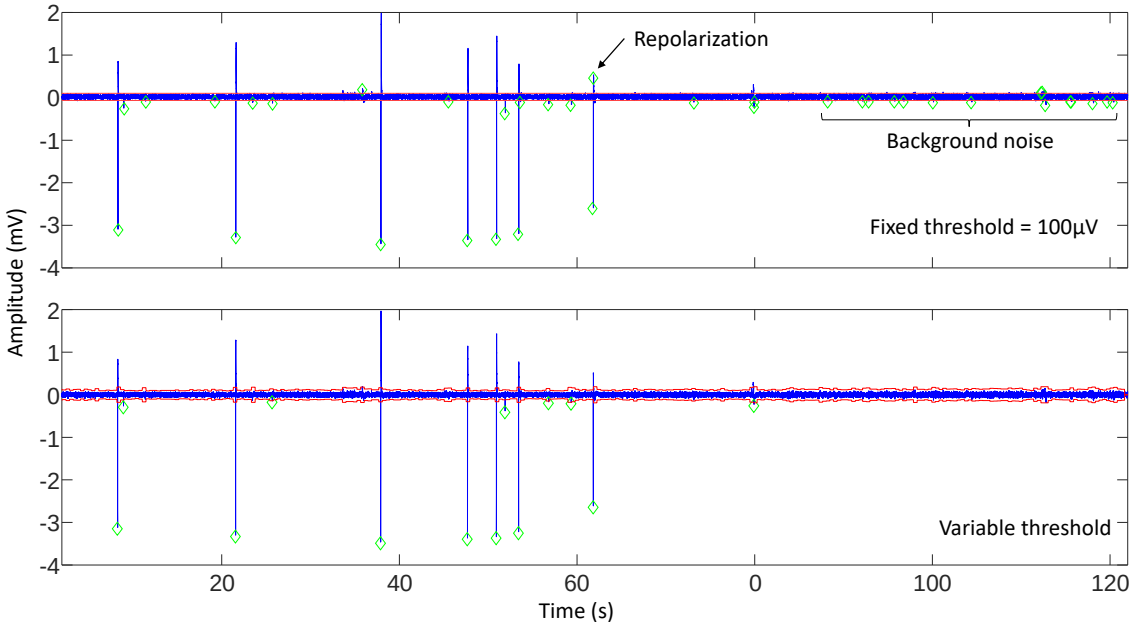

Figure 4.12: Example of a recording with high and low amplitude signal comparing fixed threshold and variable threshold for spike detection.

To understand the need of a threshold, it is shown an example in the image 4.12. In the image, two identical recordings are analysed with a fixed threshold at $100\mu V$, the top one, and a variable threshold based on the value of the noise, bottom one. If a fixed threshold is used, one of two problems usually appears: noise spikes are detected if the threshold is too low, or the smaller spikes are not detected if it is too high. In the example top plot, many spikes were detected even if they were part of the background electrical noise. Also an action potential repolarization was detected as a separated spike, which should not happen. On the other hand, with the variable threshold it is avoided having it adapting its value. It can argued that some of the minor spikes, that barely can be distinguish from the background noise, were not detected with the variable threshold method. A choice had to be made to

make sure that the noise did not influenced the data analysis. Therefore, the lost of few minor spikes was chosen as the better option.

Once the threshold is defined, the peaks are searched for both positive and negative values. The peaks have to satisfy the conditions to be higher than the threshold, of course, and to be the highest point of its 500 neighbours. This is set because the sample rate is usually set at 1 point each $10\mu s$, and the minimal duration of a spike is around $5ms$, so that a spike could not be counted twice. With this part of the script the position of the spikes and their amplitude are saved. It allows to perform statistical analysis on the frequency of activation and amplitude of the recorded spikes. For example, a Raster plot can be used to visually examine the electrical cell activity. It allows to look for patterns and synchronization between different electrodes showing the timing of spikes, losing, on the other hand, information on spikes size and shape. In figure 4.13, the activation of several electrodes at the same time can be observed twice in a single recording.

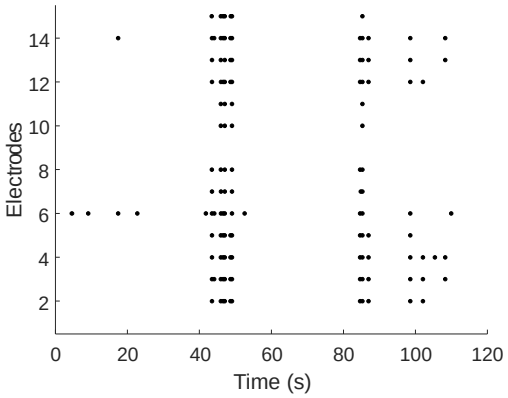

Figure 4.13: Example of Raster plot.

Notably, a difference in shape and amplitude can be observed between the recordings displayed in this manuscript. These differences were due to the diversity in the interaction between the cells and the electrodes for each experiment and between each electrode. Not reaching the cell confluence on the device surface, the variation of the cell/electrode interaction brought to changes in the recorded signals. The better engulfment of the electrode by the cell is reached the better shape and amplitude are recorded, together with an optimal signal-to-noise ratio. This aspect is addressed with the development of the system for axogenesis described in the previous chapter. With this solution the variability in recorded spike would drastically reduce. Moreover, a difference in peaks amplitude and shape can be linked to the biological development of the cell culture, at early stages and once the maturity is reached.

4.2.4 Electrical equivalent model and deconvolution

After the definition of the Hodgkin-Huxley electrical circuit model of a neural membrane and the works of Grahame and Randles for the electrode/electrolyte interface, some groups tried to link the shape of a recorded spike to the contribution of the electrode and the cell membrane. Most recent examples can be found in the works of Berdondini's and Dayeh's groups [65, 66].

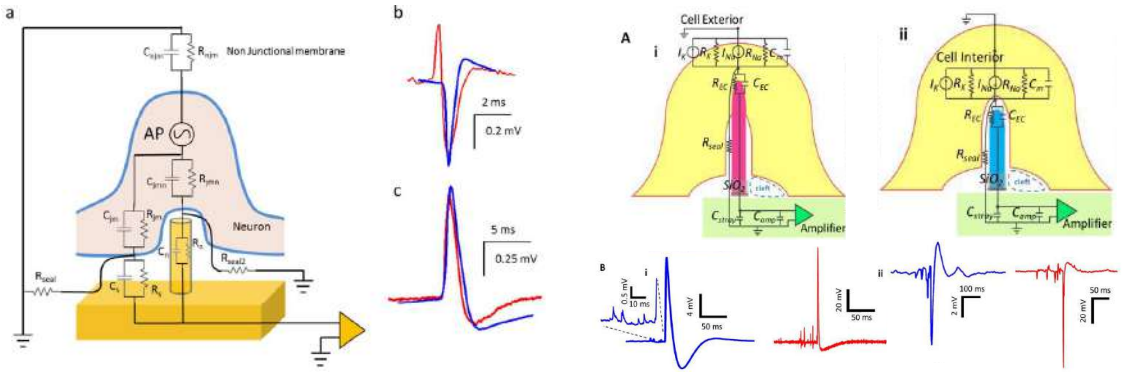

(a) MEA plasmonic 3D nano-electrode interface with a neuron cell.

(b) Intracellular and extracellular nanowire neuron interface.

Figure 4.14: a. Sketch of a neuron on a MEA electrode with a plsmonic 3d nano-electrode with the equivalent circuit used for the simulation [65]. On the right, experimental spikes (red), superposed SPICE simulation (blue). b. Electrical circuit models for intracellular and extracellular configurations[66]. Spontaneous action potentials recorded before (blue) and after (red) deconvolution.

Two methods have been mainly used to evaluate this contribution of the electrode/cell interface to the recordings. The first one is the use of the electrical equivalent model to perform simulations of the recording expected shape. It is the method used in the example of figure 4.14a. This method needs the presence of an element simulating the neuronal action potential (AP) to introduce a polarization in the circuit. By fitting of the recorded signal with the simulated one it is therefore possible to extract the values for the circuit elements. Some of these elements have values that can be previously fixed via characterization. Typically, the values of cellular membranes can be found to already be measured for most cells. For neurons cells, the membrane capacitance (C_m) is usually accepted to be equal to $0.9\mu F/cm^2$. This value must then be adapted to the surface of the nanostructures to be used in the electrical model.

Otherwise, the equivalent model can be used to define a deconvolution procedure as in the example 4.14b. Here the equivalent circuit is needed to define an analytical transfer function (TF). This allows to theoretically remove the impact of the elements between the action potential and the actual measure and therefore retrieve the the original signal. To perform this procedure, the value of each element of the equivalent circuit have to be defined in advance. The deconvolution can be done in the time domain or frequency domain. It is easier to do it in the frequency domain needing simply the ratio between the signal and the transfer function. Otherwise, in the time domain in would include complicated integral calculation.

The new elements that appear in the equivalent electrical circuit are the ones relative to the cell membranes and a resistance due to what is defined as the electrode engulfment. For the membrane characteristics, as already said, they can be

found and tuned to the particular system geometry. The seal resistance (R_{seal}), on the other hand, depends on the interaction of the cell with the electrode. It is particularly complex to define, because of the casual positioning of the cell relative to the electrode. It can be anyway assessed for each particular case. It represent the possible leakage of signal in the region called "cleft" forming a thin space between the surface of the electrode and the cellular membrane. The higher R_{seal} is, the better the cell/electrode interaction is, and the higher the engulfment is.

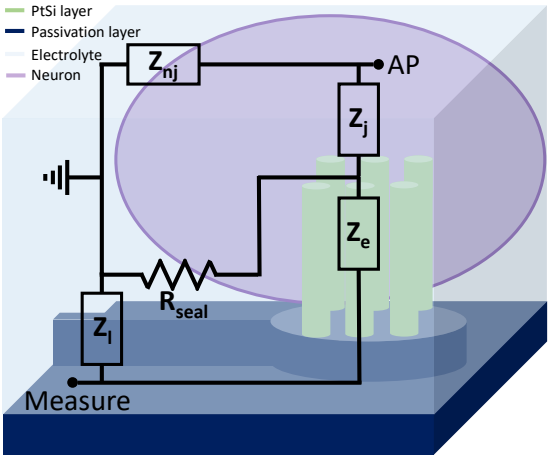

(a) Equivalent electrical circuit model for cell/electrode interface.

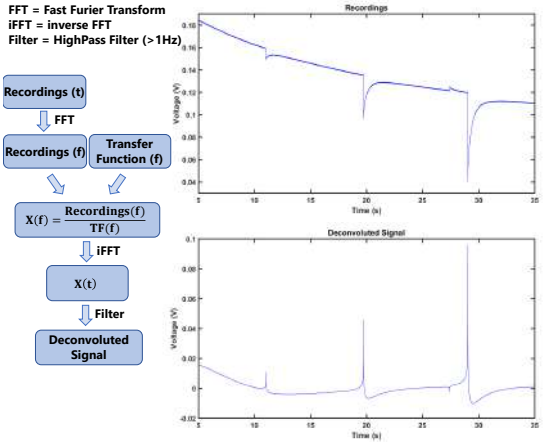

(b) Deconvolution procedure in the frequency domain and result on spontaneous recordings.

Figure 4.15: a. Sketch of the equivalent electrical circuit model for the cell/electrode interface used to extract the transfer function. b. Schematic of the deconvolution procedure steps in the frequency domain and the result of this script on spontaneous recordings.

We decided to begin to investigate the influence of our nanopillars with the deconvolution method. An equivalent electrical circuit was defined, starting from the already shown model used for the EIS characterizations (figure 4.15a). The single circuit elements are here simplified as impedances: Z_e for the electrode interface, Z_l for the insulated layers, Z_j for the junctional cell membrane and Z_{nj} for the cell membrane not interfacing the electrode. Each impedance is composed by a capacitance and a resistance in parallel. An analytical transfer function can be extracted:

$$TF = \frac{V_{out}}{V_{in}} = \frac{\frac{Z_e}{Z_j} + \frac{Z_e R_{seal}}{Z_j Z_{nj}} + \frac{Z_e}{Z_{nj}} + \frac{R_{seal}}{Z_{nj}}}{1 + \frac{Z_e R_{seal}}{Z_j Z_l} + \frac{Z_e}{Z_l} + \frac{R_{seal}}{Z_l}}. \tag{4.1}$$

The deconvolution procedure is schematically explained in the figure 4.15b. Taking a recording raw data, the Fourier Transform allows to bring it in the frequency domain. The analytical transfer function is also calculated in the frequency domain. Then the ratio between signal and TF allows to recover the original signal, or action

potential. It needs to be converted back in the time domain and filtered to avoid any long period polarizations.

The effect on a recording can be observed in the same image. It allows to reverse the sign of the spike, bringing what was supposed to be an extracellular recording to positive values. Moreover, it can restore the original amplitude, reaching the theoretical $100mV$ total amplitude of an action potential. This procedure works best for high amplitude recordings, where it exists a strong interaction between cell and electrode. This way the electrical equivalent model can actually simulate the real recording conditions. These results were obtained at the beginning of the project with a simpler recording setup, were the influence of the electrical elements of the circuit were the main factor modifying the recorded signals. In order to do that after the evolution of the recording setup, the influence of the multiplexer has to be taken in account. It would modify the electrical equivalent circuit and the transfer function.

4.3 Biological investigation

Together with the validation of the bio platform, its characterization and modelling, an objective of this project was to perform some investigation that could have actual biological interest. Two studies were identified as interesting in our context. The Amyloid Beta Peptide has been already largely studied as a model for Alzheimer's disease. Here we searched for its effect on the electrical activity on primary neuron culture. The second chosen study was performed on the Borna disease virus type-1 (BoDV-1). These studies were possible because of the collaboration with Elsa Suberbielle, a researcher in Daniel Dunia's group at the Infinity laboratory. Her expertise on the topic was fundamental to approach this subject [168, 169]. Considering only the micro structured bio platforms, very few biological investigation were performed, and those were done on cardiomyocytes, or cardiac tissue cells. In these studies, it was investigated the response of cardiomyocytes to drug stimulation [58, 63]. Otherwise, a large amount of bibliography can be done biological investigations on neural cells with MEA or CMOS technology.

4.3.1 Amyloid Beta Peptide study

The first study was performed on the effect of amyloid beta oligomers on the cell activity. These oligomers have already been largely studied, so we wanted to use it as a validation and to verify if any new type of information could be extracted. Accumulation of abnormal quantities of soluble amyloid beta (Aβ) oligomers is believed to cause malfunctioning of neurons in Alzheimer's disease. It has been shown that Aβ oligomers impair synaptic plasticity, thereby altering the ability of the neuron to store information [170, 171]. In Alzheimer's disease, dementia severity correlates strongly with decreased synapse density in hippocampus and cortex. Numerous studies report that hippocampal long-term potentiation can be inhibited by soluble oligomers of Aβ, but the synaptic elements that mediate this effect remain unclear [172, 173]. The soluble monomers can assemble sequentially into soluble oligomers, protofibrils and fibrils that accumulate in the brains of Alzheimer's disease subjects, forming insoluble amyloid plaques.

Different hypotheses link the Aβ to an unregulated calcium current into neurons. Oligomers in particular are considered as cytotoxic and neurons are particularly vulnerable to channel toxins because of their reliance on concentration gradients and membrane potentials for proper functioning. Because of all of these known effects of the Aβ on the neurons, we expected to be able to record some differences in the electrical activity.

In order to perform this experiment, the Aβ oligomer solution was prepared at the Infinity laboratory maximum 24 hours prior to the recording session. Waiting

for longer period would give the time to the monomers to form longer polymers losing the cytotoxicity of the oligomers. The oligomer solution is used at $1\mu M$ in the culture media, the solution is directly added to the culture well.

The recording session is divided in three parts. The recording of a baseline activity is the first step. It is necessary to determine the spontaneous activity of the cell culture to then compare any variation in terms of frequency or spikes amplitude. After having measured the baseline, the solution Aβ oligomers is added to the culture media. The activity is then recorded right after the addition of this solution for several minutes to assess any eventual perturbation. Then, the culture is left to rest for a minimum of one hour and a half. This rest period is necessary to see effect of the oligomers on the cell culture.

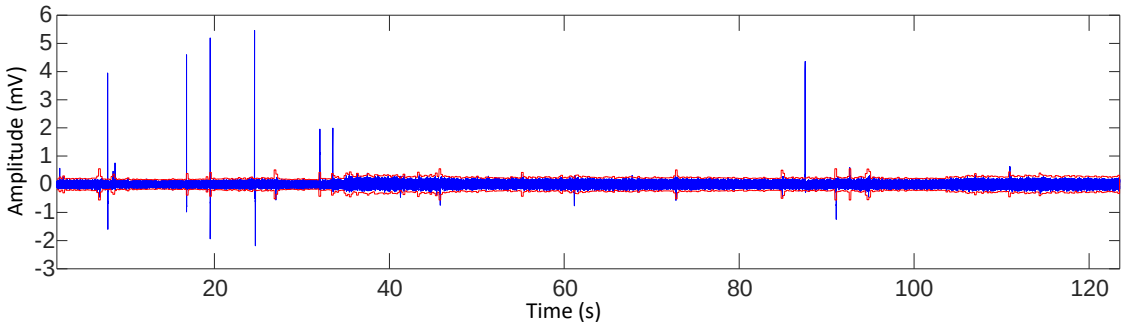

(a) Example of an electrode recording the neuronal culture.

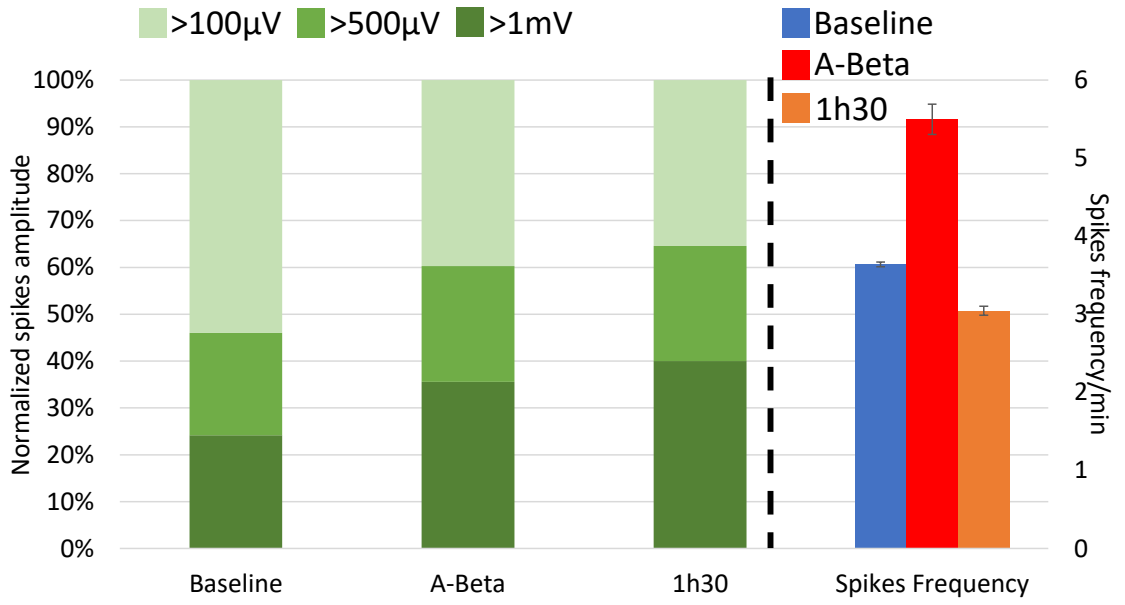

(b) Results of the three part Aβ experiments.

Figure 4.16: Primary rat cortical neurons at 15 DIV, each time one device was used for two separated experiments a. Plot of a passive electrode recording the activity of the primary neurons. Both high and small amplitude spikes are recorded. The threshold level averages at $150\mu V$. b. Bar charts representing the variation of the normalized spike recorded amplitudes and the frequency of activation for the three parts of the recording session.

In the figure 4.16b, the bar charts are summarizing the data analysis results of the experiment. The recordings were done on two different cell cultures at $15DIV$, with the exact same conditions and treatments, obtaining the same statistical trends. The cells were plated to obtain $1200cells/mm^2$, 60 passive electrodes on the device were recorded 4.16a. It can be observed that the mean spike frequency increased at the moment of the oligomers addition to the culture. Once the resting period of the culture was passed, the spike frequency was found to be decreased from the baseline. An interesting result was found also regarding the spike amplitudes variation. The Aβ oligomers were demonstrated to have an influence on presynaptic calcium current [170], essentially involved in neurotransmission and synaptic plasticity in the brain. Here we found that the amount of smaller spikes (between $100\mu V$ and $500\mu V$) recorded from the device decreased with the addition of the oligomers. It may seem to coherently represent the reduction of presynaptic activity that, as previously shown, can be detected by the bio platform. It can also be argued that an evidenced hyper-excitability of the network immediately after Aβ is detected, followed by a period of synaptic depression, revealed by a decrease in the spike frequency and changes in percentages of large amplitude spikes. These results positively validated the possibility to investigate biologically relevant topics with the bio platform.

4.3.2 Borna Disease Virus results

The experiments on Borna Disease Virus type-1 (BoDV-1) were performed in collaboration with another PhD student from the Infinity laboratory, Florent Marty, as well as the data analysis and interpretations. The virus used is a single negative strand RNA virus, it can infect a wide range of vertebrate species, humans included. In animal models, BoDV-1 causes behavioural impairment in infected host in absence of over neuronal loss and persists lifelong in its host neurons [174, 175].

As parasites, viruses have to rely on the host cells to complete their life cycle. Damages to DNA represent perfect spots to be targeted for a virus infection, where it can persist and propagate. The experiment was focused on the effect of this virus interaction with the most severe form of DNA damage, the double strand breaks (DSB). The DSB were considered to be only deleterious to genome stability. It has been shown that DSB can also occur during physiological conditions. Responses to DSB in the central nervous system, in particular on neurons, is not much studied up to date. DSB occur physiologically in healthy post-mitotic mature neurons upon activation by sensory or cognitive challenges.

The accumulation of DSB in neurons has been previously shown to cause neuronal dysfunction. Accumulation of DSB caused by BoDV-1 infection may durably alter neuronal function and impact its spontaneous electric activity. The experiment

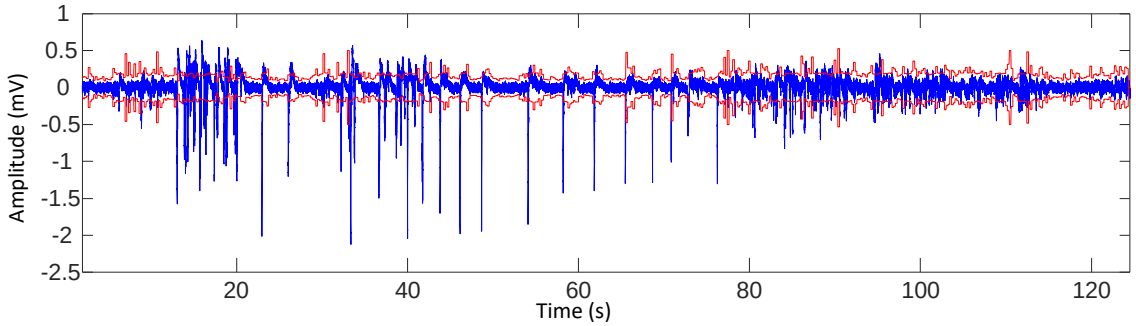

(a) Example of an electrode recording the neuronal culture.

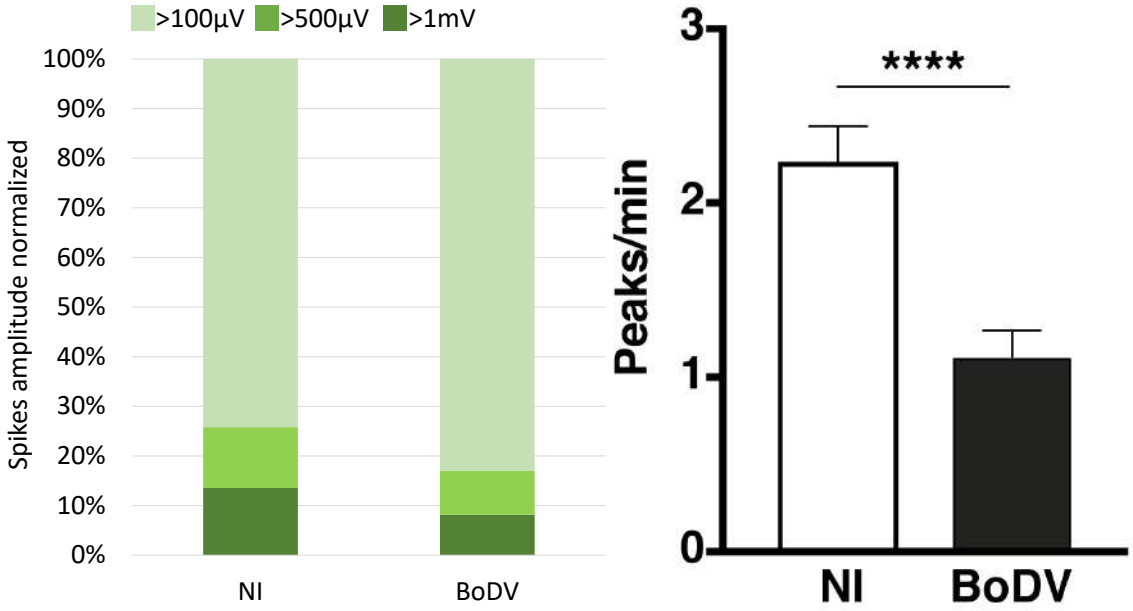

(b) Results of the BoDV experiments.

Figure 4.17: Primary rat cortical neurons at 16 DIV, each time two devices (one with infected cells and the other with the control culture) were used for three separated experiments. a. Plot of a passive electrode recording the activity of the primary neurons. The threshold level oscillates for the high level of activity, it averages at $200\mu V$. b. Left, bar charts representing the variation of the normalized spike recorded amplitudes between infected and non-infected neurons. Right, unpaired Student t-test for the frequency of activation. The p value is < 0.0001. Bars represent the standard error of the mean (SEM).

was therefore designed to compare the spontaneous electrical activity of infected and not infected cells. It was repeated three times, with two different devices each time after 16 days-in-vitro, at a concentration of $1200 cells/mm^2$, 60 passive electrodes were recorded 4.17a. All the results were following the same trends.

BoDV-1 infected cultures showed more silent nano electrodes compared to non-infected controls (NI). In particular, there was a 25% decrease in the number of active electrodes in infected neuronal networks compared to non-infected ones. Moreover, as observed in figure 4.17b, the frequency of recorded spikes for BoDV-1 infected cells were half the value for non-infected ones. The Student t-test that can be seen

in the same image was done by the PhD student collaborating with us for this experiment. Moreover, a reduction in the normalized number of spikes for higher amplitudes were observed for BoDV-1 infected cells. Thus, BoDV-1 infection seems to impair spontaneous electric firing in neuronal networks, supporting the hypothesis that DSB may durably alters neuronal network functions.

Chapter conclusion

In this last chapter the electrophysiology recording system was presented. The multiplexer main elements and their functions were described, and its performance were shown in terms of electrical background noise. Some examples of spontaneous electrical activity were shown proving the possibility to record high amplitude spikes (several millivolts) as well as smaller spikes (few hundreds microvolts). The validation of the recording setup was proved by classical neuronal activity silencing and stimulation. In order to perform data analysis a script on MATLAB was developed and here its main steps effect were shown. The deconvolution principles are described as its effects on spontaneous recordings. Finally, the results of two biological investigation are presented, validating the ability of the bio platform to assess meaningful variation in the electrical behaviour of primary neurons.

General conclusions and perspectives

The history of electrophysiology was presented and until today's most relevant research topics. Our understanding of the brain functioning has deeply improved during the years, but still we are far from knowing exactly how information are elaborated and transmitted. Nowadays, there is the need of more advanced instruments to open the possibility of novel studies on the neuronal communication. The recording at both single cell level and up to cell network is necessary to unravel the remaining unknown facts of this extremely complex organ. Also, more than one parameter have to be taken in account, so the more advanced bio platform should perform multiples type of detection.

In this manuscript, the first chapter is dedicated to the presentation of the context of this project. The history of electrophysiology is narrated, reaching the modern days and the influence of micro fabrication. The functioning of a neuron is described, from the structure of the cell to the generation of an electrical signal, the action potential. Technologies for electrophysiology are presented, bot for in-vivo and in-vitro studies. Then, the focus is brought to the more advance on chip devices. Some examples of device co-integration are presented, as well as the measure with active devices as the transistors. Of course, the state-of-the-art regarding micro fabricated bio platform is described in order to introduce the reference points of this project. Here, the micro fabrication is a tool used to improve the interaction between the cells and the electrodes, in order to increase the sensitivity of the devices. After that, the previously accomplishments of the team on the topic are shown. To conclude the first chapter, the three main areas of interest and objectives are presented. Main respective topics of the three following chapters of the manuscript.

Hence, the second chapter is focused on the more technical aspects of the project. Here it is described the fabrication of the bio platform, with large scale compatible way. The most relevant and critical steps are presented, as the first two critical photolithographies and plasma etchings. Also, the intricacies of the co-integration are described, allowing to fabricate both structured electrodes and finFETs on the same substrate. Here, the electrical field potential measurement theory is described with theoretical models and physical characterisation. An equivalent electrical circuit is used to simulate the interface between electrode and electrolyte. Together with the

characterisation of the electrodes themselves, it allowed to extract the values for each element of the circuit via data fitting. The devices performances are comparable wit the state-of-the-art. Moreover, the sensing of chemical environment is presented. The finFETs on the bio platform are used as ISFET device. Their sensitivity to pH variation is presented, with reasoning and proofs relative to each result. At the end, an extremely well performing pH sensor is obtained, with a higher than Nernst response and optimal integration on the bio platform.

Then, in the third chapter, the methodology to culture primary rat neurons is described. It is a complex procedure because primary neurons are extremely delicate cells and obtaining a mature and active culture is a difficult task. Here, the possibilities to guide the neuronal growth are presented. In order to obtain the axogenesis of neurons, the fabrication of microchannels was the chosen approach. The state-of-the-art about it is presented with the achievements of other research teams. Two different ways were explored in order to fabricate microchannels compatible with our bio platform. The first one consists in a structuration via photolithography of the SU-8 resist. The second, in the fabrication of a mould to create a PDMS system to integrate on the chip. Both methods have advantages and drawbacks that are discussed.

In the last chapter the recording setup is described. Our setup has evolved during the project, reaching its final form with the integration of the "multiplexer". The system is described together with its possibilities and performances. After that, some examples of spontaneous activity recorded from primary rat cell culture are presented. The validation of the setup is done via chemical silencing and stimulation of the culture electrical activity. A script was developed in order to perform data analysis, here the logic and result of its algorithm are shown. The script allows to perform spike detection and extract statistical trends regarding spikes frequency and amplitude. Also, the complete equivalent circuit, including the cell/electrode interface is described, together with its use for signal deconvolution. To conclude, the results obtained on two biologically relevant series of experiment are presented. The Amyloid Beta Peptide is used as an Alzheimer's disease model. Its effect on the neuronal culture electrical activity is analysed resulting in a reduction of the spike activation due to the decrease of smaller spikes as pre and post synaptic activity. The second experiment was performed on Borna Disease Virus, showing how this virus reduce the activity of a cell culture probably because of its interaction with the neuronal genome.

Perspectives

The project reached the achievement of a well performing bio platform, both in terms of electrical and chemical sensitivity. The devices were carefully characterised and modelled, proving the control on their working parameters and the understanding of the physical reason behind that. Nonetheless, the bio platform as the recording setup went through major changes during the years. It needed a large amount of time and patience to iterate the micro fabrication processes and the characterisations, but the final form of the bio platform has yet to be established. Two type of objectives are foreseeable for this work to continue, short-term perspectives and new investigations to go towards.

Short-term perspectives

It was unfortunately not possible to perform a last series of experiments proving the synchronous recording of electrical activity and pH detection, due to time and technical limitations on the project. As it can be seen in the image 4.18, culture tests on these device have already been performed showing optimal conditions for this type of experiment. When the working situation will be stable again, everything is be ready to perform this final validation step, closing the circle on this topic.

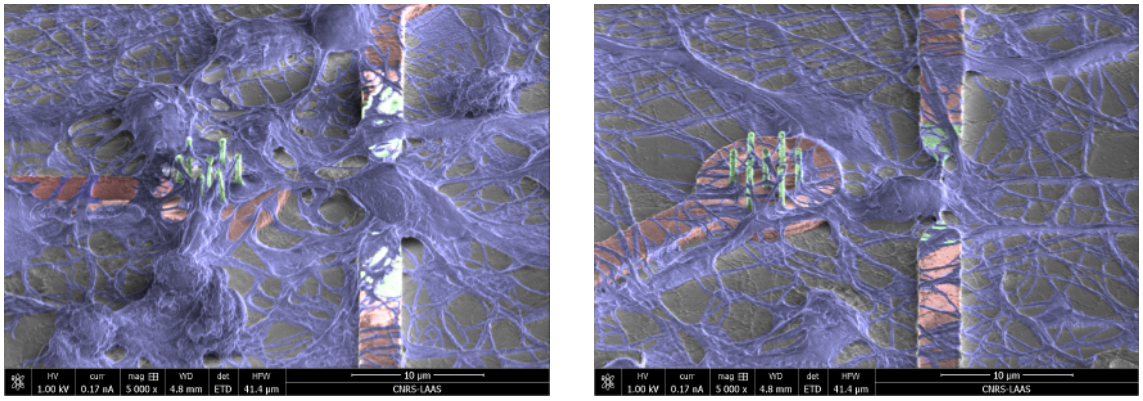

Figure 4.18: Colourized SEM images of fixed cells on the bio platform. It is possible to see the excellent interaction between both passive and active electrodes and the cell in culture.

Without doing any major modification to the device as it is, the bio platform final design should also be defined soon. It was demonstrated that is possible to co-integrate passive and active devices, with optimal performances respectively in terms of electrical and pH sensitivity, on the same substrate. Also, two methodology for the axogenesis of neuronal culture were proved to be compatible with the bio platform. It is now possible to plan the merging og this two aspects defining a novel

bio platform able to interface neurons at the subcellular level and at the same time perform multiple type of detection.

Finally, the recording setup, and therefore the data analysis, are currently limited to 16 channels at the same time. To fully take advantage of the bio platform, all the 60 electrodes should be recorded at the same time. Reaching this milestone would establish the maturity of the recording setup. Recording the electrodes for the whole bio platform simultaneously would allow to plan experiment to record signal exchange for the entire cell network.

On the other hand, changing something of the device characteristics could also bring some improvements. Studying the packaging, it was clear that the aluminium was an optimal choice for the ease of fabrication and simple structuration. On the other hand, the contact between aluminium and the gold PCB can form intermetallic contact which are known to cause problems in microelectronics. It may be interesting to investigate the use of a different metals to obtain stabler alloys. Gold-to-gold junctions or aluminium-to-aluminium junctions would prevent most of the contact failures. Also, as previously said, it exists some alternatives to the currently used insulating layer. One of the most promising material is silicon nitride. This is both a good electrical insulator, often used for devices in saline media, and a good gate oxide for pH sensing. It would reduce the number of oxide depositions in the micro fabrication process without adding much complexity to it, and could improve the lifespan of the chip in saline media together with its performances.

Future perspectives

The electrode interface optimization is fundamental for this type of technology. To go further, this interface can be improved with the deposition of conductive bio compatible materials. Different methods for surface functionalization have been developed, as micro patterning, physical vapour deposition or electrochemical deposition. This can be applied both to the passive electrodes to further improve their performances. For example, PEDOT is a classically used polymer that can be electrochemically deposited on conductive surfaces improving the interface impedance. Otherwise, molecules can be grafted to the surface granting sensitivity to specific chemical or biological agents.

The device in its actual form is based on the MEA technology. It would be possible to conceive its integration in a CMOS based substrate, maintaining the electrode structuration. The micro fabrication process was designed to be compatible for large scale integration on purpose. The transfer of our technology on a CMOS would require some tuning, but it should be possible. A post-doc has recently started working on this process for another project in our team. This would

greatly increase the spatial measurement possibilities of the bio platform, giving us the possibility to address new biological investigations.

As discussed in the manuscript, a focus point of modern electrophysiology is also the study of communication between different type of cells. The developed microchannel system can be used for this type of investigation. The two main chamber can be filled separately, and the electrodes along the microchannels would be able to measure the electrical signals exchanged between the two cell cultures. It can be interesting to determine the pattern underlying cells electrical communication and how these are influenced in case of stress or diseases.

To finish, I find that current bibliography lacks of a reference to precisely compare this type of bio platforms. In most published papers, only the best obtained recording are showed, and they lack of a discussion on general or average expected performances. Numerous type of approaches to improve some performance aspects were investigated and published, highlighting the pros of each one, but without a general fair comparison with the rest of the developed platform or available commercial devices. It should be a priority now to define a method to correctly determine which bio platform performs better with a series of unbiased rules.

Acknowledgements

First of all, I am grateful to the Univeristé Paul Sabatier Toulouse III and the Region Occitanie Pyrénées Méditeranée for the opportunity given me with the APR Intraneuro funding to pursue this thesis project. This jurney started even before the start of the PhD project as I rejoined the MPN team for an internship during the last year of university. It is thanks to Guilhem Larrieu and Daniel Gonzalez-Dunia who trusted me that I had the opening for this project as PhD student.

I have to sincerely thanks Guilhem for his support during these three years, his knowledge both scientifically and technologically was fundamental for the project. Even more, his availability on a day-to-day basis and his strict methodology helped me improving on some of my weaker points. Daniel too was an important pillar of the thesis, even if our exchanges were less frequent, the meetings with him were always rich in ideas and solutions for the project. I thank Daniel for his experienced suggestions and support too.

I am thankful to the LAAS-CNRS and the GEETS doctoral school for the excellent environment both directorate where able to create to fulfil a thesis. I want to thank also the INSA Toulouse, in particular Michel Bonnet, for the two years as teaching assistant in the department of Physical Engineering. I thank the thesis jury members for the extremely interesting discussion the defence day, and in particular the examiners Anne Charrier and Cécile Delacour for the feedbacks and corrections on the manuscript.

I thank the MPN at the LAAS where I was lucky to work, both researchers and PhD students or post-docs, in particular: Fuccio, Emmanuel, Sébastien, Peter and Abhishek. I thank also, the Dunia team at the Infinity, with Elsa, Florent, Karine, Hélène, Anne and Frédérique.

I thank the engineers at the LAAS from TEAM and I2C for their availability and help during these years. In particular from TEAM, Aurélie Lecestre and Laurent Mazenq for their help in the clean room. Their knowledge and skills with the most complex machines was often essential. Also from I2C, Marie-Charline Blatche and Fabrice Mathieu were two of the most involved people in the project. They taught me several things extremely useful for the success of this thesis and I have to thank them for the long hours spent together on the experiments and for their dedication.

I want to personally thank al the people that were in the F2 office with me during these years. Adrien Casanova, who taught me everything I needed to know on the project and was the best host you can think for the numerous evening at his place. Nicolas Mallet, the guy that taught me French via sarcasm and was known for his everlasting smile. Tiphaine Pelé-Joly who joined us to work on the project and obliged me to get used to the fast pace speaking of people from Paris. More recently, Inès Muguet who was never an intern but someone may know her as one and daily shared with me tasteful music. Finally, Aziliz Lecomte that brought a little bit me back to Italy chatting in my mother language and showed all her experience from the first moment in the office.

I also have a lot of people to thank for all the fun moments in Toulouse. Some that were there at the beginning: Julien, Aurélie, Audrey and Gautier. More that were always around: Valentin, Baptiste A., Paul, Baptiste J., Mathieu, Felipe, Alessandro and Nicola. And most of all the people that will stick with me: Clara, Benjamin, Marion, Ségolène, Anais, Andréa and Jeremy.

To finish, I want to thanks my family that constantly supported me even from a thousand kilometres distance and all my friends from Italy that I was always extremely happy to see coming back to Milan. Lastly, I thank my girlfriend Alexiane who helped me remaining mentally sane and encouraged me every day, especially when it was most difficult and the motivation was tough to find.

Résumé thèse

Contents

Chapter 1

Introduction

Pour réaliser une bio-plateforme fonctionnelle, il est nécessaire de connaitre l'évolution historique de l'électrophysiologie et des derniers développements technologiques. Dans le premier chapitre, l'histoire de l'électrophysiologie est racontée, avec une description du fonctionnement des neurones. Ensuite, les plus récentes avancées technologiques sont décrites et les objectifs de la thèse sont expliqués.

1.1 Histoire de l'électrophysiologie

L'électrophysiologie est l'étude des phénomènes électriques et des propriétés des cellules. Les racines de l'électrophysiologie prennent place dans la description de l'électricité statique par Thales. La révolution majeure de l'électrophysiologie est arrivée entre 1700 et 1900. Les travaux de Volta et Galvani ont défini les bases pour étudier l'électricité dans les muscles des animaux. La bio-électricité a été étudiée par Matteucci et Nobili. En 1850, Bois-Reymond est le premier à mesurer un potentiel d'action avec un galvanomètre. Depuis ce point, l'électrophysiologie a évolué énormément avec le premier ECG par Einthoven en 1904 et le premier EEG par Berger en 1924.

L'électrophysiologie moderne a commencé avec le prix Nobel de Edgar Adrian en 1923 et la loi de "all-or-none". Ensuite, Hogdkin et Huxley ont défini le mode de fonctionnement des canaux ioniques pour la membrane neuronale. En collaboration avec Goldman ils ont également défini l'équation pour le calcul du potentiel de membrane dépendant de la conductivité ionique:

$$E_m = \frac{RT}{F} \ln\left(\frac{P_{Na^+}[Na^+]_{ext} + P_{K^+}[K^+]_{ext} + P_{Cl^-}[Cl^-]_{ext}}{P_{Na^+}[Na^+]_{int} + P_{K^+}[K^+]_{int} + P_{Cl^-}[Cl^-]_{int}}\right)$$

Finalement, le patch-clamp a été développé et c'est depuis la technologie la plus utilisée pour faire de l'électrophysiologie. Le patch-clamp a permis l'étude du rôle de chaque canal ionique. Aujourd'hui, l'influence des nanotechnologies a permis le développement de nouvelles bio-plateformes, de MEAs (multi electrode arrays) et de probes corticales.

1.2 Cellules électrogéniques

1.2.1 Le neurone

Le système nerveux humain est composé de cellules spécialisées : les neurones, connue comme matière grise, et les cellules gliales, oligodendrocytes et astrocytes, la matière blanche. Le neurone est la brique de base du système nerveux: ils envoient des informations sur de longues distances grâce à des signaux électriques, les potentiels d'action. Dans un cerveau humain, il y a 100 milliards de neurones avec plus de 100 trillions de connections synaptiques. Un neurone a trois fonctions principales: recevoir des signaux, analyser ces signaux et communiquer avec d'autres signaux électriques. Ces fonctions sont bien définis dans l'anatomie des cellules (figure 1.1a).

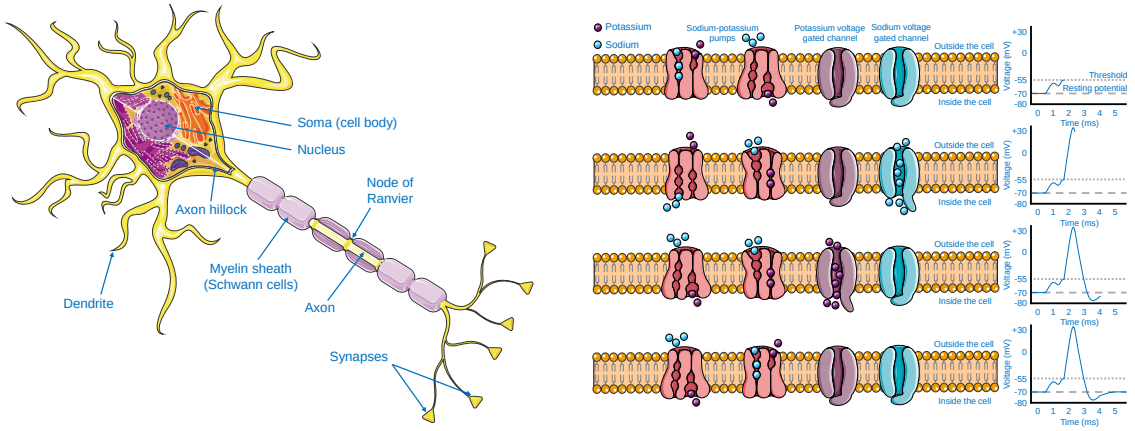

(a) Neurone. (b) Potentiel d'action.

Figure 1.1: a. Représentation schématique d'un neurone. b. Les quatre parties principales pour la génération d'un potentiel d'action. [Images composé avec SMART]

1.2.2 Signaux électriques

Les cellules électrogéniques sont des cellules capables de générer des signaux électriques, les neurones font partie de cette famille de cellules. Pour générer ces signaux, la différence de potentiel entre l'intérieur et l'extérieur des cellules doit varier. Pour cela, la perméabilité de la membrane à différentes espèces ioniques peut varier en réponse à des stimuli par les synapses (figure 1.1b).

1.2.3 Maladies neurodégénératives

Les maladies neurodégénératives sont causées par la perte des fonctionnalités du cerveau. Les plus importantes sont la maladie d'Alzheimer, la maladie de Parkinson et la maladie de Huntington. Ces maladies sont liées a la dégénération de la plasticité neuronale, mais leur fonctionnement n'est pas encore totalement connu et les médicaments actuels ne sont pas efficaces. Des études ont prévu que les cas d'Alzheimer vont plus que doubler dans les trente prochaines années.

1.3 Technologies pour l'enregistrement neuronal

Les technologies modernes pour enregistrer l'activité électrique neuronale sont divisées en *in-vivo* et *in-vitro*, chacune présentant des avantages et inconvénients.

1.3.1 In-vivo

L'électroencéphalographie (EEG) est la technologie qui nous permet d'enregistrer l'activité du cerveau sur une échelle globale avec des électrodes placées sur la surface du crane. Les sondes intra-corticales sont une alternative très intrusive mais nous permettent d'enregistrer plus précisément des zones spécifiques du cerveau.

1.3.2 In-vitro

Les technologies *in-vitro* sont divisées en deux catégories : le patch-clamp et les MEAs. Ces dispositifs sont utilisés pour étudier des groupes de cellules plus simples que pour le *in-vitro*.

(a) Patch-clamp.

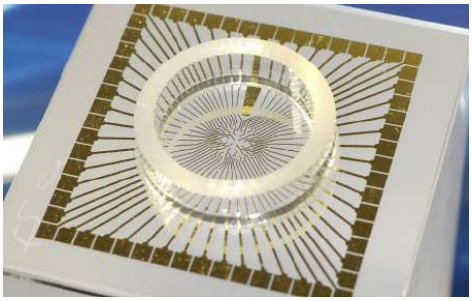

(b) MEA.

Figure 1.2: a. Image d'une patch-clamp setup. b. Example d'un dispositif MEA.

Le patch-clamp est une technologie puissante et versatile pour les études d'électrophysiologie. C'est la technique avec la plus grande sensibilité permettant d'enregistrer la totalité de l'amplitude d'un potentiel d'action. En revanche, le patch-clamp demande beaucoup d'expertise et c'est une technologie limitée car il est impossible d'enregistrer l'activité de plusieurs cellules en même temps. De plus, le patch-clamp ne permet pas d'enregistrer sur une longue période ou de répéter les expériences plusieurs fois (figure 1.2a).

Les MEAs sont fabriquées avec des techniques de micro fabrication comme la photolithographie et la gravure par plasma. Cette technologie a été commercialisée avec le développement de la micro fabrication et les MEAs sont maintenant largement utilisées. L'avantage des MEA est la possibilité d'enregistrer l'activité électrique d'une culture complète de cellules en même temps. Cependant, la limite principale des électrodes planaires est la sensibilité des enregistrements (figure 1.2b).

1.3.3 Co-integration et multi-sensing

La possibilité de rajouter plusieurs types d'enregistrement sur une seule plateforme a été étudiée par de nombreux groupes de recherche. Différentes combinaisons ont été démontrées comme la possibilité d'enregistrer et de stimuler électriquement des

cellules ; de mesurer et de quantifier des molécules spécifiques ou encore de faire des mesures optiques.

1.3.4 Mesures avec dispositif actif

Grâce à leur influence, l'application des transistors pour les biotechnologies a été étudiée par plusieurs groupes de recherche. Le premier a été le groupe de Fromherz, au milieu des années 90, qui a mesuré l'activité électrique des neurones avec des transistors avec des performances similaires à celles des MEAs. Le groupe de Lieber est également, depuis le début des années 2000, fortement impliqué dans le développement de capteurs pour des espèces biologiques, virus ou marqueurs pour le cancer. Des études encore plus particulières ont été tentées avec des OGFET, des nanotubes et des hétérostructures pour réaliser des mesures intracellulaires.

1.4 État-de-l'art

1.4.1 Dispositif avec électrodes tridimensionnels

De nombreuses alternatives pour améliorer les performances des MEAs ont été étudiées. Chronologiquement, le premier groupe à avoir réussi est celui de Spira avec des électrodes en forme de micro champignons (gMμE). Avec cette structuration des électrodes, ils ont démontré une meilleure interaction entre les cellules et les électrodes avec une amélioration conséquente des enregistrements électriques. Une solution similaire a été adoptée par le groupe de Offenhauser : le couplage électrique avec les cinétiques de membranes a été décrit grâce à l'enregistrement sur plusieurs électrodes en même temps. Le groupe de Park a réussi à obtenir des résultats optimaux avec l'utilisation de nanofils de silicium. Le couplage avec le patch-clamp a aussi permis de démontrer la possibilité de enregistrer et stimuler au même temps. De plus, l'utilisation de la technologie CMOS a été validée pour la première fois avec des électrodes structurées. Le groupe de Cui a étudié aussi l'utilisation de matériaux et de structures différentes pour les électrodes, par exemple des nanotubes en IrOx, démontrant d'excellents résultats. En plus, l'optoporation avec l'utilisation de lasers pour obtenir des enregistrements intracellulaires et améliorer les amplitudes des potentiels d'actions a été démontré par le groupe de Berdondini. Finalement, le groupe de Dayeh a réussi à obtenir d'excellents enregistrements en termes d'amplitude grâce à des nanofils très grands et à leur interaction mécanique avec les cellules.

1.4.2 Résultats précédents de notre groupe

Cette thèse est la suite d'un travail de thèse amené par Adrien Casanova. Une première génération de bioplateforme a été développée et des enregistrements électriques d'activité neuronale ont été démontrés avec des électrodes passives nanostructurées et avec des finFETs.

La micro fabrication de ces dispositifs est exécutée grâce à des procédés compatibles avec la fabrication à large échelle. Le matériau choisi pour la surface des électrodes passives c'est le PtSi pour sa très bonne conductivité, sa stabilité et sa biocompatibilité. La co-intégration de dispositifs actifs et passifs a également été

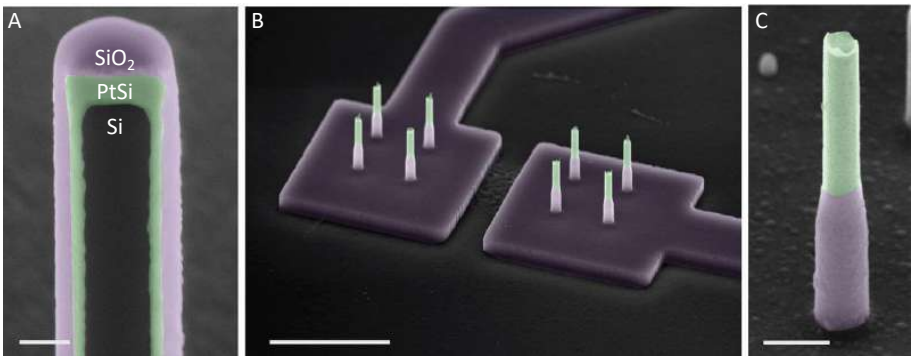

(a) Électrodes nanostructurées.

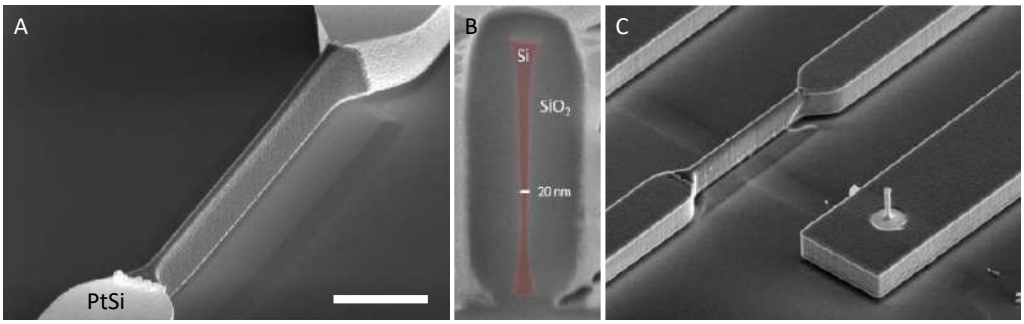

(b) FinFETs.

Figure 1.3: a. Électrodes structurées avec des nanofils verticaux. [Scale bars, 200nm (A), 5μm (B) et 500nm (C).] b. Exemple de dispositif finFET couplé avec des sondes verticales passives. [Scale bar (A) 2μm]

validé. Des premiers enregistrements de neurones primaires de rats ont été démontrés et la plateforme d'enregistrement a été validée avec des stimulations chimiques. De plus, une étude a été menée pour guider la croissance des neurones avec une fonctionnalisation de la surface de la bioplateforme. Avec la déposition de FDTS, des zones hydrophobes ont été obtenues avec de bons résultats pour le conditionnement de la croissance neuronale en deux dimensions.

1.5 Objectifs du projet de thèse

Les objectifs de ce projet de thèse sont partagés en trois parties principales. L'amélioration de performances de la plateforme et la co-intégration de différents types de mesures ainsi que l'enregistrement électrique avec des sondes passives et la mesure de pH avec des finFETs. Le contrôle de la croissance neuronale pour arriver à une interfaçage précis des axones et dendrites et l'obtention d'un enregistrement à une échelle subcellulaire. Et finalement, la caractérisation des dispositifs et la modélisation théorique pour arriver à l'investigation de questions biologiques.

Chapter 2

Fabrication et caractérisation des puces: vers une plateforme multi-détection

Dans le deuxième chapitre, la fabrication de la bioplateforme est décrite avec le packaging de la puce. Ensuite, les performances des dispositifs sont caractérisés et modélisés.

2.1 Fabrication d'une puce NEA

Pour obtenir une interface optimale entre cellule et électrodes, la structuration et le choix des matériaux utilisés sont fondamentaux.

2.1.1 Fabrication à large échelle

La première étape pour réaliser une puce Nano Electrode Arrays est la fabrication d'un jeu de masques pour la photolithographie. Notamment, les différentes étapes de photolithographie sont faites avec deux machines: Canon FPA $3000i4$ projection stepper et MA6 gen4 SUSS MicroTec mask aligner. Plus spécifiquement, le stepper est utilisé pour les deux premières étapes particulièrement critiques, avec un résolution de $400nm$, et la MA6 pour les autres étapes nécessitant moins de difficulté.

La structuration des dispositifs est faite avec un approche top-down, donc la gravure plasma est également fondamentale pour réaliser les nanopiliers des électrodes et la structure des transistors. Pour compléter la fabrication de la bioplateforme, plusieurs étapes sont nécessaires:

Oxide sacrificiel Pour contrôler les dimensions des nanopiliers après la photolithographie.

Dopage du silicon Nécessaire pour la définition des contacts de source et de drain des transistors.

Déposition des métaux Pour la création de l'interface des électrodes et des lignes conductrices.

Rapid thermal processing Cette étape permet d'obtenir du PtSi, un alliage biocompatible et conducteur.

Déposition d'oxides Pour garantir l'isolation entre les lignes conductrices et le milieu liquide.

Le résultat final peut être observé dans les images 2.1a et 2.1b. Les électrodes sont disposées en forme de matrice et les transistors sont positionnés pour avoir 8 couples d'électrodes passives et actives.

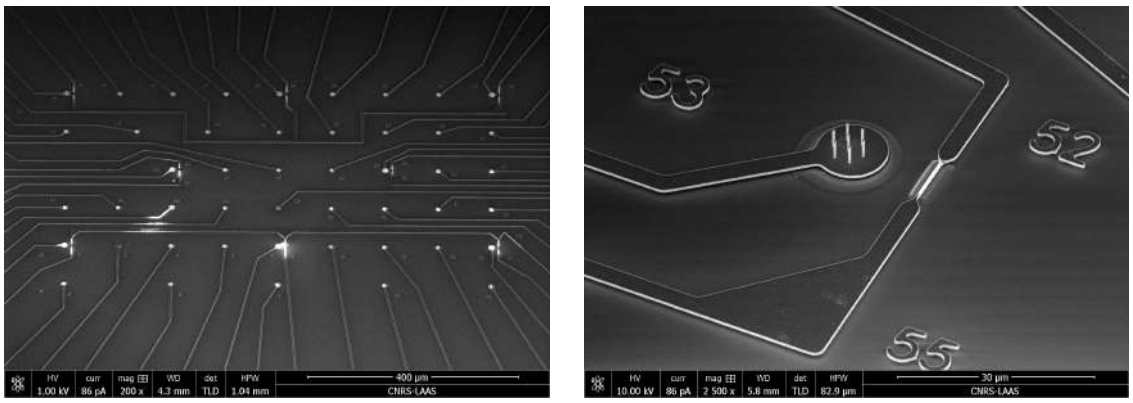

(a) Electrodes array. (b) Example of device co-integration.

Figure 2.1: a. Image SEM de la matrice d'électrodes. b. Image SEM d'une couple d'électrodes active et passive.

2.1.2 Co-intégration de dispositifs actifs

La co-intégration de différentes méthodes de mesure est une des plus récentes avancées en recherche. Ce projet veut amener la possibilité d'enregistrer l'activité électrique des cellules avec les sondes passives et de mesurer les variations de pH avec les transistors. De plus, les dimensions des dispositifs nous permettent d'obtenir une interface avec des cellules uniques. Le contrôle de chaque étape de fabrication est fondamental pour obtenir les deux dispositifs parfaitement fonctionnels. L'interface des FinFETs a été étudiée ainsi que ses performances avec l'utilisation de deux oxydes de grille: l'oxyde natif du silicium et l'oxyde d'aluminium.

2.1.3 Packaging

Après la micro fabrication des dispositifs, une étude sur le packaging des puces a été faite. Deux alternatives ont été étudiées, le flip chip avec des bumps d'or et la sérigraphie avec de la pâte à braser. Le packaging est composé de différentes étapes.

Bumps d'or ou pâte à braser Déposition manuelle des bumps d'or ou préparation de la pâte à braser.

Alignement Les contacts de la puce et du PCB son alignés.

Recuit Un traitement thermique est fait pour créer le contact métallique.

Colle epoxy Finalement une colle epoxy permet d'isoler les contacts entre eux.

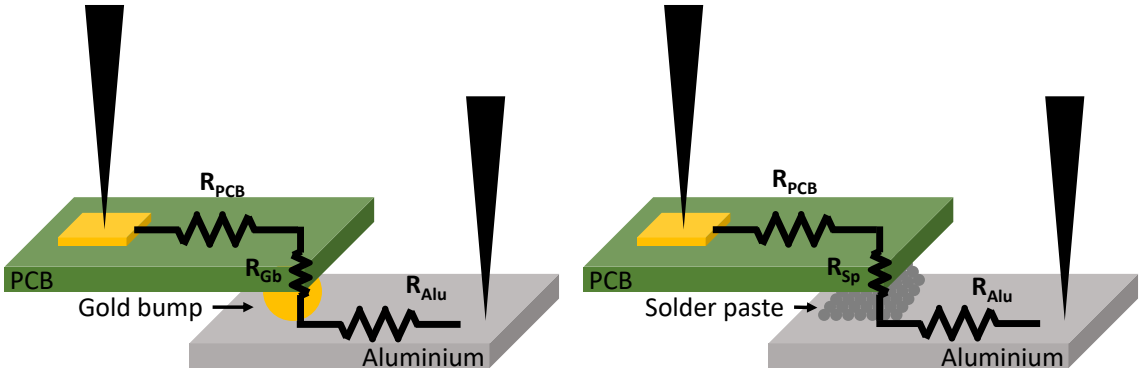

Figure 2.2: Représentation schématique de la mesure de résistance.

Des mesures de résistance électrique ont été faites pour déterminer quelle technique présente le plus d'avantages. Les résultats sont que le taux d'échec de la pâte à braser est inférieure par rapport aux bumps d'or. De plus, la résistance rajoutée à l'interface est négligeable dans les deux cas.

2.2 Mesure de champ électrique

La mesure de l'activité des cellules électrogéniques est basée sur la variation de potentiel électrique.

2.2.1 Théorie de la mesure du potentiel

Plusieurs modèles pour décrire l'interface métal liquide existent. Le plus récent et complet est le modèle de Grahame, crée en 1947. Ce modèle est composé de deux couches, les plans de Helmoltz intérieur et extérieur.

2.2.2 Les sondes passives

Utilisant ce modèle électrique, les sondes passives ont été caractérisées. Les résultats des mesures d'impédance ont déterminé la possibilité de séparer les électrodes par rapport au nombre de nanopilier, notamment 7 ou 3. L'interface entre le PtSi et le milieu liquide est représenté dans l'image 2.3a. L'impédance des sondes à $1KHz$ et les caractérisations sont présentés dans les graphes des images 2.3b, 2.3c, 2.3d.

Pour compléter la caractérisation des sondes, une modélisation a été faite également. Sur la base du modèle présenté précédemment, des simulations théoriques sont faites. Un très bon accord a été obtenu entre mesures et simulations. Depuis les simulations, il est donc possible d'extraire des valeurs pour chaque élément du circuit équivalent.

2.3 Mesure chimique

Comme expliqué auparavant, sur la plateforme sont intégrés des transistors utilisés pour la mesure du pH. Le mode de fonctionnement de ces dispositifs est ici expliqué avec leur caractérisation.

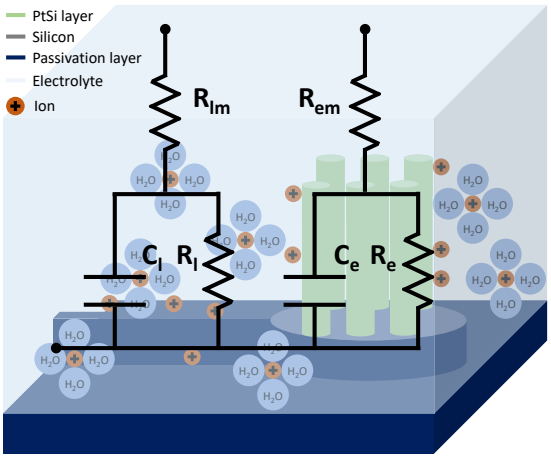

(a) Circuit équivalent.

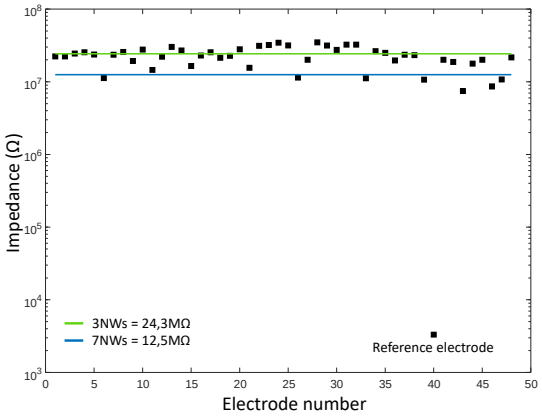

(b) Valeur d'impédance à $1KHz$.

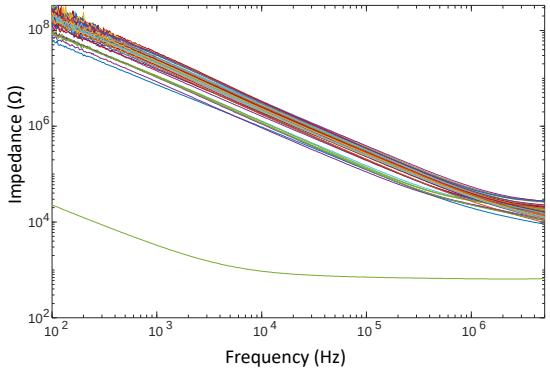

(c) Mesures d'impédances.

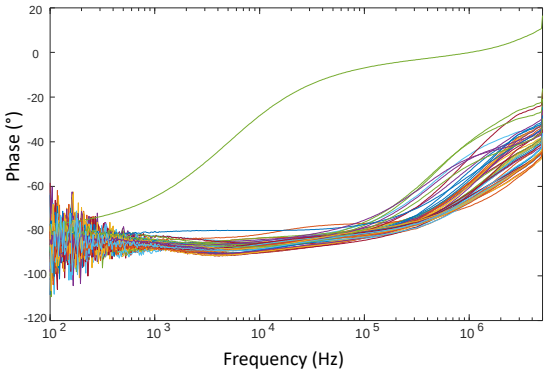

(d) Mesures de phase.

Figure 2.3: a. Schéma du circuit équivalent. b. Valeurs d'impédances pour 7 et 3 nanopiliers à $1KHz$. c et d. Plots de mesures d'impédance et de phase.

2.3.1 Théorie des ISFET

Les transistors ont la possibilité d'être utilisés comme ISFET et ces dispositifs suivent la loi de Nernst:

$$\Delta\phi = \frac{RT}{F} \ln \frac{a_{i1}}{a_{i2}}. \tag{2.1}$$

L'électricité dans le transistor dépend des caractéristiques géométriques des dispositifs mais aussi de l'interface entre l'oxyde de grille et le milieu liquide.

$$I_d = \beta(V_{gs} - V_T - \frac{1}{2}V_{ds})V_{ds} \qquad with \qquad \beta = \frac{\mu C_{ox} W}{L}. \tag{2.2}$$

Pour un ISFET en particulier, la sensibilité au pH est:

$$\frac{\delta\Psi_0}{\delta pH} = -2.3\frac{kT}{q}\alpha \qquad with \qquad \alpha = \frac{1}{\frac{2.3kTC_{dif}}{q^2\beta_{int}} + 1}. \tag{2.3}$$

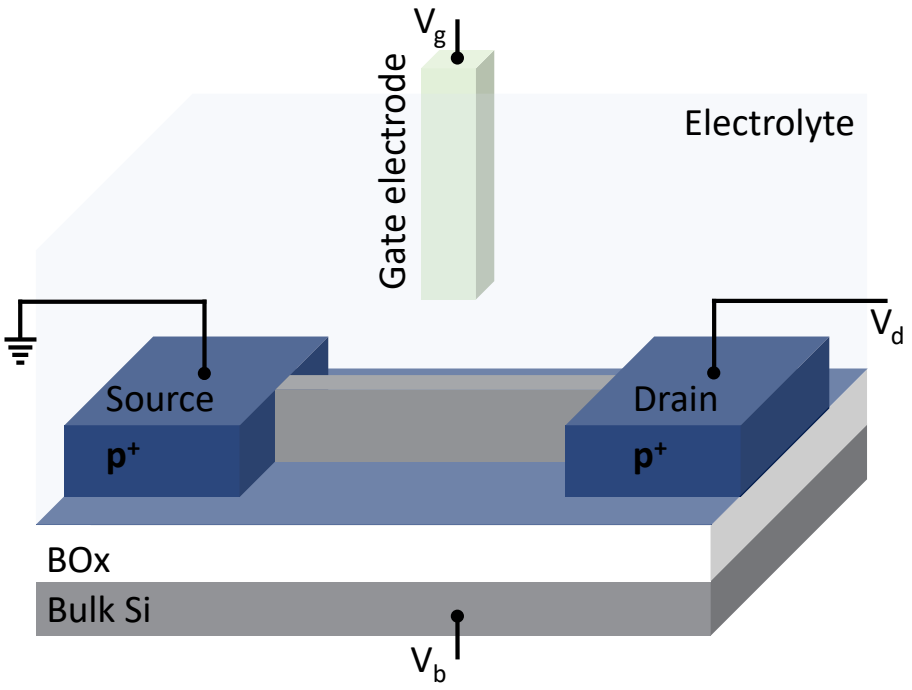

Figure 2.4: Schéma d'un dispositif ISFET

2.3.2 ISFET comme sonde de pH

Dans les années 60 a eu lieu la principale évolution de la technologie MOSFET. Beaucoup de groupes de recherche ont travaillé dans le domaine et maintenant les ISFET utilisés comme sondes de pH sont une technologie bien connue. L'influence des dimensions des dispositifs, comme des matériaux utilisés et de la possibilité d'aller au delà de la limite de Nernst ont été largement étudiés.

2.3.3 Caractérisation des FinFET comme sondes pH

En premier lieu, le fonctionnement correct des dispositifs est vérifié avec l'utilisation d'une polarisation par le bulk de la puce. Cette méthode permet de ne pas utiliser du liquide et de vérifier rapidement la bonne fabrication des transistors.

Après les premiers tests, les transistors sont caractérisés en milieu liquide avec une polarisation de grille imposée grâce à l'électrode de référence. Les dispositifs ont démontré des performances optimales avec des polarisations très faibles. Un avantage majeur pour l'utilisation avec des cellules est de pouvoir éviter des effets d'échauffement (image 2.5a).

La sensibilité au pH a été vérifiée avec de l'oxyde natif du silicium. Les résultats pour des pas de pH très grands étaient cohérents avec la loi de Nernst. Par contre, les dispositifs ne sont pas assez stables pour plusieurs utilisations consécutives. Pour cette raison l'utilisation de $5nm$ d'oxyde d'aluminium comme oxyde de grille est donc la meilleure solution. Cet oxyde est connu pour ses excellentes propriétés d'isolation et de sensibilité au pH. Avec l'utilisation de cet oxyde, les performances des transistors sont optimales et avec l'utilisation d'une polarisation de bulk la possibilité d'aller au delà de la limite de Nernst a été vérifiée.

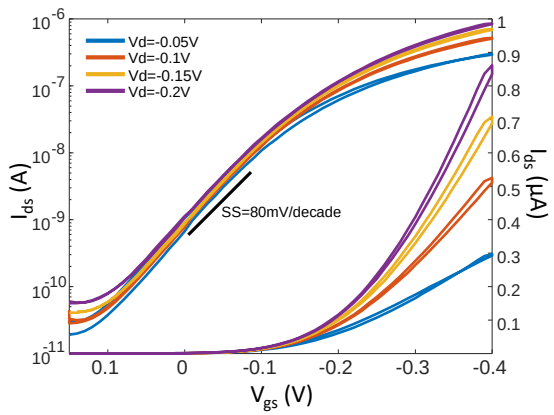

(a) Caractérisation du transistor avec PBS.

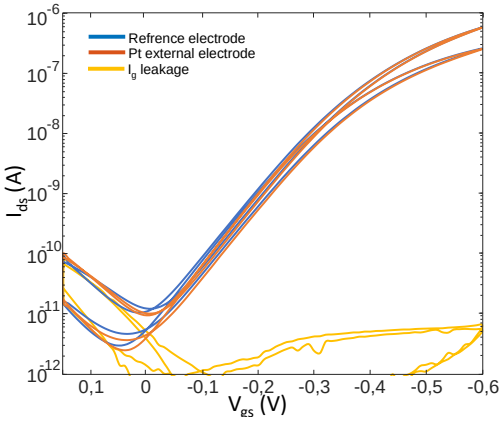

(b) Caractérisation des électrodes.

Figure 2.5: a. Caractérisation du ISFET avec PBS à différentes polarisations. b. Caractérisation des électrodes pour la polarisation du milieu.

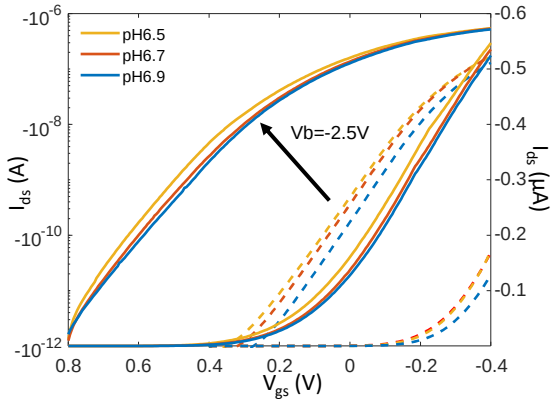

(a) Caractérisation ISFET avec Al_2O_3 et polarisation de bulk.

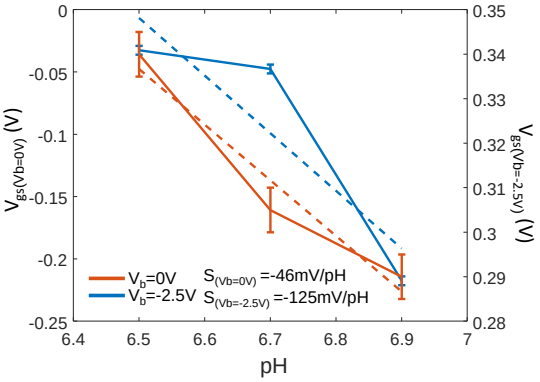

(b) Sensibilité au pH.

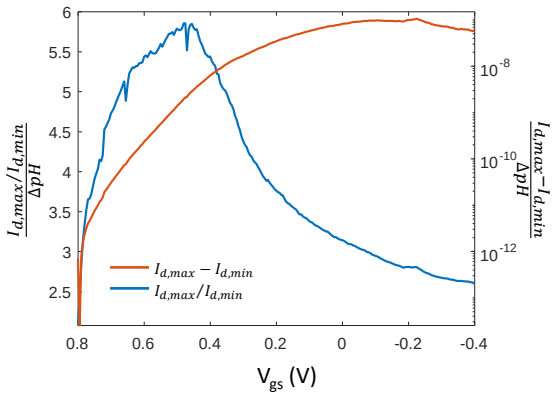

(c) Sensibilité de l'ISFET par unité de pH.

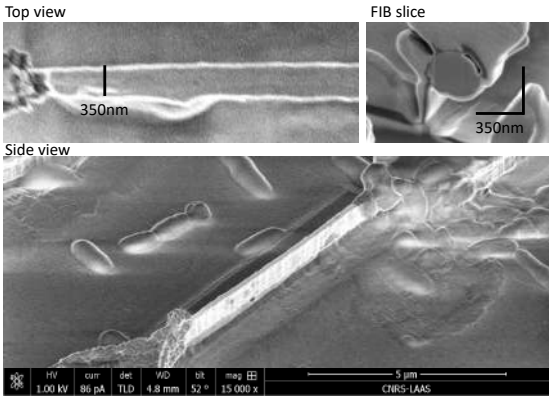

(d) Image SEM du dispositif.

Figure 2.6: a. Caractérisation des ISFET avec des solutions à différentes pH. b. Sensibilité au pH des ISFET, au delà de la limite de Nernst avec polarisation de bulk. c. Sensibilité des transistors par unité de pH avec Al_2O_3. d. Images SEM du dispositif après plusieurs utilisations.

Chapter 3

Vers l'interfaçage subcellulaire et l'axogénèse

Pour étudier les réseaux neuronaux, de nouvelles technique ont été étudiées pour guider les prolongements de cellules. Ici en particulier, l'axogénèse est conduite avec des micro canaux fabriqués avec deux méthodes différentes.

3.1 Culture cellulaire

Pendant le projet, des cellules primaires de rat ont été utilisées. Ce sont des cellules qui ne sont pas encore développées au moment de la mise en culture et qui vont créer des connexions directement sur les dispositifs.

3.1.1 Neurones primaires de rat

La culture primaire a été rendue possible grâce à la collaboration de l'équipe de Daniel Gonzalez-Dunia. C'est au laboratoire Infinity-Inserm que la dissection était effectuée, puis la mise en culture était faite au LAAS. Les deux procédés suivent des protocoles précis qui on été mis au point par les équipes. Notamment, le protocole pour la mise en culture sur dispositif est:

Stérilisation Les dispositifs sont stérilisés avec de l'éthanol 70%.

Premier coating Une molécule d'adhésion, la Poly ornithine, est déposée sur les puces.

Deuxieme coating Après rinçage de la PO, de la laminine est déposée sur les puces pour favoriser l'adhésion.

Mise en culture La concentration des cellules est corrigée et elles sont mises en culture avec un milieu préparé précédemment.

Un exemple de cellules en culture est visible dans les images 3.1a et 3.1b pour 1 jour en culture (1DIV) et 3 jours en culture (3DIV).

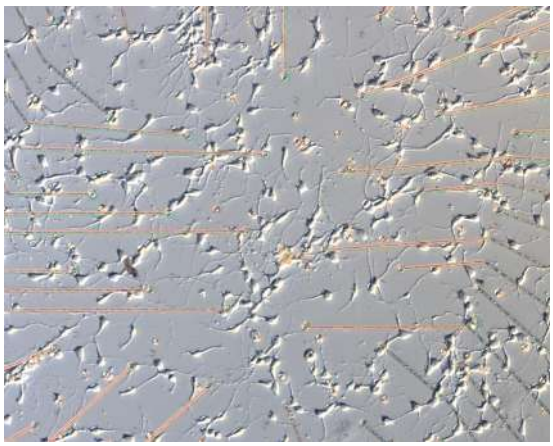

(a) Image optique des cellules en culture après 1DIV.

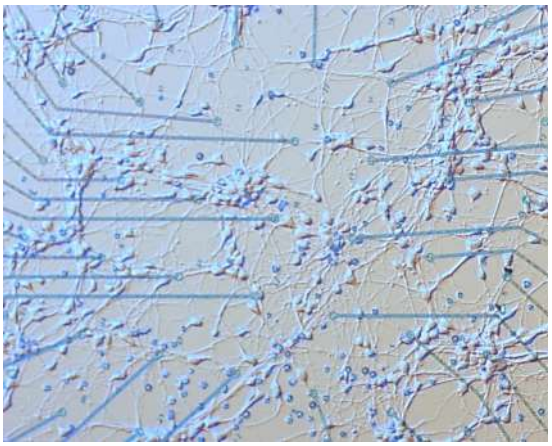

(b) Image optique des cellules en culture après 3 DIV.

Figure 3.1: Exemple d'une culture cellulaire sur une puce. La plupart des connexions sont établies en trois jours.

3.2 Possibilités pour guider la croissance neuronale

Pour guider les prolongements neuronaux, différentes solutions ont été étudiées:

Topographic structuration Structures en trois dimensions pour contraindre les prolongements cellulaires.

Surface functionalization Fonctionnalisation basée sur le dépôt de molécules chimiques avec des propriétés particulières.

Microchannels Fabrication de micro canaux pour limiter et guider les prolongements dans des directions définies.

Dans le passé, notre groupe de recherche avait déjà obtenu de très bons résultats avec une fonctionnalisation de surface décrite dans l'image 3.2.

Pour ce projet, nous avons choisi d'étudier la possibilité d'intégrer des micro canaux sur les réseaux d'électrodes de nos puces.

3.2.1 État-de-l'art

Les micro canaux ont été largement étudiés pour plusieurs applications: chimie, biologie, médecine et physique. Le design typique de ces structures est composé de deux chambre connectées par plusieurs canaux. Des exemples de cette technologie sont visibles dans les images 3.3a et 3.3b.

3.3 Micro canaux sur puces NEA

Nous avons étudié deux méthodes pour fabriquer des micro canaux:

SU-8 La structuration de la résine SU8 par photolithographie peut être directement intégrée sur la puce.

PDMS Le PDMS peut être structuré avec un moule pour obtenir des micro canaux.

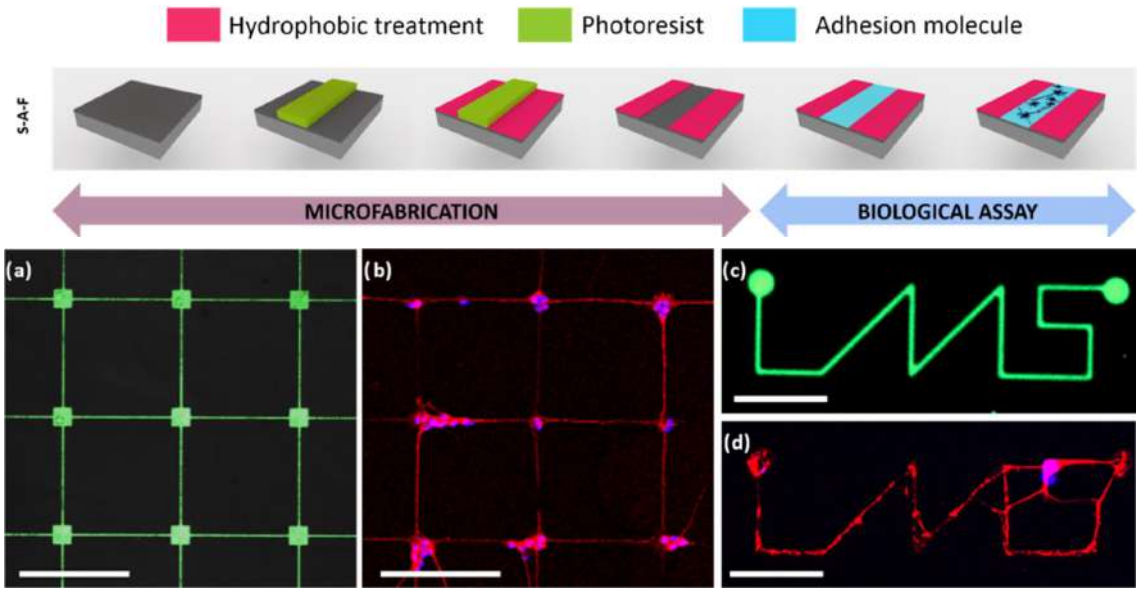

Figure 3.2: Fonctionnalisation de surface par photolithographie.

Le deux méthodes ont des avantages mais également des inconvénients et ces points vont être décrits dans ce chapitre.

3.3.1 Photolithographie SU-8

La structuration de la résine SU8 est faite avec une photolithographie qui profite d'un effet optique particulier du stepper, le "diabolo effect". Cet effet permet de modifier la position de la mise au point de la lumière UV et d'obtenir des micro canaux enterrés dans la résine. Pour cela, un jeu de masque a été fabriqué, les détails sont visibles dans l'image 3.4. Cette méthode garantit un parfait alignement avec le réseau d'électrodes sur la puce, mais c'est également une étape très sensible qui peut échouer. Dans ce cas, étant la dernière étape du processus de micro fabrication, cela pouvait faire perdre une plaque entière.

3.3.2 Structuration du PDMS

En alternative, la structuration du PDMS peut être facilement obtenue avec une plaque utilisée comme moule. Les dimensions des micro canaux obtenues dépendent uniquement de la résolution de la résine utilisée pour le moule. Cette méthode permet de fabriquer très facilement des micro canaux, mais limite fortement l'alignement. Cet alignement est fait à la main, sous un microscope. Cependant, cette méthode est beaucoup moins contraignante que la précédente. Les tests avec cette méthode de fabrication de micro canaux ont permis d'obtenir d'excellents résultats comme dans l'image 3.5. Les cellules ont crée des connexions dans les micro canaux entre les deux chambres principales (image 3.6).

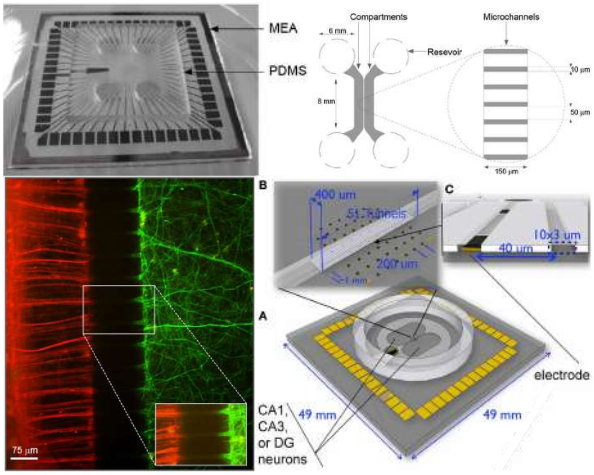

(a) Micro canaux sur dispositif MEA.

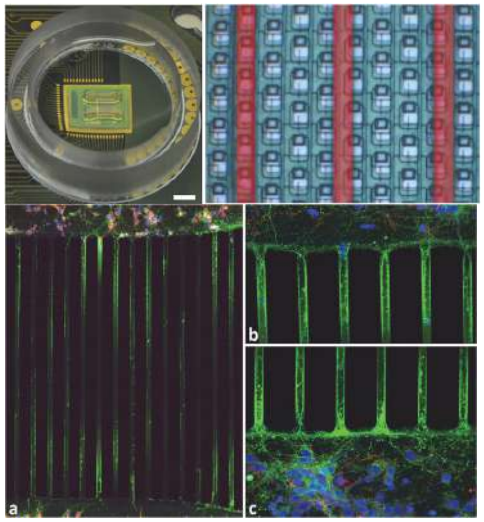

(b) Micro canaux sur dispositif CMOS.

Figure 3.3: a. Schéma de la structure fabriquée sur une puce MEA, les connexions entre cellules sont possibles exclusivement dans les micro canaux. b. Exemple des structures composée de micro canaux sur un réseau d'électrodes CMOS.

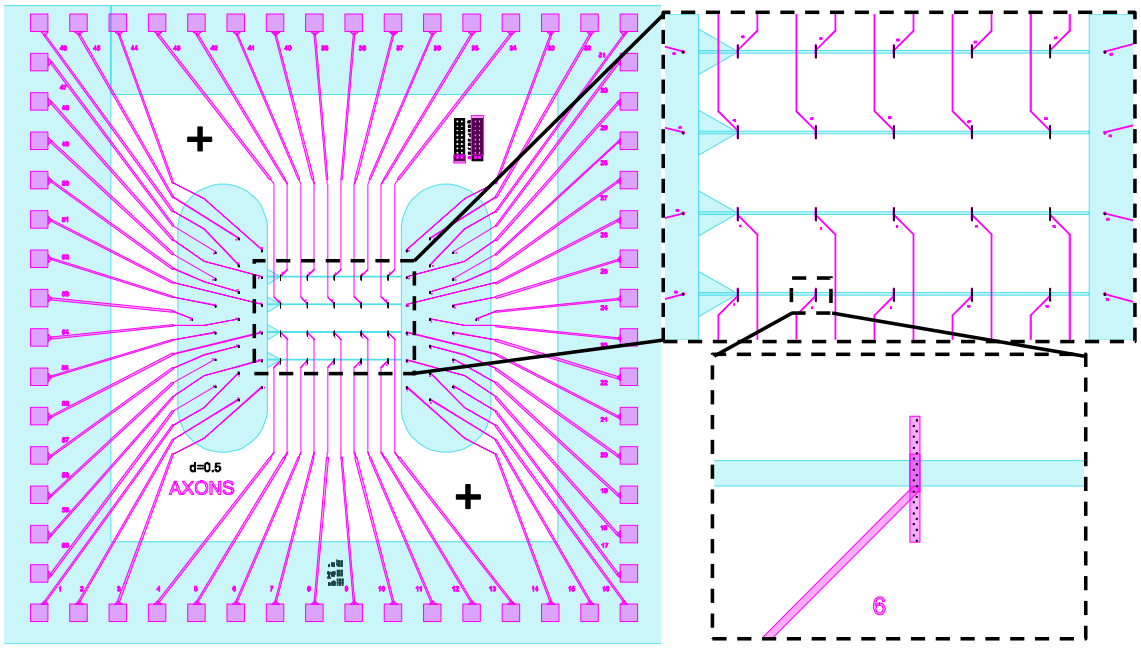

Figure 3.4: Schéma du design de masque pour la photolithographie de la résine SU8.

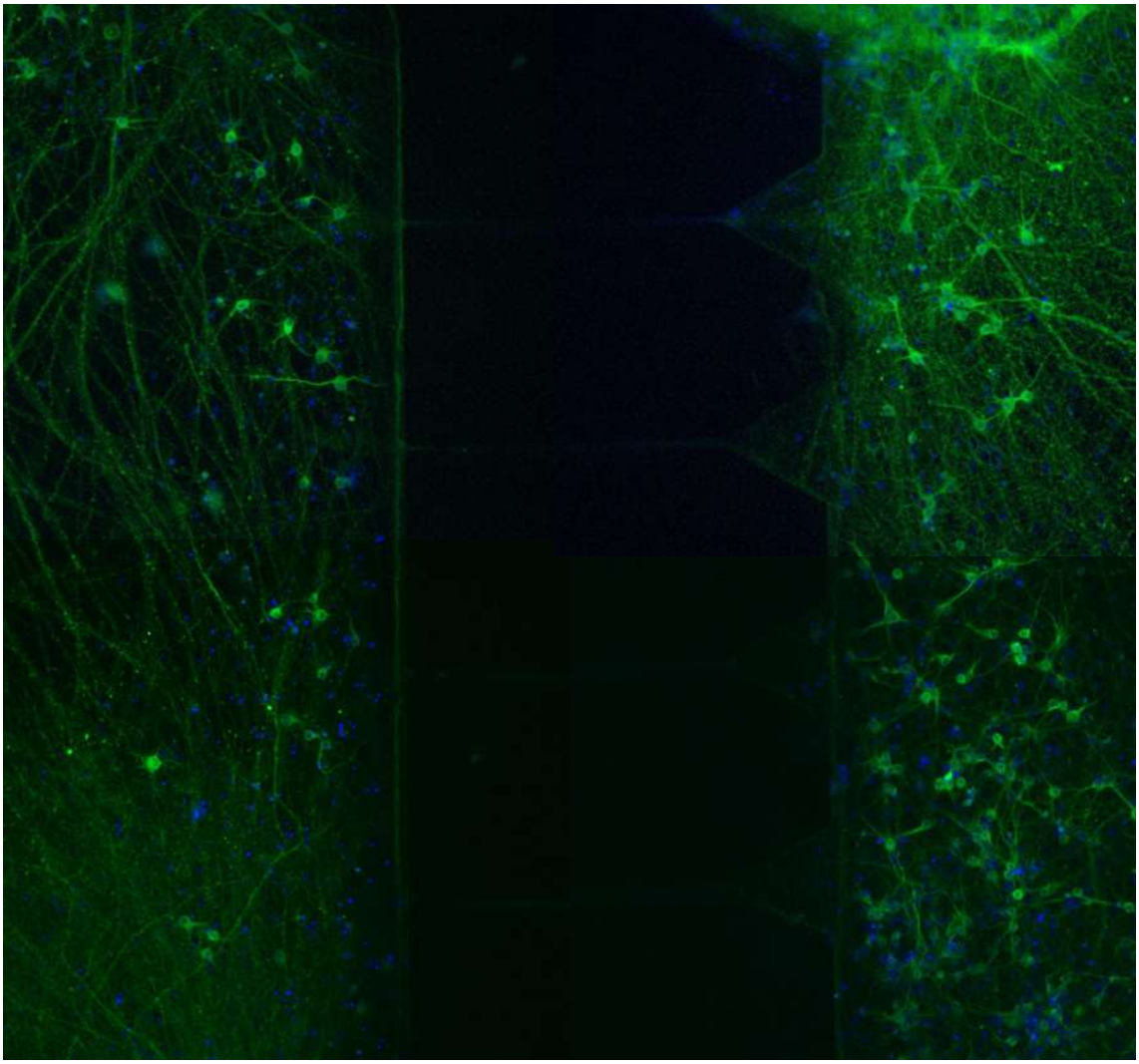

Figure 3.5: Image en fluorescence des cellules en culture après 7DIV.

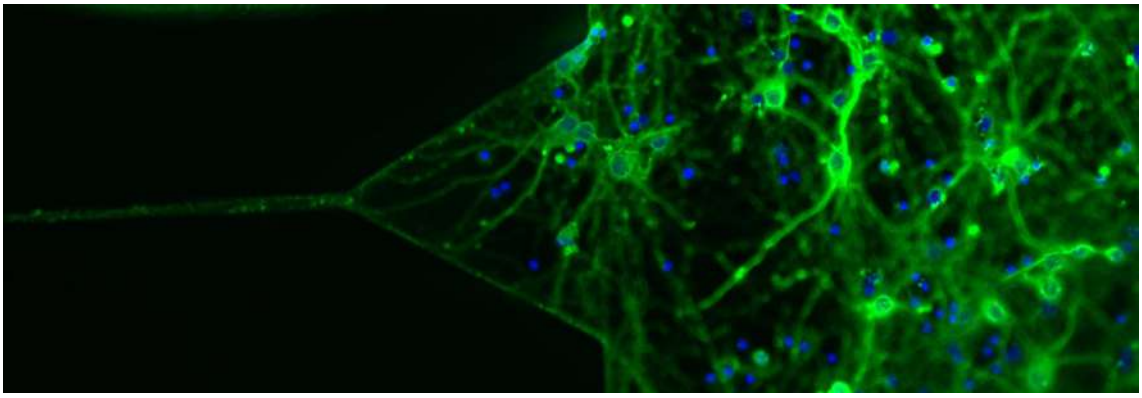

Figure 3.6: Image en fluorescence des cellules à l'entrée d'un micro canal après 7DIV.

Chapter 4

Modélisation théorique et applications pour études biologiques

Un système dédié est nécessaire pour faire des enregistrements d'activité électrique cellulaire. Ce système est décrit dans ce chapitre et des exemples d'expériences sont présentés avec l'analyse de data.

4.1 Système d'enregistrement d'électrophysiologie

Le système d'enregistrement a été conçu au laboratoire avec le software permettant de le contrôler. Un schéma descriptif peut être observé dans l'image 4.1. Il est composé d'un support pour les puces connecté au multiplexeur et d'une carte électronique conçue au laboratoire qui nous permet de changer la méthode d'enregistrement sur chaque électrode. Ce multiplexeur est connecté à une carte d'acquisition qui transfère les datas à l'ordinateur.

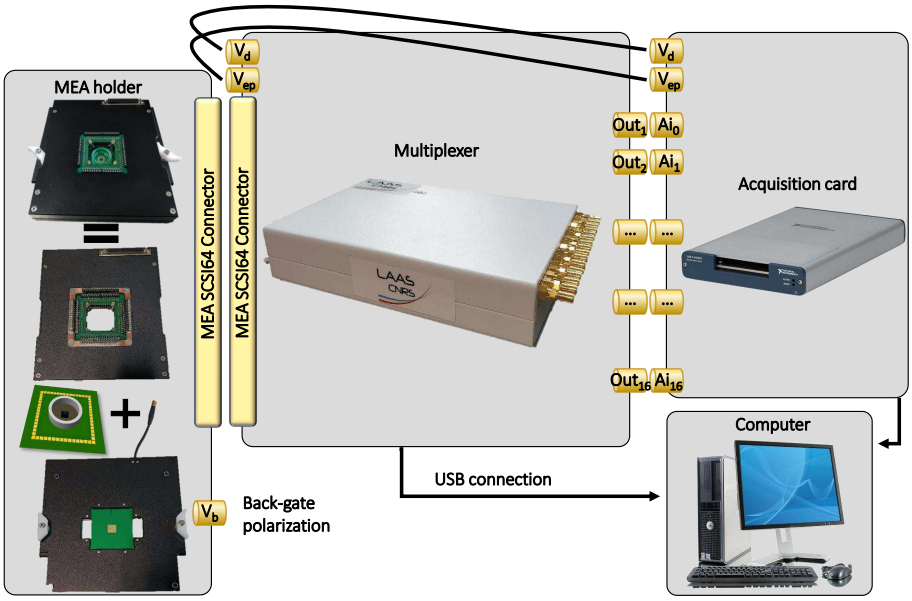

Figure 4.1: Parties principales du système d'enregistrement.

4.2 Enregistrement électrique

Pendant le projet, nous avons pu obtenir de nombreuses expériences d'enregistrement d'activité électrique de cellules. Nous avons également pu valider le système d'enregistrement avec des protocoles pour modifier l'activité des cellules.

4.2.1 Enregistrement d'activité spontanée

La mesure de l'activité spontanée des cellules est classiquement utilisée pour vérifier la performance des électrodes. Ici un exemple de l'activité électrique enregistrée est visible dans l'image 4.2. L'amplitude enregistrée est de plusieurs millivolts pour le pic le plus grand et au même moment des pics liés à l'activité synaptique sont visibles juste avant et après les pics principaux. La possibilité d'enregistrer l'activité principale et l'activité synaptique simultanément a très rarement été démontrée dans l'état-de-l'art et n'est pas possible avec des dispositifs commerciaux.

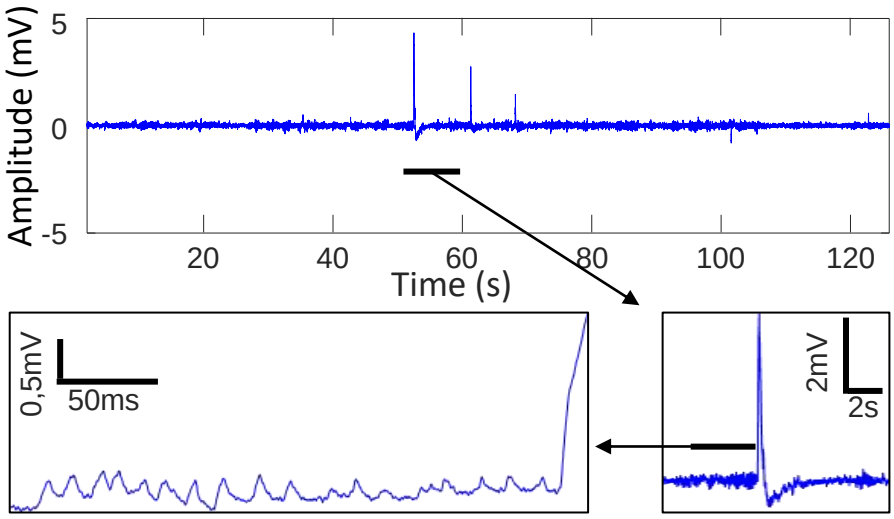

Figure 4.2: Exemple d'un enregistrement d'activité électrique spontanée.

4.2.2 Validation du système d'enregistrement

La validation du système d'enregistrement est faite avec un protocole précis qui utilisent trois molécules en particulier:

TTX Neurotoxine qui empêche l'activation des canaux ioniques sodium.

APV C'est un antagoniste des récepteurs NMDA.

CNQX C'est un antagoniste des récepteurs AMPA.

Ce cocktail de molécules assure que l'activité des cellules soit provisoirement bloquée. Dans l'image 4.3, il est possible d'observer que l'activité spontanée initiale est désactivée avec le cocktail de molécules. Logiquement, l'enregistrement ne donne pas de pics quand les molécules sont actives mais une fois le rinçage fait, l'activité spontanée est rétablie. De plus, l'activité peut être augmentée avec une stimulation chimique à base de KCl.

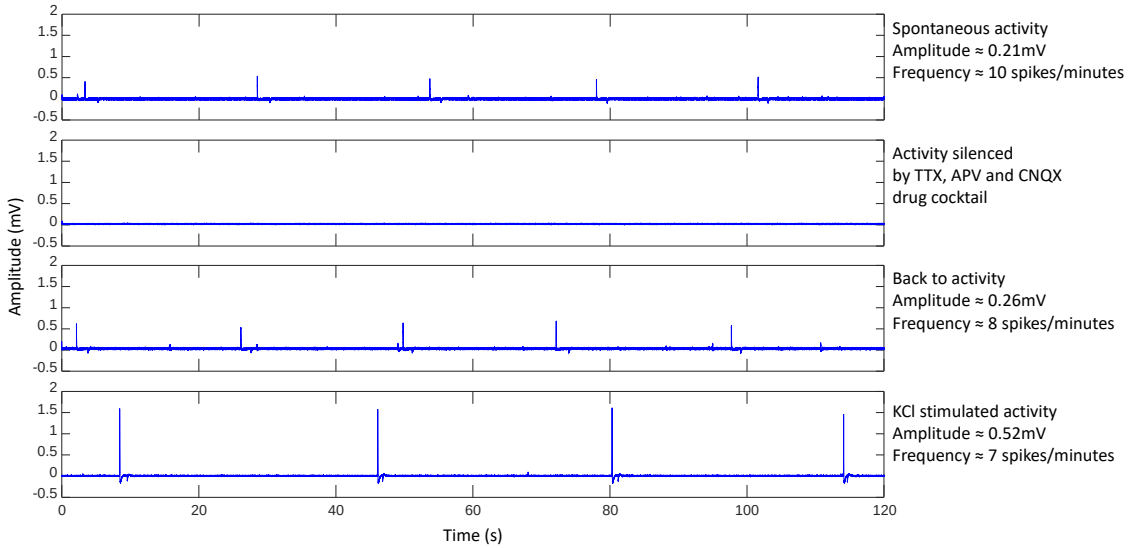

Figure 4.3: Exemple d'une expérience pour la validation du système d'enregistrement.

4.2.3 Détection de pics et analyses de data

La quantité de data enregistrée pour chaque expérience était très importante, donc un script pour l'analyse de data était nécessaire. Pour cela, MATLAB a été utilisé afin de réaliser un script pour filtrer les datas et détecter les pics. Le filtre est utile pour la réduction du bruit électrique de fond. La détection de pics est faite avec un seuil qui se déplace avec le bruit électrique pour éviter la détection de pics qui ne provient pas de l'activité neuronale. De plus, le script permet d'obtenir les tendances pour les fréquences et les amplitudes de l'activité enregistrées.

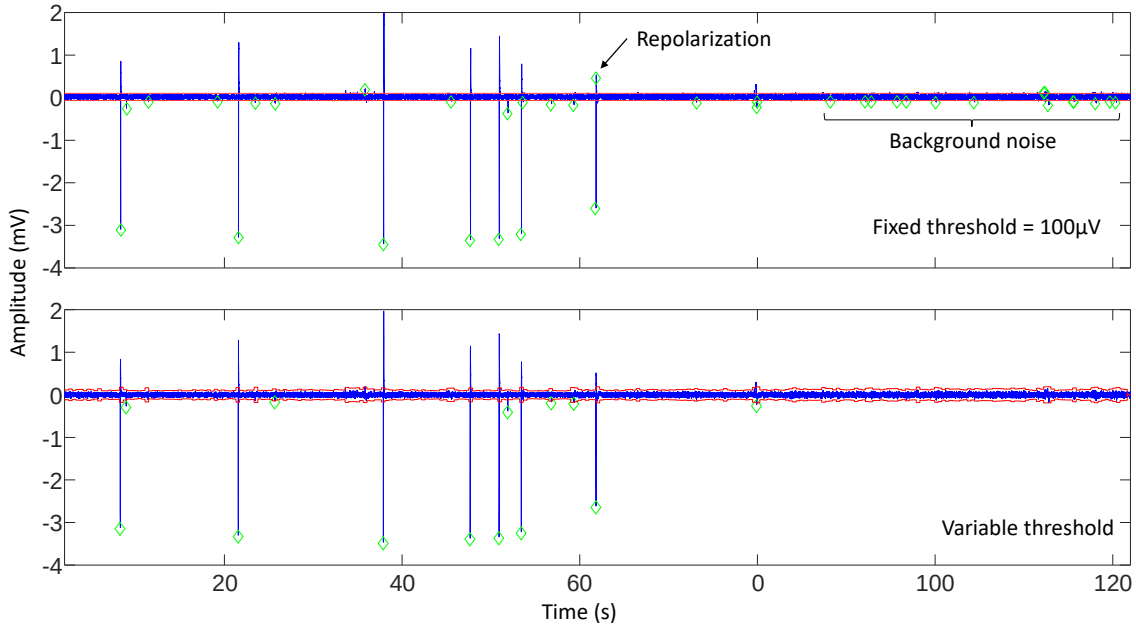

Figure 4.4: Exemple de détection de pics avec seuil fixe ou variable.

4.2.4 Modèle électrique équivalent et déconvolution

Après la définition du modèle de Hodgkin-Huxley, plusieurs groupes de recherche ont essayé d'extraire l'effet des interfaces et du système d'enregistrement pour récupérer le signal original des cellules. Avec la caractérisation des sondes précédentes et les modèles existants dans la littérature nous avons calculé la fonction de transfert du modèle équivalent et traité les signaux enregistrés. Le modèle est visible dans l'image 4.5a et le résultat de la procédure de déconvolution dans l'image 4.5b.

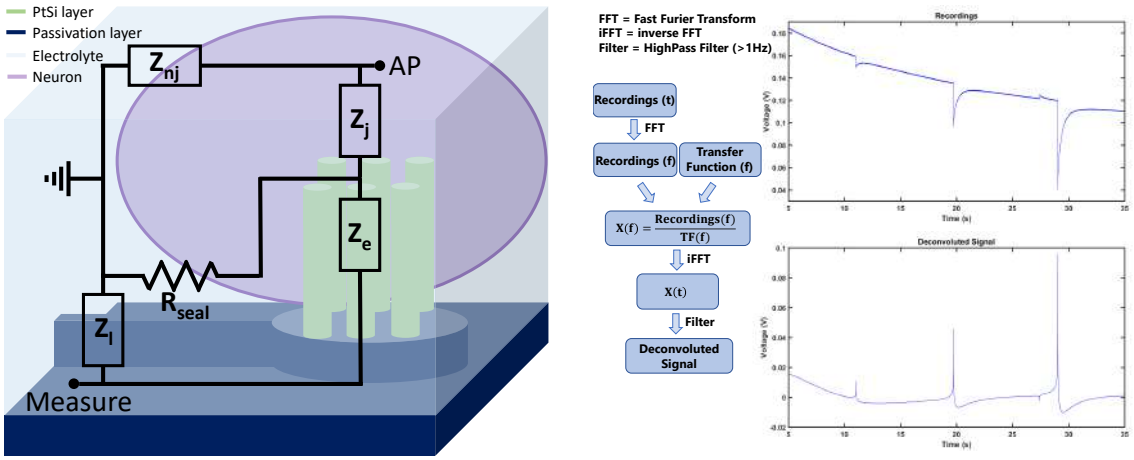

(a) Circuit équivalent.

(b) Procédure de déconvolution.

Figure 4.5: a. Schéma du modèle électrique équivalent du système d'interface entre cellules et sondes. b. Schéma de la procédure de déconvolution et du résultat obtenu avec un exemple d'enregistrement.

4.3 Investigations biologiques

Après la validation de la plateforme d'enregistrement, encore en collaboration avec l'équipe du laboratoire Infinity, des expériences ont été faites pour étudier l'effet de l'Amyloid Beta Peptide et du Borna Disease Virus sur l'activité électrique des neurones.

4.3.1 Résultats pour Amyloid Beta Peptide

La première étude a été faite sur l'Amyloid Beta Peptide. Ce peptide est souvent utilisé comme modèle pour la maladie d'Alzheimer. Il a été déjà largement étudié et ses effets sur la plasticité neuronale sont connus. Les enregistrements faits avec l'effet de ce peptide ont permis d'extraire les résultats visibles dans l'image 4.6. L'effet sur l'amplitude des pics est une diminution du nombre de pics avec une basse amplitude et une augmentation relative des pics avec une grande amplitude. De plus, la fréquence d'activation des cellules augmente dans un premier temps pour ensuite être réduite sur le long terme.

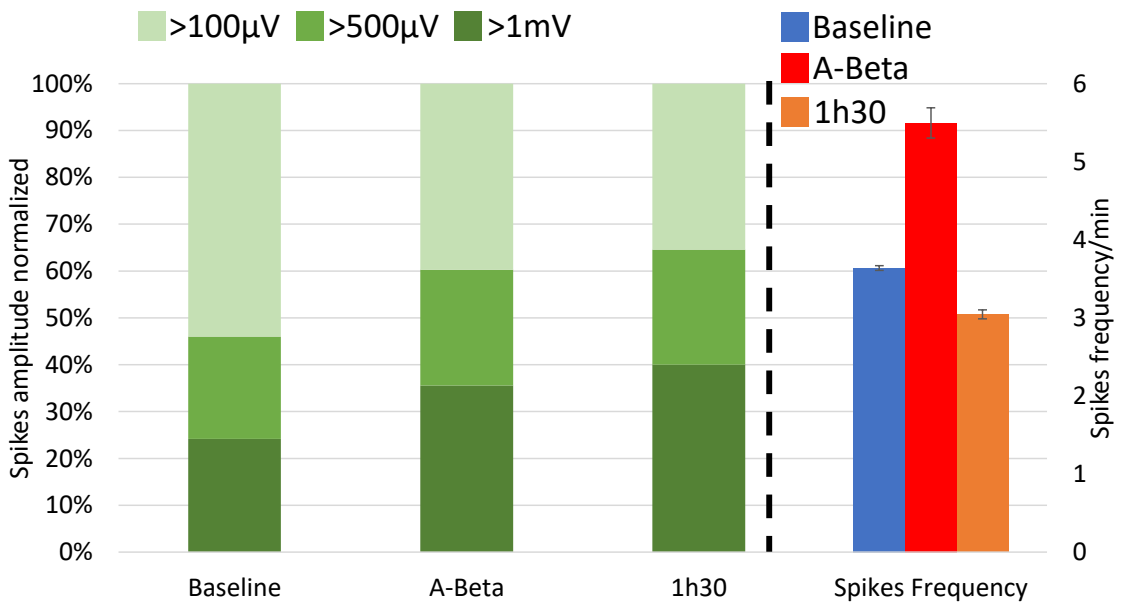

Figure 4.6: Résultats de l'expérience avec Amylolid Beta Peptide.

4.3.2 Résultats pour Borna Disease Virus

La deuxième expérience a été réalisée avec l'utilisation du Borna Disease Virus. Ce virus a été récemment étudié pour ces proprietés de multiplication liés à des cassures de l'ADN des cellules. De plus, l'accumulation de ces cassures cause aussi des altérations de l'activité électrique des neurones. Les résultats obtenus sont visibles dans l'image 4.7. L'activité électrique est énormément réduite pour les cellules infectées, et le nombre de pics avec une grande amplitude est réduite.

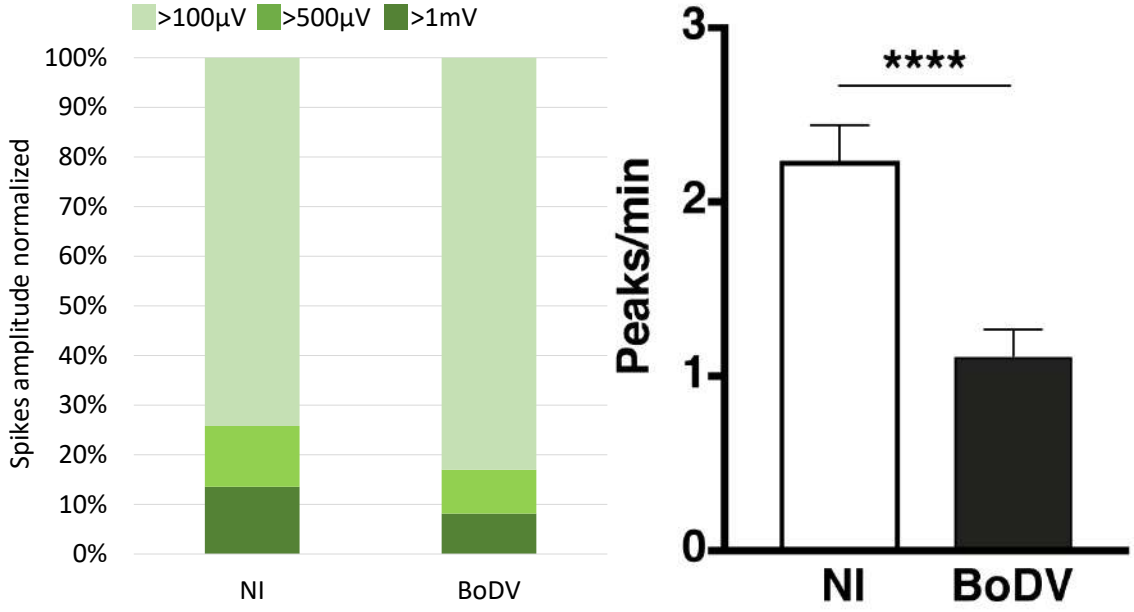

Figure 4.7: Résultats de l'expérience avec Borna Disease Virus.

Bibliography

[1] H. Berger, *Uber das Elektrenkephalogramm des Menschen*, vol. 102. 1924.

[2] W. Einthoven, "The string galvanometer and the human electrocardiogram," *Huygens Institute-Royal Netherlands Academy of Arts and Sciences (KNAW)*, 1904.

[3] A. L. Hodgkin and A. F. Huxley, "A quantitative description of membrane current and its application to conduction and excitation in nerve," *J. Physiol*, pp. 500–544, 1952.

[4] O. P. Hamill, A. Marty, E. Neher, B. Sakmann, and F. J. Sigworth, "Improved patch-clamp techniques for high-resolution current recording from cells and cell-free membrane patches," *Pfltigers Archiv European Journal of Physiology*, vol. 391, pp. 85–100, 1981.

[5] A. D. Gitler, P. Dhillon, and J. Shorter, "Neurodegenerative disease: Models, mechanisms, and a new hope," 5 2017.

[6] K. D. Wise, A. M. Sodagar, Y. Yao, M. N. Gulari, G. E. Perlin, and K. Najafi, "Microelectrodes, microelectronics, and implantable neural microsystems," *Proceedings of the IEEE*, vol. 96, pp. 1184–1202, 2008.

[7] T. J. Blanche, M. A. Spacek, J. F. Hetke, and N. V. Swindale, "Polytrodes: High-density silicon electrode arrays for large-scale multiunit recording," *Journal of Neurophysiology*, vol. 93, pp. 2987–3000, 5 2005.

[8] J. Csicsvari, D. A. Henze, B. Jamieson, K. D. Harris, A. Sirota, P. Barthó, K. D. Wise, and G. Buzsáki, "Massively parallel recording of unit and local field potentials with silicon-based electrodes," *Journal of Neurophysiology*, vol. 90, pp. 1314–1323, 8 2003.

[9] K. D. Wise, D. J. Anderson, J. F. Hetke, D. R. Kipke, and K. Najafi, "Wireless implantable microsystems: High-density electronic interfaces to the nervous system," vol. 92, pp. 76–97, Institute of Electrical and Electronics Engineers Inc., 2004.

[10] I. D. Ruz and S. R. Schultz, "Localising and classifying neurons from high density mea recordings," *Journal of Neuroscience Methods*, vol. 233, pp. 115–128, 8 2014.

[11] M. Ganji, A. C. Paulk, J. C. Yang, N. W. Vahidi, S. H. Lee, R. Liu, L. Hossain, E. M. Arneodo, M. Thunemann, M. Shigyo, A. Tanaka, S. B. Ryu, S. W. Lee, Y. Tchoe, M. Marsala, A. Devor, D. R. Cleary, J. R. Martin, H. Oh, V. Gilja, T. Q. Gentner, S. I. Fried, E. Halgren, S. S. Cash, and S. A. Dayeh, "Selective formation of porous pt nanorods for highly electrochemically efficient neural electrode interfaces," *Nano Letters*, vol. 19, pp. 6244–6254, 9 2019.

[12] R. Perin, T. K. Berger, and H. Markram, "A synaptic organizing principle for cortical neuronal groups," *Proceedings of the National Academy of Sciences of the United States of America*, vol. 108, pp. 5419–5424, 3 2011.

[13] C. Wood, C. Williams, and G. J. Waldron, "Patch clamping by numbers," *DDT*, vol. 9, 2004.

[14] K. Weale, "A new micro-electrode for electro-physiological work," *Nature*, 1951.

[15] W. Franks, F. Heer, S. Taschini, R. Sunier, C. Hagleitner, A. Hierlemann, and H. Baltes, "Cmos monolithic microelectrode array for stimulation and recording of natural neural networks," 2003.

[16] L. Berdondini, K. Imfeld, A. Maccione, M. Tedesco, S. Neukom, M. Koudelka-Hep, and S. Martinoia, "Active pixel sensor array for high spatio-temporal resolution electrophysiological recordings from single cell to large scale neuronal networks," *Lab On A Chip*, 2009.

[17] J. Abbott, T. Ye, K. Krenek, R. S. Gertner, S. Ban, Y. Kim, L. Qin, W. Wu, H. Park, and D. Ham, "A nanoelectrode array for obtaining intracellular recordings from thousands of connected neurons," *Nature Biomedical Engineering*, vol. 4, pp. 232–241, 2 2020.

[18] B. Eversmann, M. Jenkner, F. Hofmann, C. Paulus, R. Brederlow, B. Holzapfl, P. Fromherz, M. Merz, M. Brenner, M. Schreiter, R. Gabl, K. Plehnert, M. Steinhauser, G. Eckstein, D. Schmitt-Landsiedel, and R. Thewes, "A 128 $\times$ 128 cmos biosensor array for extracellular recording of neural activity," vol. 38, pp. 2306–2317, 12 2003.

[19] U. Frey, U. Egert, F. Heer, S. Hafizovic, and A. Hierlemann, "Microelectronic system for high-resolution mapping of extracellular electric fields applied to brain slices," *Biosensors and Bioelectronics*, 2008.

[20] U. Frey, U. Egert, F. Heer, S. Hafizovic, and A. Hierlemann, "Microelectronic system for high-resolution mapping of extracellular electric fields applied to brain slices," *Biosensors and Bioelectronics*, vol. 24, pp. 2191–2198, 3 2009.

[21] E. Wanke, F. Gullo, E. Dossi, G. Valenza, and A. Becchetti, "Neuron-glia cross talk revealed in reverberating networks by simultaneous extracellular recording of spikes and astrocytes' glutamate transporter and k+ currents," *J Neurophysiol*, vol. 116, pp. 2706–2719, 2016.

[22] I. Colombi, F. Tinarelli, V. Pasquale, V. Tucci, and M. Chiappalone, "A simplified in vitro experimental model encompasses the essential features of sleep," *Frontiers in Neuroscience*, vol. 10, 2016.

[23] J. Suresh, M. Radojicic, L. L. Pesce, A. Bhansali, J. Wang, A. K. Tryba, J. D. Marks, and W. van Drongelen, "Network burst activity in hippocampal neuronal cultures: the role of synaptic and intrinsic currents," *J Neurophysiol*, vol. 115, pp. 3073–3089, 2016.

[24] S. Joo and Y. Nam, "Slow-wave recordings from micro-sized neural clusters using multiwell type microelectrode arrays," *IEEE Transactions on Biomedical Engineering*, vol. 66, pp. 403–410, 2 2019.

[25] A. Hierlemann, U. Frey, S. Hafizovic, and F. Heer, "Growing cells atop microelectronic chips: Interfacing electrogenic cells in vitro with cmos-based microelectrode arrays," *Proceedings of the IEEE*, vol. 99, pp. 252–284, 2011.

[26] M. E. J. Obien, K. Deligkaris, T. Bullmann, D. J. Bakkum, and U. Frey, "Revealing neuronal function through microelectrode array recordings," 2015.

[27] F. Heer, S. Hafizovic, T. Ugniwenko, U. Frey, W. Franks, E. Perriard, J.-C. Perriard, A. Blau, C. Zieger, and A. Hierlemann, "Single-chip microeletronic system to interface with living cells," *Biosensors and Bioelectronics*, 2007.

[28] U. Frey, J. Sedivy, F. Heer, R. Pedron, M. Ballini, J. Mueller, D. Bakkum, S. Hafizovic, F. D. Faraci, F. Greve, K. U. Kirstein, and A. Hierlemann, "Switch-matrix-based high-density microelectrode array in cmos technology," *IEEE Journal of Solid-State Circuits*, vol. 45, pp. 467–482, 2 2010.

[29] W. Baumann, M. Lehmann, A. Schwinde, R. Ehret, M. Brischwein, and B. Wolf, "Microeletronic sensor system for microphysiological application on livin cells," *Sensors and Actuators*, 1999.

[30] K. Sawada, T. Ohshina, T. Hizawa, H. Takao, and M. Ishida, "A novel fused sensor for photo- and ion-sensing," *Sensors and Actuators*, 2005.

[31] T. Tokuda, A. Yamamoto, K. Kagawa, M. Nunoshita, and J. Ohta, "A cmos image sensor with optical and potential dual imaging function for on-chip bioscientific applications," *Sensors and Actuators*, 2006.

[32] B. Johnson, S. T. Peace, T. A. Cleland, and A. Molnar, "A scalable cmos sensor array for neuronalrecording and imaging," *IEEE Sensors*, 2011.

[33] B. Johnson, S. T. Peace, A. Wang, T. A. Cleland, and A. Molnar, "A 768-channel cmos microelectrode array with angle sensitive pixels for neuronal recording," *IEEE Sensors Journal*, vol. 13, pp. 3211–3218, 2013.

[34] A. Romani, N. Manaresi, L. Marzocchi, G. Medoro, A. Leonardi, L. Altomare, M. Tartagni, and R. Guerrieri, "Capacitive sensor array for localization of bioparticles in cmos lab-on-a-chip," *BIOMICROSYSTEMS*, 2004.

[35] V. Saunier, E. Flahaut, M.-C. Blatché, C. Bergaud, and A. Maziz, "Microeletrodes from pedot-carbon nanofiber composite for high performance neural recording, stimulation and neurochemical sensing," *MethodsX*, 2020.

[36] V. A. Magnotta, H. Y. Heo, B. J. Dlouhy, N. S. Dahdaleh, R. L. Follmer, D. R. Thedens, M. J. Welsh, and J. A. Wemmie, "Detecting activity-evoked ph changes in human brain," *Proceedings of the National Academy of Sciences of the United States of America*, vol. 109, pp. 8270–8273, 5 2012.

[37] J. A. Wemmie, M. P. Price, and M. J. Welsh, "Acid-sensing ion channels: advances, questions and therapeutic opportunities," 10 2006.

[38] M. Tresguerres, J. Buck, and L. R. Levin, "Physiological carbon dioxide, bicarbonate, and ph sensing," 11 2010.

[39] P. Fromherz, C. O. Muller, and R. Weis, "Neuron transistor: Electrical transfer function measured by the patch-clamp technique," 1993.

[40] P. Fromherz and A. Stett, "Silicon-neuron junction: Capacitive stimulation of an individual neuron on a silicon chip," 1995.

[41] A. Offenhä, C. Sprö, M. Matsuzawa, and W. Knoll, "Field-effect transistor array for monitoring electrical activity from mammalian neurons in culture," 1997.

[42] B. Besl and P. Fromherz, "Transistor array with an organotypic brain slice: field potential records and synaptic currents," *European Journal of Neuroscience*, 2002.

[43] A. Lambacher, M. Jenkner, M. Merz, B. Eversmann, R. A. Kaul, F. Hofmann, R. Thewes, and P. Fromherz, "Electrical imaging of neuronal activity by multitransistor-array (mta) recording at 7.8 um resolution," *Applied Physics A: Materials Science and Processing*, vol. 79, pp. 1607–1611, 11 2004.

[44] M. Voelker and P. Fromherz, "Signal transmission from individual mammalian nerve cell to field-effect transistor," *Small*, vol. 1, pp. 206–210, 2 2005.

[45] Y. Cui, Q. Wei, H. Park, and C. M. Lieber, "Nanowire nanosensors forhighly sensitive and selectivedetection of biological andchemical species," *Science reports*, 2001.

[46] Y. Huang and C. M. Lieber, "Integrated nanoscale electronics and optoelectronics: Exploring nanoscale science and technology through semiconductor nanowires," vol. 76, pp. 2051–2068, Walter de Gruyter GmbH, 1 2004.

[47] F. Patolsky, G. Zheng, O. Hayden, M. Lakadamyali, X. Zhuang, and C. M. Lieber, "Electrical detection of single viruses," 2004.

[48] G. Zheng, F. Patolsky, Y. Cui, W. U. Wang, and C. M. Lieber, "Multiplexed electrical detection of cancer markers with nanowire sensor arrays," *Nature Biotechnology*, vol. 23, pp. 1294–1301, 10 2005.

[49] F. Patolsky, B. Timko, G. Yu, Y. Fang, A. Greytak, G. Zheng, and C. Lieber, "Detection, stimulation, and inhibition of neuronal signals with high-density nanowire transistor arrays," *Science*, vol. 313, pp. 1098–1100, 8 2006.

[50] S. R. Chang, C. H. Chang, J. S. Lin, S. C. Lu, Y. T. Lee, S. R. Yeh, and H. Chen, "Die-level, post-cmos processes for fabricating open-gate, field-effect biosensor arrays with on-chip circuitry," *Journal of Micromechanics and Microengineering*, vol. 18, 11 2008.

[51] F. Larramendy, A. Bendali, M. C. Blatché, F. Mathieu, S. Picaud, P. Temple-Boyer, and L. Nicu, "Misfet-based biosensing interface for neurons guided growth and neuronal electrical activities recording," *Sensors and Actuators, B: Chemical*, vol. 203, pp. 375–381, 2014.

[52] T. M. Fu, X. Duan, Z. Jiang, X. Dai, P. Xie, Z. Cheng, and C. M. Lieber, "Sub-10-nm intracellular bioelectronic probes from nanowire-nanotube heterostructures," *Proceedings of the National Academy of Sciences of the United States of America*, vol. 111, pp. 1259–1264, 1 2014.

[53] R. Gao, S. Strehle, B. Tian, T. Cohen-Karni, P. Xie, X. Duan, Q. Qing, and C. M. Lieber, "Outside looking in: Nanotube transistor intracellular sensors," *Nano Letters*, vol. 12, pp. 3329–3333, 6 2012.

[54] M. E. Spira and A. Hai, "Multi-electrode array technologies for neuroscience and cardiology," 2013.

[55] A. Casanova, M. C. Blatche, C. A. Ferre, H. Martin, D. Gonzalez-Dunia, L. Nicu, and G. Larrieu, "Self-aligned functionalization approach to order neuronal networks at the single-cell level," *Langmuir*, vol. 34, pp. 6612–6620, 6 2018.

[56] A. Fendyur, N. Mazurski, J. Shappir, and M. E. Spira, "Formation of essential ultrastructural interface between cultured hippocampal cells and gold mushroom-shaped mea- towards "in-cell" recordings from vertebrate neurons," *Frontiers in Neuroengineering*, 11 2011.

[57] F. Santoro, S. Dasgupta, J. Schnitker, T. Auth, E. Neumann, G. Panaitov, G. Gompper, and A. Offenhäusser, "Interfacing electrogenic cells with 3d nanoelectrodes: Position, shape, and size matter," *ACS Nano*, vol. 8, pp. 6713–6723, 7 2014.

[58] F. Santoro, J. Schnitker, G. Panaitov, and A. Offenhäusser, "On chip guidance and recording of cardiomyocytes with 3d mushroom-shaped electrodes," *Nano Letters*, vol. 13, pp. 5379–5384, 11 2013.

[59] A. Hai and M. E. Spira, "On-chip electroporation, membrane repair dynamics and transient in-cell recordings by arrays of gold mushroom-shaped microelectrodes," *Lab on a Chip*, vol. 12, pp. 2865–2873, 8 2012.

[60] N. Shmoel, N. Rabieh, S. M. Ojovan, H. Erez, E. Maydan, and M. E. Spira, "Multisite electrophysiological recordings by self-assembled loose-patch-like junctions between cultured hippocampal neurons and mushroom-shaped microelectrodes," *Scientific Reports*, vol. 6, 6 2016.

[61] J. T. Robinson, M. Jorgolli, A. K. Shalek, M. H. Yoon, R. S. Gertner, and H. Park, "Vertical nanowire electrode arrays as a scalable platform for intracellular interfacing to neuronal circuits," *Nature Nanotechnology*, vol. 7, pp. 180–184, 2012.

[62] Z. C. Lin, C. Xie, Y. Osakada, Y. Cui, and B. Cui, "Iridium oxide nanotube electrodes for sensitive and prolonged intracellular measurement of action potentials," *Nature Communications*, vol. 5, 2 2014.

[63] J. Abbott, T. Ye, L. Qin, M. Jorgolli, R. S. Gertner, D. Ham, and H. Park, "Cmos nanoelectrode array for all-electrical intracellular electrophysiological imaging," *Nature Nanotechnology*, vol. 12, pp. 460–466, 5 2017.

[64] C. Xie, Z. Lin, L. Hanson, Y. Cui, and B. Cui, "Intracellular recording of action potentials by nanopillar electroporation," *Nature Nanotechnology*, vol. 7, pp. 185–190, 2012.

[65] M. Dipalo, H. Amin, L. Lovato, F. Moia, V. Caprettini, G. C. Messina, F. Tantussi, L. Berdondini, and F. D. Angelis, "Intracellular and extracellular recording of spontaneous action potentials in mammalian neurons and cardiac cells with 3d plasmonic nanoelectrodes," *Nano Letters*, vol. 17, pp. 3932–3939, 6 2017.

[66] R. Liu, R. Chen, A. T. Elthakeb, S. H. Lee, S. Hinckley, M. L. Khraiche, J. Scott, D. Pre, Y. Hwang, A. Tanaka, Y. G. Ro, A. K. Matsushita, X. Dai, C. Soci, S. Biesmans, A. James, J. Nogan, K. L. Jungjohann, D. V. Pete, D. B. Webb, Y. Zou, A. G. Bang, and S. A. Dayeh, "High density individually addressable nanowire arrays record intracellular activity from primary rodent and human stem cell derived neurons," *Nano Letters*, vol. 17, pp. 2757–2764, 5 2017.

[67] A. Casanova, *Développement de nanosystèmes à base de nanofils pour l'interfaçage neuronal*. PhD thesis, 2016. Thèse de doctorat dirigée par Larrieu, Guilhem et Nicu, Liviu Micro et nanosystèmes Toulouse 3 2016.

[68] A. Casanova, M.-C. Blatche, F. Mathieu, L. Bettamin, H. Martin, D. Gonzalez-Dunia, L. Nicu, and G. Larrieu, "Integration of finfets and 3d nanoprobes devices on a common bio-platform for monitoring electrical activity of single neurons," *IEDM IEEE*, 2017.

[69] B. J. Lin and B. J. Lin, "Optical lithography: here is why," SPIE Bellingham, 2010.

[70] H. Levinson, "Principles of lithography, vol. pm198," 2011.

[71] F. Ayazi and K. Najafi, "High aspect-ratio polysilicon micromachining technology," *Sensors and Actuators, A: Physical*, vol. 87, no. 1-2, pp. 46–51, 2000.

[72] F. Ayazi and K. Najafi, "High aspect-ratio combined poly and single-crystal silicon (HARPSS) MEMS technology," *Journal of Microelectromechanical Systems*, vol. 9, no. 3, pp. 288–294, 2000.

[73] B. He, Y. Yang, M. F. Yuen, X. F. Chen, C. S. Lee, and W. J. Zhang, "Vertical nanostructure arrays by plasma etching for applications in biology, energy, and electronics," *Nano Today*, vol. 8, no. 3, pp. 265–289, 2013.

[74] A. Zeniou, K. Ellinas, A. Olziersky, and E. Gogolides, "Ultra-high aspect ratio Si nanowires fabricated with plasma etching: Plasma processing, mechanical stability analysis against adhesion and capillary forces and oleophobicity," *Nanotechnology*, vol. 25, no. 3, 2014.

[75] R. M. W.R. Thurber and Y. Liu., "Resistivity-Dopant Density Relationship for Phosphorus-Doped Silicon," *A Century of Excellence in MEASUREMENTS, STANDARDS, and TECHNOLOGY*, pp. 289–290, 2018.

[76] Y. Cui, X. Duan, J. Hu, and C. M. Lieber, "Doping and electrical transport in silicon nanowires," *Journal of Physical Chemistry B*, vol. 104, no. 22, pp. 5215–5216, 2000.

[77] S. S. Stensaas and L. J. Stensaas, "Histopathological evaluation of materials implanted in the cerebral cortex," *Connective Tissue*, vol. 155, pp. 145–155, 1978.

[78] B. W. Kristensen, J. Noraberg, P. Thiébaud, M. Koudelka-Hep, and J. Zimmer, "Biocompatibility of silicon-based arrays of electrodes coupled to organotypic hippocampal brain slice cultures," *Brain Research*, vol. 896, no. 1-2, pp. 1–17, 2001.

[79] N. Lago, K. Yoshida, K. P. Koch, and X. Navarro, "Assessment of biocompatibility of chronically implanted polyimide and platinum intrafascicular electrodes," *IEEE Transactions on Biomedical Engineering*, vol. 54, no. 2, pp. 281–290, 2007.

[80] J. M. Poate and T. C. Tisone, "Kinetics and mechanism of platinum silicide formation on silicon," *Applied Physics Letters*, vol. 24, no. 8, pp. 391–393, 1974.

[81] J. B. Bindell, J. W. Colby, D. R. Wonsidler, J. M. Poate, D. K. Conley, and T. C. Tisone, "An analytical study of platinum silicide formation," *Thin Solid Films*, vol. 37, no. 3, pp. 441–452, 1976.

[82] S. S. Cohen, P. A. Piacente, G. Gildenblat, and D. M. Brown, "Platinum silicide ohmic contacts to shallow junctions in silicon," *Journal of Applied Physics*, vol. 53, no. 12, pp. 8856–8862, 1982.

[83] A. A. Naem, "Platinum silicide formation using rapid thermal processing," *Journal of Applied Physics*, vol. 64, no. 8, pp. 4161–4167, 1988.

[84] Y. Guerfi, *Réalisation et caractérisation de transistors MOS à base de nanofils verticaux en silicium.* PhD thesis, 2015.

[85] N. Yoshizawa, T. Sato, and T. Hashizume, "Fundamental study of InP-based open-gate field-effect transistors for application to liquid-phase chemical sensors," *Japanese Journal of Applied Physics*, vol. 48, no. 9 Part 1, pp. 0911021–0911024, 2009.

[86] D. C. Li, P. H. Yang, and M. S. Lu, "Cmos open-gate ion-sensitive field-effect transistors for ultrasensitive dopamine detection," *IEEE Transactions on Electron Devices*, vol. 57, pp. 2761–2767, 10 2010.

[87] J.-C. Chou and C.-Y. Weng, "Sensitivity and hysteresis effect in al 2 o 3 gate ph-isfet," 2001.

[88] S. Chen, J. G. Bomer, E. T. Carlen, and A. Van Den Berg, "Al2O3/silicon nanoISFET with near ideal nernstian response," *Nano Letters*, vol. 11, no. 6, pp. 2334–2341, 2011.

[89] S. K. Kang and S. Purushothaman, "Development of conducting adhesive materials for microelectronic applications," 1999.

[90] A. J. G. Strandjord, S. Popelar, and C. Jauernig, "Interconnecting to aluminum-and copper-based semiconductors (electroless-nickel/gold for solder bumping and wire bonding)."

[91] M. A. Uddin, M. O. Alam, Y. C. Chan, and H. P. Chan, "Adhesion strength and contact resistance of flip chip on flex packages - effect of curing degree of anisotropic conductive film," *Microelectronics Reliability*, vol. 44, pp. 505–514, 3 2004.

[92] M. Nielsen, M. E., Bjorketun, M. H. Hansen, and J. Rossmeisl, "Towards first principles modeling of electrochemical electrode-electrolyte interfaces," *Surface Science*, 2015.

[93] S. Sakong, M. Naderian, K. Mathew, R. G. Hennig, and A. Grob, "Density functional theory study of the electrochemical interface between a pt electrode and an aqueous electrolyte using an implicit solvent method," *Journal of Chemical Physics*, vol. 142, 6 2015.

[94] M. F. Toney, J. N. Howard, J. Richer, G. L. Borges, J. G. Gordon, O. R. Melroy, D. G. Wiesler, D. Yee, and L. B. Sorensen, "Voltage-dependent ordering of water molecules at an electrode-electrolyte interface," *Letters to Nature*, 1994.

[95] H. Fiedmann, O. Amiri, and A. Ait-Mokhtar, "Physical modeling of the electrical double layer effects on multispecies ions transport in cement-based materials," *Cement and Concrete Research*, 2008.

[96] L. A. Geddes, "Historical evolution of circuit models for the electrode-electrolyte interface," 1997.

[97] P. Bergveld, "Development, operation, and application of the ion-sensitive field-effect transistor as a tool for electrophysiology," 1972.

[98] R. E. G. V. Hal, J. C. T. Eijkel, and P. Bergveld, "A novel description of isfet sensitivity with the buffer capacity and double-layer capacitance as key parameters," 1995.

[99] M. Gupta, S. Santermans, A. Veloso, Z. Tao, W. Li, G. Hellings, L. Lagae, W. V. Roy, and K. Martens, "Size independent ph sensitivity for ion sensitive finfets down to 10 nm width," *IEEE Sensors Journal*, vol. 19, pp. 6578–6586, 8 2019.

[100] D. K. Wise and T. Matsuo, "An integrated field-effect electrode for biopotential recording," 1974.

[101] B. Palán, F. V. Santos, J. M. Karam, B. Courtois, and M. Husák, "New isfet sensor interface circuit for biomedical applications," 1999.

[102] R. A. Rani and O. Sidek, "Isfet ph sensor characterization: towards biosensor microchip application," 2004.

[103] E. Stern, J. F. Klemic, D. A. Routenberg, P. N. Wyrembak, D. B. Turner-Evans, A. D. Hamilton, D. A. LaVan, T. M. Fahmy, and M. A. Reed, "Label-free immunodetection with cmos-compatible semiconducting nanowires," *Nature*, vol. 445, pp. 519–522, 2 2007.

[104] P. Xie, Q. Xiong, Y. Fang, Q. Qing, and C. M. Lieber, "Local electrical potential detection of dna by nanowire-nanopore sensors," *NATURE NANOTECHNOLOGY* /, vol. 7, 2012.

[105] S. Swaminathan', S. A. Krishnan', W. Lim, Z. Khiann', and G. C. Ahamed', "Microsensor characterization in an integrated blood gas measurement system," 2002.

[106] J. M. Rothberg, W. Hinz, T. M. Rearick, J. Schultz, W. Mileski, M. Davey, J. H. Leamon, K. Johnson, M. J. Milgrew, M. Edwards, J. Hoon, J. F. Simons, D. Marran, J. W. Myers, J. F. Davidson, A. Branting, J. R. Nobile, B. P. Puc, D. Light, T. A. Clark, M. Huber, J. T. Branciforte, I. B. Stoner, S. E. Cawley, M. Lyons, Y. Fu, N. Homer, M. Sedova, X. Miao, B. Reed, J. Sabina, E. Feierstein, M. Schorn, M. Alanjary, E. Dimalanta, D. Dressman, R. Kasinskas, T. Sokolsky, J. A. Fidanza, E. Namsaraev, K. J. McKernan, A. Williams, G. T. Roth, and J. Bustillo, "An integrated semiconductor device enabling non-optical genome sequencing," *Nature*, 2011.

[107] I. Humenyuk, B. Torbiéro, S. Assié-Souleille, R. Colin, X. Dollat, B. Franc, A. Martinez, and P. Temple-Boyer, "Development of pnh 4-isfets microsensors for water analysis," *Microelectronics Journal*, vol. 37, pp. 475–479, 6 2006.

[108] F. Larramendy, F. Mathieu, S. Charlot, L. Nicu, and P. Temple-Boyer, "Parallel detection in liquid phase of n-channel mosfet/chemfet microdevices using saturation mode," *Sensors and Actuators, B: Chemical*, vol. 176, pp. 379–385, 2013.

[109] H. M. K. T. Y. Miyahara, Y. Shibata, "An integrated chemical sensor with multiple ion and gas sensors," *Sensors and Actuators B: Chemical*, 1990.

[110] E. Lauwers, J. Suls, W. Gumbrecht, D. Maes, G. Gielen, and W. Sansen, "A cmos multiparameter biochemical microsensor with temperature control and signal interfacing," 2001.

[111] S. P. S. L. Li, "Mapping neutral microclimate ph in plga microspheres," *Journal of Controlled Release*, 2004.

[112] S. R. Chang and H. Chen, "A cmos-compatible, low-noise isfet based on high efficiency ion-modulated lateral-bipolar conduction," *Sensors*, vol. 9, pp. 8336–8348, 10 2009.

[113] F. Mariani, I. Gualandi, D. Tonelli, F. Decataldo, L. Possanzini, B. Fraboni, and E. Scavetta, "Design of an electrochemically gated organic semiconductor for ph sensing," *Electrochemistry Communications*, vol. 116, 7 2020.

[114] N. Kumar, D. Bhatt, M. Sutradhar, and S. Panda, "Interface mechanisms involved in a-igzo based dual gate isfet ph sensor using al2o3 as the top gate dielectric," *Materials Science in Semiconductor Processing*, vol. 119, 11 2020.

[115] H.-K. Liao, J.-C. Chou, W.-Y. Chung, T.-P. Sun, and S.-K. Hsiung, "Study of amorphous tin oxide thin films for isfet applications," 1998.

[116] K. Bedner, A. Guzenko, A. Tarasov, M. Wipf, R. L. Stoop, D. Just, S. Rigante, W. Fu, R. A. Minamisawa, C. David, M. Calame, J. Gobrecht, and C. Schönenberger, "ph response of silicon nanowire sensors: Impact of nanowire width and gate oxide," 2013.

[117] A. Tarasov, M. Wipf, R. L. Stoop, K. Bedner, W. Fu, V. A. Guzenko, O. Knopfmacher, M. Calame, and C. Schönenberger, "Understanding the electrolyte background for biochemical sensing with ion-sensitive field-effect transistors," *ACS Nano*, vol. 6, pp. 9291–9298, 10 2012.

[118] O. Knopfmacher, A. Tarasov, M. Wipf, W. Fu, M. Calame, and C. Schönenberger, "Silicon-based ion-sensitive field-effect transistor shows negligible dependence on salt concentration at constant ph," *ChemPhysChem*, vol. 13, pp. 1157–1160, 4 2012.

[119] O. Knopfmacher, A. Tarasov, W. Fu, M. Wipf, B. Niesen, M. Calame, and C. Schönenberger, "Nernst limit in dual-gated si-nanowire fet sensors," *Nano Letters*, vol. 10, pp. 2268–2274, 6 2010.

[120] O. Knopfmacher, D. Keller, M. Calame, and C. Schönenberger, "Dual gated silicon nanowire field effect transistors," vol. 1, pp. 678–681, 9 2009.

[121] A. Casanova, M. C. Blatche, C. A. Ferre, H. Martin, D. Gonzalez-Dunia, L. Nicu, and G. Larrieu, "Self-aligned functionalization approach to order neuronal networks at the single-cell level," *Langmuir*, vol. 34, pp. 6612–6620, 6 2018.

[122] V. Onesto, L. Cancedda, M. L. Coluccio, M. Nanni, M. Pesce, N. Malara, M. Cesarelli, E. D. Fabrizio, F. Amato, and F. Gentile, "Nano-topography enhances communication in neural cells networks," *Scientific Reports*, vol. 7, 12 2017.

[123] V. Onesto, R. Narducci, F. Amato, L. Cancedda, and F. Gentile, "The effect of connectivity on information in neural networks," *Integrative Biology (United Kingdom)*, vol. 10, pp. 121–127, 2 2018.

[124] M. Dipalo, A. F. McGuire, H. Y. Lou, V. Caprettini, G. Melle, G. Bruno, C. Lubrano, L. Matino, X. Li, F. D. Angelis, B. Cui, and F. Santoro, "Cells adhering to 3d vertical nanostructures: Cell membrane reshaping without stable internalization," *Nano Letters*, vol. 18, pp. 6100–6105, 9 2018.

[125] D. Iandolo, F. A. Pennacchio, V. Mollo, D. Rossi, D. Dannhauser, B. Cui, R. M. Owens, and F. Santoro, "Electron microscopy for 3d scaffolds–cell biointerface characterization," *Advanced Biosystems*, vol. 3, 2 2019.

[126] X. Li, L. Matino, W. Zhang, L. Klausen, A. F. McGuire, C. Lubrano, W. Zhao, F. Santoro, and B. Cui, "A nanostructure platform for live-cell manipulation of membrane curvature," *Nature Protocols*, vol. 14, pp. 1772–1802, 6 2019.

[127] P. Clark, P. Connolly, A. S. G. Curtis, J. A. T. Dow, and C. D. W. Wilkinson, "Cell guidance by ultrafine topography in vitro," *Journal of Cell Science*, 1991.

[128] M. R. Hynd, J. P. Frampton, N. Dowell-Mesfin, J. N. Turner, and W. Shain, "Directed cell growth on protein-functionalized hydrogel surfaces," *Journal of Neuroscience Methods*, vol. 162, pp. 255–263, 5 2007.

[129] S. B. Jun, M. R. Hynd, N. Dowell-Mesfin, K. L. Smith, J. N. Turner, W. Shain, and S. J. Kim, "Low-density neuronal networks cultured using patterned poly-l-lysine on microelectrode arrays," *Journal of Neuroscience Methods*, vol. 160, pp. 317–326, 3 2007.

[130] M. Jungblut, W. Knoll, C. Thielemann, and M. Pottek, "Triangular neuronal networks on microelectrode arrays: An approach to improve the properties of low-density networks for extracellular recording," *Biomedical Microdevices*, vol. 11, pp. 1269–1278, 12 2009.

[131] N. S. Baek, J. H. Lee, Y. H. Kim, B. J. Lee, G. H. Kim, I. H. Kim, M. A. Chung, and S. D. Jung, "Photopatterning of cell-adhesive-modified poly(ethyleneimine) for guided neuronal growth," *Langmuir*, vol. 27, pp. 2717–2722, 3 2011.

[132] E. Marconi, T. Nieus, A. Maccione, P. Valente, A. Simi, M. Messa, S. Dante, P. Baldelli, L. Berdondini, and F. Benfenati, "Emergent functional properties of neuronal networks with controlled topology," *PLoS ONE*, vol. 7, 4 2012.

[133] M. Suzuki, K. Ikeda, M. Yamaguchi, S. N. Kudoh, K. Yokoyama, R. Satoh, D. Ito, M. Nagayama, T. Uchida, and K. Gohara, "Neuronal cell patterning on a multi-electrode array for a network analysis platform," *Biomaterials*, vol. 34, pp. 5210–5217, 7 2013.

[134] J. Cheng, G. Zhu, L. Wu, X. Du, H. Zhang, B. Wolfrum, Q. Jin, J. Zhao, A. Offenhäusser, and Y. Xu, "Photopatterning of self-assembled poly (ethylene) glycol monolayer for neuronal network fabrication," *Journal of Neuroscience Methods*, vol. 213, pp. 196–203, 3 2013.

[135] J. Wang, L. Ren, L. Li, W. Liu, J. Zhou, W. Yu, D. Tong, and S. Chen, "Microfluidics: A new cosset for neurobiology," *Lab on a Chip*, 2008.

[136] M. K. Lewandowska, D. J. Bakkum, S. B. Rompani, and A. Hierlemann, "Recording large extracellular spikes in microchannels along many axonal sites from individual neurons," *PLoS ONE*, vol. 10, 3 2015.

[137] Y. W. Fan, F. Z. Cui, S. P. Hou, Q. Y. Xu, L. N. Chen, and I. S. Lee, "Culture of neural cells on silicon wafers with nano-scale surface topograph," *Journal of neuroscience methods*, 2002.

[138] T. M. Pearce, J. A. Wilson, S. G. Oakes, S.-Y. Chiu, and J. C. Williams, "Integrated microelectrode array and microfluidics for temperature clamp of sensory neurons in culture," *Lab on a Chip*, 2005.

[139] R. Stepanyan, B. Hollins, S. E. Brock, and T. S. Mcclintock, "Primary culture of lobster (homarus americanus) olfactory sensory neurons," *Chemical Senses*, vol. 29, pp. 179–187, 2004.

[140] C. Métin, D. Deléglise, T. Serafini, T. E. Kennedy, and M. Tessier-Lavigne, "A role for netrin-1 in the guidance of cortical efferents," *Development*, 1997.

[141] J. Henley and M. M. Poo, "Guiding neuronal growth cones using ca2+ signals," 6 2004.

[142] F. Tang and K. Kalil, "Netrin-1 induces axon branching in developing cortical neurons by frequency-dependent calcium signaling pathways," *Journal of Neuroscience*, vol. 25, pp. 6702–6715, 7 2005.

[143] M. P. Maher, J. Pine, J. Wright, and Y.-C. Tai, "The neurochip: a new multi-electrode device for stimulating and recording from cultured neurons," 1999.

[144] S. Turner, K. L., I. M., C. H.G., S. W., and T. J., "Cell attachment on silicon nanostructures," *Journal of Vacuum Science and Technology B: Microelectronics and Nanometer Structures*, vol. 15, p. 2848, 11 1997.

[145] M. J. Mahoney, R. R. Chen, J. Tan, and W. M. Saltzman, "The influence of microchannels on neurite growth and architecture," *Biomaterials*, vol. 26, pp. 771–778, 3 2005.

[146] B. Vahidi, J. W. Park, H. J. Kim, and N. L. Jeon, "Microfluidic-based strip assay for testing the effects of various surface-bound inhibitors in spinal cord injury," *Journal of Neuroscience Methods*, vol. 170, pp. 188–196, 5 2008.

[147] M.-H. Wu, J. P. G. Urban, Z. Cui, . Zhan, F. Cui, M.-H. Wu, Z. F. Cui, J. P. G. Urban, and Z. Cui, "Development of pdms microbioreactor with well-defined and homogenous culture environment for chondrocyte 3-d culture," *Biomed Microdevices*, vol. 8, pp. 331–340, 2006.

[148] J. M. K. Ng, I. Gitlin, A. D. Stroock, and G. M. Whitesides, "Components for integrated poly(dimethylsiloxane) microfluidic systems," *Electrophoresis*, 2002.

[149] A. M. Rajnicek, S. Britland, and C. D. McCaig, "Contact guidance of cns neurites on grooved quartz: influence of groove dimensions, neuronal age and cell type," *Journal of Cell Science*, 1997.

[150] A. M. P. Turner, N. Dowell, S. W. P. Turner, L. Kam, M. Isaacson, J. N. Turner, H. G. Craighead, and W. Shain, "Attachment of astroglial cells to microfabricated pillar arrays of different geometries," *Journal of Biomedical Material Research*, 2000.

[151] H. G. Craighead, S. W. Turner, R. C. Davis, C. James, A. M. Perez, P. M. S. John, M. S. Isaacson, L. Kam, W. Shain, J. N. Turner, and G. Banker, "Chemical and topographical surface modi®cation for control of central nervous system cell adhesion," 1998.

[152] A. M. Taylor, M. Blurton-Jones, S. W. Rhee, D. H. Cribbs, C. W. Cotman, and N. L. Jeon, "A microfluidic culture platform for cns axonal injury, regeneration and transport," *Nature Methods*, vol. 2, pp. 599–605, 8 2005.

[153] E. Claverol-Tinturé, J. Cabestany, and X. Rosell, "Multisite recording of extracellular potentials produced by microchannel-confined neurons in-vitro," *IEEE Transactions on Biomedical Engineering*, vol. 54, pp. 331–335, 2 2007.

[154] J. M. Peyrin, B. Deleglise, L. Saias, M. Vignes, P. Gougis, S. Magnifico, S. Betuing, M. Pietri, J. Caboche, P. Vanhoutte, J. L. Viovy, and B. Brugg, "Axon diodes for the reconstruction of oriented neuronal networks in microfluidic chambers," *Lab on a Chip*, vol. 11, pp. 3663–3673, 11 2011.

[155] P. A. Wieringa, R. W. Wiertz, E. D. Weerd, and W. L. Rutten, "Bifurcating microchannels as a scaffold to induce separation of regenerating neurites," *Journal of Neural Engineering*, vol. 7, 2010.

[156] S. Moorjani, S.-E. Huh, N. Bhattacharjee, and A. Folch, "Study of axon-guidance interaction in controlled microfluidic environments," *16th Interna-*

tional Conference on Miniaturized Systems for Chemistry and Life Sciences, 2012.

[157] N. Bhattacharjee, N. Li, T. M. Keenan, and A. Folch, "A neuron-benign microfluidic gradient generator for studying the response of mammalian neurons towards axon guidance factors," *Integrative Biology*, vol. 2, pp. 669–679, 11 2010.

[158] L. Pan, S. Alagapan, E. Franca, T. Demarse, G. J. Brewer, and B. C. Wheeler, "Large extracellular spikes recordable from axons in microtunnels," *IEEE Transactions on Neural Systems and Rehabilitation Engineering*, vol. 22, pp. 453–459, 2014.

[159] E. Claverol-Tinturé, M. Ghirardi, F. Fiumara, X. Rosell, and J. Cabestany, "Multielectrode arrays with elastomeric microstructured overlays for extracellular recordings from patterned neurons," *Journal of Neural Engineering*, vol. 2, 6 2005.

[160] B. J. Dworak and B. C. Wheeler, "Novel mea platform with pdms microtunnels enables the detection of action potential propagation from isolated axons in culture," *Lab on a Chip*, vol. 9, pp. 404–410, 2009.

[161] T. T. Kanagasabapathi, P. Massobrio, R. A. Barone, M. Tedesco, S. Martinoia, W. J. Wadman, and M. M. Decré, "Functional connectivity and dynamics of cortical-thalamic networks co-cultured in a dual compartment device," *Journal of Neural Engineering*, vol. 9, 6 2012.

[162] G. J. Brewer, M. D. Boehler, S. Leondopulos, L. Pan, S. Alagapan, T. B. DeMarse, and B. C. Wheeler, "Toward a self-wired active reconstruction of the hippocampal trisynaptic loop: Dg-ca3," *Frontiers in Neural Circuits*, vol. 7, 10 2013.

[163] L. Pan, S. Alagapan, E. Franca, G. J. Brewer, and B. C. Wheeler, "Propagation of action potential activity in a predefined microtunnel neural network," vol. 8, 8 2011.

[164] M. K. Lewandowska, M. Radivojević, D. Jäckel, J. Müller, and A. R. Hierlemann, "Cortical axons, isolated in channels, display activity-dependent signal modulation as a result of targeted stimulation," *Frontiers in Neuroscience*, vol. 10, 3 2016.

[165] B. J. Dickson, "Molecular mechanisms of axon guidance," 2001.

[166] F. Larramendy, L. Mazenq, P. Temple-Boyer, and L. Nicu, "Three-dimensional closed microfluidic channel fabrication by stepper projection single step lithography: The diabolo effect," *Lab on a Chip*, vol. 12, pp. 387–390, 1 2012.

[167] F. Larramendy, M. C. Blatche, L. Mazenq, A. Laborde, P. Temple-Boyer, and O. Paul, "Microchannel-connected su-8 honeycombs by single-step projec-

tion photolithography for positioning cells on silicon oxide nanopillar arrays," *Journal of Micromechanics and Microengineering*, vol. 25, 4 2015.

[168] E. Suberbielle, P. E. Sanchez, A. V. Kravitz, X. Wang, K. Ho, K. Eilertson, N. Devidze, A. C. Kreitzer, and L. Mucke, "Physiologic brain activity causes dna double-strand breaks in neurons, with exacerbation by amyloid-beta," *Nature Neuroscience*, vol. 16, pp. 613–621, 5 2013.

[169] E. Suberbielle, B. Djukic, M. Evans, D. H. Kim, P. Taneja, X. Wang, M. Finucane, J. Knox, K. Ho, N. Devidze, E. Masliah, and L. Mucke, "Dna repair factor brca1 depletion occurs in alzheimer brains and impairs cognitive function in mice," *Nature Communications*, vol. 6, 11 2015.

[170] V. Nimmrich, C. Grimm, A. Draguhn, S. Barghorn, A. Lehmann, H. Schoemaker, H. Hillen, G. Gross, U. Ebert, and C. Bruehl, "Amyloid beta oligomers (abeta1-42 globulomer) suppress spontaneous synaptic activity by inhibition of p/q-type calcium currents," *Journal of Neuroscience*, vol. 28, pp. 788–797, 1 2008.

[171] T. Yang, S. Li, H. Xu, D. M. Walsh, and D. J. Selkoe, "Large soluble oligomers of amyloid beta-protein from alzheimer brain are far less neuroactive than the smaller oligomers to which they dissociate," *Journal of Neuroscience*, vol. 37, pp. 152–163, 1 2017.

[172] S. Li, M. Jin, T. Koeglsperger, N. E. Shepardson, G. M. Shankar, and D. J. Selkoe, "Soluble a beta oligomers inhibit long-term potentiation through a mechanism involving excessive activation of extrasynaptic nr2b-containing nmda receptors," *Journal of Neuroscience*, vol. 31, pp. 6627–6638, 5 2011.

[173] F. Tamagnini, S. Scullion, J. T. Brown, and A. D. Randall, "Intrinsic excitability changes induced by acute treatment of hippocampal ca1 pyramidal neurons with exogenous amyloid beta peptide," *Hippocampus*, vol. 25, pp. 786–797, 7 2015.

[174] M. Szelechowski, A. Bétourné, Y. Monnet, C. A. Ferré, A. Thouard, C. Foret, J. M. Peyrin, S. Hunot, and D. Gonzalez-Dunia, "A viral peptide that targets mitochondria protects against neuronal degeneration in models of parkinson's disease," *Nature Communications*, vol. 5, 10 2014.

[175] A. Bétourné, M. Szelechowski, A. Thouard, E. Abrial, A. Jean, F. Zaidi, C. Foret, E. M. Bonnaud, C. M. Charlier, E. Suberbielle, C. E. Malnou, S. Granon, C. Rampon, and D. Gonzalez-Dunia, "Hippocampal expression of a virus-derived protein impairs memory in mice," *Proceedings of the National Academy of Sciences of the United States of America*, vol. 115, pp. 1611–1616, 2 2018.